

Emulsion microgel particles: from design to oral to gastrointestinal digestion

Ophélie Marie-Pierre Cécile Torres

Submitted in accordance with the requirements for the degree of

Doctor of Philosophy

The University of Leeds

School of Food Science and Nutrition

October 2018

The candidate confirms that the work submitted is his/her own, except where work which has formed part of jointly-authored publications has been included. The contribution of the candidate and the other authors to this work has been explicitly indicated below. The candidate confirms that appropriate credit has been given within the thesis where reference has been made to the work of others. Details of the jointly-authored publications and contribution of each authors are outlined on the next page.

This copy has been supplied on the understanding that it is copyright material and that no quotation from the thesis may be published without proper acknowledgement.

The right of Ophélie Marie-Pierre Cécile Torres to be identified as Author of this work has been asserted by her in accordance with the Copyright, Designs and Patents Act 1988.

Further details of the jointly-authored publications and the contributions of the candidate and the other authors to the work are included below:

Chapter 2

Torres, O., Murray, B. and Sarkar, A. 2016. Emulsion microgel particles: Novel encapsulation strategy for lipophilic molecules. *Trends in Food Science & Technology*. **55**(Supplement C), pp.98-108.

Chapter 3

Torres, O., Tena, N.M., Murray, B. and Sarkar, A. 2017. Novel starch based emulsion gels and emulsion microgel particles: Design, structure and rheology. *Carbohydrate Polymers*. **178**, pp.86-94.

Chapter 4

Torres, O., Murray, B. and Sarkar, A. 2017. Design of novel emulsion microgel particles of tuneable size. *Food Hydrocolloids*. **71**(Supplement C), pp.47-59.

Chapter 5

Torres, O., Andablo-Reyes, E., Murray, B. S. and Sarkar, A. 2018. Emulsion microgel particles as high-performance bio-lubricant. *ACS Applied Materials & Interfaces*, **10**, 26893-26905.

Chapter 6

Torres, O., Murray, B. and Sarkar, A. 2019. Overcoming in vitro gastric destabilisation of emulsion droplets using emulsion microgel particles for targeted intestinal release of fatty acids. *Food Hydrocolloids*. **89**, pp.523-533.

Details of authorship contributions:

Ophelie Torres: designed the experiments and conducted the measurements, data analysis and interpretation as well as drafted and edited the manuscripts and replied to the comments from reviewers.

Anwesha Sarkar and Brent S. Murray: provided supervision, feedback and contributed to the proofreading and editing of the manuscript.

Nidia M. Tena: conducted the preliminary experiments to identify the concentration of OSA starch to form stable OSA starch emulsion, under the supervision of Ophelie Torres.

Efren E. Andablo-Reyes: provided feedback on mathematical modelling of the Hertz contact and drag force.

List of accepted conference abstracts

Poster presentation:

Torres, O., Murray, B. and Sarkar, A. Emulsion microgels: a novel approach for delivery of lipophilic molecules. (2016). Innovations in Encapsulation – Edinburgh, UK.

Oral presentations:

Torres, O., Murray, B. and Sarkar, A. Emulsion microgels: a novel approach for delivery of lipophilic molecules. (2016). 30th EFFoST International Conference – Vienna, Austria.

Torres, O., Murray, B. and Sarkar, A. Emulsion microgels: a novel approach for delivery of lipophilic molecules. (2016). 3rd Food Science & Nutrition PhD Conference – Leeds, UK.

Torres, O., Tena, N.M., Murray, B. and Sarkar, A. Preparation of novel emulsion gels and emulsion microgel particles using modified starch. (2017). 19th Gums & Stabilisers for the Food Industry Conference: Hydrocolloid multifunctionality – Berlin, Germany.

Torres, O., Tena, N.M., Murray, B. and Sarkar, A. Novel starch based emulsion gels and emulsion microgel particles: Design, structure and rheology. (2017). 3rd UK Hydrocolloids Symposium – Nottingham, UK.

Torres, O., Murray, B. and Sarkar, A. Oral tribology of starch based emulsion microgel particles. (2017). International Symposium on Delivery of Functionality in Complex Food Systems – Auckland, New Zealand.

Torres, O., Murray, B. and Sarkar, A. Oral tribology of starch based emulsion microgel particles. (2018). 17th Food Colloids Conference – Leeds, UK.

Torres, O., Andablo-Reyes, E., Murray, B. S. and Sarkar, A. Lubrication properties of emulsion microgel particles under in vitro oral processing. (2018). 4th International Conference on BioTribology – Montreal, Canada.

Acknowledgements

First and foremost I would like to sincerely thank my main supervisor Dr. Anwesha Sarkar and co-supervisor Professor Brent S. Murray for all their help, time and academic guidance throughout this project. Their support has truly been crucial, from the start of this research project up to the submission of my thesis. I am deeply grateful to have been able to conduct my PhD thesis with two incredibly knowledgeable and resourceful supervisors.

I would also like to acknowledge the financial sponsorship from the University of Leeds 110th Anniversary Research Scholarship, the industrial sponsor and the European Research Council (ERC, grant agreement number: 757993). I would like to extend my thanks to all staff, lecturers and colleagues in the School of Food Science and Nutrition, for supporting me throughout my research and making my time in the laboratories enjoyable. I particularly would like to thank: Linda Pravinata, Feng Xu, Efren Andablo-Reyes, Alessandro Gullota, Pallab Borah, Melvin Holmes, Martin Fuller, Miles Ratcliff, Joanne Burke, Nataricha Phisarnchananan and Neil Rigby, who were always there to help and offer valuable support during my PhD.

I would like to express my gratitude to my parents, family and friends, for all their support, interest, motivation and encouragements to persevere through the difficult times of my research. A special “*merci*” to my Mum, my Aunt and my little Cousins, who all helped in their own special ways. I am also extremely thankful towards my Grandma who helped me become a stronger woman throughout the years. Many thanks also go to my closest friends, Lisa for her great support in graphical designs and Elise, who tried her best to keep my fed, but also for both of their listening ears. And of course none of this would gone as smoothly without my partner, Alexandre, who gave me the courage to do a PhD as well as provided countless suggestions, guidance, moral support and patience during this critical time. I dedicate this thesis to all of you.

Abstract

Lipophilic active molecules, such as fat soluble vitamins, flavourings and fatty acids pose challenges for their application in food matrices due their water-insolubility, rapid oxidation and degradation during physiological transit. Based on the perceived knowledge gap from the literature review, a novel encapsulation strategy, targeting the delivery of lipophilic molecules, was developed in this thesis: emulsion microgel particles. These engineered smart particles are soft gel like particles encapsulating several oil droplets. These particles can alter their network structure, swelling behaviour, permeability or mechanical strength in response to internal physiological stimuli (*e.g.*, change in pH, ionic strength, temperature, mechanical shear, enzymatic action, etc.).

By investigating the nature of two specific biopolymer networks (*i.e.*, starch gel or whey protein gel) and the interactions between the filler (*i.e.*, emulsion droplets) and the matrix (*i.e.*, the gel), two different approaches (top-down or bottom-up) were used to design these emulsion microgel particles. The unique design of the emulsion microgel particles developed in this PhD was that both the emulsifying agent and the matrix material were composed of the same biopolymer without the need of additional hydrocolloids. The characterization techniques used in this thesis included particle sizing, microscopy at various length scales, zeta-potential, rheology, tribology, sodium dodecyl sulphate polyacrylamide gel electrophoresis, pH-stat titrimetric measurements supported by theoretical calculations.

In view of the above, the rheological properties and microstructural breakdown of the model emulsion gels were first analysed. The oil content, particle size, filler to matrix ratio and matrix polymer properties were also examined. Emphasis was then placed on the different response mechanisms of the starch- or whey protein-based emulsion microgel particles when subjected to different environmental stresses, such as acidic pH, enzyme activity (α -amylase for oral relevance, pepsin or trypsin for gastrointestinal relevance) and mechanical shear. Successfully, the emulsion microgel particles contributed to the improvement of food based delivery systems for lipophilic materials. Starch-based emulsion microgel particles were found to be suitable for the protection of lipophilic molecules against oral shear and coalescence whilst providing appropriate lubrication *via* both enzyme and shear-response mechanism. Whey protein-based emulsion microgel particles were established to protect the lipophilic molecules from harsh gastric environment

whilst enabling complete release of free fatty acid during the intestinal phase due to both enzyme and pH-assisted mechanisms.

The findings from this PhD thesis thus provide guidelines to develop new bio-responsive materials where these emulsion microgel particles can be used to offer excellent site-dependent controlled release properties for lipophilic materials.

Table of Contents

List of accepted conference abstracts	iv
Acknowledgements	v
Abstract	vi
Table of Contents	viii
List of Tables	x
List of Figures	xii
List of Abbreviations	xviii
Chapter 1 General Introduction	1
1.1 Overall research aim	1
1.2 General insight on emulsions and gels.....	2
1.3 Rationale behind the selection of biopolymers	4
1.4 Rationale behind the selection of characterization techniques	13
1.5 Outline of the thesis	36
1.6 References	38
Chapter 2 Emulsion microgel particles: novel encapsulation strategy for lipophilic molecules	47
Abstract.....	47
2.1 Introduction	48
2.2 Formation of Emulsion Gels	51
2.3 Filler-Matrix Interactions	55
2.4 Emulsion microgel particle formation	62
2.5 Delivery of lipophilic molecules using emulsion microgel particles...	66
2.6 Conclusions	69
2.7 References	70
Chapter 3 Novel starch-based emulsion gels and emulsion microgel particles: design, structure and rheology	81
Abstract.....	81
3.1 Introduction	82
3.2 Materials and Methods.....	84
3.3 Results and Discussion.....	89
3.4 Conclusions	102
3.5 References	102
Chapter 4 Design of novel whey protein based-emulsion microgel particles of tuneable size	107
Abstract.....	107

4.1	Introduction	108
4.2	Materials and Methods	111
4.3	Results and discussion.....	118
4.4	Conclusions	135
4.5	References	136
Chapter 5 <i>In vitro</i> oral processing of starch-based emulsion microgel particles: from protection to lubrication performances		143
	Abstract.....	143
5.1	Introduction	144
5.2	Materials and Methods	147
5.3	Results and discussion.....	150
5.4	Conclusions	169
5.5	References	170
Chapter 6 Whey protein-based emulsion microgel particles for targeted intestinal release of lipophilic components		175
	Abstract.....	175
6.1	Introduction	176
6.2	Materials and Methods	179
6.3	Results and Discussion.....	184
6.4	Conclusions	197
6.5	References	198
Chapter 7 General Discussion		203
7.1	Introduction	203
7.2	Summary of the main results.....	205
7.3	Concluding remarks and future directions	223
7.4	References	225
Appendix A Supplementary information for Chapter 3		229
Appendix B Supplementary information for Chapter 4.....		231
Appendix C Supplementary information for Chapter 5		232
Appendix D Supplementary information for Chapter 6		242

List of Tables

Table 2.1 Definitions and microstructures (at various length scales) of different emulsion gel-based strategies for delivery of lipophilic molecules. (A) Transmission electron micrograph (TEM) of emulsion gels (reproduced from Anton et al. (2001)). (B) Scanning electron micrograph (SEM) of emulsion microgel particle (reproduced from Egan, et al., 2013).	50
Table 2.2 Effects of active and inactive filler on the rheological behaviour of emulsion gels (G' : storage modulus; ϕ : volume fraction; \uparrow : increase; \downarrow : decrease).....	56
Table 2.3 Filler-matrix interactions and rheological behaviour of whey protein emulsion gels (G' : storage modulus, ϕ : volume fraction; $[]$: concentration, \uparrow : increase; \downarrow : decrease; $=>$: leads to).	59
Table 3.1 Initial and final concentrations of wheat starch and 40 wt% oil-in-water emulsion stabilised by 4 wt% OSA starch as well as mixing ratios for the formation of the different emulsion gels.	87
Table 4.1 Key processing conditions for Buchi Encapsulator B-390 [®] and Leeds Jet homogenizer, respectively.	114
Table 4.2 Final storage modulus (G') measurement at 25 °C and 1 Hz, and mesh size (ζ) and standard deviation for the various rheological measurements of HT-WPI emulsion gel at different $[Ca^{2+}]$; line containing mean with similar subscript letter are not significantly different ($p > 0.05$).	125
Table 4.3 Summary of the flux of Ca^{2+} ions to HT-WPI adsorbed at oil droplet surface as a function of different $[Ca^{2+}]$ and turbulent diffusion.	135
Table 5.1 Relative indentation and drag force calculations of the emulsion droplets of radius 0.08 μm and particles of radius 15 μm at $U = 3 \text{ mm s}^{-1}$ and $\phi p = 20\%$	166
Table 7.1 Sauter mean diameter (d_{32}) and ζ -potential at pH 7, columns with symbol (*) are significantly different ($p < 0.05$).....	205
Table 7.2 Final experimental elastic modulus (G'_b), phase angle ($\tan \delta$), limiting deformation value (γL) of the emulsion gel containing different starch and oil concentrations, and estimated elastic modulus (G'_m) and phase angle ($\tan \delta_m$) of the starch gel matrix and derivative mesh size (ζ), columns containing symbol (*) are significantly different ($p < 0.05$) to their corresponding starch gel (15 or 20 wt%) without oil droplets, in the same column.	209
Table 7.3 Final experimental elastic modulus (G'_b), phase angle ($\tan \delta$), limiting deformation value (γL) of the whey protein emulsion gel prepared at different Ca^{2+} concentrations without or with 20 wt% oil, and estimated elastic modulus (G'_m) and phase angle ($\tan \delta_m$) of the whey protein gel matrix and derivative mesh size (ζ), columns containing symbol (*) are significantly different ($p < 0.05$) to their corresponding whey protein gel without oil droplets.	211
Table 7.4 Summary of mixing time (t_{mix}), diffusive molecular flux of Ca^{2+} (J) and whey protein-based emulsion microgel particle size (d_{32}) as function of the different processing routes and Ca^{2+} concentrations.....	215

Table 7.5 Summary of the physiological-specific trigger mechanisms in relation to the biopolymer used to engineer the emulsion microgel particles	216
Table 7.6 Amino acid composition of β -lactoglobulin and the pK _a values of the amino acid residue side chains (from (Alexander et al., 1989; Damodaran et al., 2008).....	222

List of Figures

Figure 1.1 Schematic representation of an emulsion microgel particle designed in this thesis.....	2
Figure 1.2 Schematic representation of the structure and chemical composition of amylopectin and amylose molecules, adapted from Sweedman et al. (2013).....	5
Figure 1.3 Schematic representation of the behaviour of starch granules during heating, cooling and shearing (\nearrow : increase, \searrow : decrease), adapted from Iida et al. (2008) and Wang et al. (2015).	7
Figure 1.4 OSA-starch modification: starch glucose unit with added OSA groups, adapted from Sweedman et al. (2013).	9
Figure 1.5 Schematic representation of heat-set versus cold-set gelation of whey protein, adapted from Ryan et al. (2013).	12
Figure 1.6 Schematic representation of a negatively charged particle and the presence of its ions at the “Slipping plane”, “Double layer” and “Diffuse layer”, figure from Malvern Instruments Ltd (2011).	15
Figure 1.7 Schematic representation of light scattered from small and large particles.	17
Figure 1.8 Schematic representation of the differences between optical microscopy and confocal laser scanning microscopy, adapted from Hardham (2012) and Microscopegenius.com	18
Figure 1.9 Schematic representation of commonly used geometries in rheology with the sample in blue.	20
Figure 1.10 Relationship between the force and velocity of an applied stress on the displacement of a material, adapted from Mezger (2014).	20
Figure 1.11 Schematic representation of the oscillatory rheology of a viscoelastic material, showing the sinusoidal stress input (σ), the sinusoidal resulting strain (γ) and the phase shift angle (δ) occurring between the input stress and measured strain response, adapted from Mezger (2014).	22
Figure 1.12 Comparison of viscosity functions of Newtonian and non-Newtonian fluids.....	24
Figure 1.13 Oral processing: from bulk rheology to thin layer lubrication.	25
Figure 1.14 Schematic representation of a tribometer set-up.....	26
Figure 1.15 Typical Stribeck curve as a function of the Hersey number, adapted from de Vicente et al. (2006) and Stokes (2012).	27
Figure 1.16 Schematic representation of the proteolysis of a polypeptide, comprised of four amino acid, via pepsin attacking a peptide bond.	32
Figure 1.17 Schematic representation of polyacrylamide gel electrophoresis (M_w : molecular weight), figure from Bio-Rad Laboratories (2015).....	33
Figure 1.18 Schematic representation of the lipolysis of triglycerides into diglycerol and monoglycerol and fatty acids.	35

Figure 1.19 Schematic framework of this thesis.	36
Figure 2.1 Schematic representation of emulsion gel formation using whey protein.....	52
Figure 2.2 Schematic diagram illustrating the effect of fillers on G' . (Solid line: inactive filler; dotted line: active filler).....	58
Figure 2.3 Schematic representation of controlled release of lipophilic molecules from emulsion microgel particle via swelling or matrix erosion.	67
Figure 3.1 Schematic diagram and corresponding micrographs of the formation of OSA starch-stabilised emulsion (A), sheared wheat starch gel (B) and starch emulsion gel and emulsion microgel particles (indicated within dashed box).	88
Figure 3.2 Elastic modulus (G' , filled symbols) and viscous modulus (G'' , empty symbols) as a function of time and temperature (full black line) of 15 wt% wheat starch gel (A) and 20 wt% wheat starch gel (B) prepared with different OSA starch concentrations (0 wt%, ■; 0.5 wt%, ●; 1 wt%, ▲; 1.5 wt%, ◆; 2 wt%, ▼) at 1 Hz and 0.5 % strain.	90
Figure 3.3 Elastic modulus (G' , filled symbols) and viscous modulus (G'' , empty symbols) as a function of strain of 15 wt% wheat starch gel (A) and 20 wt% wheat starch gel (B) prepared with different OSA starch concentrations (0 wt%, ■; 0.5 wt%, ●; 1 wt%, ▲; 1.5 wt%, ◆; 2 wt%, ▼). The limiting deformation value (γ_L) of wheat starch gels at 15 wt% (black) and 20 wt% (white) is reported as a function of OSA concentration (C), samples with symbol (†) are not significantly different ($p > 0.05$) to wheat starch gel (15 or 20 wt%) without OSA starch.	92
Figure 3.4 Droplet size distribution (A) indicating d_{32} and d_{43} values of 40 wt% oil-in-water emulsion stabilised by 1 wt% OSA (red dashed line), 2 wt% OSA (blue dotted line) and 4 wt% OSA (black full line) and CLSM micrograph (B) of 40 wt% oil-in-water emulsion stabilised by 4 wt% OSA, oil droplets in red stained using Nile Red and OSA starch in blue stained using Methylene Blue. Scale bar represents 10 μm	94
Figure 3.5 Elastic modulus (G' , filled symbols) and viscous modulus (G'' , empty symbols) as a function of time and temperature (full line) of 15 wt% wheat starch gel (A) and 20 wt% wheat starch gel (B) prepared using different oil fractions (0 wt%, ■; 5 wt%, ●; 10 wt%, ▲; 15 wt%, ◆; 20 wt%, ▼), at 1 Hz and 0.5 % strain. Final elastic modulus of wheat starch gels at 15 wt% (black) and 20 wt% (white) is shown as a function of oil concentration (C) measured at 25 °C, 1 Hz and 0.5 % strain, samples with symbol (†) are not significantly different ($p > 0.05$) to wheat starch gel (15 or 20 wt%) without oil droplets.....	96
Figure 3.6 Elastic modulus (G' , filled symbols) and viscous modulus (G'' , empty symbols) as a function of strain of 15 wt% wheat starch gel (A) and 20 wt% wheat starch gel (B) prepared using different oil fractions (0 wt%, ■; 5 wt%, ●; 10 wt%, ▲; 15 wt%, ◆; 20 wt%, ▼). The limiting deformation value (γ_L) of wheat starch gels at 15 wt% (black) and 20 wt% (white) is reported as a function of oil concentration (C), samples with symbol (†) are not significantly different ($p > 0.05$) to wheat starch gel (15 or 20 wt%) without oil droplets.....	98

- Figure 3.7** CLSM micrograph with superimposed droplet size distribution and d_{32} and d_{43} values of emulsion microgel particles produced at 15 wt% wheat starch + 5 wt% oil (A), 15 wt% wheat starch + 10 wt% oil (B), 20 wt% wheat starch + 10 wt% oil (C) and 20 wt% wheat starch + 15 wt% oil (D). Dotted circles highlight the emulsion microgel particles in the images. Wheat starch in green, stained with Nile Blue and oil droplets in red stained with Nile Red.**99**
- Figure 3.8** Cryo-SEM micrograph of starch emulsion microgel particles produced using 10 wt% OSA-stabilised emulsion encapsulated into 15 wt% wheat starch, scale bar represents 20 μm (A) and higher magnification image showing the external surface of the emulsion microgel particles, scale bar represents 5 μm (B). The arrows point to the individual emulsion microgel particles.**101**
- Figure 4.1** Schematic diagram of the formation of emulsion microgel particles using cold Ca^{2+} ion-induced gelation process.....**117**
- Figure 4.2** Influence of temperature (75 °C, ▲; 80 °C, ● and 85 °C, ■) on relative bound/ unbound ratio (A) and absolute bound/ unbound ratio (B) of ANS to whey protein. Solid and dashed lines indicate 12 wt% and 9.6 wt% WPI, respectively.**119**
- Figure 4.3** Mean hydrodynamic diameter (nm) of whey protein aggregates when subjected to temperature conditions (75 °C, ▲; 80 °C, ● and 85 °C, ■). Solid and dashed lines indicate 12.5 wt% and 9.6 wt% WPI, respectively.**120**
- Figure 4.4** CLSM micrograph, superimposed droplet size distribution and d_{32} , d_{43} values of 20 wt% oil-in-water emulsion stabilised by 9.6 wt% HT-WPI at 25 °C and pH 7; oil droplets stained using Nile Red. Scale bar represents 20 μm**122**
- Figure 4.5** Storage modulus (G') as a function of time (A) and strain (B) of emulsion gel with 9.6 wt% HT-WPI and 20 wt% oil prepared using different concentration of Ca^{2+} ions (0.02 M, ●; 0.1 M, ■; 1 M, ▲; 1.4M, ×) and insert of emulsion gel (■) versus protein gel (●) at 0.1 M Ca^{2+} **124**
- Figure 4.6** Micrographs of the emulsion microgel particles (9.6 wt% WPI, 20 wt% oil) produced with Leeds Jet Homogenizer (0.1 M Ca^{2+}) (A) and Buchi Encapsulator (1 M Ca^{2+}) (B) via optical microscope, 20× magnification (A1) and 1.5× magnification (B1) and CLSM (20× and 40× magnification) with the oil droplets stained in Nile Red (2) and the protein network stained in Rhodamine B (3).**128**
- Figure 4.7** Particle size distribution of emulsion microgel particles formed with Leeds jet homogeniser (A) at 0.02 M (dashed red line) and 0.1 M (full black line) and with Buchi Encapsulator (B) at 1 M (empty) and 1.4 M (full) Ca^{2+} , respectively.**129**
- Figure 4.8** CLSM micrograph of emulsion microgel particles produced with Leeds jet homogenizer encapsulating several oil droplets at 0.02 M Ca^{2+} ions (A) and single emulsion droplet encapsulation at 0.1 M Ca^{2+} ions (B), protein network stained in green and black represents oil droplets or background.**130**

Figure 4.9 Scanning electron micrograph of hexane washed emulsion microgel particle (A) and inner distribution of oil droplets within an emulsion microgel particle (B) produced using a Buchi Encapsulator at 1 M Ca^{2+}	131
Figure 5.1 (A) Cryo-SEM micrograph of the external structure and (B) internal structure of starch emulsion microgel particles (15 wt% starch – 10 wt% oil), respectively. Scale bar represents 20 and 5 μm , respectively.....	150
Figure 5.2 (A) Viscosity versus shear rate of the oil-in-water emulsion at 37 °C before and after tribological shear in the absence or presence of buffer and α -amylase; viscosity versus shear rate of the emulsion microgel particles (15 wt% starch) at different concentrations of oil at 37 °C, before and after tribological shear in the absence of buffer (B); in the presence of buffer (C) and α -amylase (D), respectively.....	152
Figure 5.3 (A) Coefficient of friction as function of entrainment speed for sunflower oil, buffer without α -amylase and OSA starch stabilized emulsion in absence or presence of buffer and/or α -amylase subjected to a normal load of 2 N and at 37 °C; (B) Particle size distribution of the OSA starch stabilised-emulsion (40 wt% oil) with and without α -amylase before and after being subjected to tribological shear.....	154
Figure 5.4 Confocal fluorescence images of the emulsion 0 s (A), 60 s (B) after the addition of α -amylase before tribological shear ($\lambda = 488$ nm, oil droplets); (C) photographs of the emulsions in the absence or presence of buffer and/or α -amylase in the tribometer.....	156
Figure 5.5 Coefficient of friction as function of entrainment speed of starch microgel particles encapsulating different oil contents measured at 2 N and 37 °C in absence of buffer and α -amylase (A and B); in presence of buffer (50:50 w/w) without α -amylase (C and D); in the presence of buffer (50:50 w/w) with α -amylase (E and F). Controls are the OSA-stabilised emulsion under the same conditions.	158
Figure 5.6 Particle size distribution of 15 wt% starch particles encapsulating different oil concentrations before or after being sheared by the tribometer in the absence (A) or presence of α -amylase (B); (C) photographs of the emulsion microgel particles after tribology in the absence or presence of buffer and/or α -amylase.	162
Figure 5.7 Confocal fluorescence images of the emulsion microgel particles 0 s (A) and 60 s (B) after the addition of α -amylase ($\lambda = 488$ nm, oil droplets and 639 nm, starch shell), scale bar represents 20 μm	163
Figure 5.8 Schematic representation of OSA starch stabilized oil-in-water emulsion in the mixed regime of a tribometer in the absence (A) or presence of buffer without (B) and with α -amylase (C).	167
Figure 5.9 Schematic representation of native starch particles in the mixed regime of a tribometer at low (A) and high (B) starch concentration in the absence or presence α -amylase (C); schematic representation of starch based emulsion microgel particles at low (D) or high (E) particle volume fraction without or with α -amylase (F).	168

Figure 6.1 Emulsion (A) and emulsion microgel particle (B) size distribution (black full line: before digestion, black dashed line: in buffer pH 3; after <i>in vitro</i> gastric digestion blue full line: 5 min, blue dashed line: 60 min, blue dotted line: 120 min) and confocal microstructure of emulsion droplets (C and D) and emulsion microgel particles (E and F) under <i>in vitro</i> gastric digestion over time (oil droplets stained in red by Nile Red and protein matrix stained in green by Rhodamine B in Figure E only whereas only oil droplets stained in red by Nile Red in Figure C, D and F).	185
Figure 6.2 Zeta-potential of 9.6 wt% WPI stabilized emulsion (A) and emulsion microgel particles (B) at pH 7 (black) and pH 3 (blue slashed) and under <i>in vitro</i> gastric digestion (blue). Error bars represent standard deviations, mean with symbol (*) are statistically different at a level of $p < 0.05$) to all other samples.....	186
Figure 6.3 SDS-PAGE pattern before and after <i>in vitro</i> gastric digestion (A) of 9.6 wt% native WPI solution (a and a'), 9.6 wt% WPI microgel particles (b and b'), 9.6 wt% interfacial WPI stabilised emulsion (c and c') and 9.6 wt% WPI emulsion microgel particles (d and d') and relative quantification (B) of intact β - (black) and α -lactalbumin (white) bands by densitometric analysis of the gel.....	187
Figure 6.4 Schematic diagram of the protective properties of emulsion microgel particles against complete <i>in vitro</i> gastric digestion by pepsin.....	190
Figure 6.5 Confocal micrograph with superimposed particle size distribution of 9.6 wt% WPI stabilized emulsion and 9.6 wt% WPI based emulsion microgel particles under intestinal and sequential gastric + intestinal static <i>in vitro</i> digestion after 30 and 180 min, scale bar represents 10 μm	193
Figure 6.6 Zeta-potential of 9.6 wt% WPI stabilized emulsion (A) and emulsion microgel particles (B) at pH 7 (black) and under intestinal <i>in-vitro</i> digestion (blue) and under <i>in-vitro</i> gastric + intestinal digestion (blue slashed), mean with symbol (*, †) are statistically different at a level of $p < 0.05$) to all other samples undergoing the same digestion conditions.	194
Figure 6.7 Free fatty acid release during <i>in vitro</i> intestinal digestion (post-gastric digestion) over time and release schematics of 9.6 wt% WPI stabilised emulsion (■) and 9.6 wt% WPI emulsion microgel particles (●) and mathematical modelling fit (grey line). Maximum free fatty acid release (Φ_{max} , %), rate constant after 60 min (k , $\mu\text{mol s}^{-1} \text{m}^{-2}$) of <i>in vitro</i> intestinal digestion of different samples in the inset table (* mean statistical different at a level of $p < 0.05$).....	196
Figure 7.1 Approach of the thesis: linking polymer and emulsifier properties to control the release of nutrient during oral or gastrointestinal processing.	204
Figure 7.2 Schematic representation of emulsion droplets (denoted by yellow circles) stabilization mechanisms as a function of the emulsifiers, OSA starch with hydrophobic OSA groups in red (left) and WPI (blue) (right) at pH 7.....	206
Figure 7.3 Schematic representation of starch-based emulsion gel with zooming in the region of interactions between OSA starch molecules and native starch molecules.	210

Figure 7.4 Schematic representation of whey protein-based emulsion gel with zoom in the region of interactions between WPI molecules and Ca^{2+} **212**

Figure 7.5 Schematic representation of the top-down and bottom-up techniques used to produce starch- or whey protein-based emulsion microgel particles, respectively..... **214**

Figure 7.6 Effect of oil content and enzyme on the friction force of 15 wt% starch emulsion microgel particles depending on the lubrication regime, sample with symbol (*) are statistically different ($p < 0.05$)..... **219**

List of Abbreviations

ANS	7.8-aniline-1-naphthalebsulfonic acid
CLSM	Confocal laser scanning microscope
DLS	Dynamic light scattering
DS	Degree of substitution
FDA	Food and Drug Administration
FFA	Free fatty acid
HT-WPI	Heat-treated whey protein
LVER	Linear viscoelastic region
O/W	Oil-in-water emulsion
OSA	Octenyl succinic anhydride
PDMS	Polydimethylsiloxane
PMMA	Poly(methyl methacrylate)
PSD	Particle size distribution
SDS-PAGE	Sodium dodecyl sulphate polyacrylamide gel electrophoresis
SEM	Scanning electron microscope
SGF	Simulated gastric fluid
SIF	Simulated intestinal fluid
WPI	Whey protein isolate
WS	Wheat starch

Nomenclature

A	Area
a_H	Hertz contact radius
a_{TP}	Contact area
C	Concentration
C_0	Initial concentration
d	Diameter
D_m	Displacement
d_{32}	Sauter mean diameter
d_{43}	De Broukere mean diameter
d_H	Hydrodynamic diameter
D	Diffusion coefficient
D_t	Turbulent diffusion coefficient
E^*	Reduced elastic modulus
E_f	Electric field
E_ε	Dissipation energy
F	Force
$f(k_a)$	Henry's function
F_d	Drag force
G^*	Complex modulus
G'	Elastic (or storage) modulus
G''	Viscous (or loss) modulus
h	Height
J	Diffusive molecular flux
k	Digestion rate constant
k_b	Boltzmann constant
K_d	Dissociation constant
LB	Concentration of ANS bound
LF	Concentration of ANS unbound
M	Molar
m	Mass
M_w	Molecular weight
n_p	Number of particles

P	Power input
P_n	Power number
q	Volumetric flow rate
Q	Amount of active molecule release
Q_c	Conversion factor
R	Radius
R_a	Surface roughness
Re	Reynolds number
T	Temperature
t	Time
$t_{1/2}$	Half-time
t_{mix}	Mixing time
U_E	Electrophoretic mobility
\bar{U}	Entrainment speed
V	Volume
v	Velocity
v_p	Velocity of particles
W	Normal load
W_L	Normal load supported by the lubricant
W_p	Normal load supported by the particles
w	Weight
w_d	Dry weight
w_w	Wet weight
γ	Shear strain
γ_T	Interfacial tension
$\dot{\gamma}$	Shear rate
δ	Indentation of the contact
$\tan \delta$	Phase angle
ε	Dielectric constant
ζ	Zeta-potential
η	Viscosity
η_k	Kinematic viscosity
ϑ	Angular variation
μ	Friction coefficient

μ_B	Friction coefficient of the continuous phase
ν	Poisson ratio
ζ	Average mesh size
ρ	Solvent density
σ	Shear stress
Φ	Amount of free fatty acids
ϕ	Volume fraction
ϕ_p	Effective fraction of particles

Chapter 1

General Introduction

1.1 Overall research aim

Lipophilic active molecules, such as fat soluble vitamins, flavourings, fatty acids and essential oils pose considerable challenges for their application in food matrices as they are water-insoluble. They tend to oxidize rapidly in the presence of air, light and heat. Additionally, due to their hydrophobic nature, most of these compounds are difficult to deliver in human physiology (the latter is largely aqueous-based) and are generally partially absorbed by the body or their biological activity is partly or fully degraded during their oral-to-gastrointestinal transit. Thus, there is a huge need to protect these lipophilic compounds without environmental degradation and tailor their release to target physiological sites, such as targeted release of flavours in the mouth or protection of omega-3 fatty acids during gastric transit and release during intestinal digestion.

A wide range of technologies have been developed to encapsulate lipid molecules, such as emulsions, emulsion gels, liposomes, micelles, nanoparticles, etc. Each of these have their own specific advantages and disadvantages in terms of protection, delivery, cost, regulatory status, ease of use, biodegradability and biocompatibility (McClements and Li, 2010).

Thesis Objective. In this thesis, the main objective was to design novel soft emulsion microgel particles of discrete size to allow the control release of the encapsulated emulsion droplets during either oral or gastrointestinal processing. Emulsion microgel particles are “smart” soft solid vehicles, where several emulsion droplets are encapsulated within a biopolymer hydrogel particle (Figure 1.1). With that in mind, different biopolymers and processing technologies were used to engineer emulsion microgel particles that can respond to internal physiological stimuli, allowing to control the delivery of the encapsulated material. The innovative aspect of this thesis is that these emulsion microgel particles were prepared using

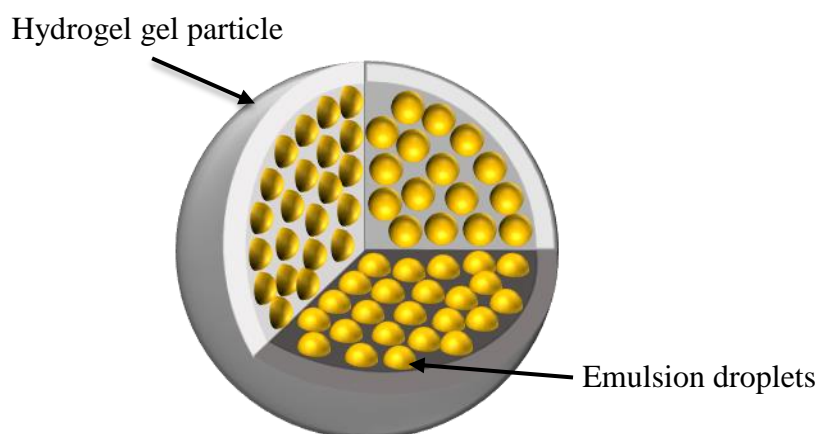


Figure 1.1 Schematic representation of an emulsion microgel particle designed in this thesis.

one biopolymer (whey protein or starch) *i.e.*, the same category of biopolymer was used as the interfacial material and as the gelling agent.

Thesis Hypothesis. The hypothesis behind this thesis was that by tuning the properties of the emulsion microgel particles, such as oil volume fraction, properties of the polymeric matrix and the interactions between the encapsulated droplets and the matrix, site-dependent release of the emulsion droplets during either *in vitro* oral or gastrointestinal regimes could be controlled.

1.2 General insight on emulsions and gels

1.2.1 Emulsions in food

Emulsions are a mixture of two or more immiscible liquids, where oil-in-water or water-in-oil emulsions can be formed such that one liquid is dispersed as small droplets (*i.e.*, the oil or dispersed phase) into a second liquid (*i.e.*, the water or continuous phase). The size of the droplets can vary between 0.1 to 100 μm (Dickinson, 1992; McClements, 2004). The immiscibility of the two liquids causes the emulsion to be thermodynamically unstable *i.e.*, the free energy of the emulsion is greater than if the two immiscible liquids remained as separate phases. Hence, emulsification only occurs under mechanical agitation via mixing or homogenization.

Over time, the formed emulsion will gradually separate back into two phases through various destabilisation mechanisms, such as flocculation, creaming, coalescence. Flocculation occurs when oil droplets are attracted to each other leading to the formation of flocs. Creaming arises from the density difference between the two immiscible liquids, resulting in the lower density liquid rising to the top of the emulsion. Coalescence is induced by irreversible collision of droplets resulting in the formation of larger droplets, so that over time the average droplet size increases until phase separation occurs (Dickinson, 1994).

Surface active compounds can be added to increase the stability of the emulsion via either electrostatic or steric stabilisation. Electrostatic stabilisation occurs when charged polar surfactants adsorbed at the droplet interface repel each other, overcoming van der Waals attractive forces. The repulsion incurred by the surfactant will prevent the droplets from colliding, aggregating and coalescing. The strength of the electrostatic repulsion will depend on pH and ionic strength. Steric stabilisation results from the formation of a steric layer at the surface of the oil droplets (with the use of amphiphilic polymers or protein) protruding into the continuous phase. As the droplets come closer together, the large polymer chains protruding from the droplets will prevent adjacent droplets to collide due to Brownian motion and van der Waals force (Dickinson, 1994; Tesch et al., 2002). In food, natural emulsifiers or stabilisers are used such as proteins and polysaccharides.

1.2.2 Biopolymer gels

It is usually recognized that gels are soft solid materials that do not flow under shear. Although under some conditions, gels have been observed to store the energy applied to them and recover their original shape upon removal of the strain. Hence, gels can also be defined as elastic materials, where the elastic modulus (G') of the gel is larger than its viscous modulus (G''). Gels are usually composed of two substances, the major constituent is usually a solvent (i.e., water for hydrogels) and the second component is a high molecular weight polymer or colloidal particle. The elasticity of the gel is caused by the entrapment of the solvent into the three-dimensional network formed by the polymer or colloidal particles (Clark, 1991).

Biopolymer gels are composed of either protein or polysaccharides. The properties of the gel will depend on the molecular characteristics of the biopolymer

such as, the number and sequence of monomers and the type of interactions occurring between the polymer chains, which will result in different types of network (i.e., associative or particulate network) (Clark, 1996). An associative network is formed through molecular random coils undergoing entanglement and physical cross-linking. Particulate gels arise from globular biopolymers, which associate via hydrophobic or electrostatic interactions into either filamentous structures or randomly branched aggregates.

Gelation can occur through several approaches. For instance, changing the temperature of a biopolymer in solution might lead to the change in the polymer conformational state leading to the association of polymer chains. The addition of ions, enzymes, alcohols, urea or a change in pH can also lead to aggregation and gelation of the biopolymer. For instance, ions might screen the electrostatic charge of a biopolymer resulting in its electrostatic attraction. Whilst enzymes can hydrolyse the biopolymer exposing the hydrophobic groups of the biopolymer resulting in its aggregation (Clark, 1991; Creusot and Gruppen, 2007). Additionally, these compounds might directly associate with the biopolymers, such as with the formation of ionic-bridges (Clark, 1991).

1.3 Rationale behind the selection of biopolymers

This thesis focused on both oral and intestinal targeted release of oil droplets, with the intent of paving the way to the development of a novel controlled delivery system for lipophilic bio-active molecules. Specific biopolymers were used to design model emulsion microgel particles depending on the biopolymer degradability and protective properties at specific environmental conditions. To target the delivery of emulsion droplets in the oral phase, emulsion microgel particles were designed from starch, as starch can be broken down by α -amylase. On the other hand, for the targeted release of emulsion droplets in the gastrointestinal regime, whey protein was used, as whey protein is not affected by α -amylase in the oral phase. These particles allowed to investigate the relationship between the physicochemical properties of biopolymers and their protective effects on the encapsulated emulsion droplets. Aspects of both biopolymers used are discussed in the following section.

1.3.1 Native starch and OSA-modified starch for starch-based microgel particles

Targeting the release and/or protection of emulsion droplet during oral processing is of great significant in the food but also pharmaceutical industry. One of the important aspects of oral processing is the palatability of the product, whilst protection of nutrients or active ingredients is also of great concern for enhanced bioavailability during intestinal digestion. During oral processing, mainly two mechanisms might trigger the breakdown of particles: oral shear and salivary digestive enzymes, such as α -amylase. The breakdown of the particles would release the encapsulated lipophilic compounds, which might lead to the degradation of the active compound, limiting the absorption of the molecule during gastrointestinal digestion (Golding and Wooster, 2010; Singh and Sarkar, 2011). It is also important to remember that during oral processing, emulsion coalescence is strongly associated with the desired lubrication properties, which might provide a creamy mouthfeel (Dickinson, 2017; de Wijk et al., 2006). Therefore, during oral processing emulsion microgel particles should be designed to protect the encapsulated emulsion droplets from destabilisation whilst retaining similar lubrication properties as conventional emulsions.

Starch is the second-most abundant natural biopolymer after cellulose and is the main carbohydrate in the human diet. During oral processing, but also whilst in the small intestine, most starches will be hydrolysed by α -amylase, although some starches show resistance (Ai et al., 2013). Therefore, it was hypothesised that starch will allow the design of particles that can alter their integrity in response to

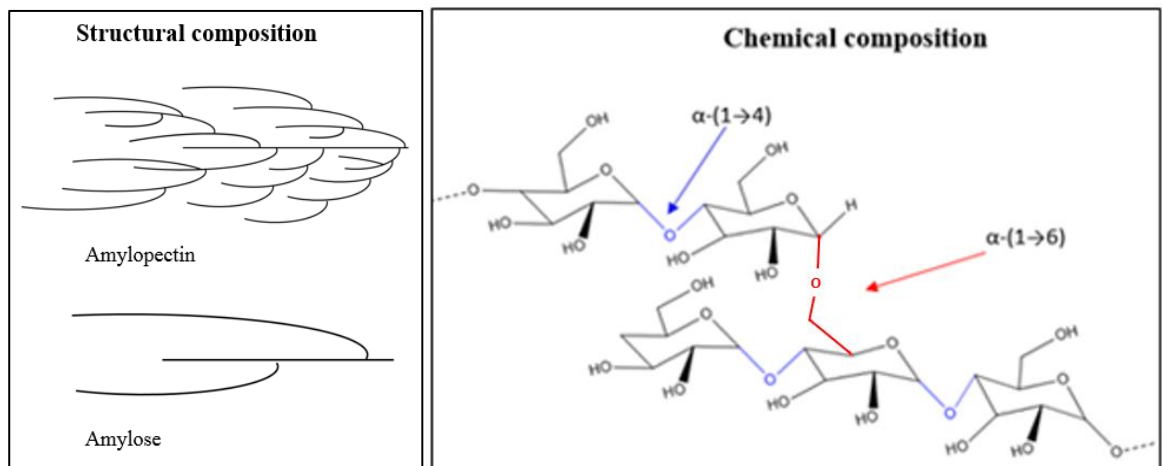


Figure 1.2 Schematic representation of the structure and chemical composition of amylopectin and amylose molecules, adapted from Sweedman et al. (2013).

specific enzymes (namely α -amylase) (Zhang et al., 2015). During oral processing, these emulsion microgel particles engineered using two starch types (native starch to form the gel matrix and modified starch to stabilize the oil droplets) should provide lubrication, whilst still protecting the emulsion droplets from complete degradation and coalescence.

Native starch is a branched polymer composed of glucose units bound together via glycosidic bonds either through linear links (α -(1 \rightarrow 4)) or branched links (α -(1 \rightarrow 6)) (Figure 1.2) (Sweedman et al., 2013). The lightly branched long glucose chains form the amylose molecules ($M_w \sim 10^6$ Da), whereas the highly branched short glucose chains form the amylopectin molecules ($M_w \sim 10^8 - 10^9$ Da). Starch mainly occurs in the form of semi-crystalline granules composed of amorphous regions surrounded by semi-crystalline growth rings alternating with amorphous growth rings (Hornung, 2018; Wang et al., 2015).

Upon heating the starch granules in the presence of water, the granules become hydrated and swell, leading to the collapse of the structured crystalline granules (Figure 1.3). As the granules swell, amylose molecules leach into the continuous phase and form an interconnected network increasing the viscosity of the system (Teyssandier et al., 2011). This process is known as the gelatinization of starch. On cooling, the amylose and amylopectin chains gradually retrograde into partly organized structures, around the remaining collapsed granules, leading to the formation of a three-dimensional gel network via hydrogen bonding (Wang et al., 2015). The composition of the starch granules, such as the amylose content will largely influence the microstructure of the gel formed. High amylose content ($\geq 20\%$) starch granules lead to strong elastic gel networks, whereas waxy starch (0% amylose) will form weak aggregates due to the limited intermolecular hydrogen bonding (Wang et al., 2015).

However, the microstructure of the starch gel can drastically change upon shearing of starch granules undergoing gelatinization (Figure 1.3). Previous studies have shown that upon shear and heat treatment, the viscosity and complex modulus of starch significantly decreased whilst the phase angle significantly increased (Svegmark, 1991; Svegmark and Hermansson, 1991). Shear treatment but also ultrasound treatment have shown to breakdown and disintegrate the starch granules allowing further amylose to leach out, but also releasing fragments of amylopectin into the continuous phase (Svegmark and Hermansson, 1991; Iida et al., 2008). The

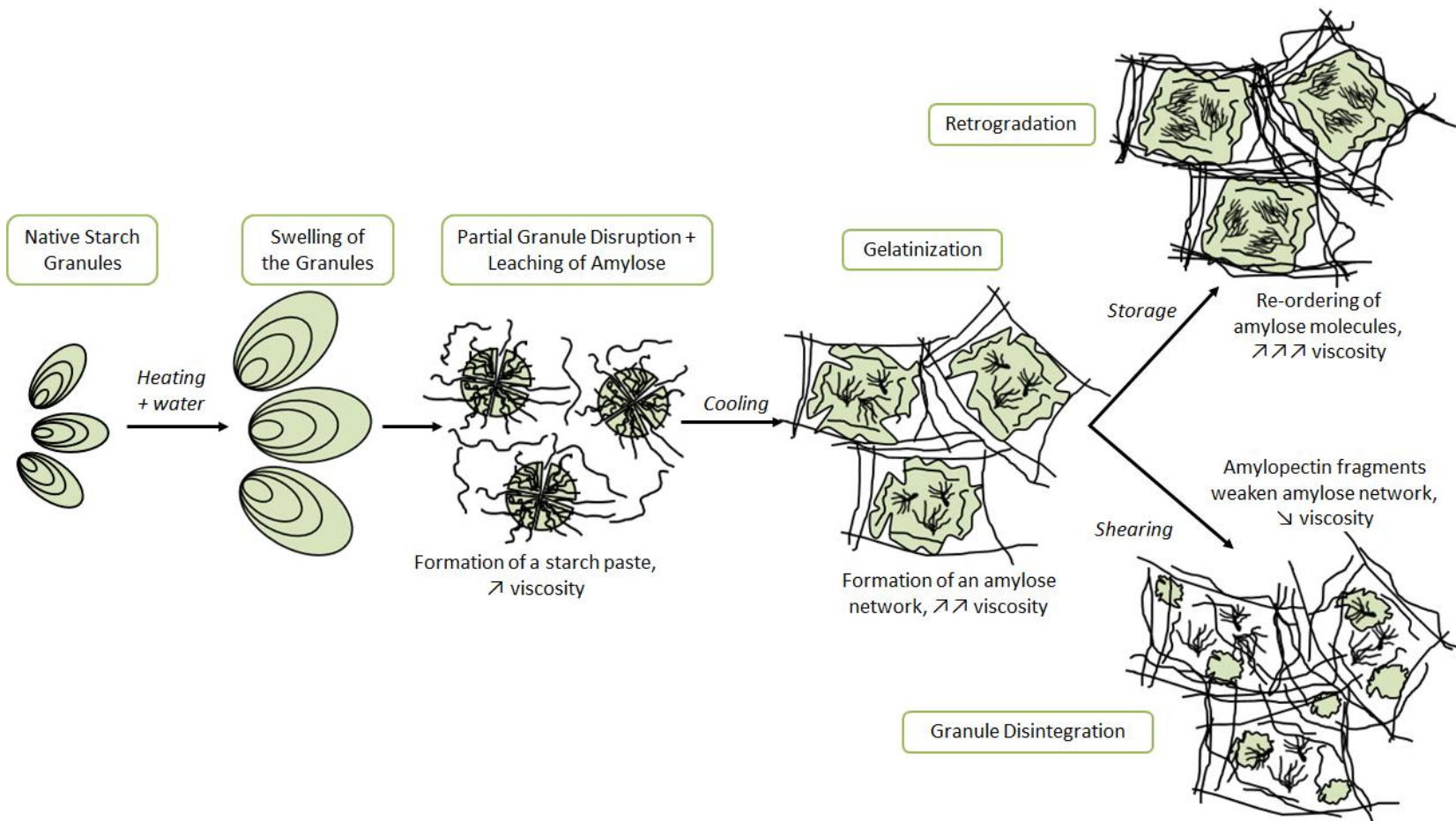


Figure 1.3 Schematic representation of the behaviour of starch granules during heating, cooling and shearing (↑: increase, ↓: decrease), adapted from Iida et al. (2008) and Wang et al. (2015).

amylopectin fragments and disintegrated granules might interfere with the amylose network, resulting in a lower cross-linked polymer.

In this thesis, native wheat starch was used to form the gel matrix due to its high amylose content (~ 20%) (Phillips and Williams, 2009). To optimize the production of emulsion microgel particles, shear treatment was performed in combination with heat treatment to produce the starch gels. The viscosity of the starch gel was of great importance to produce emulsion microgel particles via homogenization, as a highly viscous gel would obstruct the homogenizer during particle creation. Additionally, the disintegration of the granules was also important to optimize the binding between the emulsion droplets and the amylose molecules. Both aspects have been discussed in more detail in **Chapter 3** and *in vitro* oral processing is discussed in **Chapter 5**.

Native starch faces several limitations such as thermal degradation, limited water solubility and industrial applications (Sweedman et al., 2014). Hence, starch can be modified to improve its functional properties, such as attaching hydrophobic groups to the glucose units to produce an amphiphilic starch or hydrolysing starch into smaller molecules to increase its solubility in water (Bai and Shi, 2011; Sweedman et al., 2013). Esterification of native starch with octenyl succinic anhydride (OSA) is a common modification, which imparts hydrophobic properties to starch. In aqueous dispersions, under mild alkaline conditions the hydroxyl groups (-OH), mainly at C-2 and C-3 on the glucose units of the amorphous branch point of amylopectin, can be modified by adding OSA groups. Alkaline conditions are necessary to decrease hydrogen bonding between starch molecules, resulting in the swelling of the starch granules and the incorporation of the OSA molecules into the granules (Agama-Acevedo and Bello-Perez, 2017; Sweedman et al., 2013; Bai et al., 2014; Bai and Shi, 2011; Nilsson and Bergenståhl, 2006). This addition produces esters (RCOOR'), which allows the starch to become amphiphilic, with the starch backbone being hydrophilic and the OSA group being hydrophobic (though also charged) (Figure 1.4).

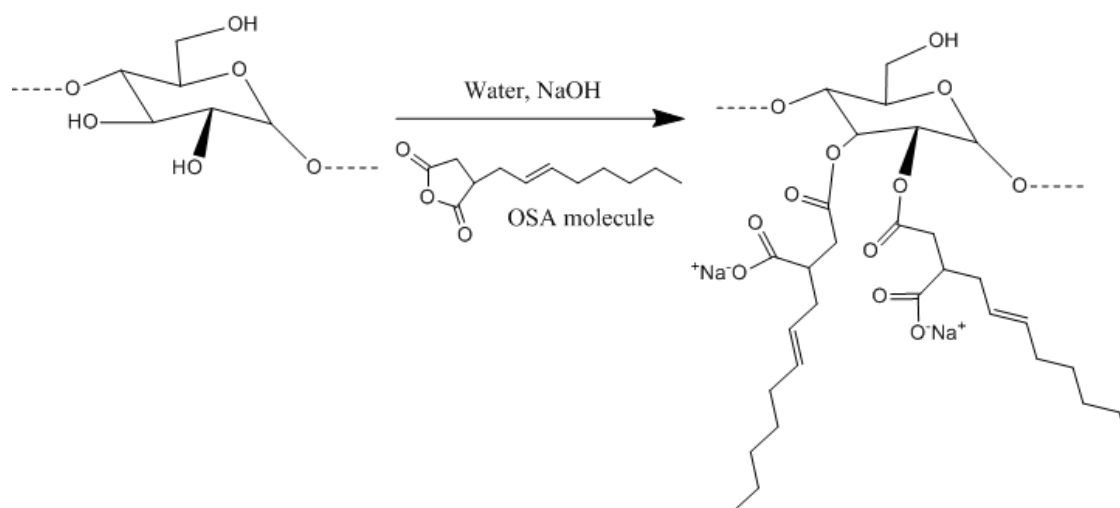


Figure 1.4 OSA-starch modification: starch glucose unit with added OSA groups, adapted from Sweedman et al. (2013).

However, it should be noted that distribution of OSA groups on the starch has been shown to be highly uneven between different types of starches but also between different granules in the same sample. The modification of the physical and functional properties of the OSA starch will depend on the degree of substitution (DS), which is the average number of OSA derivatives per glucose units. The DS can be determined through titration which has been reported to have limited reproducibility and accuracy. Another technique widely used to determine the DS is NMR (Nuclear Magnetic Resonance), which requires controlled conditions to allow both the starch and OSA groups to be visible in the same analysis (Tizzotti et al., 2011; Zhang et al., 2011).

In the food and beverage industry, OSA starch has been widely used as an emulsifier and stabiliser due to its amphiphilic properties, which allows OSA starch to adsorb to the oil-in-water (O/W) interface (Tesch et al., 2002; Dokić et al., 2012). However, the FDA established a maximum of 3% OSA treatment (DS ~ 0.02). In comparison to higher OSA treatment (e.g. 0.07 – 0.11), OSA starch at DS 0.02 was not found to significantly affect the emulsification properties of OSA starch. Several studies have hypothesised that at high DS, OSA group might not be available to interact with the hydrophobic phase due to their midsection position within the starch chain (Agama-Acevedo and Bello-Perez, 2017; Bhosale and Singhal, 2007; Liu et al., 2008; Nilsson and Bergenståhl, 2006; Sweedman et al., 2013). The emulsifying ability of OSA starch arises primarily through the hydrophobic nature of the OSA groups that are able to adsorb to the oil-water interface. Once the emulsification process is

complete, the oil droplets are protected against coalescence via steric stabilization provided by the large molecular size of OSA starch. The steric stabilisation properties of OSA starch provides several advantages over protein stabilised emulsion (via electrostatic stabilisation), such as their capacity to be independent to temperature, pH and ionic strength (Tesch et al., 2002).

1.3.2 Whey protein and cold set gelation for preparing whey protein-based emulsion microgel particles

Following the same concept as the starch-based emulsion microgel particles used for the protection of lipophilic molecules during oral processing, a second biopolymer matrix was investigated to protect bioactive molecules from gastric conditions whilst optimizing their delivery in the intestinal phase.

Globular proteins, such as whey protein, are widely known to be resistant to pepsin due to their globular structure limiting the diffusion of pepsin to the active sites (Guo et al., 1995; Macierzanka et al., 2012; Luo et al., 2017). Hence, due to the resistance of whey protein to pepsinolysis and its known emulsification and gelling properties, whey protein was chosen to design the second type of emulsion microgel particles in **Chapter 4** and its gastrointestinal protection against proteolysis and lipolysis is discussed in **Chapter 6**.

Whey protein is primarily composed of β -lactoglobulin (M_w : 18.4 kDa, pI \sim 5.2), which contains a high proportion of hydrophobic groups, two internal disulphide bridges and one free thiol, imparting the protein its globular structure. The second most prevalent protein is α -lactalbumin (M_w 14.2 kDa, pI \sim 4.8 - 5.1), which contains four disulphide bonds (Wolz and Kulozik, 2015). Two other proteins, bovine serum albumin and immunoglobulins, are also found in whey protein (Phillips and Williams, 2011).

At neutral pH, β -lactoglobulin occurs as non-covalently linked native dimers, which can separate into modified monomers with a change in pH or an increase in temperature. Above 60 °C, the dissociation of the dimers becomes irreversible and the protein undergoes conformational changes and partial unfolding, leading to the loss of its native tertiary and secondary structures, which results in a more mobile molecule (Figure 1.5) (Nicolai et al., 2011; Phillips and Williams, 2011; Khaydukova et al., 2017). The hydrophobic and sulfhydryl groups normally buried between monomers of

the native protein become exposed and interact with adjacent protein monomers, via physical (van der Waals, ionic, hydrophobic interactions) and/or chemical (S-S bonding, H-bonding) reactions (Wijayanti et al., 2014; Zúñiga et al., 2010; Phillips and Williams, 2011). Small oligomers are formed until a critical amount is exceeded, where these then arrange into monodispersed primary aggregates. Over further heating, the size of aggregates increases resulting in the formation of a gel network that entraps water by capillary forces (Nicolai et al., 2011). However, it should be noted that the importance of disulphide (S-S) bonds in the formation of a whey protein gel has recently been reinvestigated and discrepancy between results have been found. New results suggests that S-S bonding might be less important in the initial aggregation of β -lactoglobulin as originally thought, where hydrophobic interaction dominates. In contrast, S-S bonds will play a role in reinforcing the gel network over further heat-treatment (Havea et al., 2004; Havea et al., 2009; Phillips and Williams, 2011). The type and extent of aggregation reactions taking place will depend on the temperature, pH, ionic strength and protein concentration (Wijayanti et al., 2014; Iametti et al., 1995; Wolz and Kulozik, 2015). For instance, chemical reactions mainly arise at high temperature ($> 85\text{ }^{\circ}\text{C}$), high pH ($> \text{pH } 6$) and low ionic strength ($< 0.1\text{ M NaCl}$), whilst physical reactions occur at lower temperature ($< 85\text{ }^{\circ}\text{C}$), low pH ($< \text{pH } 6$) and high ionic strength ($< 1\text{ M NaCl}$) (Roefs and De Kruif, 1994; Wijayanti et al., 2014).

Heat-treated whey protein gels are extensively used in the food industry due to their improved organoleptic properties. However, the heat treatment process required to produce such gels have seen some limitations when used with heat sensitive material such as certain vitamins or flavours (Sok et al., 2005). Cold-set gelation of whey protein offers an alternative method involving either ionic (*i.e.*, sodium chloride or calcium chloride) or acidic (*i.e.*, glucono- δ -lactone) treatment of whey protein (for the purpose of this thesis, only ionic treatment-induced cold gelation will be discussed further) (Britten and Giroux, 2001; Barbut and Foegeding, 1993; Bryant and McClements, 1998; Bryant and McClements, 2000). This cold-set gelation can be achieved using two processing steps (Figure 1.5). First, preheating whey protein allows its denaturation and unfolding. Secondly, addition of ions to the cold solution of

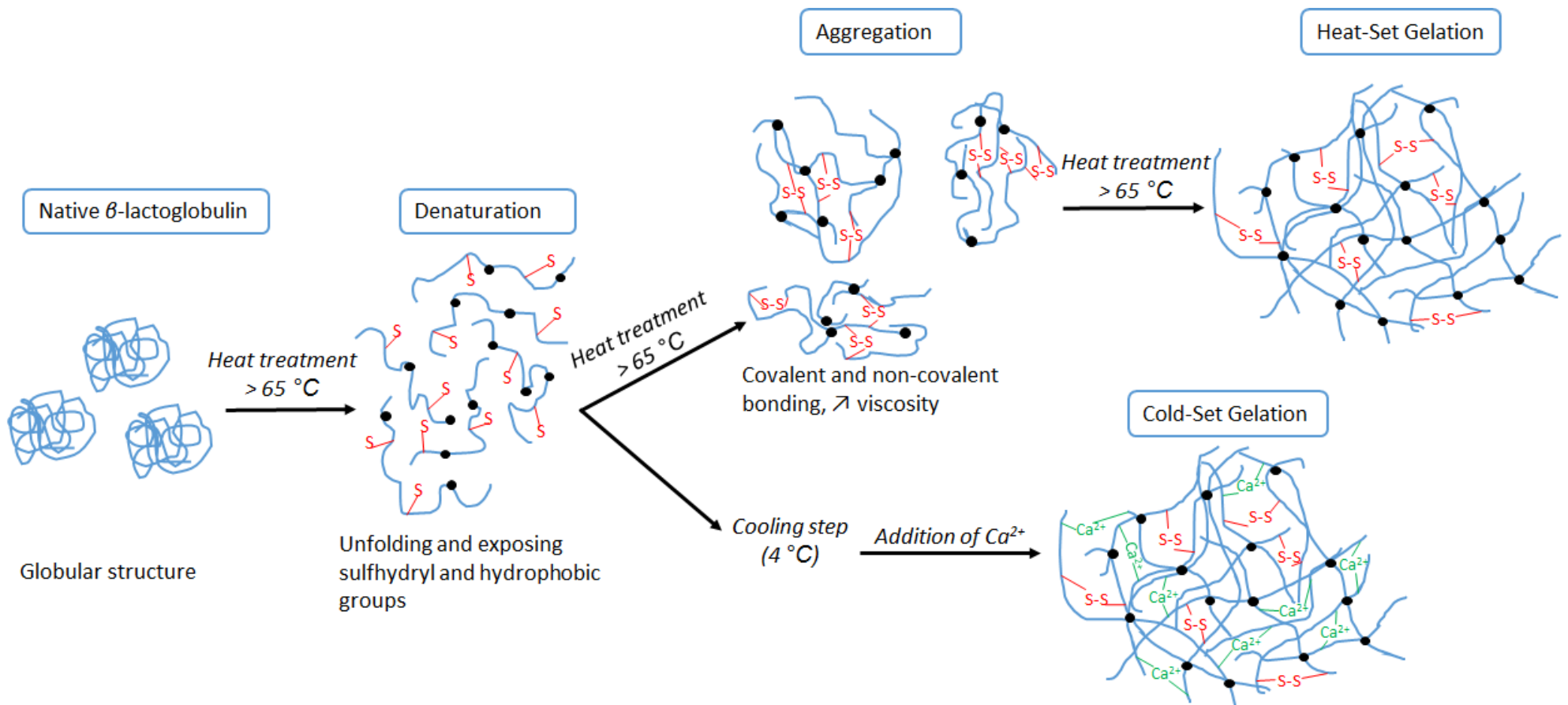


Figure 1.5 Schematic representation of heat-set versus cold-set gelation of whey protein, adapted from Ryan et al. (2013).

preheated whey protein results in spontaneous gelation due to the screening of the repulsive force of the protein as well as the formation of ionic-bridges, depending on the valency of the ions incorporated (Hongprabhas and Barbut, 1997; Hongprabhas et al., 1999; Kharlamova et al., 2018). For instance, divalent ions, such as CaCl_2 or MgCl_2 will be able to bind to the carboxyl groups of β -lactoglobulin, inducing the cross-linking of protein and promoting gelation at a lower concentration as compared to monovalent ions such as NaCl (Bryant and McClements, 2000).

The emulsification properties of whey protein have been extensively studied. Whey protein has been shown to effectively emulsify O/W emulsions due to its large amount of hydrophobic groups and globular nature. Upon adsorption to the O/W interface, β -lactoglobulin partially unfolds and rearranges its structure to form intermolecular β -sheets allowing the formation of a strong, elastic and densely packed layer interacting strongly through hydrophobic interaction and H-bonding and possibly intermolecular disulphides (Dickinson, 1998; Phillips and Williams, 2011; Amine et al., 2014). The charged nature of β -lactoglobulin results in the emulsion being mainly stabilised via electrostatic repulsion, although steric repulsion also occurs. Hence, the stability of the emulsion will largely depend on the environment conditions (*i.e.*, temperature, pH and ionic strength).

1.4 Rationale behind the selection of characterization techniques

To fully understand the different microstructures but also physicochemical and functional characteristics of both starch and whey protein emulsions, gels, emulsion gels, particles and emulsion microgel particles, several analytical instruments were employed. The theoretical and technical properties of the main characterization tools employed during this PhD are discussed below.

1.4.1 Emulsion and emulsion microgel particles characterization

Emulsions and emulsion microgel particles were characterized using different techniques to determine their size, shape, charge and stability over time.

1.4.1.1 Dynamic light scattering (DLS)

The denaturation and aggregation rate of whey protein was analysed via dynamic light scattering to identify an optimized temperature and time at which the protein would unfold allowing spontaneous gelation when in contact with calcium ions (Ca^{2+}). In solution, particles such as aggregated protein, undergo Brownian motion, which is commonly used as a method to examine particle size, since smaller particles will have a faster Brownian motion than larger ones. Although, it should be noted that temperature affects the Brownian motion of particles – at high temperature particles move faster. DLS is a common method to measure the size of particles below the submicron region (*i.e.*, between 1 nm to $1\mu\text{m}$), illuminated via a laser beam. The size of the particles affects the fluctuation rate of the scattered light intensity (Nobmann et al., 2007). For instance, a fast fluctuation rate is obtained from small particles that have rapid Brownian motion. The hydrodynamic diameter of the particle (d_H) is then calculated using the Stokes-Einstein equation (1.1), which defines the velocity of the Brownian motion as the translational diffusion coefficient (D):

$$d_H = \frac{k_b T}{3\pi\eta D} \quad (1.1)$$

where k_b is the Boltzmann constant, T is the temperature and η is the viscosity of the medium. It should be noted that the translational diffusion coefficient and hence d_H also depends on any surface structures, such as adsorbed polymer layers, and ions in the media. The particle size distribution can be calculated by the autocorrelation function of the instrument's software and then fitted to obtain the average particle diameter, the z-average, defined as the intensity-weighted mean diameter (Malvern Instruments Ltd, 2005).

1.4.1.2 Zeta-potential

A key characteristic of emulsions and particles is their surface charge, which allows to examine their electrostatic stability and response to changes with pH and ionic strength. In this thesis, the ζ -potential of the different emulsions and emulsion microgel particles was analysed at constant environmental conditions as well as, during oral or gastrointestinal *in vitro* conditions.

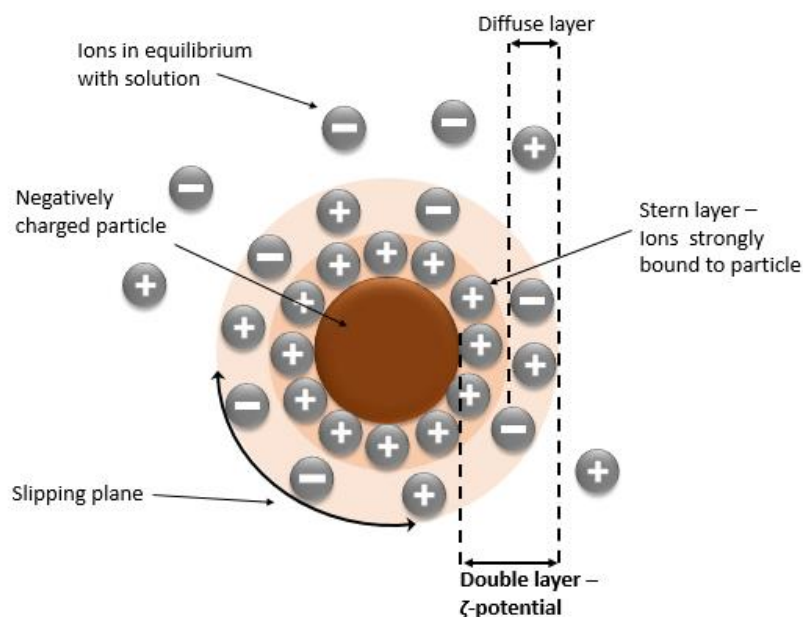


Figure 1.6 Schematic representation of a negatively charged particle and the presence of its ions at the “Slipping plane”, “Double layer” and “Diffuse layer”, figure from Malvern Instruments Ltd (2011).

Figure 1.6 illustrates the double layer model of a negatively charged particle that describes the surface charge of particles resulting in their electrostatic repulsion. In solution, some counter-ions (in this case positive ions) are strongly attracted to the negatively charged particle, forming the “Stern layer”. Further away from the particle, counter-ions are less strongly associated to the particle and form the “Diffuse layer”. The “Stern layer” and “Diffuse layer” form the “Double layer”, where a boundary region between the layer of immobile liquid and associated ions forms the “Slipping plane”. The ζ -potential measures the electrostatic potential at the “Slipping plane”, which indicates the potential stability of an emulsion. For instance, emulsion droplets with a large positive or negative ζ -potential ($> +$ or $- 30$ mV) will repel each other via electrostatic repulsion, limiting flocculation and coalescence. However, a change in pH or ionic strength will affect the ζ -potential and potentially destabilise the emulsion (Malvern Instruments Ltd, 2011).

The electrostatic potential of particles or emulsion droplets is measured via electrophoresis. The sample is injected into a capillary cell comprised of two oppositely charged electrodes, of distance 6 cm. Under an applied electric field ($50 < E_f < 150$ V), particles in equilibrium with the dispersion media move (at a constant velocity) towards the oppositely charge electrode. The velocity of the particles (v_p) is referred to their electrophoretic mobility ($U_E = v_p / E_f$) and is dependent on the

strength of the electric field (E_f), the dielectric constant (ϵ), the viscosity (η) of the medium (*i.e.*, water, $\eta = 8.9 \cdot 10^{-4}$ Pa s, at 20 °C) and the ζ -potential of the particles. The strength of an electric field can be calculated from equation 1.2:

$$E_f = \frac{\text{Voltage applied}}{\text{Distance between electrodes}} \quad (1.2)$$

Hence, at a voltage of 150 V the electric field is calculated to be around 25 V cm⁻¹.

From Henry's equation (1.3), the ζ -potential can be related to the electrophoretic mobility of the particles:

$$U_E = \frac{2\epsilon\zeta f(k_a)}{3\eta} \quad (1.3)$$

where $f(k_a)$ is the Henry's function which refers to the ratio of the particle radius (a) to the electrical double layer thickness (k). Based on the Smoluchowski approximation, in aqueous polar media $f(k_a) = 1.5$. However, the Smoluchowski approximation is only valid if the thickness of the double layer is smaller than the mean particle radius (*i.e.*, thin double layer). For particles in a non-polar media with a thick double layer, the Hückel approximation should be used instead where $f(k_a) = 1$.

1.4.1.3 Laser Diffraction particle size measurements

Another technique to measure particle size is via laser diffraction, which is based on the angular variation (ϑ) in the intensity of the scattered light as the laser beam passes through a dispersed sample. This technique is most accurate for a particles ranging between 100 nm to 1 mm. As described in Figure 1.7, large particles scatter light at a small angle whereas, small particles scatter light at a larger angle. The angular scattering intensity pattern is then converted into a particle size distribution using the "Mie Theory", assuming that the particles are dispersed (to avoid multiple scattering effects), homogeneous spheres and knowing the refractive index of both the particles and dispersion medium.

The measured particle size can be expressed as d_{32} which is the Sauter mean diameter or d_{43} which is the De Broukere mean diameter. The d_{32} refers to the surface area mean and is most sensitive to the presence of fine particles, whereas, the d_{43}

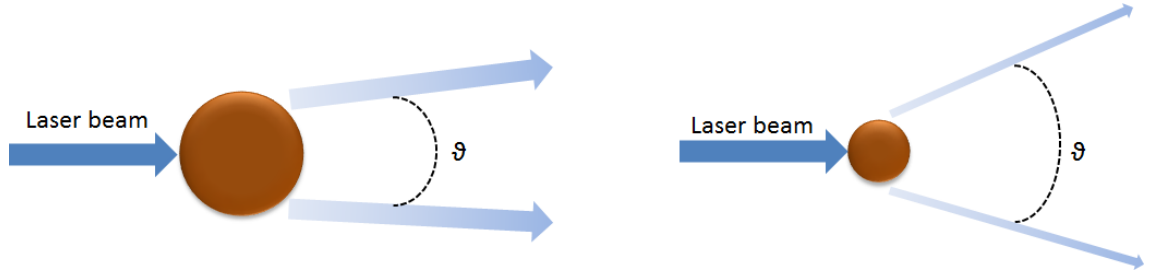


Figure 1.7 Schematic representation of light scattered from small and large particles.

refers to the volume of the particle and most sensitive to large particles (McClements, 2015; Malvern Instruments Ltd, 2015).

These two means can be calculated from equation 1.4 and 1.5, respectively:

$$d_{32} = \frac{\sum n_{pi} A_i d_i}{\sum n_{pi} A_i} \quad (1.4)$$

$$d_{43} = \frac{\sum n_{pi} V_i d_i}{\sum n_{pi} V_i} \quad (1.5)$$

where n_{pi} is the number of particles, A_i is the particle surface area, V_i is the particle volume, d_i is the diameter of the particles.

1.4.1.4 Microscopy across length scales

The morphology and surface of emulsion droplets and emulsion microgel particles were studied using different types of microscopy (*i.e.*, optical, confocal and electron microscope) relying on different physical principles.

The most basic microscopy method is the optical microscope which uses reflected light to image the surface of a sample. This microscope consist of a light source, several lenses and an eye piece or digital camera (Figure 1.8). The wide-field illumination employed by the optical microscope leads to the uniform illumination of the focus plane but also of the plane above and below the focus plane. Therefore, only thin and relatively transparent samples can be imaged (Auty, 2013). The resolution of an optical microscope is governed by the wavelength of the light source (which can be as low as 200 nm) and the objective. However, due to the design and manufacturing of certain microscope as well as the Brownian motion of small particles, objects smaller than 1 μm are hardly detectable. Another limitation of the

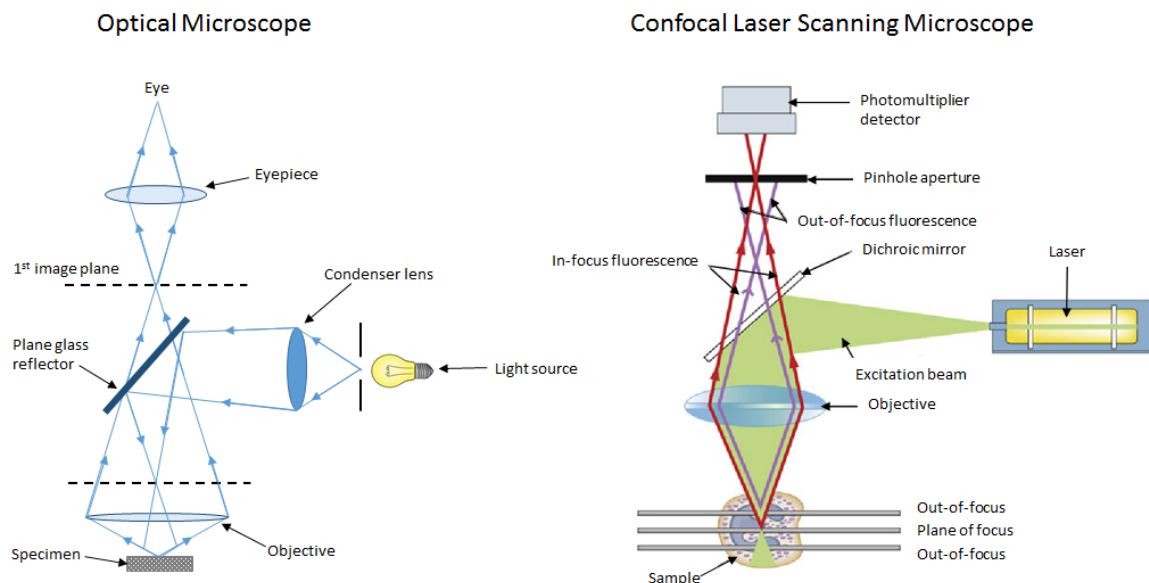


Figure 1.8 Schematic representation of the differences between optical microscopy and confocal laser scanning microscopy, adapted from Hardham (2012) and Microscopegenius.com

optical microscope is the limited contrast between different components in a sample due to their similar refractive indices (McClements, 2015). Therefore, other types of microscope have been developed to overcome these limitations, such as the confocal laser scanning microscope (CLSM), which can be used as a fluorescence technique that can analyse both two-dimensional and three-dimensional images.

The principle behind CLSM is highlighted in Figure 1.8. This microscope allows the illumination of the whole sample by scanning one or more laser beams. The photomultiplier detector (PMT) then detects the emitted light from the focal plane and transforms the light signal into live data images using a computer software. A pinhole apparatus is used to eliminate out-of-focus light from the areas below and above the in-focus plane (Auty, 2013). The use of fluorescent dyes to stain different components in a sample such as proteins and fats also allows to easily analyse the morphology and microstructure of a sample. The incident light can be absorbed by fluorophores incorporated to the sample and emitted at different wavelengths. The dichroic mirror then deflects the signal onto the PMT. The dyes can be covalently or non-covalently bound to the sample. In this thesis, Rhodamine B was used to stain starch particles via non-covalent interactions (hydrogen bonding), Nile Blue stained whey protein particles through electrostatic interactions and Nile Red stained oil

droplets via hydrophobic interactions (Auty, 2013). Nevertheless, similarly to optical microscope the maximum resolution obtained with CLSM is around 200 nm.

Electron microscopy is a good alternative to characterize smaller samples (< 200 nm), which uses electron beams rather than light beams. A series of magnetic fields are used to direct the electron beams instead of optical lenses. A scanning electron microscopy (SEM) allows to visualize features as small as 3 – 20 nm (McClements, 2015). In this thesis only SEM was used to visualise the topography of whey protein or starch emulsion microgel particles. In SEM, an electron beam is focused on the surface of a specimen, some energy is absorbed by the sample and generates secondary electrons, which upon leaving the sample are recorded by a detector and imaged with a software. For non-conductive materials, samples need to be sputter coated with a conductive metal, such as platinum or gold, to enhance the intensity signal of the secondary electron generated by the bombardment of electron. Additionally, the samples need to be placed under high vacuum since electrons can be easily scattered by gas molecules resulting in poor image quality. The main disadvantage of the high vacuum is the need to remove the aqueous phase to avoid any interferences. Hence, extensive drying or evaporation of the sample is required which might disrupt its structure, shape and size causing artefacts (McClements, 2015). Cryo-SEM can overcome the need to extensively dry aqueous samples. Here, samples are cryogenically treated by rapidly freezing the sample with liquid nitrogen, for example to replace water with amorphous ice crystals. The sample is then sublimated and coated with a conductive metal to be imaged in a similar manner than with a conventional SEM (JEOL Ltd, 2011).

1.4.2 Rheology

Rheology, from its Greek word “rheos” meaning “flowing”, is the study of flow and deformation of liquid, semi-solid or solid matter subjected to a normal and tangential stress. Liquid materials are often characterized via shear viscosity, which investigates the flow behaviour of the liquid by measuring the materials resistance to flow when a shear stress is applied. In comparison, the rheological behaviour of semi-solid materials are commonly characterized via dynamic oscillatory rheology, which examines the elastic modulus and fracture properties of the material. The elastic or storage modulus (G') of a semi-solid material is a measure of the deformation energy

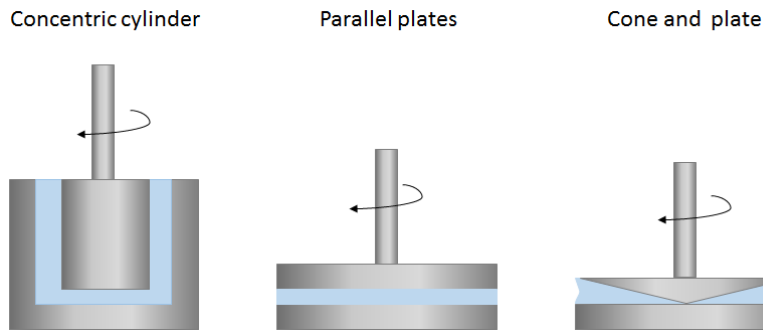


Figure 1.9 Schematic representation of commonly used geometries in rheology with the sample in blue.

stored by the material during the shearing process. The fracture properties of a semi-solid material refers to the tendency of the material to break under stress. For a semi-solid material to fracture, the applied stress has to be greater than the fracture stress (stress required to cause fracture) of the material (McClements, 2015).

The rheological characterization of different samples can be achieved using different three types of geometries, where the concentric cylinder (*i.e.*, cup and bob), the parallel plates, and the cone and plate are the most commonly used (Figure 1.9). In this thesis, a cone and plate geometry was used, where the cone has a slight angle ($\sim 4^\circ$), which resulted in a uniform shear stress across the sample (as compared to the parallel plates geometry) (Gunasekaran, 2002).

Upon rheological deformation of a material, shear stress (σ), shear strain (γ) and shear rate ($\dot{\gamma}$) are three parameters used to describe deformation. Shear stress is defined as the amount of force (F) per unit area (A) and shear strain is the displacement of the material due to stress, whilst shear rate is the rate at which shear progresses (Mezger, 2014). Figure 1.10 demonstrates the relationship between shear,

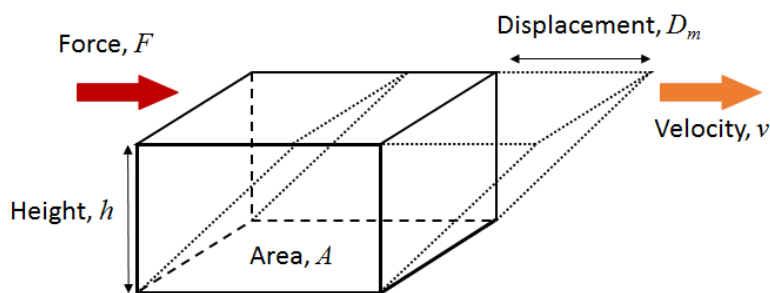


Figure 1.10 Relationship between the force and velocity of an applied stress on the displacement of a material, adapted from Mezger (2014).

stress, shear strain and shear rate, which can be obtain from equation 1.6, 1.7 and 1.8, respectively:

$$\sigma = \frac{F}{A} \quad (1.6)$$

$$\gamma = \frac{D_m}{h} \quad (1.7)$$

$$\dot{\gamma} = \frac{v}{h} \quad (1.8)$$

where D_m is the displacement, h is the height and v is the velocity, obtained from: $v = \frac{D_m}{t}$ with t representing time.

In this thesis (**Chapters 3 and 4**), dynamic oscillatory rheological studies were carried out to understand and optimize the properties (*i.e.*, gelation kinetics, strength and fracture properties) of the whey protein and starch gels and emulsion gels as a function of biopolymer concentration and oil content. The shear viscosity (via rotational rheology) of the subsequently formed emulsion microgel particles was also of great interest to examine their lubrication properties and delivery mechanism during oral processing. The principles and implications of the different measurements conducted throughout this thesis are discussed below.

1.4.2.1 Viscoelastic behaviour of gels and emulsion gels – Oscillatory rheology

Semi-solid materials such as gels are usually characterized in terms of their viscoelastic properties, *i.e.*, complex shear modulus G^* , which is determined by equation 1.9:

$$G^* = \frac{\sigma}{\gamma} \quad (1.9)$$

The principle behind this measurement is to apply a constant sinusoidal stress to the semi-solid material and measure its resulting strain as a function of amplitude stress, frequency, temperature or time (Figure 1.11). Upon shearing, the semi-solid material will store and lose the deformation energy, described by the storage modulus (G'), which represents the elastic behaviour of the material, and the loss modulus (G''), representing the viscous behaviour of the sample. Another description of this measurement is the phase angle (δ), defined as the lag angle between the applied shear

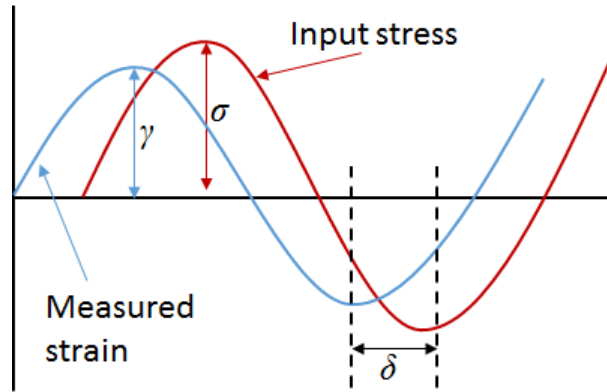


Figure 1.11 Schematic representation of the oscillatory rheology of a viscoelastic material, showing the sinusoidal stress input (σ), the sinusoidal resulting strain (γ) and the phase shift angle (δ) occurring between the input stress and measured strain response, adapted from Mezger (2014).

and the strain response of the material, which describes the damping ability of a semi-solid material (*i.e.*, how the applied shear oscillation decays due to viscous dissipation). The phase angle is the ratio between the viscous and elastic modulus, equation 1.10:

$$\tan \delta = \frac{G''}{G'} \quad (1.10)$$

When the elastic modulus dominates, $\tan \delta < 1$, whereas when the viscous modulus dominates, $\tan \delta > 1$. It should be noted, that if $G' = G''$, $\tan \delta = 1$ which indicates the sol/gel transition point (Mezger, 2014).

In this thesis three oscillatory measurements were conducted on the different whey protein and starch based gels and emulsion gels: an amplitude sweep, a frequency sweep and a time/temperature sweep.

An amplitude sweep test is performed at variable amplitude shear strain, while keeping the temperature and frequency constant. This test allows to understand the linear viscoelastic region (LVER) of a sample as well as determining the limiting value ($\dot{\gamma}_L$) of the LVER (which usually represents the limit at which the material irreversibly starts to break down). All further measurements (*e.g.*, frequency sweep, time sweep) should be performed in the LVER (Mezger, 2014).

A frequency sweep test is performed at variable frequency and constant shear and temperature. This test allows one to examine the time-dependent deformation

behaviour, with high frequency simulating rapid motion/short-term behaviour and low frequency simulating slow motion/long-term behaviour. A frequency sweep also allows one to understand the degree of cross-linking in a polymer gel. A highly cross-linked polymer will exhibit constant rigidity, which will be highlighted by an almost constant elastic and viscous modulus over frequency, with $G' \gg G''$ and G' being almost parallel to G'' . In comparison, a gel with a lower degree of cross-linking will show more flexibility, with G' increasing until reaching a plateau and G'' also increasing until reaching a maximum and dropping. Additionally, the values of G' and G'' will be closer to each other (Mezger, 2014).

A time and temperature sweep is conducted at constant shear and frequency, temperature can be varied or kept constant. This test is used to understand the gelation kinetics or hardening behaviour of a sample over time (with or without the use of a temperature ramp). In the event of hardening or gelation G' will increase, highlighting the increase in structural strength of the sample. The increase in G' can be caused by an increased number of molecular entanglements or an increase in the number of cross-links via hydrogen bonding, or hydrophobic interactions, etc. Before the formation of a gel or a network $G' < G''$ emphasizing the liquid behaviour of the sample. Over time $G' = G''$, highlighting the sol/gel transition point. Further on the experiment time, $G' > G''$ showing the solid like behaviour of the formed gel (Mezger, 2014).

1.4.2.2 Flow behaviour and viscosity of emulsion microgel particles – Rotational rheology

The flow behaviour of liquids, such as colloidal dispersions, is commonly characterized via viscosity measurements, where shearing induces the sample to flow due to the rearrangement and deformation of the sample's structure. The viscosity is defined as the flow resistance given by a flowing sample. Depending on the flowing behaviour of samples, these can be classed as Newtonian or non-Newtonian fluids. For ideal Newtonian fluids, viscosity (η) is defined as the ratio between shear stress (σ) and shear rate ($\dot{\gamma}$), equation 1.11:

$$\eta = \frac{\sigma}{\dot{\gamma}} \quad (1.11)$$

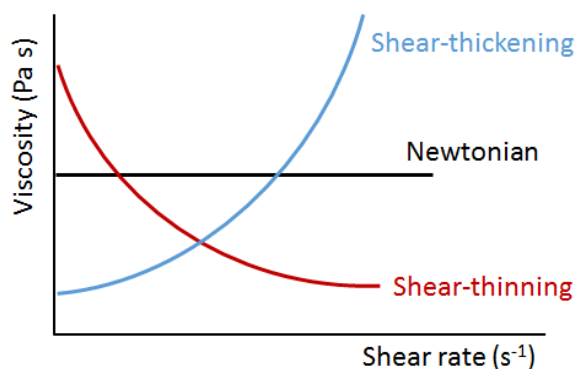


Figure 1.12 Comparison of viscosity functions of Newtonian and non-Newtonian fluids.

Hence, the viscosity of the sample is independent to the shear rate at a specific temperature (Figure 1.12). Typically, Newtonian fluids are composed of low molecular weight molecules, such as water, sugar solutions (*e.g.*, corn syrup) and milk. Samples with higher molecular weight molecules will show non-Newtonian behaviour, where the viscosity of the sample depends on the shear rate.

The behaviour of non-Newtonian fluids can be classed as shear-thinning (pseudoplastic behaviour) or shear-thickening (dilatant behaviour) (Figure 1.12). Shear-thinning samples are commonly found in food such as polymer dispersion (*i.e.*, ketchup, whipped cream, salad dressing). Under shear, the polymers deform and rearrange in the direction of the flow, leading to a decrease in viscosity with increasing shear rate. Shear-thickening samples are less commonly found in food, although starch granule dispersions (*e.g.*, corn starch) are one example. In this case, the viscosity of the sample increases with increasing shear rate due to the flocculation or compression of the dispersed particles (Mezger, 2014).

In this thesis, the viscosity of the different microgel particles and emulsion microgel particles in dispersion were studied to understand how the particles behaved under shear rate as a function of particle strength (via biopolymer concentrations), oil content and particle volume fraction.

1.4.3 *In vitro* oral processing

In order to understand the mechanical properties of emulsion microgel particles undergoing bio-mechanical shear (oral shear), in **Chapter 5**, a suitable methodology was required. Food oral processing has been demonstrated to be

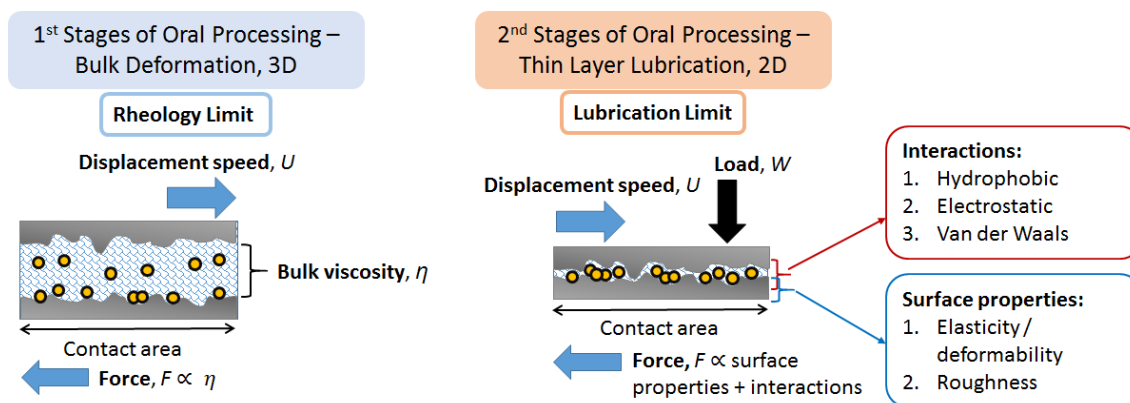


Figure 1.13 Oral processing: from bulk rheology to thin layer lubrication.

essentially a destructive process, where food is deformed and broken down into smaller particles and mixed with saliva. Most studies on oral processing have mainly focused on bulk rheological (via viscosity measurements) and mechanical response (via compression tests) of the food during the initial mastication occurring between the teeth (Prakash, 2017). However, through continuous mastication, food breaks down and changes in microstructure and moisture content due to shearing forces occurring between the tongue, palate and teeth and the incorporation of saliva, respectively. Therefore, bulk rheology becomes less dominant whereas thin film properties become important as these take into account the surface friction and lubrication occurring in between the tongue and palate in relative motion (Figure 1.13) (Chen and Stokes, 2012; Chen and Engelen, 2012).

In this thesis, the tribological properties (*i.e.*, friction and lubrication properties) of the emulsion microgel particles in the absence or presence of artificial saliva was studied for a better understanding of their controlled release mechanism.

1.4.3.1 Tribology

Tribology, from its Greek word “tribos” meaning “rubbing” or “sliding” is the study of friction, wear and lubrication of interacting surfaces in relative motion (Figure 1.14). It was first developed to study and improve the friction and wear of industrial engines undergoing extreme mechanical shear. Under these conditions, stainless steel tribo-pairs (*i.e.*, ball and disc) were used to study the lubrication properties of different lubricants to minimize wear.

Recently, tribology has gained great interest in the area of food oral processing due to the possibility of measuring the interactions between the oral surfaces (*i.e.*, tongue and palate), saliva and food or beverages occurring after

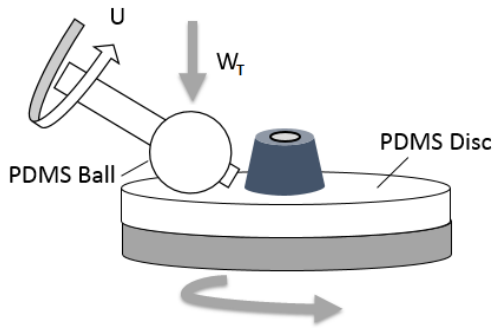


Figure 1.14 Schematic representation of a tribometer set-up.

mastication. These interactions give rise to oral lubrication properties and allow textural properties based on rubbing and squeezing, such as creaminess and smoothness (linked to the presence of lipids), to be analysed (Stokes, 2012). However, tribometers have to be adapted to better mimic oral conditions. For instance, lower load and speed are used due to the low pressure and speed exerted between the tongue and palate during oral processing and swallowing (Kennedy et al., 2010). Additionally, soft contacting surfaces were designed from silicone elastomer (*i.e.*, PDMS), which have closer elasticity (3 MPa) and roughness (~ 50 nm), to human oral cavity as compared to the original smooth stainless steel tribo-pairs.

Tribology measurements determines the friction (*i.e.*, the resistance) between two interacting surfaces in motion (Figure 1.14), expressed as a constant, the friction coefficient (μ) which is calculated from the measured friction force (F) and the normal load (W), equation 1.12:

$$\mu = \frac{F}{W} \quad (1.12)$$

In dry conditions, the friction coefficient depends only on the properties of the contacting surfaces, such as hydrophobicity, adhesion, roughness and deformability. The incorporation of a fluid will significantly affect the friction coefficient, depending on the properties of the lubricating fluid (*i.e.*, flow behaviour), the interactions between the fluid and the surfaces (*i.e.*, hydrophobic, electrostatic or van der Waals) and the rolling-sliding motion of the surfaces (*i.e.*, entrainment speed, \bar{U}) (Figure 1.14). The rolling-sliding speed will influence the entrainment of the fluid, causing the separation of the surfaces due to a thick fluid layer or preventing the surfaces from contacting each other due to a thin fluid layer.

In general, the friction behaviour of fluid lubricants is presented as a Stribeck curve, which plots the friction coefficient as a function of the lubrication parameters, although the friction coefficient can also be plotted as a function of entrainment speed alone (Figure 1.15). The lubrication parameters are defined as the Hersey number which takes into account the dynamic viscosity of the fluid (η), the entrainment speed (\bar{U}) and the normal load (W), equation 1.13:

$$\text{Hersey number} = \frac{\eta \bar{U}}{W} \quad (1.13)$$

Based on the progression of the Stribeck curve, three different lubrication regimes can be observed as a function of entrainment speed: the boundary, mixed and hydrodynamic regime (Figure 1.15). At low entrainment speed (and with a fluid of low viscosity or a high load), the fluid is not entrained in between the contacting surfaces, resulting in a high friction coefficient. This condition is known as the “boundary regime”. In this regime, the properties of the contacting surfaces, such as their roughness, will dominate the friction behaviour. For instance, rough surfaces will lead to higher friction due to the asperities of the two surfaces interacting and possibly locking-up. As the entrainment speed increases, the fluid enters the contacting surfaces and forms a thin layer capable of supporting some of the load,

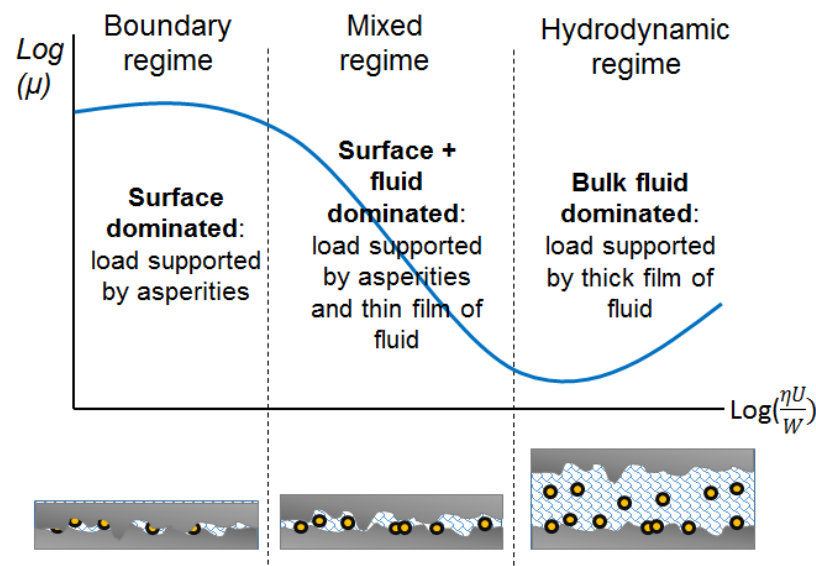


Figure 1.15 Typical Stribeck curve as a function of the Hersey number, adapted from de Vicente et al. (2006) and Stokes (2012).

resulting in the decrease of the friction coefficient, known as the “mixed regime”. In this case, the thin film of fluid separates the two surfaces so that only large asperities from the surfaces are in contact. Hence, the properties of both the fluid and the surfaces but also the interactions between the fluid and surfaces are of great importance in the determination of the friction coefficient. For instance, a fluid which highly interacts with the surfaces will more easily be entrained in between the surface resulting in a larger decrease of the friction coefficient. As the entrainment speed increases further, the fluid layer increases resulting in further separation of the surfaces and the friction coefficient decreases further, until the “hydrodynamic regime” is reached. At this point, a thick film of fluid totally separates the surfaces by sustaining the applied load. Here, the bulk properties (*i.e.*, viscosity) of the fluid dominate the friction behaviour of the fluid (Sarkar et al., 2017; Stokes et al., 2013). However, the friction coefficient increases back due to the fluid drag force (F_d), which is define as equation (1.14):

$$F_d = 6\pi R\eta\bar{U} \quad (1.14)$$

where R , is the radius of the particles found in a fluid, η is the viscosity of the fluid and \bar{U} is the entrainment speed. Hence, for the entrainment speed to increase further, the friction force of the entire fluid has to increase, resulting in the increase of the friction coefficient.

In this thesis, to fully understand the behaviour of emulsion microgel particles during simulated oral processing, both bulk rheology and thin film tribology were measured. The bulk rheology of the emulsion microgel particles was analysed through the viscosity of the samples since viscosity is highly relevant to understand the lubrication behaviour of the samples during the mixed regime. It was also of interest to understand the viscosity changes towards the breakdown of the particles, hence the viscosity of each samples was also measured before and after tribological shear. Therefore, the understanding of both viscosity and lubrication behaviours of the different samples would allow to understand the breakdown properties and release mechanism of the emulsion microgel particles, which would have not been possible by simply looking at bulk rheology.

1.4.3.2 Artificial saliva: the role of α -amylase

The systematic presence of saliva in the oral cavity plays a crucial role during oral processing to wet and lubricate food systems. Saliva has the ability to absorb onto different substrates (*i.e.*, teeth, tongue), interact with food systems and lubricate and protect the oral surfaces (Carpenter, 2012). Saliva is composed of 99% water, the other 1% is composed of several electrolytes (*i.e.*, sodium, potassium, calcium, magnesium, bicarbonate, and phosphates), immunoglobulins, enzymes (*i.e.*, α -amylase), mucins and nitrogenous compounds (*i.e.*, urea and ammonia) (Minekus et al., 2014). The presence of large glycoproteins such as mucins provide saliva with a non-Newtonian shear thinning viscosity, resulting in the lubricating behaviour of saliva (Mosca and Chen, 2017).

During food oral processing, food interacts with components of saliva, which destabilises food products through different processes depending on the food structure. In this work, the focus was put on the enzymatic degradation of starch-based systems via the main digestive enzyme in saliva, α -amylase. Salivary α -amylase initiates starch hydrolysis at the α -(1 \rightarrow 4) glycosidic bonds by exerting a torsion to the glucose unit at the catalytic site (α -(1 \rightarrow 4)) (French, 1981; Reilly, 2007). The activity of salivary α -amylase is at its optimum at pH 6.8 (and 37 °C) whilst in acidic conditions (*i.e.*, gastric conditions) the enzyme is inactivated. This enzymatic breakdown has shown to reduce the viscosity of starchy products in a time scale relevant to food oral processing (*i.e.*, semi-solid food have a residence time between 5 to 30 s (Chen and Engelen, 2012; Minekus et al., 2014)).

In this thesis, *in vitro* oral processing was studied to understand the breakdown and controlled release of starch-based emulsion microgel particles triggered by both oral shear and oral enzymes (α -amylase). Hence, artificial saliva was produced following the standardized static *in vitro* digestion protocol (Minekus et al., 2014).

1.4.4 *In vitro* gastrointestinal processing

In order to understand the controlled release mechanisms of the whey protein-based emulsion microgel particles, their degradation was analysed via *in vitro* gastrointestinal digestion. Several *in vitro* gastrointestinal digestion models have been developed to study the biological fate of food and pharmaceuticals, although *in*

vivo analysis of the gastrointestinal digestion of food is still considered as reference (Minekus et al., 2014). However, the large cost of equipment and labour, but also ethical constraints, inter-individual variation, lack of standardized methods and limited experimental design, results in the highly limited use of *in vivo* methods (Alegría et al., 2015). In comparison, *in vitro* models require less labour, are more rapid (due to easier sampling methods and higher reproducibility rates) and do not have ethical constraints. Recent studies have shown correlation between the extent of milk proteolysis obtained from *in vivo* data using pigs and static *in vitro* digestion methods (Egger et al., 2017). Therefore, *in vitro* digestion models are deemed suitable to examine the influence of digestion on food of different structures, compositions and processing conditions in order to investigate the bioaccessibility (*i.e.*, amount of a compound released from food and available for intestinal absorption) of nutrients.

Three main *in vitro* digestion models have been developed: the static, the semi-dynamic and the dynamic model. All three typically include two to three digestion phases (*i.e.*, oral, gastric and small intestinal phase) and try to mimic *in vivo* physiological conditions by using relevant temperature, enzymes, pH, digestion times and salt concentrations.

The static model is considered as the simplest method as the samples reside largely in a single static digestion phase (*i.e.*, the secretions and enzymes are not added periodically to simulate the *in vivo* process) and also the digestion products are not removed. This model can be used adequately to understand the mechanistic digestion process of a simple food or purified food components, such as investigating the digestion process of milk, bread or vitamins and nutrients, under specific conditions. The main disadvantage of this model is that dynamic physiological parameters, such as hydration, changes in conditions (*i.e.*, pH, enzyme concentration) over time and peristalsis and gradual removal of digestion products, are not taken into considerations (Alegría et al., 2015). The fraction of product released during digestion, such as macronutrients, is also complicated to separate from the undigested fraction, which will strongly affects the analysis. For instance, the use of centrifugation to separate the digested product from the undigested fraction can be limited because of their density similarity (Minekus et al., 2014). Therefore, the static *in vitro* model is not suitable to assess the release, adsorption and transport kinetics of macronutrients (*i.e.*, glucose, amino-acids) over time. Hence other methods have been developed to overcome these limitations such as the dynamic *in vitro* model and

the semi-dynamic *in vitro* model (Barroso et al., 2015; Molly et al., 1993; Mulet-Cabero et al., 2018; Mulet-Cabero et al., 2017). It should be noted however, that the release of free fatty acid over time via the use of pH-Stat titration can accurately be examined using a static model, since the produced fatty acids are assumed to be equivalent to the amount of neutralizing alkali titrated over time (Minekus et al., 2014).

In this thesis, the investigation of the protection and breakdown mechanisms of the emulsion microgel particles as compared to O/W emulsions, during gastrointestinal digestion, was the main research question (**Chapter 6**). The release kinetics of the encapsulated emulsion droplets or lipids being accurately measured using pH-Stat titration, the static *in vitro* model was chosen to examine the behaviour of the different systems during gastric and intestinal digestion. The properties of both digestion phases and techniques used to investigate the breakdown mechanism of the emulsion microgel particles are discussed below.

1.4.4.1 Gastric digestion: the role of acidic pH and pepsin

The main role of the gastric phase is to degrade and progressively deliver the chyme (*i.e.*, the digestive product collected at the end of the gastric phase) into the small intestine to optimize intestinal digestion. During the gastric phase, acidic gastric juices containing hydrochloric acid and proteolytic enzymes dilute the food bolus. Under fasting conditions, the pH of the gastric phase ranges from 1 to 3. Upon the ingestion of food, the pH increases slightly (~ pH 5) depending on the buffering capacity, composition and quantity of food ingested, followed by a gradual decrease due to the secretion of acidic gastric juices. The mixing of the food bolus via a peristaltic movement of the stomach allows some slight mixing of the food bolus with the gastric secretion.

Proteolysis (*i.e.*, peptic digestion) is achieved in the stomach through pepsin, which is an aspartic protease. Pepsin can only hydrolysis peptide bonds of non-terminal amino-acid, thus pepsin cannot break polypeptides into amino-acids but only into smaller polypeptides (Figure 1.16). The enzyme preferentially cleaves to peptide bonds between hydrophobic and aromatic amino acids (*i.e.*, phenylalanine, tryptophan and tyrosine) (Beynon and Bond, 2001). The activity of pepsin will vary depending on the pH of the gastric phase, with pH 2 – 4 (37 °C) being the optimum pH (Minekus et al., 2014).

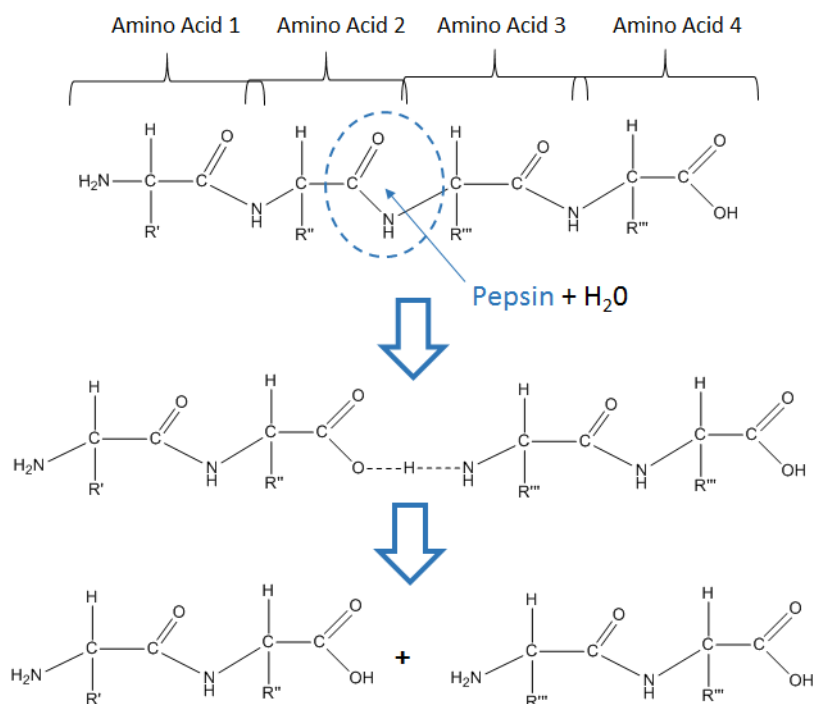


Figure 1.16 Schematic representation of the proteolysis of a polypeptide, comprised of four amino acid, via pepsin attacking a peptide bond.

Gastric lipase can also be found in gastric secretion and is responsible for less than 30% of lipolysis in healthy adults (Minekus et al., 2014; Wilde and Chu, 2011). However, due to the lower activity of gastric lipase ($10 - 120 \text{ U mL}^{-1}$) as compared to intestinal lipase ($80 - 7000 \text{ U mL}^{-1}$), owing to the low pH and the absence of surfactant (*i.e.*, bile salts), gastric lipase was omitted following the recommendation of the standardized INFOGEST static *in vitro* digestion method (Minekus et al., 2014).

1.4.4.2 Protein electrophoresis (SDS – PAGE)

The extent of proteolytic digestion of food (in the case of this thesis, whey protein stabilised oil-in-water emulsion and emulsion microgel particles) during or after gastric digestion was examined via sodium dodecyl sulphate polyacrylamide gel electrophoresis (SDS-PAGE) (Egger et al., 2016; Hu et al., 2017). Protein electrophoresis refers to the movement of charged protein in response to an electric field, leading to their separation. Under an electric field, protein will move towards the electrode of opposite charge. The migration rate of the protein is dependent on the strength of the electric field, temperature, pH, ionic strength of the buffer solution

as well as the shape, size, and charge of the protein. Hence, by using separation matrices such as acrylamide or agarose gels, which have different pore size, it is possible to separate proteins as function of their size. The gel pore structure will allow smaller proteins to move more rapidly as compared to larger proteins, yielding protein bands in the gel matrix (Figure 1.17). However generally, protein solution should be solubilised and denatured with sodium dodecyl sulphate (SDS) to allow any protein-protein interactions to be removed, resulting in the dissociation of proteins but also in the unfolding of the protein. Additionally, SDS binds to the protein (~proportionally to its molecular weight) to impart an overall negative charge to the proteins allowing the protein to move towards the positively charged cathode, so that the size of the protein is primarily what affects the rate at which it moves towards the anode rather than its charge.

Reducing agent (*i.e.*, mercaptoethanol or dithiothreitol) are also used to further disrupt disulphide bonds and totally unfold the protein. To allow the detection of the protein bands in the gel, the protein sample is usually stained, with Coomassie Blue. The protein bands can then be detected via densitometry and compared to a protein standard to estimate the molecular weight of each bands (Bio-Rad Laboratories, 2015).

In the case of proteolysis analysis, the digested protein bands can be relatively quantified as compared to the undigested protein bands (*i.e.*, control samples) to

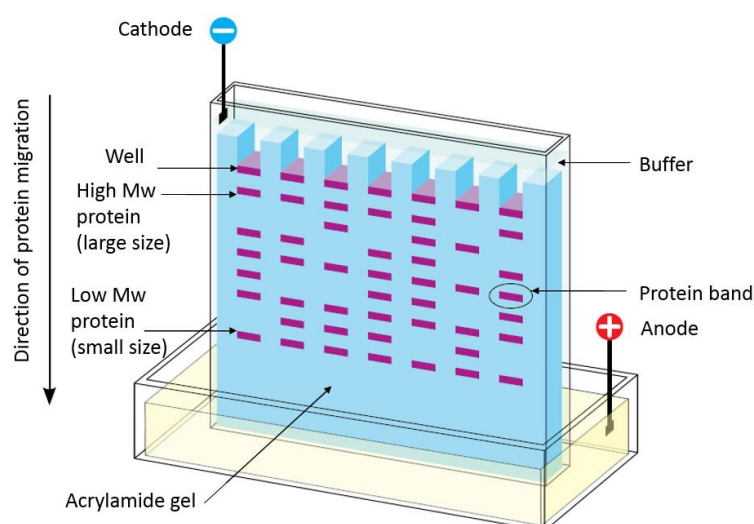


Figure 1.17 Schematic representation of polyacrylamide gel electrophoresis (*M_w*: molecular weight), figure from Bio-Rad Laboratories (2015).

understand the extent of the digestion. Low molecular polypeptide bands can also generally be observed via SDS-PAGE reinforcing the proteolysis analysis.

1.4.4.3 Intestinal digestion: the role of bile salts and pancreatic lipase

Following the 2 hours of *in vitro* gastric digestion, the gastric chyme is transferred into the small intestine. The chyme is first neutralized by secretion of sodium carbonate (or sodium hydroxide). This is conducted by increasing the pH to around 6.8 and mixed with bile and pancreatic juice, containing enzymes (Alegría et al., 2015).

In the small intestine, proteolysis is continued through trypsin and chymotrypsin, both of which are serine endopeptidase with an optimum activity at pH 8 and 37 °C. The active sites of trypsin are arginine and lysine, whilst the ones of chymotrypsin are phenylalanine, tryptophan and tyrosine (although chymotrypsin can also cleave to histidine, methionine and leucine, where slower hydrolysis occurs) (Beynon and Bond, 2001).

About 60 – 80% of lipolysis also occurs in the small intestine through the synergistic properties of pancreatic lipase/colipase and bile salts. Pancreatic lipase catalysis the hydrolysis of triglycerides, at sn-1 and sn-3 positions, producing two fatty acids and one monoglyceride (Figure 1.18) (Wilde and Chu, 2011). However, pancreatic lipase has first to adsorb to the lipid droplet interface in order to initiate the hydrolysis. In emulsions, other surface active materials are present (such as proteins), hence the displacement of these surfactants are necessary for lipase to adsorb to the oil droplets interface. Bile salts will promote the action of lipase by displacing surface active material and forming mixed micelles. Another important role of bile salts is to prevent the accumulation of inhibitory products (such as long free fatty acid and monoglycerides formed during lipolysis) at the lipid interface (Sarkar et al., 2016).

Bile salts are synthesized from cholesterol in the liver, stored in the gall bladder and released in the duodenum during digestion. The main components of bile salts are cholic acid, deoxycholic acid and chenodeoxycholic acid, which conjugate with taurine and glycine, thus imparting bile salts with amphiphilic and polar properties (Wilde and Chu, 2011). Therefore, bile salts can easily emulsify lipid products during intestinal digestion enhancing the solubilisation of lipid digestion products into mixed micelles and allowing the adsorption of lipase

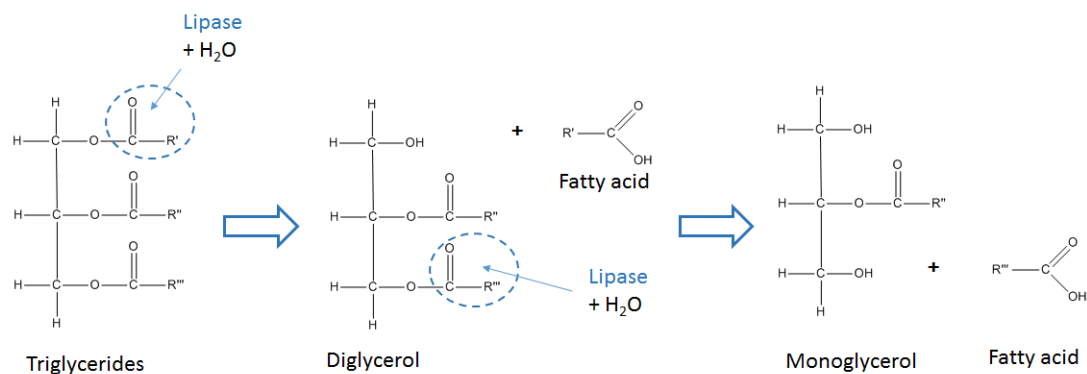


Figure 1.18 Schematic representation of the lipolysis of triglycerides into diglycerol and monoglycerol and fatty acids.

(Sarkar et al., 2016). However, it should be noted that, in comparison to conventional surfactant, bile salts have a rigid and flat molecular structure, resulting in a low packing efficiency at the lipid interface (Maldonado-Valderrama et al., 2008). In the presence of emulsified lipids (such as protein stabilised emulsions) bile salts can displace the proteins from the interface by adsorbing into small defects of the protein network, known as the orogenic displacement process. This will lead to the formation of small pools of surfactant, which have a higher surface pressure than the protein network itself. These surfactant pools will grow, compressing the protein network into thick aggregates, until the network collapses, resulting in the displacement of the protein at the oil/water interface and the possible adsorption of lipase (Mackie et al., 2000). However, the high surface activity of bile salts as compared to pancreatic lipase, will result in competitive adsorption between both molecules, which can inhibit the activity of pancreatic lipase. Previous studies have also suggested the bile salts might bind to the active site of pancreatic lipase further inhibiting the adsorption of lipase. Pancreatic lipase cofactor, *i.e.*, colipase, can interact electrostatically with bile salts as well as form complexes with lipase, enabling pancreatic lipase to overcome the inhibition by bile salts and adsorb to the oil interface, resulting in enhanced lipolysis (Wilde and Chu, 2011).

1.4.4.4 Free fatty acid release: pH-Stat titration

The rate of lipolysis during *in vitro* intestinal digestion is often analysed via a pH-stat titration method. As mentioned above, upon lipolysis of triglycerides, two fatty acids are released, resulting in a decrease in pH. Hence, by maintaining the *in vitro* intestinal solution at a constant pH via titration of sodium hydroxide over time,

it is possible to examine the amount of free fatty acid released. It is assumed that the neutralization of one mole of digested triglyceride is obtained via the addition of two moles of sodium hydroxide. However, it should be noted that this is only true if all the free fatty acid released are readily ionized, which will depend on the pH of the solution as well as the pK_a of the fatty acids (Li and McClements, 2010; Mat et al., 2016).

In this thesis, pH-stat titration was conducted to understand the different release rates of the free fatty acid in a conventional oil-in-water emulsion as compared to the ones in emulsion microgel particles. This investigation would allow to further understand the control release mechanism imparted by the emulsion microgel particles during *in vitro* digestion.

1.5 Outline of the thesis

With this overview, this thesis includes a continuum of literature review and research studies from the design and characterization of emulsion microgel particles, encapsulating lipophilic molecules, to the *in vitro* oral and gastrointestinal release properties of the encapsulated emulsion droplets. The outline of each chapter is highlighted in Figure 1.19.

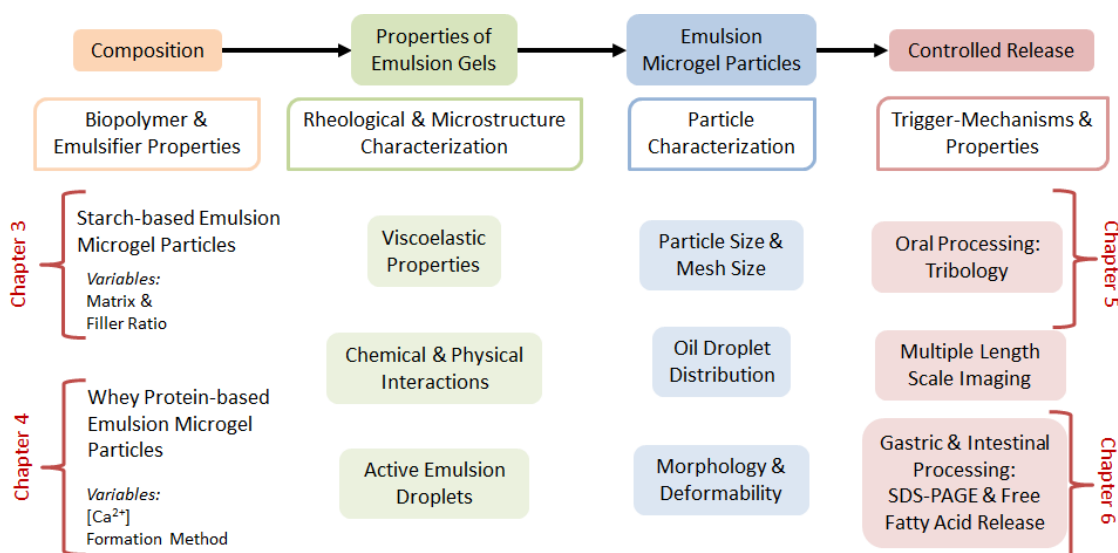


Figure 1.19 Schematic framework of this thesis.

Chapter 2 includes a literature review allowing to understand the key technologies available for the design of emulsion gels and emulsion microgel

particles in general, whilst also focusing on the different release mechanisms of emulsion microgel particles. A clear knowledge gap is identified to pursue the experimental studies. The literature review forming this chapter was published in peer-reviewed journal, *Trends in Food Science & Technology*.

Chapter 3 discusses the formation of starch based emulsion gels as well as the top-down approach to form starch based emulsion microgel particles followed by the characterization of structural and rheological properties of these starch based emulsion microgel particles. The innovative aspect was that for the first time OSA-starch stabilized emulsion droplets were reported to act as active fillers (*i.e.*, bound) in sheared starch gels. The formation of starch emulsion microgel particles was also reported for the first time. This chapter was published in peer-reviewed journal, *Carbohydrate Polymers*.

Chapter 4 explores two bottom-up processing techniques (jet homogenization versus extrusion) to design different sized whey protein based emulsion microgel particles using Ca^{2+} -induced cold gelation technique. The detailed processing parameters of both techniques are discussed in relation to the size of the emulsion microgel particles obtained from these methods, supported by theoretical calculations. The results from this chapter was published in peer-reviewed journal, *Food Hydrocolloids*.

Chapter 5 demonstrates the lubrication properties of starch based emulsion microgel particles during *in vitro* oral processing, using experimental (tribology, rheology, imaging) and theoretical (drag force, Hertz' theory and particles indentation) approaches. This application of the starch based emulsion microgel particles for oral lubrication while protecting the droplets against coalescence was published in peer-reviewed journal, *ACS Applied Materials and Interfaces*.

Chapter 6 presents the ability of whey protein based emulsion microgel particles to protect droplets from coalescence during *in vitro* gastric digestion followed by their free fatty acid release during *in vitro* intestinal digestion. The controlled digestion behaviour of whey protein based emulsion microgel particles was published in the peer-reviewed journal *Food Hydrocolloids*.

Chapter 7 includes a general summary and discussion of the main results as well as a conclusion in relation to the principal research problem and areas for future studies.

1.6 References

- Agama-Acevedo, E. and Bello-Perez, L.A. 2017. Starch as an emulsions stability: the case of octenyl succinic anhydride (OSA) starch. *Current Opinion in Food Science*. **13**, pp.78-83.
- Ai, Y. et al. 2013. In vitro and in vivo digestion of octenyl succinic starch. *Carbohydrate Polymers*. **98**(2), pp.1266-1271.
- Alegría, A. et al. 2015. Static Digestion Models: General Introduction. In: Verhoeckx, K., et al. eds. *The Impact of Food Bioactives on Health: in vitro and ex vivo models*. Cham: Springer International Publishing, pp.3-12.
- Amine, C. et al. 2014. Investigation of emulsifying properties and emulsion stability of plant and milk proteins using interfacial tension and interfacial elasticity. *Food Hydrocolloids*. **39**, pp.180-186.
- Auty, M.A.E. 2013. 4 - Confocal microscopy: principles and applications to food microstructures. In: Morris, V.J. and Groves, K. eds. *Food Microstructures*. Woodhead Publishing, pp.96-98.
- Bai, Y. et al. 2014. Position of modifying groups on starch chains of octenylsuccinic anhydride-modified waxy maize starch. *Food Chemistry*. **153**, pp.193-199.
- Bai, Y. and Shi, Y.-C. 2011. Structure and preparation of octenyl succinic esters of granular starch, microporous starch and soluble maltodextrin. *Carbohydrate Polymer*. **83**(2), pp.520-527.
- Barbut, S. and Foegeding, E.A. 1993. Ca²⁺-Induced Gelation of Pre-heated Whey Protein Isolate. *Journal of Food Science*. **58**(4), pp.867-871.
- Barroso, E. et al. 2015. Development of human colonic microbiota in the computer-controlled dynamic SIMulator of the GastroIntestinal tract SIMGI. *LWT - Food Science and Technology*. **61**(2), pp.283-289.
- Beynon, R.J. and Bond, J.S. 2001. *Proteolytic enzymes: a practical approach*. 2nd ed. Oxford: Oxford University Press.
- Bhosale, R. and Singhal, R. 2007. Effect of octenylsuccinylation on physicochemical and functional properties of waxy maize and amaranth starches. *Carbohydrate Polymers*. **68**(3), pp.447-456.
- Bio-Rad Laboratories, I. 2015. A Guide to Polyacrylamide Gel Electrophoresis and Detection.

- Britten, M. and Giroux, H.J. 2001. Acid-induced gelation of whey protein polymers: effects of pH and calcium concentration during polymerization. *Food Hydrocolloids*. **15**(4–6), pp.609-617.
- Bryant, C.M. and McClements, D.J. 1998. Molecular basis of protein functionality with special consideration of cold-set gels derived from heat-denatured whey. *Trends in Food Science & Technology*. **9**(4), pp.143-151.
- Bryant, C.M. and McClements, D.J. 2000. Influence of NaCl and CaCl₂ on Cold-Set Gelation of Heat-denatured Whey Protein. *Journal of Food Science*. **65**(5), p804.
- Carpenter, G. 2012. Role of Saliva in the Oral Processing of Food. *Food Oral Processing*. Wiley-Blackwell.
- Chen, J. and Engelen, L. 2012. Food oral processing: fundamentals of eating and sensory perception. Chichester: Wiley-Blackwell.
- Chen, J. and Stokes, J.R. 2012. Rheology and tribology: Two distinctive regimes of food texture sensation. *Trends in Food Science & Technology*. **25**(1), pp.4-12.
- Clark, A.H. 1991. Structural and Mechanical Properties of Biopolymer Gels. In: Dickinson, E. ed. *Food Polymers, Gels and Colloids*. Woodhead Publishing, pp.322-338.
- Clark, A.H. 1996. Biopolymer gels. *Current Opinion in Colloid & Interface Science*. **1**(6), pp.712-717.
- Creusot, N. and Gruppen, H. 2007. Enzyme-induced aggregation and gelation of proteins. *Biotechnology Advances*. **25**(6), pp.597-601.
- de Vicente, J. et al. 2006. Viscosity Ratio Effect in the Emulsion Lubrication of Soft EHL Contact. *Journal of Tribology*. **128**(4), pp.795-800.
- de Wijk, R.A. et al. 2006. Perceived creaminess of semi-solid foods. *Trends in Food Science & Technology*. **17**(8), pp.412-422.
- Dickinson, E. 1992. Structure and composition of adsorbed protein layers and the relationship to emulsion stability. *Journal of the Chemical Society, Faraday Transactions*. **88**(20), pp.2973-2983.
- Dickinson, E. 1994. Protein-stabilized emulsions. *Journal of Food Engineering*. **22**(1), pp.59-74.

- Dickinson, E. 1998. Proteins at interfaces and in emulsions Stability, rheology and interactions. *Journal of the Chemical Society, Faraday Transactions*. **94**(12), pp.1657-1669.
- Dickinson, E. 2017. On the road to understanding and control of creaminess perception in food colloids. *Food Hydrocolloids*.
- Dokić, L. et al. 2012. Physicochemical characteristics and stability of oil-in-water emulsions stabilized by OSA starch. *Food Hydrocolloids*. **29**(1), pp.185-192.
- Egger, L. et al. 2016. The harmonized INFOGEST in vitro digestion method: From knowledge to action. *Food Research International*. **88**, pp.217-225.
- Egger, L. et al. 2017. Physiological comparability of the harmonized INFOGEST in vitro digestion method to in vivo pig digestion. *Food Research International*. **102**, pp.567-574.
- French, D. 1981. Amylases: Enzymatic Mechanisms. In: Hollaender, A., et al. eds. *Trends in the Biology of Fermentations for Fuels and Chemicals*. Boston, MA: Springer US, pp.151-182.
- Golding, M. and Wooster, T.J. 2010. The influence of emulsion structure and stability on lipid digestion. *Current Opinion in Colloid & Interface Science*. **15**(1), pp.90-101.
- Gunasekaran, M.M.A.a.S. 2002. Fundamental Rheological Methods. *Cheese Rheology and Texture*. CRC Press.
- Guo, M.R. et al. 1995. Susceptibility of β -Lactoglobulin and Sodium Caseinate to Proteolysis by Pepsin and Trypsin. *Journal of Dairy Science*. **78**(11), pp.2336-2344.
- Hardham, A.R. 2012. Confocal microscopy in plant-pathogen interactions. *Methods Mol Biol*. **835**, pp.295-309.
- Havea, P. et al. 2004. The role of disulphide and non covalent bonding in the functional properties of heat-induced whey protein gels. *Journal of Dairy Research*. **71**(3), pp.330-339.
- Havea, P. et al. 2009. Heat-Induced Whey Protein Gels: Protein-Protein Interactions and Functional Properties. *Journal of Agricultural and Food Chemistry*. **57**(4), pp.1506-1512.
- Hongsprabhas, P. and Barbut, S. 1997. Ca²⁺-Induced cold gelation of whey protein isolate: effect of two-stage gelation. *Food Research International*. **30**(7), pp.523-527.

- Hongsprabhas, P. et al. 1999. The Structure of Cold-Set Whey Protein Isolate Gels Prepared With Ca⁺⁺. *LWT - Food Science and Technology*. **32**(4), pp.196-202.
- Hornung, P. 2018. Brazilian yam and turmeric native starches: characterization, modification and application. Thesis.
- Hu, B. et al. 2017. Gelation of soybean protein and polysaccharides delays digestion. *Food Chemistry*. **221**, pp.1598-1605.
- Iametti, S. et al. 1995. Modifications of High-Order Structures upon Heating of .beta.-Lactoglobulin: Dependence on the Protein Concentration. *Journal of Agricultural and Food Chemistry*. **43**(1), pp.53-58.
- Iida, Y. et al. 2008. Control of viscosity in starch and polysaccharide solutions with ultrasound after gelatinization. *Innovative Food Science & Emerging Technologies*. **9**(2), pp.140-146.
- JEOL Ltd. 2011. Introducing Cryo Scanning Electron Microscopy. *JEOL Application Data Sheet, SEM, SM-B-004-00E*.
- Kennedy, D. et al. 2010. Tongue Pressure Patterns During Water Swallowing. *Dysphagia*. **25**(1), pp.11-19.
- Kharlamova, A. et al. 2018. Calcium-induced gelation of whey protein aggregates: Kinetics, structure and rheological properties. *Food Hydrocolloids*. **79**, pp.145-157.
- Khaydukova, M. et al. 2017. Critical view on drug dissolution in artificial saliva: A possible use of in-line e-tongue measurements. *European Journal of Pharmaceutical Sciences*. **99**, pp.266-271.
- Li, Y. and McClements, D.J. 2010. New Mathematical Model for Interpreting pH-Stat Digestion Profiles: Impact of Lipid Droplet Characteristics on in Vitro Digestibility. *Journal of Agricultural and Food Chemistry*. **58**(13), pp.8085-8092.
- Liu, Z. et al. 2008. Production of Octenyl Succinic Anhydride-Modified Waxy Corn Starch and Its Characterization. *Journal of Agricultural and Food Chemistry*. **56**(23), pp.11499-11506.
- Luo, Q. et al. 2017. Pepsin diffusivity in whey protein gels and its effect on gastric digestion. *Food Hydrocolloids*. **66**, pp.318-325.

- Macierzanka, A. et al. 2012. The effect of gel structure on the kinetics of simulated gastrointestinal digestion of bovine β -lactoglobulin. *Food Chemistry*. **134**(4), pp.2156-2163.
- Mackie, A.R. et al. 2000. Orogenic Displacement of Protein from the Oil/Water Interface. *Langmuir*. **16**(5), pp.2242-2247.
- Maldonado-Valderrama, J. et al. 2008. Interfacial Characterization of β -Lactoglobulin Networks: Displacement by Bile Salts. *Langmuir*. **24**(13), pp.6759-6767.
- Malvern Instruments Ltd. 2005. *Zetasizer Nano Series User Manual MAN0317*. Worchestershire, UK: Malvern Instruments Ltd.
- Malvern Instruments Ltd. 2011. Simplifying the Measurement of Zeta Potential Using M3-PALS, Technical note. *Malvern Instruments Ltd*.
- Malvern Instruments Ltd. 2015. A basic guide to particle characterization. *Malvern Instruments Ltd*.
- Mat, D.J.L. et al. 2016. In vitro digestion of foods using pH-stat and the INFOGEST protocol: Impact of matrix structure on digestion kinetics of macronutrients, proteins and lipids. *Food Research International*. **88**, pp.226-233.
- McClements, D.J. 2004. *Food Emulsion principles and properties*. Boca Raton: CRC Press.
- McClements, D.J. 2015. Nanoparticle- and Microparticle-Based Delivery Systems: Encapsulation, Protection, and Release of Active Compounds. Boca Raton, Florida: Taylor and Francis Group.
- McClements, D.J. and Li, Y. 2010. Structured emulsion-based delivery systems: controlling the digestion and release of lipophilic food components. *Adv Colloid Interface Sci*. **159**(2), pp.213-28.
- Mezger, T.G. 2014. *The rheology handbook*. 4th ed. Hanover, Germany: Vincentz Network.
- Microscopegenius.com. *Metallurgical microscopes*. [Online]. Available from: <http://microscopegenius.com/microscope-basics/compound-microscopes/metallurgical-microscopes/>
- Minekus, M. et al. 2014. A standardised static in vitro digestion method suitable for food – an international consensus. *Food & Function*. **5**(6), pp.1113-1124.

- Molly, K. et al. 1993. Development of a 5-step multi-chamber reactor as a simulation of the human intestinal microbial ecosystem. *Applied Microbiology and Biotechnology*. **39**(2), pp.254-258.
- Mosca, A.C. and Chen, J. 2017. Food-saliva interactions: Mechanisms and implications. *Trends in Food Science & Technology*. **66**(Supplement C), pp.125-134.
- Mulet-Cabero, A.-I. et al. 2018. Structural mechanism and kinetics of in vitro gastric digestion are affected by process-induced changes in bovine milk. *Food Hydrocolloids*.
- Mulet-Cabero, A.-I. et al. 2017. Dairy food structures influence the rates of nutrient digestion through different in vitro gastric behaviour. *Food Hydrocolloids*. **67**, pp.63-73.
- Nicolai, T. et al. 2011. β -Lactoglobulin and WPI aggregates: Formation, structure and applications. *Food Hydrocolloids*. **25**(8), pp.1945-1962.
- Nilsson, L. and Bergenståhl, B. 2006. Adsorption of Hydrophobically Modified Starch at Oil/Water Interfaces during Emulsification. *Langmuir*. **22**(21), pp.8770-8776.
- Nobbmann, U. et al. 2007. Dynamic light scattering as a relative tool for assessing the molecular integrity and stability of monoclonal antibodies. *Biotechnol Genet Eng Rev*. **24**, pp.117-28.
- Phillips, G.O. and Williams, P.A. 2009. *Handbook of hydrocolloids*. 2nd ed. Cambridge; Boca Raton, FL;: CRC Press.
- Phillips, G.O. and Williams, P.A. 2011. *Handbook of Food Proteins*. Woodhead Publishing. Available from: <https://app.knovel.com/hotlink/toc/id:kpHFP00021/handbook-food-proteins/handbook-food-proteins>
- Prakash, S. 2017. Chapter 4 - From Rheology to Tribology: Applications of Tribology in Studying Food Oral Processing and Texture Perception. In: Ahmed, J., et al. eds. *Advances in Food Rheology and Its Applications*. Woodhead Publishing, pp.65-86.
- Reilly, P.J. 2007. Chapter 5 - Amylase and Cellulase Structure and Function. In: Yang, S.-T. ed. *Bioprocessing for Value-Added Products from Renewable Resources*. Amsterdam: Elsevier, pp.119-130.

- Roefs, S.P.F.M. and De Kruif, K.G. 1994. A Model for the Denaturation and Aggregation of β -Lactoglobulin. *European Journal of Biochemistry*. **226**(3), pp.883-889.
- Ryan, K.N. et al. 2013. Use of Whey Protein Soluble Aggregates for Thermal Stability—A Hypothesis Paper. *Journal of Food Science*. **78**(8), pp.R1105-R1115.
- Sarkar, A. et al. 2017. Aqueous Lubrication, Structure and Rheological Properties of Whey Protein Microgel Particles. *Langmuir*. **33**(51), pp.14699-14708.
- Sarkar, A. et al. 2016. On the role of bile salts in the digestion of emulsified lipids. *Food Hydrocolloids*. **60**, pp.77-84.
- Singh, H. and Sarkar, A. 2011. Behaviour of protein-stabilised emulsions under various physiological conditions. *Advances in Colloid and Interface Science*. **165**(1), pp.47-57.
- Sok, L.V.L. et al. 2005. Cold gelation of β -lactoglobulin oil-in-water emulsions. *Food Hydrocolloids*. **19**(2), pp.269-278.
- Stokes, J.R. 2012. 'Oral' Tribology. *Food Oral Processing*. Blackwell Publishing Ltd.
- Stokes, J.R. et al. 2013. Oral processing, texture and mouthfeel: From rheology to tribology and beyond. *Current Opinion in Colloid & Interface Science*. **18**(4), pp.349-359.
- Svegmark, K. and Hermansson, A.-M. 1991. Changes induced by shear and gel formation in the viscoelastic behaviour of potato, wheat and maize starch dispersions. *Carbohydrate Polymers*. **15**(2), pp.151-169.
- Svegmark, K., Hermansson, A. M. 1991. Distribution of Amylose and Amylopectin in Potato Starch Pastes: Effects of Heating and Shearing. *Food Structure*. **10**(2).
- Sweedman, M.C. et al. 2014. Aggregate and emulsion properties of enzymatically-modified octenylsuccinylated waxy starches. *Carbohydrate Polymers*. **111**, pp.918-927.
- Sweedman, M.C. et al. 2013. Structure and physicochemical properties of octenyl succinic anhydride modified starches: A review. *Carbohydrate Polymers*. **92**(1), pp.905-920.
- Tesch, S. et al. 2002. Stabilization of emulsions by OSA starches. *Journal of Food Engineering*. **54**(2), pp.167-174.

- Teysandier, F. et al. 2011. Sol–gel transition and gelatinization kinetics of wheat starch. *Carbohydrate Polymers*. **83**(2), pp.400-406.
- Tizzotti, M.J. et al. 2011. New ¹H NMR Procedure for the Characterization of Native and Modified Food-Grade Starches. *Journal of Agricultural and Food Chemistry*. **59**(13), pp.6913-6919.
- Wang, S. et al. 2015. Starch Retrogradation: A Comprehensive Review. *Comprehensive Reviews in Food Science and Food Safety*. **14**(5), pp.568-585.
- Wijayanti, H.B. et al. 2014. Stability of Whey Proteins during Thermal Processing: A Review. *Comprehensive Reviews in Food Science and Food Safety*. **13**(6), pp.1235-1251.
- Wilde, P.J. and Chu, B.S. 2011. Interfacial & colloidal aspects of lipid digestion. *Advances in Colloid and Interface Science*. **165**(1), pp.14-22.
- Wolz, M. and Kulozik, U. 2015. Thermal denaturation kinetics of whey proteins at high protein concentrations. *International Dairy Journal*. **49**, pp.95-101.
- Zhang, B. et al. 2011. Effects of octenylsuccinylation on the structure and properties of high-amylose maize starch. *Carbohydrate Polymers*. **84**(4), pp.1276-1281.
- Zhang, Z. et al. 2015. Designing hydrogel particles for controlled or targeted release of lipophilic bioactive agents in the gastrointestinal tract. *European Polymer Journal*. **72**, pp.698-716.
- Zúñiga, R.N. et al. 2010. Kinetics of Formation and Physicochemical Characterization of Thermally-Induced β -Lactoglobulin Aggregates. *Journal of Food Science*. **75**(5), pp.E261-E268.

Chapter 2

Emulsion microgel particles: novel encapsulation strategy for lipophilic molecules¹

Abstract

Lipophilic molecules such as flavours, essential oils, vitamins and fatty acids are difficult to deliver in food matrices owing to their limited solubility, rapid oxidation and degradation during physiological transit. Among the technologies available to deliver lipophilic molecules, emulsion microgel particles are a relatively new class of soft solid particles of discrete size, shape, and interesting release properties.

Relevant literature concerning the processing of emulsion gels and emulsion microgel particles has been reviewed. Factors affecting the mechanical properties of protein-stabilized emulsion gels with key emphasis on the role of “active” and “inactive fillers” are discussed. Technologies for creation of emulsion gel particles using top-down and bottom-up approaches have been covered. Special attention was dedicated to the release mechanisms from emulsion microgel particles via swelling and erosion.

Emulsion gels with “active fillers” offer the potential to create emulsion microgel particles using top-down approaches. Polymer extrusion, multiple emulsion templating, fluid gels are few routes for creating emulsion microgel particles using bottom-up approaches. Although whey protein has been well researched, modified starch and plant proteins need to be investigated for design of new emulsion microgel particles that can act as surfactant and bulk gelling agents in their own right through intelligent tuning of processing conditions. If designed

¹ Published as: Torres, O., Murray, B. and Sarkar, A. 2016. Emulsion microgel particles: Novel encapsulation strategy for lipophilic molecules. *Trends in Food Science & Technology*. **55** (Supplement C), pp.98-108. DOI: <https://doi.org/10.1016/j.tifs.2016.07.006>

carefully with an end goal of “controlled delivery” in mind, responsiveness to oral temperature, biological enzymes, intestinal pH etc., can be built into emulsion microgel particles so that they may find novel applications in food, pharmaceutical and personal care industries.

2.1 Introduction

Lipophilic active molecules, such as fat soluble vitamins, flavourings, fatty acids and essential oils pose challenges for their application in food matrices as they are water insoluble. They tend to oxidize rapidly in the presence of air, light and heat. Additionally, due to their hydrophobic nature, most of these compounds are difficult to deliver in human physiology and are generally partially absorbed by the body or their biological activity is partly or fully degraded during their transit. Thus, there is a huge need to protect these lipophilic compounds towards environmental degradation and tailor their release at specific physiological sites, such as burst release of flavours or essential oils in the mouth or the protection of omega-3 fatty acids during gastric transit and their release in the intestine.

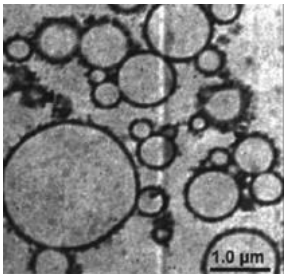
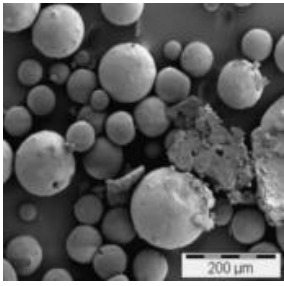
A wide range of technologies have been developed to encapsulate lipid molecules, such as emulsions, emulsion gels, liposomes, micelles, nanoparticles, etc. Each of these have their own specific advantages and disadvantages in terms of protection, delivery, cost, regulatory status, ease of use, biodegradability and biocompatibility (McClements and Li, 2010). Among these, emulsions gels are an alternative technique that allows stabilization and delivery of lipophilic compounds in food matrices. Emulsion gels are frequently produced in food products, such as, sausages, yogurt, dairy desserts, cheese, etc. (Mun et al., 2015b). Currently, there has been an upsurge in research efforts in the domain of emulsion gels resulting in engineering novel soft solids, such as emulsion fluid gels and emulsion microgel particles. To understand different terminologies used in the literature, definitions of each of these classes of emulsion gels with their corresponding microstructures are included in Table 2.1.

Emulsion microgel particles are a relatively new class of soft solids, particularly in food research. Emulsion microgel particles have similar polymer chemistry to emulsion gels though their physical arrangement and scale differs. Both

emulsion gels and emulsion microgel particles have oil and gel phases but microgels are much smaller discrete particles with well-defined spherical shape (Thorne et al., 2011). In emulsion gels, the emulsion droplets are stabilised by emulsifiers and heterogeneously distributed in a continuous gel matrix whereas in emulsion microgel particles, emulsion droplets are stabilised by an emulsifier and gelling agent, creating a soft solid shell around several emulsion droplets which are then incorporated into a continuous gel matrix. Therefore, in emulsion gels before gelation of the matrix, emulsion droplets are rather mobile due to Brownian motion and can be unstable due to faster flocculation, coalescence and creaming. Meanwhile, in emulsion microgel particles, several emulsion droplets are entrapped into a soft solid shell providing better control of droplet size, mobility and mechanical properties (Mun et al., 2015a; Ruffin et al., 2014; Zhang et al., 2015b; Zhang et al., 2015c). Additionally, microgel particles have been demonstrated to protect lipophilic compound (such as polyunsaturated fatty acids) against oxidation (Beaulieu et al., 2002; Augustin and Sanguansri, 2012; Chung et al., 2013; Mao and Miao, 2015; Velikov and Pelan, 2008; Matalanis et al., 2011). Therefore, by encapsulating lipophilic molecules into these emulsion microgel particles, lipophilic bioactives can be easily protected and dispersed into aqueous food media, such as dairy products (*i.e.*, yogurt, ice cream, cheese) but also meat products (*i.e.*, sausages).

The microgel particle encapsulation method has been described as “smart” because the size, physicochemical properties of these particles are tuneable and allow the microgel to swell or de-swell, as well as degrade in response to specific temperature, pH, ionic strength and enzymatic conditions (Ballauff and Lu, 2007; Shewan and Stokes, 2013; Wei et al., 2016; Kawaguchi, 2014). Hence, emulsion microgel particles can be effective for site-dependent release of lipophilic bioactives (Ching et al., 2016). For instance, incorporation of filled hydrogel particles in low fat dairy products have been found to retain the sensory attributed of the dairy product by controlling the release of lipophilic aroma and mimicking fat droplet functionality (*i.e.*, creamy mouthfeel with a lower fat content) (Joye and McClements, 2014; Pizzoni et al., 2015; Malone and Appelqvist, 2003; Malone et al., 2003; Oliver et al., 2015a; Oliver et al., 2015b; Zhang et al., 2015a; Chung et al., 2013). Hydrogel particles encapsulating hydrophilic compounds have been well studied and reviewed by Joye and McClements (2014) and McClements (2015) as

Table 2.1 Definitions and microstructures (at various length scales) of different emulsion gel-based strategies for delivery of lipophilic molecules. (A) Transmission electron micrograph (TEM) of emulsion gels (reproduced from Anton et al. (2001)). (B) Scanning electron micrograph (SEM) of emulsion microgel particle (reproduced from Egan, et al., 2013).

Nomenclature and Microstructure	Description	References
<p data-bbox="226 480 465 515">(A) Emulsion gel</p> 	<p data-bbox="517 480 1653 858">“Emulsion gels”, also named as “emulsion hydrogel”, “emulgel”, “emulsion-filled gel” are defined as soft solids where emulsified lipid droplets are entrapped in a gel matrix. Generally, the emulsified lipid droplets are referred to as “fillers” and the gelled aqueous phase is referred to as the “matrix”. They are formed either by suitable application of temperature, pH, ionic strength, enzymes to the emulsion made with high concentration of biopolymer (especially protein in the case of protein-based emulsion gel) or by addition of a gelling agent to the continuous phase forming physical cross-links between emulsion droplets. It has the advantages of both hydrogels (<i>i.e.</i>, thermodynamic stability) and emulsions (<i>i.e.</i>, delivery of lipid soluble molecules).</p>	<p data-bbox="1688 523 1960 778">(Briuglia et al., 2014; Dickinson, 2012; Oliver et al., 2015; Sarkar et al., 2015; Satapathy et al., 2015; Ma and An, 2016)</p>
<p data-bbox="226 863 465 943">(B) Emulsion microgel particle</p> 	<p data-bbox="517 927 1653 1177">“Emulsion microgel particles”, “emulsion filled hydrogel particles”, “emulsion gel beads” or “fluid emulsion gel” are new class of particles formed by encapsulating several emulsion droplets into a soft gel shell either using a top-down approach or a bottom-up approach. Fluid emulsion gels are a specific case of emulsion microgel particles as they are formed by applying shear to the continuous phase whilst gelling the emulsion droplets.</p>	<p data-bbox="1688 863 1960 1241">(Beaulieu et al., 2002; Ching et al., 2016; Dickinson, 2015; Egan et al., 2013; Sung et al., 2015; Garrec and Norton, 2012; Moakes et al., 2015b)</p>

well as protein-based microgels by Dickinson (2015). Nevertheless, to our knowledge, no review on emulsion microgel particles encapsulating lipophilic compounds is available. Hence, this review aims to detail the formation of emulsion microgel particles and their application for controlled release of lipophilic compounds.

We begin by covering the basic processing steps of emulsion gels since this sets the scene for the top-down approach of making emulsion microgel particles from the parent emulsion gel. In the second section, we discuss the role of oil droplet, “filler” and gel “matrix”, and interactions that govern the mechanical properties of emulsion gels. We have focussed mainly on whey protein (from bovine milk) and also covered the few available publications on modified starch-based systems, since both these biopolymers have potential to act as surfactants and gelling agent when subjected to suitable processing conditions. The third section deals with the bottom-up approach to design emulsion microgel particles using polymer extrusion, multiple emulsion-based templating or the fluid gel route. Finally, we discuss the different release mechanisms of these emulsion microgel particles.

2.2 Formation of Emulsion Gels

The formation of emulsion gels is generally a two-step process as shown in Figure 2.1. The first step involves the formation of an oil-in-water emulsion. During high shear mixing, such as high pressure homogenization, colloid milling, etc., globular whey proteins unfold and adsorb onto the surface of oil droplets due to their surface active properties, decreasing the interfacial tension between the oil and the aqueous phase and stabilizing the oil droplets via electrostatic repulsion and steric stabilization (Dickinson, 2012; Kakran and Antipina, 2014; Sala et al., 2008; Sarkar and Singh, 2016). The second step involves the formation of a three-dimensional protein network entrapping the emulsified oil droplets by gelling the continuous phase (Figure 2.1) by heat, salt and/or acid treatment.

In the same way, modified starch, which has been modified by attaching hydrophobic octenyl succinic acid (OSA) moieties has been well reported in literature as an emulsifier, whilst starch is well known as a thickening agent. Because of the free carboxylic acid side chain present in OSA, OSA-starch could be considered as a weakly negatively surface active charged polyelectrolyte (Shogren et al., 2000).

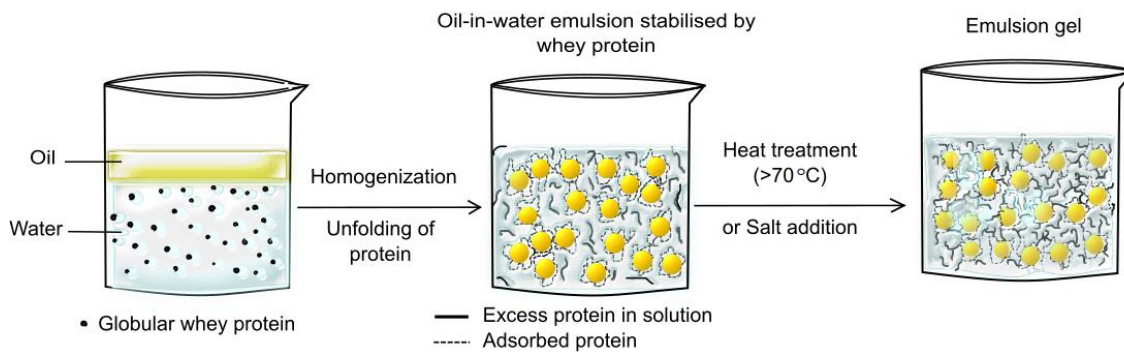


Figure 2.1 Schematic representation of emulsion gel formation using whey protein.

Tesch et al. (2002) investigated the use of OSA starches as a surfactant. They reported that OSA starch has similar surface activity and surface tension to whey protein due to its amphiphilic nature (Wang et al., 2011). The stabilisation mechanism imparted to emulsions is primarily steric due to the adsorbed branched amylopectin chains (Domian et al., 2015; Tesch et al., 2002; Chivero et al., 2016; Ettelaie et al., 2016). Many authors have been studying the gelatinization properties of OSA starches since compared to native starches which swell and melt at high temperature, OSA-starches exhibit lower gelatinization temperatures (Bao et al., 2003; Bhosale and Singhal, 2007; Ortega-Ojeda et al., 2005; Sweedman et al., 2013; Thirathumthavorn and Charoenrein, 2006). OSA-starches cold gelatinization properties have been attributed to the weakening of the interactions between amylopectin and amylose, caused by the improved steric repulsion disrupting starch crystalline structure after OSA modification, increasing the solubility of the modified starch and allowing OSA starch to entrap higher amounts of water (Sweedman et al., 2013; Ettelaie et al., 2016). Additionally, not all hydrophobic groups on the backbone of the polymer adsorb at the oil-water interface thus, hydrophobic interactions between OSA chains on neighbouring amylopectin branches can enhance the viscosity of the solution and form a polymer network (Ettelaie et al., 2016; Ortega-Ojeda et al., 2005; Sweedman et al., 2013; Thirathumthavorn and Charoenrein, 2006). Interestingly, no literature was found on the formation of an emulsion gel using OSA starch alone without any added surfactant or gelling agent: studies focused either on the stabilisation properties of OSA starch or on its thermal and pasting properties.

In general, different kinds of processing methods can be employed to gel the continuous phase. The key ones are heat, acid or salt treatment. Acid milk gels have deliberately been excluded here as they have been covered extensively in other reviews (Loveday et al., 2013; Lucey and Singh, 1997).

2.2.1 Thermal treatment of protein stabilised emulsions

Heat treatment induces denaturation and/or thermal gelation of several biopolymers. The sol-gel transition of biopolymers can either be irreversible (whey protein) or partly reversible (starch) depending on the physical or chemical interactions involved.

On heating above the denaturation temperature (65 °C) of the key globular protein of WPI (β -lactoglobulin), the molecule unfolds and the gelation process happens in three connected steps: denaturation, aggregation and three-dimensional network formation (Alting et al., 2003; Dang et al., 2009; Nicolai et al., 2011). Structural, physical and chemical changes are induced on heating between 70 and 90 °C for between 5 to 60 min. When, β -lactoglobulin unfolds it retains its dimeric form, exposing its sulfhydryl and hydrophobic groups causing the protein molecule to become reactive (Moakes et al., 2015a; Wolz and Kulozik, 2015). Further rearrangement of β -lactoglobulin secondary structure provides association points via intermolecular β -sheets forming high molecular mass oligomers. Simultaneously, aggregation of these activated molecules occurs when two unfolded molecules collide, forming the primary polymers, resulting in higher molecular weight aggregates and increasing the viscosity of the system (Moakes et al., 2015a; Wijayanti et al., 2014; Wolz and Kulozik, 2015). These clusters arise from physical non-covalent interactions, such as hydrophobic, electrostatic and hydrogen bond interactions between unfolded protein molecules (Boutin et al., 2007; Fitzsimons et al., 2008; Livney, 2010; Monahan et al., 1996). Different protein aggregation degrees can be obtained by varying environmental conditions, such as protein concentration, temperature, time, pH and addition of ions (Chen and Dickinson, 1998; Dang et al., 2009; Nicolai et al., 2011; Ruffin et al., 2014). For instance, the protein concentration strongly influences the aggregation kinetics of WPI. Increasing the concentration of protein increases the collision probability between molecules resulting in the increase

of the denaturation kinetics and aggregation rate (Dissanayake et al., 2013; Wolz and Kulozik, 2015).

During further heat treatment, the aggregation process continues through chemical covalent cross links such as intermolecular disulphide bonds and sulfhydryl-disulphide interchange that reinforces the network permanently (Monahan et al., 1996; Nicolai et al., 2011). In the case of whey protein-stabilized emulsions, both intra- and inter- droplet interactions occur. As explained by Monahan et al. (1996), denatured whey protein molecules adsorbed at the oil-water interface have their hydrophobic residues located at the interface and hydrophilic residues located in the continuous phase. With time, proteins located in the continuous phase denature enabling their interaction with adjacent unfolded protein adsorbed onto oil droplets, forming an emulsion gel. These interactions can generate even thicker interfacial layers (Sarkar et al., 2016a) and inter-droplet aggregation via disulphide interchange reactions which contributes to the formation of the protein gel network (Monahan et al., 1996).

2.2.2 Cationic treatment

Addition of salts such as monovalent or divalent salts (NaCl, CaCl₂, ZnCl₂, MgCl₂) to an emulsion is another technique inducing gelation, so called cold gelation. The higher valency of multivalent ions means that they are much more effective at screening electrostatic repulsion between droplets. Furthermore, multivalent ions such as Ca²⁺ ions can specifically bind to adsorbed protein carboxylate groups on different droplet surfaces forming ion bridges (Sarkar et al., 2016b).

With regard to whey protein stabilised emulsions and cold gelation induced by the addition of salts, the system must first be heat-treated to allow proteins to unfold and expose their hydrophobic patches (Dickinson, 2012). Hydrophobic patches from protein adsorbed to oil droplets can combine with hydrophobic patches located on other protein moieties leading to oil droplet aggregation. These aggregates constitute the building blocks leading to the cationic gel 3D network (Sok et al., 2005). Addition of calcium ions on cooling leads to further aggregation and gelation through calcium ion-mediated interactions (Bryant and McClements, 1998; Hongsprabhas and Barbut, 1997; Kuhn et al., 2010).

2.3 Filler-Matrix Interactions

The rheological behaviour of emulsion filled gels has been extensively studied due to their importance in pharmaceuticals, cosmetics and foods. In 1956, Kerner established a model for gels filled with strongly bound particles, which predicts that these particles increase the storage modulus of a gel (Oliver et al., 2015b; Kerner, 1956). Oil droplets have been reported to behave in a similar manner (Dickinson, 2012; Sala et al., 2007). The rheological properties of an emulsion gel depend on (Dickinson and Chen, 1999; Sala et al., 2008):

- i. the properties of the background gel matrix (biopolymer composition, crosslinking density, biopolymer concentration, etc.) and the properties of the emulsified oil droplets, *i.e.*, the filler (fatty acid composition, droplet size);
- ii. the filler volume fraction;
- iii. the filler - matrix interactions;
- iv. the state of aggregation of the filler.

In general, the final rigidity of emulsion gels is often greater than the rigidity of the corresponding protein gels without the filler due to denatured protein adsorbed on the oil droplets forming crosslinks with protein unfolded in the matrix (Dickinson, 2012).

2.3.1 Theoretical models

In emulsion gels, oil droplets are often hypothesized to behave like solid particles. In this case, both van der Poel theory (1958) and Kerner theory (1956) of the shear modulus, G' , of a composite gelled material can be applied (Oliver et al., 2015b), which are based on three assumptions (Sala et al., 2007):

- i. The filler particles are entirely adherent to the matrix,
- ii. The filler particles remain as independent particles and do not interact with each other, *i.e.*, emulsion droplets are not flocculated,
- iii. The filler particles are homogeneously distributed throughout the matrix.

These theories predict three different regimes of mechanical behaviour during small deformation depending upon the filler volume fraction for given moduli of the matrix (G'_m) and filler particles (G'_f):

- i. $G'_f < G'_m$: Filler particles deform more than the matrix,

- ii. $G'_f = G'_m$: Filler particles deform equally to the matrix,
- iii. $G'_f > G'_m$: Filler particles deform less than the matrix.

The shear modulus of liquid filler particles G'_f was later estimated by van Vliet (1988) according to the Laplace pressure $G'_f = \frac{2\gamma_T}{R}$, where R is the radius of monodispersed oil droplet and γ_T is the oil-water interfacial tension (Sala et al., 2007; van Vliet, 1988). In this study, van Vliet included the aspect of non-interacting filler particles, where the storage moduli of non-interacting filled gels approached the theoretical behaviour of unfilled gel with increasing filler volume fraction (*i.e.*, the filled gel modulus decreases with increasing filler volume fraction under small deformation).

Filler-matrix interactions are theoretically dependent on the composition of the adsorbed layer at the oil interface. Some layers can chemically interact with the polymer matrix (*e.g.*, protein adsorbed onto oil droplets can interact with the protein gel network) whereas other layers may weakly interact with the matrix (*e.g.*, surfactant coated oil droplets weakly interact with the protein gel network) (Dickinson, 2012). The extent and strength of filler-matrix interactions are difficult to quantify since different thermal processing and distribution of surface active components between bulk and interface lead to different filler-matrix interactions. To our knowledge, no adequate method exists to directly quantify the extent and strength of the filler- matrix

Table 2.2 Effects of active and inactive filler on the rheological behaviour of emulsion gels (G' : storage modulus; ϕ : volume fraction; \uparrow : increase; \downarrow : decrease).

	Active / Bound filler	Inactive / Unbound filler
Definition	Fillers are mechanically connected to the matrix. Such interaction can occur via electrostatic, hydrogen bonding, covalent bonding and/or hydrophobic interaction	Little or no chemical or physical affinity of the fillers for the surrounding matrix; fillers behave like small holes or “voids” within the matrix
Effect on elastic modulus of the filled emulsion gel (G' , Pa)	\uparrow or $\downarrow G'$ depending on $\frac{G_f}{G_M}$	$\downarrow G'$
Filler volume fraction (ϕ , %)	$\uparrow \phi \Rightarrow \uparrow G'$	Little effect of ϕ on G'
Filler droplet size (μm)	\uparrow droplet size $\Rightarrow \downarrow G'$	G' is independent to filler droplet size

interactions. Rheological measurement can, however, be an indirect method in understanding the type of interactions taking place.

In summary (Table 2.2), fillers can be classed as bound (“active”) or unbound (“inactive”) and have different effects with regards to the rheological behaviour of the emulsion gel (Dickinson and Chen, 1999; Dickinson, 2012).

2.3.2 Factors affecting the mechanical properties of emulsion gels

The presence of oil droplets affects the overall rheological behaviour of emulsion gels depending on several factors. Extensive studies have been carried out on filler-matrix interactions, particularly in whey protein emulsion gels (Dickinson, 1998). Table 2.3 shows a compilation (non-exhaustive) of various whey protein-based emulsion gels, where the emulsion droplets act as active fillers, the factors which dictate different kinds of interactions and the resultant rheological behaviour are also highlighted. In this section, we describe some of these systems with respect to two key variables, *i.e.*, filler and matrix properties.

2.3.2.1 Effect of filler

Types of emulsifier

The type of emulsifying agent dictates the nature of interactions between the droplet surface and matrix (*i.e.*, active or inactive filler). Whey protein stabilised emulsion droplets in a whey protein gel generally acts as “active” or “bound” fillers and enhance the gel strength. On the other hand, droplets stabilised by non-ionic or ionic surfactant will interact weakly with protein gel matrix, decreasing the storage modulus (Chen et al., 2001; Dickinson and Chen, 1999; McClements et al., 1993). These “inactive” or “unbound fillers” will decrease the elastic modulus – except if the droplets are small and rigid – compared to active fillers, regardless of droplet size, droplet volume fraction, etc., (Dickinson and Chen, 1999) (Figure 2.2). In the case of a mixed monolayer protein and surfactants, such as Tween 20, surfactants tend to displace proteins due to their stronger interaction with the oil droplet interfaces. Hence, oil droplets will not interact with the protein matrix, weakening the chemical affinities between the filler and the matrix, which results in the decrease of the gel strength (Chen et al., 2000; Dickinson and Chen, 1999; Dickinson, 2012; Sala et al., 2008). For

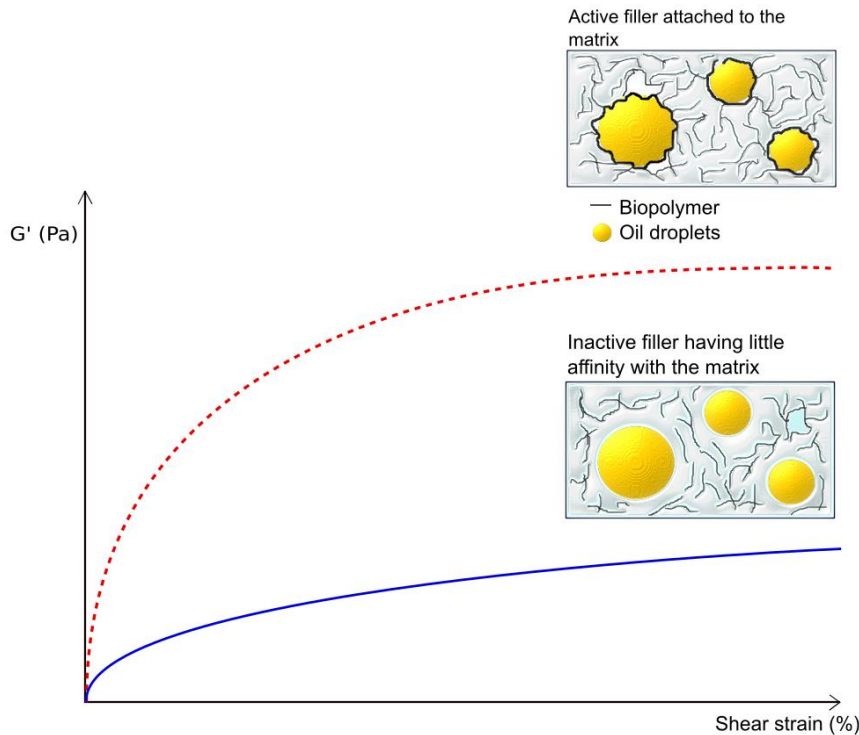


Figure 2.2 Schematic diagram illustrating the effect of fillers on G' . (Solid line: inactive filler; dotted line: active filler).

instance, Chen et al. (2000) investigated the viscoelastic properties of heat set WPI stabilised emulsion gels in presence or absence of added emulsifier. The study showed that the G' of whey protein emulsion gel was five times higher ($G' = 5.05$ kPa) as compared to that of mixed whey protein + Tween 20-stabilized emulsion gel ($G' = 0.95$ kPa).

Droplet volume fraction

Several authors have reported that increasing the concentration of active fillers increases G' (Dickinson and Chen, 1999; Sok et al., 2005; Yost and Kinsella, 1992). Chen and Dickinson (1998) studied the effect of droplet volume fraction (0 – 45 vol%) on 10 wt% whey protein emulsion gels and observed a significant increase in gel strength when droplet volume fraction was above 20 vol% (Table 2.3).

Emulsion droplet size and emulsifier concentration

A balance has to be found between emulsion droplet size and emulsifying agent concentration. Small droplets have a larger surface area which needs to be covered by surfactant. Thus, a high concentration of emulsifier is required to avoid bridging

Table 2.3 Filler-matrix interactions and rheological behaviour of whey protein emulsion gels (G' : storage modulus, ϕ : volume fraction; []: concentration, \uparrow : increase; \downarrow : decrease; \Rightarrow : leads to).

Processing condition	Oil:WP I ratio	[WPI] (wt%)	Processing conditions	Mechanical Behaviour	References
<i>Thermal treatment</i>	2 : 1 10 : 1	10-15	pH \approx 7 90 °C 15 – 30 min 0 – 200 mM NaCl	<ul style="list-style-type: none"> • Active filler $\Rightarrow \uparrow G'$ 	(Sung et al., 2015; McClements et al., 1993)
	5 : 1, 10 : 1	6-9	pH \approx 7 85 °C 30 min	<ul style="list-style-type: none"> • $\uparrow \phi \Rightarrow \uparrow G'$ • \uparrow number of crosslinks $\Rightarrow \uparrow G'$ • \downarrow oil droplet size $\Rightarrow \uparrow G'$ • Interfacial aging of the emulsion $\Rightarrow \downarrow G'$ 	(Chen and Dickinson, 1998; Chen and Dickinson, 1999a; Chen and Dickinson, 1999b; Chen et al., 2000)
	1 : 4, 1 : 1, 33 : 1,	5-30	pH \approx 4.6 – 5 50 – 90 °C 15 min	<ul style="list-style-type: none"> • \uparrow [protein] $\Rightarrow \uparrow$ gel strength • WPI precipitates at pH close to its pI (5.2) \Rightarrow random aggregation and $\uparrow G'$ 	(Moakes et al., 2015b; Yost and Kinsella, 1992)
<i>Divalent ions</i>	1 : 1, 1.5 : 1, 2 : 1, 2.8 : 1, 4.3 : 1	8-10	pH 4 – 6.8 12 – 140 mM CaCl ₂	<ul style="list-style-type: none"> • $\uparrow \phi$ + same [Ca²⁺] \Rightarrow structural changes from particulate to both fine stranded and random aggregates • Same ϕ + \uparrow [Ca²⁺] \Rightarrow larger gel pores + protein aggregates • \uparrow [Ca²⁺] \Rightarrow particulate structure of random aggregates + oil droplets flocculation (calcium bridging) • \downarrow [Ca²⁺] \Rightarrow filamentous network 	(Beaulieu et al., 2002; Egan et al., 2013; Sok et al., 2005)

flocculation and aggregation. With larger droplets an excess of micellar emulsifier might lead to depletion flocculation which can be beneficial in increasing a gel's strength as discussed in the next section (Boutin et al., 2007; Chen and Dickinson, 1998; Yost and Kinsella, 1992).

In terms of emulsion droplets size McClements et al. (1993) reported that emulsion gels prepared with 10 wt% whey protein isolate (WPI) and 40 wt% oil showed a 100 % increase in G' on decreasing the mean droplet diameter (d_{32} value) from approximately 4 to 0.7 μm . Decreasing emulsion droplet size at a constant volume fraction increases the total droplet surface area. With this increase in surface area-to-volume ratio, they become more closely packed and the number of protein interactions between droplets increases (Sala et al., 2009). Therefore, smaller droplets reinforce the matrix and increase the elastic modulus to a greater extent. In comparison, large droplets have been observed to have a lower impact on strengthening the gel matrix (McClements, et al., 1993; Yost & Kinsella, 1992).

Flocculation of emulsion droplets

Recently, Oliver et al. (2015a) showed the effects of emulsion droplet clustering using emulsions (1 wt% WPI, 40 wt% oil) in a gelatin matrix (4 to 10 wt%). At a slow gelation rates, depletion interactions allowed aggregation of droplets in the absence of other attractive interactions between adjacent droplets. This led to a heterogeneous distribution of droplets distribution in a homogeneously gelled matrix (Oliver et al., 2015a). Clustering of emulsion droplet thus lead to an increase in the G' . Sala et al. (2007) also showed that aggregated emulsion droplets had a greater impact on the rheological properties of the emulsion gels due to the increase in localized volume fraction. van Aken et al. (2015), explained the effect of particle clustering using a theoretical model. This model recognizes that the deformability of aggregated particles is linked to the volume fraction inside each cluster and their firmness.

Solid fat content

The firmness of aggregated droplets can also be increased by increasing the solid fat content of droplets, which increases G' . The effective modulus of liquid oil droplets is related to their Laplace pressure $\Delta P = \frac{2\gamma_T}{R}$ where R is the radius of monodispersed oil droplet and γ_T is the oil-water interfacial tension for an emulsion (Oliver et al., 2015b; van Vliet, 1988). The modulus of solid fat droplets is related to

the presence of a fat crystal network enhancing the droplets rigidity. Therefore, a higher solid fat content containing larger fat crystal network increases the firmness of the emulsion droplet which in turn increases G' of the emulsion gel. Oliver et al. (2015b) showed that at 4 °C, 9 % (w/w) WPI stabilised emulsion gel with low solid fat content (27%) had a 20-fold lower tangential stress (12.1 kPa), compared to that with higher solid fat content (61.6%, 251.7 kPa). Furthermore, compared to liquid oil droplets, higher solid fat droplets are more prone to partial coalescence due to fat needles from one droplet protruding into adjacent droplets. Such partial coalescence can significantly increase the effective droplet volume fraction, which strengthens the emulsion gel further (Dickinson, 2006; Oliver et al., 2015b; Yost and Kinsella, 1992).

Interfacial ageing

In case of emulsion gels with active fillers, the extent of strengthening is also dependent on the age of the interfacial adsorbed layer if it consists of a biopolymer (Dickinson, 2012). Studies conducted by Chen and Dickinson (1999b) have indicated that aged (1 day to 1 week) protein-stabilised emulsion droplets have weaker affinities for the protein in the matrix ($G' < 1$ kPa) as compared to freshly prepared emulsion gel ($G' > 3$ kPa). Interactions can occur between folded and unfolded protein in the bulk and protein already adsorbed at the surface of the emulsion droplets within the solution although the aged adsorbed protein will be unfolded in a different way. The sulfhydryl groups can lose their reactivity due to rapid conformational changes of the adsorbed protein structure during surface ageing. Therefore, the filler and matrix are less bound to each other, which decreases G' (Chen and Dickinson, 1999b).

2.3.3 Matrix properties

The concentration of gelling agent influences the rheology of emulsion gels as explained by the van Vliet theory of emulsion gels with either active or inactive fillers. The modulus increases or decreases depending on the ratio between the matrix modulus and the filler modulus (Table 2.2). For the matrix itself, variation of gelling agent concentration typically alters the G' according to a power law relation, *i.e.*, $G' \approx C^n$ (C: concentration of protein; n: power law) (Puyol et al., 2001). At high concentrations of gelling agent, the number of bonds between molecules are more important than at lower concentrations. Decreasing the amount of voids (free space)

in gels leads to denser gels (Boutin et al., 2007). Studies conducted on emulsion gels, as described in Table 2.3, also show similar results, *i.e.*, higher matrix concentration leads to firmer gels (Fitzsimons et al., 2008; Oliver et al., 2015b; Sala et al., 2009; Tesch et al., 2002). For instance, Chen and Dickinson (1998) reported that increasing the concentration of WPI from 1 wt% to 8 wt% in an emulsion gel containing 20 vol% oil nearly doubled the G' of the emulsion gel. Nevertheless, a critical gelling agent concentration was noticed by Chen and Dickinson (1998) for active oil droplets, which depends on the oil volume fraction and the source of the protein. For instance, a pure protein gel formed with 14 wt% WPI had the same strength as an emulsion gel formed with 3 wt% WPI and a high filler volume fraction (45 vol% oil). Above this critical matrix concentration, the storage modulus of the matrix G'_m is so high that the effect of the filler is insignificant (Chen and Dickinson, 1998; van der Poel, 1958).

In summary, the mechanical behaviour of a gel can be controlled by tuning the properties of the inner phase (emulsion droplets) and the biopolymer matrix. Interestingly, most literature on emulsion gels with active fillers has focussed on whey protein-based emulsion gels. Literature on starch-based emulsion gels where modified starch acts as both surfactant and gelling agent appears largely unexplored. This might be an interesting field of research to explore systematically to understand if OSA starch-stabilized droplets act as active fillers or not, and whether interfacial OSA starch interacts with the starch present at the continuous phase during thermal gelation.

2.4 Emulsion microgel particle formation

Emulsion microgel particles can be formed using two routes – a top-down' approach or a bottom-up' approach. In the top-down approach, large materials are broken down into small particles with the use of specific shearing equipment (McClements, 2014). For instance, emulsion gels with or without added lipophilic bioactive molecules, can be sheared in a controlled manner resulting in small gel particles. It can be hypothesized that the properties of filler-matrix interaction will be critical for the break-up of such microgel particles. This facile processing route has been successfully used in whey protein-based microgels (Sarkar et al., 2016c), and also holds potential for the creation of emulsion microgel particles too. In theory, emulsion gels with active fillers should be better for this top-down processing so that the oil

droplets contained within do not coalesce and leak out of the gel particles during the shearing process. This is a research question which needs exploration.

In comparison the bottom-up approach is based on the spontaneous formation of particles due to alteration of molecular interactions forcing molecules to rearrange themselves (McClements, 2014). In this case, the starting emulsion is directly gelled into micron-sized soft emulsion particles using different techniques under appropriate conditions such as ionic strength, temperature, pH, etc.

2.4.1 Formation of emulsion microgel particles using bottom-up approaches

2.4.1.1 Polymer extrusion route

Polymer extrusion is a process in which a polymer at relatively high concentration is forced through a nozzle at a certain pressure, flow rate and temperature. The polymer extruded through the nozzle usually changes texture due to the release of steam or reaction with ions, leading to its gelation (Harper and Clark, 1979). Whey protein microgel particles without filler emulsions have been successfully prepared using this technique by extruding denatured WPI into CaCl_2 solution (Egan et al., 2014). This method required a heating step during which whey proteins were denatured and polymerized into soluble aggregates, followed by a cooling step and the subsequent addition of calcium ions, which results in the formation of a network via Ca^{2+} -mediated interactions of soluble aggregates. This Ca^{2+} -mediated cold gelation of whey protein may be compared to alginate gelation, which results from a dimeric association of guluronic and mannuronic acid regions with Ca^{2+} in the “egg box” formation.

Formation of emulsion microgel particles via extrusion can also be achieved by passing the emulsion through a nozzle where gelled emulsion particles would exit the extrusion device due to heat, salt or acid treatment or their combination. Pre-treated whey protein-stabilised emulsions have been reported to successfully gel into emulsion microgel particles or “emulsion gel beads” using such an external gelation method (Beaulieu et al., 2002; Egan et al., 2013; Ruffin et al., 2014). The technique involved extruding emulsion droplets stabilised by denatured WPI through a syringe into a bath containing CaCl_2 solution (Egan, Jacquier, Rosenberg, & Rosenberg, 2013). Calcium ions had numerous effects on the elasticity, size and morphology of the

resultant particles (Beaulieu et al., 2002; Liang et al., 2010). Higher concentrations of CaCl_2 led to a decrease in the size of the microgel particle as well as an increase in their sphericity. Beaulieu et al. (2002) related this effect to the increase in kinetics of gelation via calcium ions. An increase in Ca^{2+} concentration increases the amount of ionic bridges formed between calcium ions and sulfhydryl groups on the protein which increases protein-protein interactions and aggregation, leading to an accelerated formation of a three-dimensional network. As the gelation kinetic is accelerated droplets do not have enough time to destabilize via screening of electrostatic repulsion by Ca^{2+} and small emulsion microgel particles can be produced. In the case of the internal gelation technique, the first step is to emulsify the oil, containing insoluble calcium in the form of CaCO_3 , with denatured WPI. The subsequent addition of acid results in the release of calcium ions and the gelation of the denatured WPI.

As compared to the top-down approach, the bottom-up approach of polymer extrusion excludes the use of high temperature on the encapsulated bioactive molecule since it is a cold gelation technique. However, the main disadvantage of the polymer extrusion technique is the large size of the microgel particles formed ($> 500 \mu\text{m}$), though internal gelation has the ability to form smaller particles ($< 100 \mu\text{m}$). The size of the particles formed via external gelation mainly depends on the nozzle or syringe diameter which has a restricted range of sizes. In comparison, particles size formed via internal gelation depends on the emulsion droplet size generated by the multiple emulsion which can be controlled by the concentration of CaCO_3 , stirring rate and oil volume fraction allowing better control over particle size than the former. As particles over $100 \mu\text{m}$ impact the sensory perception of food, these might have some adverse sensory aspects when incorporated in food.

As well as external or internal gelation via polymer extrusion, co-extrusion techniques have also been investigated in literature. In this case, a surfactant stabilised emulsion is first prepared and then mixed with alginate solution followed by Ca^{2+} -ion mediated gelation using a spray aerosol method. Ching et al. (2015) showed that the alginate microgel particles with filled emulsion droplets had droplet sizes in the range of $20 - 80 \mu\text{m}$. During this process (in between the period of the emulsification and the extrusion process), there is a possibility that as the droplets are gelled, shrinkage of the microgel particles might bring the droplets closer to each other, resulting in droplet coalescence. Furthermore, it requires an additional hydrocolloid (*i.e.*, alginate), which has several disadvantages such as the increase of the cost, the emulsifier might

also be thermodynamically incompatible with the biopolymer gel or depletion flocculation of the oil droplets before gelation might occur. Therefore, during the period in between the emulsification and extrusion process, flocculation and coalescence of the oil droplets will influence the distribution and size of the oil droplets entrapped within the emulsion microgel particles.

2.4.1.2 Multiple emulsion templating route

Sung et al. (2015) described a new method of producing emulsion microgel particles using a multiple emulsion templating route. In this study, Sung et al. (2015) gelled the aqueous phase of an oil-in-water-in-oil multiple emulsion via thermal gelation of the whey protein in the inner aqueous phase. The emulsion microgel particles were separated from the secondary oil phase using an organic solvent. The advantage of this method is that it produces small particles ($d_{32} \sim 12 \mu\text{m}$). However, this method is time consuming due to the number of processing steps required and the use of organic solvent limits its applications in food. Egan et al. (2013) prepared emulsion microgel particles using a combination of internal gelation method and multiple emulsion templating. Compared to external gelation, this technique was mainly affected by the stirring rate, which allowed reduction of the size of the particles below $100 \mu\text{m}$.

2.4.1.3 Fluid gel route

Recently, the new technique of fluid gels has been presented by Moakes et al. (2015b) building on research done on multiple emulsion hydrogels and shear gels. This is a bottom-up approach as shear is applied to a biopolymer solution that is undergoing sol-gel transition. The shearing process prevents the formation of a continuous protein network and instead produces discrete spherical gel particles (Garrec and Norton, 2012; Moakes et al., 2015b). The particle size and morphology of the microgels formed are controlled by the shear rate and thermal history of the biopolymers. Research on fluid gels formed with whey protein, at a typical concentration of 10 wt% shows that the shear applied to the primary aggregates of whey protein restricts particle-particle aggregation and therefore complete whey protein gelation. This restricted sol-gel transition alters whey protein interactions forcing the molecules to rearrange themselves. In terms of thermal treatment, the rapid heating rate increases particle-particle interactions (due to Brownian motion) and strengthens hydrophobic interactions between protein aggregates makes them resistant to shear. Therefore, large

aggregated particles are formed. In comparison, low heating rates decreases the protein aggregation rate and do not strengthen hydrophobic interactions. Thus, the aggregates formed are smaller and single non aggregated particles can also be produced (Moakes et al., 2015a).

Using the same design principle, emulsion fluid gel particles were prepared. An oil-in-water emulsion (5 to 20 vol% oil) was first stabilised using a solution of WPI (5 to 30 wt%). The emulsion was then heat treated (0.5 °C/min to 80 °C), which started the protein denaturation process and hydrophobic aggregation. Shear (450 rpm) was applied, preventing the entirety of the emulsion to gel. As a result, WPI adsorbed onto the oil droplets was gelled forming emulsion fluid gel particles (Moakes et al., 2015b).

2.5 Delivery of lipophilic molecules using emulsion microgel particles

In general, on ingestion, emulsion microgel particles are expected to be exposed to a wide range of physical (*e.g.*, shear and temperature) and biochemical (*e.g.*, dilution, ionic strength, pH, pepsin, amylase, pancreatin, mucins and bile salts) conditions as it passes through the mouth, the stomach and the intestines (Singh and Sarkar, 2011). During its physiological transit, the emulsion microgel particle can release the encapsulated active molecule by two approaches: 1. Swelling of the particle due to pH and environmental ionic strength and 2. Erosion due to enzymatic degradation or shear. Figure 2.3 illustrates the release of active molecules when triggered by particular physical and/or biochemical factors.

2.5.1 Swelling of emulsion microgel particles

The swelling of emulsion microgel particles containing ionized or ionisable groups can occur depending on the pH and ionic strength of the environment (Beaulieu et al., 2002). As illustrated in Figure 2.3, when emulsion microgel particles with ionisable groups are exposed to a specific pH, loss of attractive electrostatic interactions drives the charged groups apart. This repulsion might lead to the swelling of emulsion microgel particle, which increases the pore size (Zhang et al., 2015a). If the lipophilic active molecules are smaller than the stretched pores, they can more

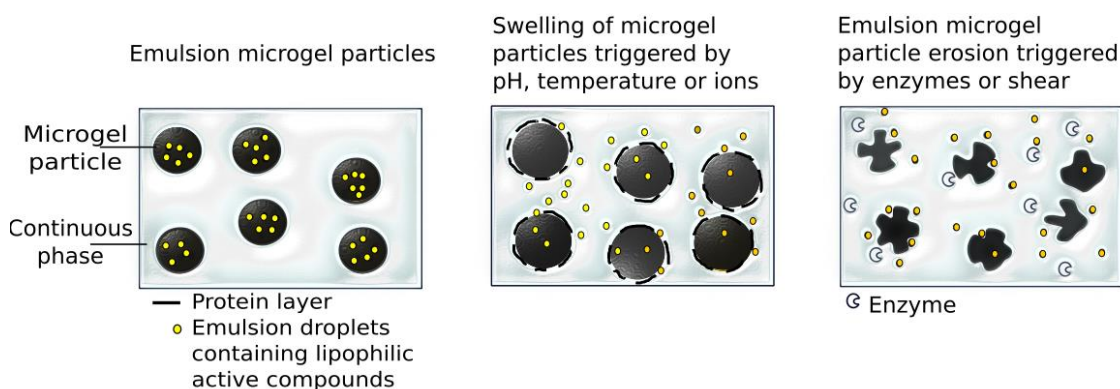


Figure 2.3 Schematic representation of controlled release of lipophilic molecules from emulsion microgel particle via swelling or matrix erosion.

easily diffuse out or, if the active molecules are electrostatically bound, they would more be easily released. The swelling of the gel pores has also shown to allow for bile salts and enzymes to diffuse into the particles, resulting in the solubilisation and digestion of the lipophilic compound by the bile salts micelles as well as the transport of the active to the intestinal walls (Liu et al., 2002; Li et al., 2011). Therefore, controlling the environment or tuning the microgel can allow control of their swelling ratio. This swelling ratio can be calculated in two different ways:

i. Fick's model of diffusion: This can be used to predict the release of the entrapped lipophilic molecules from swollen gels (Paulsson and Edsman, 2002; Ritger and Peppas, 1987);

$$Q = 2C_0K \frac{Dt^{1/2}}{\pi} \quad (2.1)$$

with Q the amount of active molecules released per unit area, C_0 the initial concentration of active molecules in emulsion microgel particles, K the partitioning coefficient defined as $K = C_g/C_o$, where C_g and C_o are the concentrations of soluble active molecules in the gel and oil phase, respectively, t the time elapsed since the release experiment started and D the diffusion coefficient of active molecules in the emulsion microgel.

i. Swelling ratio: This calculates the weight change before and after incubation of emulsion gel particles in a particular environment, such as the oral or gastrointestinal phase (Beaulieu et al., 2002; Gunasekaran et al., 2007; Liang et al., 2010)

$$\text{Swelling ratio or water uptake ability (\%)} = \frac{w_w - w_d}{w_d} \times 100 \quad (2.2)$$

with w_w the wet weight of emulsion microgel particles and w_d their dry weight.

Studies conducted on whey protein emulsion microgel particles have reported that at pre-prandial acidic / gastric pH (1.9), the particles did not extensively swell (Swelling ratio = 20%). It is expected that all negatively charged carboxyl groups at the surface of the particle are neutralized however the protein chain contains few positively charged amine groups, leading to low electrostatic repulsive forces. At a pH close to the protein pI (pH 5.2), the swelling ratio was lowest (Swelling ratio = 13%) as the net charge of the protein is close to zero. There was no electrostatic repulsion. At intestinal pH (6.9), the swelling ratio was quite high (Swelling ratio = 42%) because whey protein had a high amount of negatively charged carboxyl groups, leading to strong electrostatic repulsive forces, which allowed the uptake of water (Beaulieu et al., 2002; Gunasekaran et al., 2007; Gunasekaran et al., 2006). Additionally, several authors reported that the protein concentration had an effect on the swelling ratio of beads. At higher protein concentration, the cross-linking density of the microgel network was higher, leading to a decrease in the swelling ratio. Hence, it takes longer for particles to swell and liberate the encapsulated substance, which can be a strategy for a slow release (Egan et al., 2013; Gunasekaran et al., 2007).

In comparison to protein, OSA starch based emulsion microgel systems might not be affected by the environmental pH or ionic strength (Tesch et al., 2002), since it is only weakly charged, which is an interesting area for further research.

2.5.2 Matrix erosion by enzyme degradation

During physiological processing, enzymes degrade biopolymers enabling the erosion of the matrix and the release of the encapsulated compounds. As compared to swelling, the matrix is eroded either partly or completely, enabling a burst release. So, it can be expected that whey protein emulsion microgel particles would be digested by proteolytic enzymes, such as trypsin or pepsin, whereas OSA starch based microgel particles would be digested by α -amylase, unless their susceptible bonds were engineered to be inaccessible or partly accessible to the enzymes. Studies conducted by Beaulieu et al. (2002) reported that whey protein emulsion microgel particles were

resistant to gastric enzymes such as pepsin but were attacked by intestinal enzyme mixtures such as pancreatin, so a targeted intestinal delivery seems plausible.

This is quite unlike the behaviour of whey protein emulsions or whey protein based microgel particles which are readily hydrolysed by pepsin at gastric pH (Sarkar et al., 2009; Sarkar et al., 2016c; Singh and Sarkar, 2011). Resistance of emulsion microgel particles to pepsin might be attributable to the reburial of hydrophobic groups during the emulsification and gelation processes, with little or no accessibility to pepsin. Nevertheless, during intestinal digestion emulsion microgel particles were digested by trypsin and chymotrypsin. The former acts on the carboxyl end of peptide bond involving lysine and arginine, whereas, the later attacks peptide bonds at large hydrophobic groups (Beaulieu et al., 2002; Gunasekaran et al., 2007; Kananen et al., 2000).

In modified starch hydrogels, during oral and intestinal processing, α -amylase would hydrolyse the starch to some extent. The amount of amylose contained in the starch will affect the strength of the gel matrix (Mun et al., 2015b) – higher amounts lead to a more compressed and packed structure (Tangsrianugul et al., 2015). This increase in strength and/or compactness as well as cross-linking achieved through processing might enable prevention of immediate matrix erosion via α -amylase attack (Atyabi et al., 2006).

2.6 Conclusions

From this literature review, it seems that only few studies have been conducted on the design and characterization of emulsion microgel particles in order to control the delivery of lipophilic material. However, emulsion gels containing active or inactive fillers and their rheological properties have been well characterised. Such knowledge will enable the creation of emulsion microgel particles with triggered release properties.

Emulsion microgels particle might be carefully designed using top down approaches of controlled shearing of emulsion gels with active fillers, or bottom up approaches using polymer extrusion, fluid gels, or multiple emulsion templating. Such particles could be used to release the encapsulated lipophilic phase in a sustained or burst manner via erosion due to shear treatment or enzyme degradation, such as with

amylase or pancreatin, or swelling of the matrix due to changes of pH and ionic strength in the physiological regime. Many food proteins and polysaccharides can be used to form edible emulsion microgel particles. The use of modified starch and dairy proteins would be of great interest, since they show potential for emulsion microgel particle formation by acting as both emulsifying and bulk gelling agents. Furthermore, these biopolymers have specific responsiveness to pH, ionic strength, enzymes, etc., which can be exploited for tailored properties.

The following chapters, of this thesis, will focus on demonstrating how by using starch, “active” emulsion gels can be formed resulting in the creation of starch-based emulsion microgel particles via a top-down approach (**Chapter 3**). Additionally, the design of size tuneable whey protein-based emulsion microgel particles will be studied as a function of processing conditions (*i.e.*, looking at different gelation kinetics through the use of different concentrations of calcium ions and different mixing conditions) (**Chapter 4**). Both types of emulsion microgel particles will then be examined, as to whether the encapsulated material can be released in a controlled manner at specific physiological sites *i.e.*, oral phase (**Chapter 5**) and gastrointestinal phase (**Chapter 6**).

2.7 References

- Alting, A.C. et al. 2003. Cold-set globular protein gels: Interactions, structure and rheology as a function of protein concentration. *Journal of Agricultural and Food Chemistry*. **51**(10), pp.3150-3156.
- Anton, M. et al. 2001. Filler effects of oil droplets on the rheology of heat-set emulsion gels prepared with egg yolk and egg yolk fractions. *Colloids and Surfaces B: Biointerfaces*. **21**(1–3), pp.137-147.
- Atyabi, F. et al. 2006. Cross-linked starch microspheres: effect of cross-linking condition on the microsphere characteristics. *Arch Pharm Res*. **29**(12), pp.1179-86.
- Augustin, M.A. and Sanguansri, L. 2012. 2 - Challenges in developing delivery systems for food additives, nutraceuticals and dietary supplements A2 - Garti, Nissim. In: McClements, D.J. ed. *Encapsulation Technologies and Delivery*

- Systems for Food Ingredients and Nutraceuticals*. Woodhead Publishing, pp.19-48.
- Ballauff, M. and Lu, Y. 2007. "Smart" nanoparticles: Preparation, characterization and applications. *Polymer*. **48**(7), pp.1815-1823.
- Bao, J. et al. 2003. Physical Properties of Octenyl Succinic Anhydride Modified Rice, Wheat, and Potato Starches. *Journal of Agricultural and Food Chemistry*. **51**(8), pp.2283-2287.
- Beaulieu, L. et al. 2002. Elaboration and characterization of whey protein beads by an emulsification/cold gelation process: application for the protection of retinol. *Biomacromolecules*. **3**(2), pp.239-248.
- Bhosale, R. and Singhal, R. 2007. Effect of octenylsuccinylation on physicochemical and functional properties of waxy maize and amaranth starches. *Carbohydrate Polymers*. **68**(3), pp.447-456.
- Boutin, C. et al. 2007. Characterization and acid-induced gelation of butter oil emulsions produced from heated whey protein dispersions. *International Dairy Journal*. **17**(6), pp.696-703.
- Briuglia, M. et al. 2014. Sustained and controlled release of lipophilic drugs from a self-assembling amphiphilic peptide hydrogel. *International Journal of Pharmaceutics*. **474**(1-2), pp.103-111.
- Bryant, C.M. and McClements, D.J. 1998. Molecular basis of protein functionality with special consideration of cold-set gels derived from heat-denatured whey. *Trends in Food Science & Technology*. **9**(4), pp.143-151.
- Chen, J.S. and Dickinson, E. 1998. Viscoelastic properties of heat-set whey protein emulsion gels. *Journal of Texture Studies*. **29**(3), pp.285-304.
- Chen, J.S. and Dickinson, E. 1999a. Effect of surface character of filler particles on rheology of heat-set whey protein emulsion gels. *Colloids and Surfaces B-Biointerfaces*. **12**(3-6), pp.373-381.
- Chen, J.S. and Dickinson, E. 1999b. Interfacial ageing effect on the rheology of a heat-set protein emulsion gel. *Food Hydrocolloids*. **13**(5), pp.363-369.
- Chen, J.S. et al. 2000. Mechanical properties and microstructure of heat-set whey protein emulsion gels: Effect of emulsifiers. *Lebensmittel-Wissenschaft Und Technologie-Food Science and Technology*. **33**(4), pp.299-307.

- Chen, J.S. et al. 2001. Protein-based emulsion gels: Effects of interfacial properties and temperature. In: Dickinson, E. and Miller, R. eds. *Food Colloids: Fundamentals of Formulation*. Cambridge: Royal Soc Chemistry, pp.384-391.
- Ching, S.H. et al. 2015. Physical stability of emulsion encapsulated in alginate microgel particles by the impinging aerosol technique. *Food Research International*. **75**, pp.182-193.
- Ching, S.H. et al. 2016. Rheology of emulsion-filled alginate microgel suspensions. *Food Research International*. **80**, pp.50-60.
- Chivero, P. et al. 2016. Assessment of soy soluble polysaccharide, gum arabic and OSA-Starch as emulsifiers for mayonnaise-like emulsions. *LWT - Food Science and Technology*. **69**, pp.59-66.
- Chung, C. et al. 2013. Oil-filled hydrogel particles for reduced-fat food applications: Fabrication, characterization, and properties. *Innovative Food Science & Emerging Technologies*. **20**, pp.324-334.
- Dang, H.V. et al. 2009. Rheology and microstructure of cross-linked waxy maize starch/whey protein suspensions. *Food Hydrocolloids*. **23**(7), pp.1678-1686.
- Dickinson, E. 2006. Structure formation in casein-based gels, foams, and emulsions. *Colloids and Surfaces A: Physicochemical and Engineering Aspects*. **288**(1-3), pp.3-11.
- Dickinson, E. 2012. Emulsion gels: The structuring of soft solids with protein-stabilized oil droplets. *Food Hydrocolloids*. **28**(1), pp.224-241.
- Dickinson, E. 2015. Microgels - An alternative colloidal ingredient for stabilization of food emulsions. *Trends in Food Science & Technology*. **43**(2), pp.178-188.
- Dickinson, E. and Chen, J.S. 1999. Heat-Set Whey Protein Emulsion Gels: Role of Active and Inactive Filler Particles. *Journal of Dispersion Science and Technology*. **20**(1-2), pp.197-213.
- Dissanayake, M. et al. 2013. Denaturation of whey proteins as a function of heat, pH and protein concentration. *International Dairy Journal*. **31**(2), pp.93-99.
- Domian, E. et al. 2015. Rheological properties and physical stability of o/w emulsions stabilized by OSA starch with trehalose. *Food Hydrocolloids*. **44**, pp.49-58.
- Egan, T. et al. 2013. Cold-set whey protein microgels for the stable immobilization of lipids. *Food Hydrocolloids*. **31**(2), pp.317-324.
- Egan, T. et al. 2014. Cold-set whey protein microgels as pH modulated immobilisation matrices for charged bioactives. *Food Chemistry*. **156**, pp.197-203.

- Ettelaie, R. et al. 2016. Steric stabilising properties of hydrophobically modified starch: Amylose vs. amylopectin. *Food Hydrocolloids*. **58**, pp.364-377.
- Fitzsimons, S.M. et al. 2008. Segregative interactions between gelatin and polymerised whey protein. *Food Hydrocolloids*. **22**(3), pp.485-491.
- Garrec, D.A. and Norton, I.T. 2012. Understanding fluid gel formation and properties. *Journal of Food Engineering*. **112**(3), pp.175-182.
- Gunasekaran, S. et al. 2007. Use of whey proteins for encapsulation and controlled delivery applications. *Journal of Food Engineering*. **83**(1), pp.31-40.
- Gunasekaran, S. et al. 2006. Whey protein concentrate hydrogels as bioactive carriers. *Journal of Applied Polymer Science*. **99**(5), pp.2470-2476.
- Harper, J.M. and Clark, J.P. 1979. Food extrusion. *C R C Critical Reviews in Food Science and Nutrition*. **11**(2), pp.155-215.
- Hongsprabhas, P. and Barbut, S. 1997. Protein and salt effects on Ca²⁺-induced cold gelation of whey protein isolate. *Journal of Food Science*. **62**(2), pp.382-385.
- Joye, I.J. and McClements, D.J. 2014. Biopolymer-based nanoparticles and microparticles: Fabrication, characterization, and application. *Current Opinion in Colloid & Interface Science*. **19**(5), pp.417-427.
- Kakran, M. and Antipina, M.N. 2014. Emulsion-based techniques for encapsulation in biomedicine, food and personal care. *Current Opinion in Pharmacology*. **18**, pp.47-55.
- Kananen, A. et al. 2000. Influence of chemical modification of whey protein conformation on hydrolysis with pepsin and trypsin. *International Dairy Journal*. **10**(10), pp.691-697.
- Kawaguchi, H. 2014. Thermoresponsive microhydrogels: preparation, properties and applications. *Polymer International*. **63**(6), pp.925-932.
- Kerner, E.H. 1956. The Elastic and Thermo-elastic Properties of Composite Media. *Proceedings of the Physical Society. Section B*. **69**(8), p808.
- Kuhn, K.R. et al. 2010. Cold-set whey protein gels induced by calcium or sodium salt addition. *International Journal of Food Science & Technology*. **45**(2), pp.348-357.
- Li, Y. et al. 2011. Control of lipase digestibility of emulsified lipids by encapsulation within calcium alginate beads. *Food Hydrocolloids*. **25**(1), pp.122-130
- Liang, L. et al. 2010. In vitro release of α -tocopherol from emulsion-loaded β -lactoglobulin gels. *International Dairy Journal*. **20**(3), pp.176-181.

- Liu, X.D. et al. 2002. Characterization of structure and diffusion behaviour of Ca-alginate beads prepared with external or internal calcium sources. *Journal of Microencapsulation*. **19**(6), pp.775-782.
- Livney, Y.D. 2010. Milk proteins as vehicles for bioactives. *Current Opinion in Colloid & Interface Science*. **15**(1-2), pp.73-83.
- Loveday, S.M. et al. 2013. Innovative yoghurts: Novel processing technologies for improving acid milk gel texture. *Trends in Food Science & Technology*. **33**(1), pp.5-20.
- Lucey, J.A. and Singh, H. 1997. Formation and physical properties of acid milk gels: a review. *Food Research International*. **30**(7), pp.529-542.
- Ma, K. and An, Z. 2016. Enzymatically Crosslinked Emulsion Gels Using Star-Polymer Stabilizers. *Macromolecular Rapid Communications*. **37**(19), pp.1593-1597.
- Malone, M.E. and Appelqvist, I.A.M. 2003. Gelled emulsion particles for the controlled release of lipophilic volatiles during eating. *Journal of Controlled Release*. **90**(2), pp.227-241.
- Malone, M.E. et al. 2003. Oral behaviour of food hydrocolloids and emulsions. Part 2. Taste and aroma release. *Food Hydrocolloids*. **17**(6), pp.775-784.
- Mao, L.K. and Miao, S. 2015. Structuring Food Emulsions to Improve Nutrient Delivery During Digestion. *Food Engineering Reviews*. **7**(4), pp.439-451.
- Matalanis, A. et al. 2011. Structured biopolymer-based delivery systems for encapsulation, protection, and release of lipophilic compounds. *Food Hydrocolloids*. **25**(8), pp.1865-1880.
- McClements, D.J. 2014. Mechanical Particle Fabrication Methods. *Nanoparticle- and Microparticle-based Delivery Systems*. Boca Raton, Florida: Taylor and Francis Group, CRC Press, pp.123-148.
- McClements, D.J. 2015. Encapsulation, protection, and release of hydrophilic active components: Potential and limitations of colloidal delivery systems. *Advances in Colloid and Interface Science*. **219**, pp.27-53.
- McClements, D.J. and Li, Y. 2010. Structured emulsion-based delivery systems: controlling the digestion and release of lipophilic food components. *Adv Colloid Interface Sci*. **159**(2), pp.213-28.
- McClements, D.J. et al. 1993. Effect of emulsion droplets on the rheology of whey-protein isolate gels. *Journal of Texture Studies*. **24**(4), pp.411-422.

- Moakes, R.J.A. et al. 2015a. Preparation and characterisation of whey protein fluid gels: The effects of shear and thermal history. *Food Hydrocolloids*. **45**, pp.227-235.
- Moakes, R.J.A. et al. 2015b. Preparation and rheological properties of whey protein emulsion fluid gels. *Rsc Advances*. **5**(75), pp.60786-60795.
- Monahan, F.J. et al. 1996. Disulfide-mediated Polymerization Reactions and Physical Properties of Heated WPI-stabilized Emulsions. *Journal of Food Science*. **61**(3), pp.504-509.
- Mun, S. et al. 2015a. Control of beta-carotene bioaccessibility using starch-based filled hydrogels. *Food Chem*. **173**, pp.454-61.
- Mun, S. et al. 2015b. Control of lipid digestion and nutraceutical bioaccessibility using starch-based filled hydrogels: Influence of starch and surfactant type. *Food Hydrocolloids*. **44**, pp.380-389.
- Nicolai, T. et al. 2011. β -Lactoglobulin and WPI aggregates: Formation, structure and applications. *Food Hydrocolloids*. **25**(8), pp.1945-1962.
- Oliver, L. et al. 2015a. Influence of droplet clustering on the rheological properties of emulsion-filled gels. *Food Hydrocolloids*. **50**, pp.74-83.
- Oliver, L. et al. 2015b. Effect of fat hardness on large deformation rheology of emulsion-filled gels. *Food Hydrocolloids*. **43**, pp.299-310.
- Ortega-Ojeda, F.E. et al. 2005. Gel formation in mixtures of hydrophobically modified potato and high amylopectin potato starch. *Carbohydrate Polymers*. **59**(3), pp.313-327.
- Paulsson, M. and Edsman, K. 2002. Controlled Drug Release from Gels Using Lipophilic Interactions of Charged Substances with Surfactants and Polymers. *Journal of Colloid and Interface Science*. **248**(1), pp.194-200.
- Pizzoni, D. et al. 2015. Evaluation of aroma release of gummy candies added with strawberry flavours by gas-chromatography/mass-spectrometry and gas sensors arrays. *Journal of Food Engineering*. **167, Part A**, pp.77-86.
- Puyol, P. et al. 2001. Heat-induced gelation of whey protein isolates (WPI): effect of NaCl and protein concentration. *Food Hydrocolloids*. **15**(3), pp.233-237.
- Ritger, P.L. and Peppas, N.A. 1987. A simple equation for description of solute release II. Fickian and anomalous release from swellable devices. *Journal of Controlled Release*. **5**(1), pp.37-42.

- Ruffin, E. et al. 2014. The impact of whey protein preheating on the properties of emulsion gel bead. *Food Chemistry*. **151**, pp.324-332.
- Sala, G. et al. 2008. Matrix properties affect the sensory perception of emulsion-filled gels. *Food Hydrocolloids*. **22**(3), pp.353-363.
- Sala, G. et al. 2007. Effect of droplet-matrix interactions on large deformation properties of emulsion-filled gels. *Journal of Texture Studies*. **38**(4), pp.511-535.
- Sala, G. et al. 2009. Deformation and fracture of emulsion-filled gels: Effect of gelling agent concentration and oil droplet size. *Food Hydrocolloids*. **23**(7), pp.1853-1863.
- Sarkar, A. et al. 2016a. Microstructure and long-term stability of spray dried emulsions with ultra-high oil content. *Food Hydrocolloids*. **52**, pp.857-867.
- Sarkar, A. et al. 2009. Behaviour of an oil-in-water emulsion stabilized by β -lactoglobulin in an in vitro gastric model. *Food Hydrocolloids*. **23**(6), pp.1563-1569.
- Sarkar, A. et al. 2015. Impact of Protein Gel Porosity on the Digestion of Lipid Emulsions. *Journal of Agricultural and Food Chemistry*. **63**(40), pp.8829-8837.
- Sarkar, A. et al. 2016b. Emulsion stabilization by tomato seed protein isolate: Influence of pH, ionic strength and thermal treatment. *Food Hydrocolloids*. **57**, pp.160-168.
- Sarkar, A. et al. 2016c. In vitro digestion of Pickering emulsions stabilized by soft whey protein microgel particles: influence of thermal treatment. *Soft Matter*. **12**(15), pp.3558-69.
- Sarkar, A. and Singh, H. 2016. Emulsions and foams stabilised by milk proteins. In: McSweeney, P.L.H. and O'Mahony, J.A. eds. *Advanced Dairy Chemistry*. Springer New York, pp.133-153.
- Satapathy, S. et al. 2015. Development and Characterization of Gelatin-Based Hydrogels, Emulsion Hydrogels, and Bigels: A Comparative Study. *Journal of Applied Polymer Science*. **132**(8).
- Shewan, H.M. and Stokes, J.R. 2013. Review of techniques to manufacture microhydrogel particles for the food industry and their applications. *Journal of Food Engineering*. **119**(4), pp.781-792.

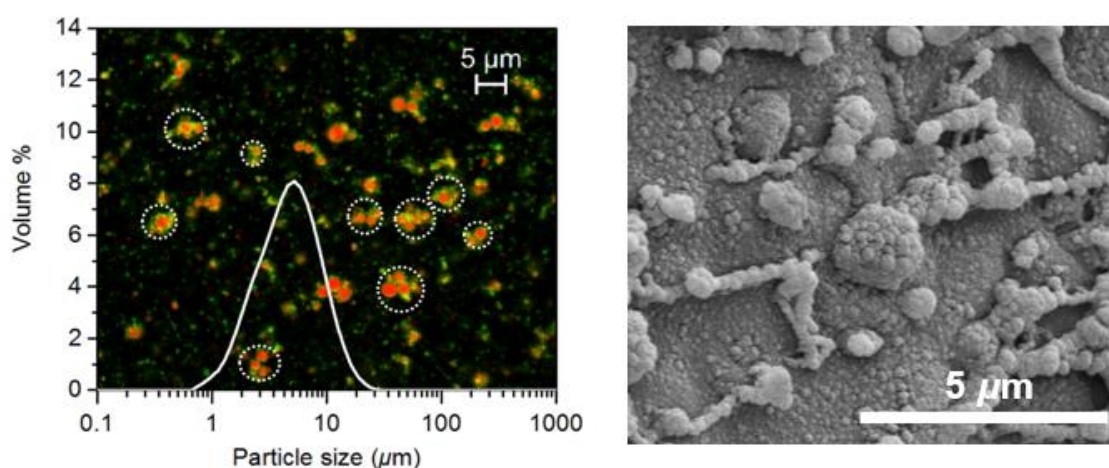
- Shogren, R.L. et al. 2000. Distribution of octenyl succinate groups in octenyl succinic anhydride modified waxy maize starch. *Starch - Stärke*. **52**(6-7), pp.196-204.
- Singh, H. and Sarkar, A. 2011. Behaviour of protein-stabilised emulsions under various physiological conditions. *Advances in Colloid and Interface Science*. **165**(1), pp.47-57.
- Sok, L.V.L. et al. 2005. Cold gelation of β -lactoglobulin oil-in-water emulsions. *Food Hydrocolloids*. **19**(2), pp.269-278.
- Sung, M.R. et al. 2015. Fabrication, characterization and properties of filled hydrogel particles formed by the emulsion-template method. *Journal of Food Engineering*. **155**, pp.16-21.
- Sweedman, M.C. et al. 2013. Structure and physicochemical properties of octenyl succinic anhydride modified starches: A review. *Carbohydrate Polymers*. **92**(1), pp.905-920.
- Tangsriangul, N. et al. 2015. Simulated gastrointestinal fate of lipids encapsulated in starch hydrogels: Impact of normal and high amylose corn starch. *Food Research International*. **78**, pp.79-87.
- Tesch, S. et al. 2002. Stabilization of emulsions by OSA starches. *Journal of Food Engineering*. **54**(2), pp.167-174.
- Thirathumthavorn, D. and Charoenrein, S. 2006. Thermal and pasting properties of native and acid-treated starches derivatized by 1-octenyl succinic anhydride. *Carbohydrate Polymers*. **66**(2), pp.258-265.
- Thorne, J.B. et al. 2011. Microgel applications and commercial considerations. *Colloid and Polymer Science*. **289**(5), pp.625-646.
- van Aken, G.A. et al. 2015. Rheological effect of particle clustering in gelled dispersions. *Food Hydrocolloids*. **48**, pp.102-109.
- van der Poel, C. 1958. On the rheology of concentrated dispersions. *Rheologica Acta*. **1**(2-3), pp.198-205.
- van Vliet, T. 1988. Rheological properties of filled gels. Influence of filler matrix interaction. *Colloid and Polymer Science*. **266**(6), pp.518-524.
- Velikov, K.P. and Pelan, E. 2008. Colloidal delivery systems for micronutrients and nutraceuticals. *Soft Matter*. **4**(10), pp.1964-1980.
- Wang, X.Y. et al. 2011. Preparation and characterisation of octenyl succinate starch as a delivery carrier for bioactive food components. *Food Chemistry*. **126**(3), pp.1218-1225.

- Wei, J. et al. 2016. Tailor-made microgel particles: Synthesis and characterization. *Colloids and Surfaces A: Physicochemical and Engineering Aspects*. **489**, pp.122-127.
- Wijayanti, H.B. et al. 2014. Stability of Whey Proteins during Thermal Processing: A Review. *Comprehensive Reviews in Food Science and Food Safety*. **13**(6), pp.1235-1251.
- Wolz, M. and Kulozik, U. 2015. Thermal denaturation kinetics of whey proteins at high protein concentrations. *International Dairy Journal*. **49**, pp.95-101.
- Yost, R.A. and Kinsella, J.E. 1992. Microstructure of Whey-Protein Isolate Gels Containing Emulsified Butterfat Droplets. *Journal of Food Science*. **57**(4), pp.892-897.
- Zhang, Z. et al. 2015a. Designing hydrogel particles for controlled or targeted release of lipophilic bioactive agents in the gastrointestinal tract. *European Polymer Journal*. **72**, pp.698-716.
- Zhang, Z. et al. 2015b. Development of food-grade filled hydrogels for oral delivery of lipophilic active ingredients: pH-triggered release. *Food Hydrocolloids*. **44**, pp.345-352.
- Zhang, Z. et al. 2015c. Food-grade filled hydrogels for oral delivery of lipophilic active ingredients: Temperature-triggered release microgels. *Food Research International*. **69**, pp.274-280.

Design of emulsion microgel particles

Chapter 3

Novel starch-based emulsion gels and emulsion microgel particles: design, structure and rheology²



Abstract

Novel starch-based emulsion microgel particles were designed using a facile top-down shear-induced approach. The emulsion droplets were stabilized using octenyl succinic anhydride (OSA) modified starch and incorporated into heat-treated and sheared wheat starch gels, forming emulsion gels. Using gelation kinetics and small deformation rheological measurements of sheared wheat starch gels and emulsion gels, OSA starch-stabilized emulsion droplets were demonstrated to act as “active fillers”. By varying starch concentrations (15 – 20 wt%) and oil fractions (5 – 20 wt%), optimal concentrations for the formation of emulsion microgel particles were identified. Microscopy at various length scales (transmission confocal laser scanning and cryo-scanning electron microscopy) and static light scattering measurements revealed emulsion microgel particles of 5 – 50 μm diameter. These novel emulsion microgel particles created via careful combination of gelatinized wheat starch and

² Published as: Torres, O., Tena, N.M., Murray, B. and Sarkar, A. 2017. Novel starch based emulsion gels and emulsion microgel particles: Design, structure and rheology. *Carbohydrate Polymers*. **178**, pp.86-94. DOI: <https://doi.org/10.1016/j.carbpol.2017.09.027>

OSA stabilised-emulsion droplets acting as active fillers may find applications in food and personal care industries for delivery of lipophilic molecules.

3.1 Introduction

Lipophilic molecules, such as flavourings, essential oils or drugs pose considerable challenges when incorporated into food, pharmaceuticals and other soft matter applications, due to their partial or complete water insolubility. Because of this and their susceptibility to oxidation, most of these compounds are difficult to deliver pre- and post-consumption (McClements, 2015). A wide range of emulsion-based approaches have been developed to encapsulate oil-soluble molecules, such as conventional emulsions, nanoemulsions, double emulsions, emulsion gels, etc., (Zhang et al., 2015).

Emulsion microgel particles are a relatively new class of soft solids vehicle that has not been explored as widely. The particles have a similar structure to emulsion gels, although their physical characteristics and length scales differ. In emulsion microgel particles, emulsion droplets are stabilised by an emulsifier and gelling agent inside a larger (microgel) particle (Torres et al., 2017; Torres et al., 2016). In other words, several emulsion droplets are encapsulated together within a soft solid shell. The soft solid shell around the oil droplets has been demonstrated to protect lipophilic compounds against oxidation (Beaulieu et al., 2002). The microgel particle itself can be dispersed in a controlled manner in an aqueous media. Additionally, microgel particles allow swelling or de-swelling as a function of environmental conditions, tuning their size and/or physicochemical properties, enabling the protection and possible release of lipophilic active compounds in a range of soft material applications (Ballauff and Lu, 2007; Wei et al., 2016). Hence, it is important to design such emulsion microgel particles using biocompatible polymers, such as starch, which is the second most abundant biopolymer in nature.

Starch is widely used in commercial applications and its versatility as a gelling agent is well-recognized (Teyssandier et al., 2011; Zhang et al., 2013). Drastic changes in the microstructure and viscoelastic properties of starch gels can be generated by shearing during gelatinization. Previous studies have shown that shear breaks down the swollen granules into smaller fragments producing a more viscous and translucent

gel. These smaller fragments have been suggested to be responsible for decreasing the rigidity by acting as inactive fillers in the amylose gel matrix (Lu et al., 2008; Svegmarm and Hermansson, 1991).

The incorporation of solubilized modified starch into non-sheared gelatinized starch has also been reported to affect the viscoelasticity and retrogradation properties of starch gels (Thirathumthavorn and Charoenrein, 2006; Tukomane and Varavinit, 2008). On the other hand, starch modified with octenyl succinic anhydride (OSA) has been widely demonstrated to stabilize oil-in-water emulsions, via the addition of hydrophobic groups to the starch molecules (Zhang et al., 2015; Nilsson and Bergenstahl, 2006; Tesch et al., 2002). The incorporation of hydrophobic groups in OSA starch molecules has been suggested to retard hydrogen bonding between amylose molecules in the starch dispersions, hindering the gelation process (Thirathumthavorn and Charoenrein, 2006; Tukomane and Varavinit, 2008; Bao et al., 2003). Aggregation of OSA groups has also been shown to allow the formation of a network via hydrophobic interactions between adjacent OSA starch chains (Ortega-Ojeda et al., 2005; Thirathumthavorn and Charoenrein, 2006; Tukomane and Varavinit, 2008). Nevertheless, no studies have been performed to understand the interaction between OSA starch at the oil/water interface and sheared gelatinized starch. It is critical to understand how OSA starch-stabilized emulsion droplets would bind to a sheared starch matrix within an emulsion gel and how this would influence processing of this starch-based emulsion gel into emulsion microgel particles via a top-down approach *i.e.*, controlled shearing.

To our knowledge, there is only one study in the literature describing production of starch-based microgel particles, however involving protein coated oil droplets (Malone and Appelqvist, 2003). In this study, starch granules were dispersed into a low oil fraction ($\leq 10\text{wt}\%$) sodium caseinate-stabilised oil-in-water emulsion, which was then heat treated to allow the starch to gelatinize, followed by moulding into gel particles of 3 mm of diameter. It is worth recognizing that thermodynamic incompatibility between the starch and the protein at the oil/water interface might result in uncontrolled release behaviour as well as instability of the particles over time if the oil fraction was increased above 10 wt%. The large particle size ($> 45 \mu\text{m}$) might also limit food applications due to possible impact on sensory perception (Imai et al., 1999). An alternative would be to explore designing OSA starch-stabilized emulsion droplets embedded into a sheared starch matrix. In addition, it would be crucial to

understand how gel stiffness and emulsion droplet binding to the starch matrix would affect the ability to break up such a system into emulsion microgel particles via a controlled shearing process (top-down approach).

Therefore, the objectives of this study were firstly to understand the interactions between OSA starch-stabilized emulsions and gelatinized sheared starch and secondly to design starch-based emulsion microgel particles using a controlled shearing process. As a control, the interactions between solubilized OSA starch and sheared starch were also studied using small deformation rheology. It is hypothesised that the OSA-stabilised emulsion droplets would strongly bind to the sheared starch gel as an “active filler” and this should enable break up of this emulsion gel into microgel particles without any oil leakage.

3.2 Materials and Methods

3.2.1 Materials

Wheat native starch was purchased from Sigma-Aldrich (Gillingham, UK). Commercial, pregelatinized OSA starch refined from waxy maize starch was used that contained a maximum of 3% OSA (Ingredion, GmbH, Germany). Sunflower oil was obtained from Morrisons (UK) supermarket. All dispersions were prepared with Milli-Q water having a resistivity of 18.2 M Ω ·cm at 25 °C (Milli-Q apparatus, Millipore, Bedford, UK). All other chemicals were of analytical grade and purchased from Sigma-Aldrich unless otherwise specified.

3.2.2 Determination of amylose content of native wheat starch and waxy OSA starch

The amylose content was determined via the iodine binding method using a spectrophotometer (6715 UV/Vis. Spectrophotometer, Jenway, Keison Ltd, UK) following the method developed by Kaufman et al. (2015). Five milligram of starch sample or standard were added to centrifuge tubes with 1 mL of DMSO (90%) and heat treated for 60 min at 95 °C with a vortexing step every 10 min. The samples were then cooled down for 5 min and 100 μ L of each sample was pipetted into new centrifuge tubes containing 100 μ L of DMSO (90w%) and 3.04 g/L iodine. The tubes

were shaken for 2 min. The different samples were then analysed for absorbance at 620 nm and 510 nm.

The amylose standard curve was prepared using different ratios of pure amylose from potato and pure amylopectin from corn starch purchased from Sigma-Aldrich (Dorset, UK).

The regression equation was determined from the standard curve using the absorbance difference between 620 and 510 nm. The amylose content of the different starch sample was then calculated using Equation 3.1:

$$\text{Amylose \%} = \frac{(\text{Abs } 620 - \text{Abs } 510) - y \text{ intercept of regression}}{\text{slope of regression}} \quad (3.1)$$

3.2.3 Preparation of stock modified starch stabilized emulsions

The OSA starch at different concentrations (1.7, 3.4 and 6.7 wt%) was dispersed in Milli-Q water and gently stirred (500 rpm) for 2 h using a magnetic stirrer.

Sunflower oil was subsequently mixed with the OSA starch dispersion at ambient temperature. The ratio of the lipid phase to aqueous phase in the emulsion was 40:60 (w/w), with a final OSA starch concentration of 1, 2 or 4 wt%. These oil-aqueous phase mixtures were pre-emulsified with a high speed rotor-stator mixer (Silverson, L5M-A, UK) at 8,000 rpm for 5 min for 1 and 2 wt% OSA starch or 10 minutes for 4 wt% OSA starch. The pre-emulsions were further homogenized in a laboratory scale two-stage valve high pressure homogenizer at 250/50 bar using two passes (Panda Plus, GEA Niro Soave, Parma, Italy). The emulsion samples were stored at 4 °C for 24 h for further analysis.

3.2.4 Particle size analysis

The particle size distribution of the emulsion droplets and emulsion microgel particles was measured via a Malvern Mastersizer 3000E hydro, (Malvern Instruments, Worcestershire, UK). Sizing of the emulsion oil droplets was conducted based on a relative refractive index (RI) of 1.097 (*i.e.*, the ratio of the RI of sunflower oil (1.46) to that of the aqueous phase (1.33)). Sizing of the emulsion microgel particles was conducted based on a relative RI of 1.150 (*i.e.*, the ratio of the RI of the particle (1.5) to that of the aqueous phase at (1.33)).

3.2.5 Preparation of mixed gels and emulsion gels

Starch gels were formed by dispersing native wheat starch in MilliQ water and heating at 80 °C for 40 minutes in a water bath. Simultaneously, shear treatment was continuously applied for two minutes with three minutes interval using a hand blender (Hand blender, XB986B, 170W, Argos, UK).

Emulsion gels containing different concentrations of starch (15 or 20 wt%), OSA starch (0.5, 1, 1.5 or 2 wt%) and oil fractions (5, 10, 15, 20 wt%) were prepared by mixing starch gels with 40 wt% oil-in-water emulsion stabilized by 4 wt% OSA starch at different ratios. Table 3.1 summarizes the different initial and final concentrations of wheat starch and OSA starch as well as oil fraction, per weight of the final emulsions. For comparison purposes, OSA starch dispersions without any oil droplets was also mixed with wheat starch using the same ratios as for the emulsion gels, forming mixed OSA starch-wheat starch gels. The different ratios of OSA starch dispersion or emulsion were first heat treated to 80 °C before being vigorously mixed with the sheared starch gel at 80 °C, allowing the formation of starch mixed gels and emulsion gels, respectively.

3.2.6 Small deformation rheology

Small deformation viscoelasticity of the different gels was investigated under dynamic oscillatory shear rheometry using a Kinexus ultra rheometer (Malvern Instruments Ltd. Worcestershire, UK). A cone-and-plate geometry system (40 mm, model: CP4/40 SS017SS) was used for all measurements. About 0.5 mL of gel was placed onto the sample plate and sealed with a thin layer of the 350 cst silicone oil to prevent evaporation.

The elastic modulus (G') and viscous modulus (G'') were measured firstly while conducting a strain sweep between 0.01 and 100 % strain, at 1 Hz and 25 °C, to determine the linear viscoelastic region. A frequency sweep was also conducted between 0.6 to 63 rad s⁻¹ at 0.5 % strain and 25 °C to determine the complex viscosity (η^*) of the different gels. The third test performed on the different gels was temperature and time sweep, carried out in the linear viscoelastic region (0.5 % strain) and 1 Hz. The sample plate was preheated to 80 °C before the addition of the samples. The G' and G'' were measured during two different temperature changes: (a) cooling at 4 °C min⁻¹ from 80 °C to 25 °C and (b) holding at 25 °C for 66 minutes. The limiting

Table 3.1 Initial and final concentrations of wheat starch and 40 wt% oil-in-water emulsion stabilised by 4 wt% OSA starch as well as mixing ratios for the formation of the different emulsion gels.

Starch gel Initial [WS] (wt%)	Oil-in-water Emulsion		Starch gel : Emulsion Ratio	Starch gel Final [WS] (wt%)	Oil-in-water Emulsion	
	Initial [oil] (wt%)	Initial [OSA] (wt%)			Final [oil] (wt%)	Final [OSA] (wt%)
17.2			87.5:12.5		5	0.5
20	40	4	75:25	15	10	1
24			62.5:37.5		15	1.5
30			50:50		20	2
22.9			87.5:12.5		5	0.5
26.7	40	4	75:25	20	10	1
32			62.5:37.5		15	1.5
40			50:50		20	2

deformation value ($\dot{\gamma}_L$) of the different gels was arbitrarily chosen as the point where the elastic modulus decreased by 20% from the first value of the modulus measured at 0.1 % strain.

3.2.7 Preparation of emulsion microgel particles

Emulsion microgel particles were produced using a top-down approach as illustrated in Figure 3.1. The sheared starch gels or emulsion gels were refrigerated at 4 °C for three hours. The refrigerated gels were then passed twice through a laboratory scale two-stage valve high pressure homogenizer at 250/50 bar (Panda Plus, GEA Niro Soave, Parma, Italy). The resulting particles were collected in a beaker and immediately diluted with Milli-Q water and stirred for 30 min at 150 rpm to limit particle aggregation.

3.2.8 Microscopy

All emulsions, emulsion gels and emulsions microgel particles (50 μL) were imaged via optical microscopy (Nikon, SMZ-2T, Japan), confocal laser scanning microscopy (CLSM) and cryo-scanning electron microscopy (cryo-SEM).

A Zeiss LSM 700 confocal microscope (Carl Zeiss MicroImaging GmbH, Jena, Germany) with a 40 \times magnification lens was used. About 10 μL of Nile Red (1 mg mL⁻¹ in dimethyl sulfoxide, 1:100 v/v) was used to stain oil (argon laser with an

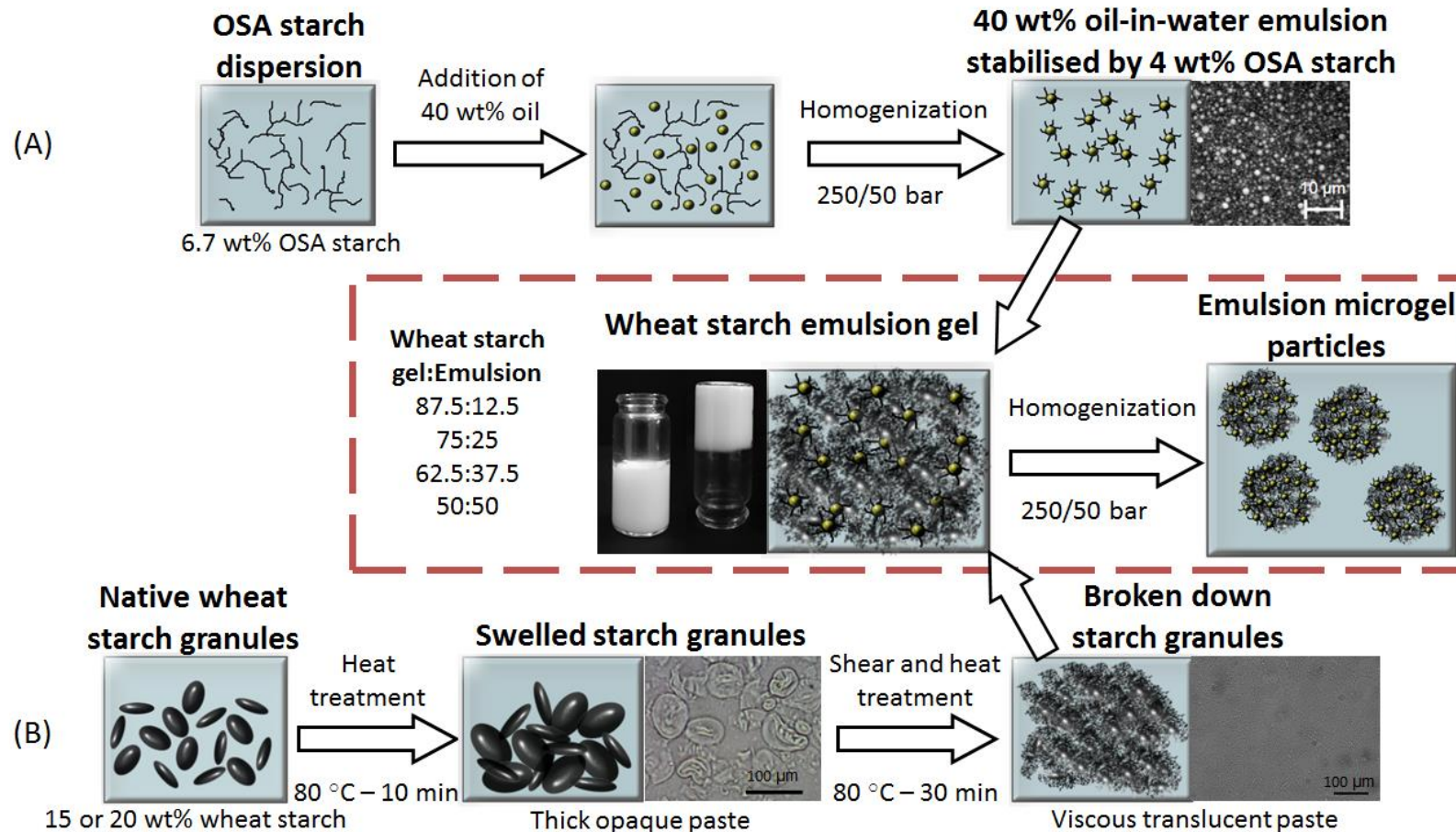


Figure 3.1 Schematic diagram and corresponding micrographs of the formation of OSA starch-stabilised emulsion (A), sheared wheat starch gel (B) and starch emulsion gel and emulsion microgel particles (indicated within dashed box).

excitation line at 488 nm), 10 μL of Nile Blue (0.1 mg mL^{-1} in Milli-Q water, 1:100 v/v) was used to stain wheat starch (HeNe with an excitation line at 639 nm) and 10 μL of 1% Methylene Blue was used to stained OSA starch (Ar laser with an excitation line at 639 nm).

A cryo-scanning electron microscope (FEI Quanta 200F FEG ESEM, Japan), equipped with a Quorum PolarPrep 2000 cryo-system was also used to study the structural features of the emulsion microgel particles. A drop of emulsion microgel particles dispersion (10 – 20 μL) was placed on rivets mounted on a cryo-SEM stub. These were then frozen in liquid nitrogen slush and then transferred into the PP2000 preparation chamber. The frozen samples were fractured with a blade and carefully etched at $-95\text{ }^{\circ}\text{C}$ for 4 min, followed by coating with platinum (5 nm). The samples were then transferred into the cryo-SEM observation chamber for imaging at 5 kV.

3.2.9 Statistical analysis

Data was obtained in triplicate and mean and standard deviation were calculated. Significant differences between samples were determined by one-way ANOVA and multiple comparison test with Tukey's adjustment was performed using SPSS software (IBM, SPSS statistics, version 24) and the level of confidence was 95%.

3.3 Results and Discussion

3.3.1 Effect of the addition of OSA starch on wheat starch gels

The first set of control experiments were carried out with OSA starch added to wheat starch without the addition of any emulsion droplets. This sets the scene to understand the interaction between dispersed OSA starch and wheat starch. Figure 3.2 shows the elastic (G') and viscous (G'') modulus of the different gels as a function of time and temperature.

All samples can be considered as gels from time 0 s since $G' \gg G''$ and G' remained relatively constant throughout the whole frequency range (0.6 to 60 rad s^{-1}) (Appendix A.1). The gels had similar rheological behaviour irrespective of the concentrations of wheat starch (15 or 20 wt%) and OSA starch (0 to 2 wt%) used. During the cooling stage, G' increased by over 70% and during the holding stage, G'

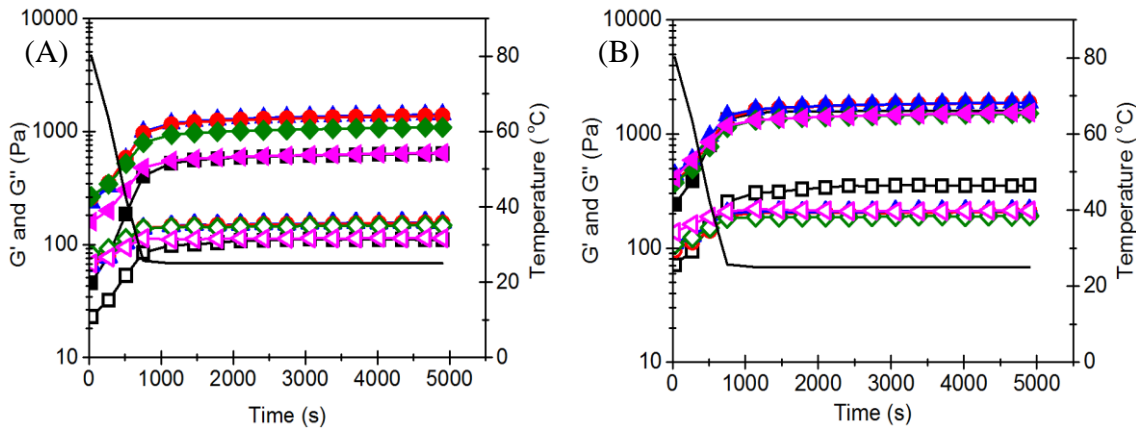


Figure 3.2 Elastic modulus (G' , filled symbols) and viscous modulus (G'' , empty symbols) as a function of time and temperature (full black line) of 15 wt% wheat starch gel (A) and 20 wt% wheat starch gel (B) prepared with different OSA starch concentrations (0 wt%, ■; 0.5 wt%, ●; 1 wt%, ▲; 1.5 wt%, ◆; 2 wt%, ▼) at 1 Hz and 0.5 % strain.

further increased by approximately 30%. This significant increase in G' can be attributed to the reorganization and association of colloidal- and molecularly-dispersed amylose and amylopectin (Teyssandier et al., 2011; Singh et al., 2003).

As expected, the concentration of wheat starch affected the initial and final elastic modulus of the gels significantly ($p < 0.05$) (Figure 3.2). For instance, the G' increased by almost one order of magnitude on increasing the wheat starch concentration by 5 wt% (0.046 ± 0.006 kPa for 15 wt% starch, 0.24 ± 0.034 kPa for 20 wt% starch). Amylose is the main starch molecule responsible for forming the three-dimensional network (via hydrogen bonding) between the starch chains during gel formation (Wang et al., 2015; Miles et al., 1985). In this study, the amylose content of the native wheat starch and commercial waxy OSA starch were measured to be 18.7% and 0.17%, respectively, in accordance with previous studies (Singh et al., 2003). Increasing the concentration of wheat starch by 5 wt% would therefore increase the amylose content by a factor of 1/4 in the final gel, which explains the significantly higher G' values (Rosalina and Bhattacharya, 2002).

The addition of OSA starch (0.5 to 2 wt%) to 20 wt% sheared starch gels did not affect the initial and final G' of the gels significantly ($p > 0.05$) (Figure 3.2 B). On the other hand, the addition of OSA starch (0.5 to 2 wt%) to 15 wt% sheared starch gels significantly increased the initial strength of the gels by over 70% (from 0.046

kPa to 0.2 kPa), respectively (Figure 3.2 A, see Appendix A.2 for statistical analysis). Over time, however, only 0.5 and 1 wt% OSA starch significantly increased the final G' of 15 wt% starch, by approximately 50%.

Previous studies have demonstrated that high amounts of OSA starch (*i.e.*, minimum ratio of 20:80 by weight, OSA starch:native starch) added to non-sheared starch affected the retrogradation phenomenon of the gels (Tukomane and Varavinit, 2008; Ortega-Ojeda et al., 2005). The retrogradation process of amylose and amylopectin was found to be retarded due to the substitution of OSA groups on the amylopectin, hindering the hydrogen bonding and re-association between starch molecules via steric hindrance (Bao et al., 2003; Thirathumthavorn and Charoenrein, 2006). Additionally, the viscosity and elastic modulus of mixed gels were found to increase significantly. These effects were attributed to the ability of OSA starch to form hydrophobic interactions with other OSA starch molecules (Bhosale and Singhal, 2007; Krstonošić et al., 2011). Hydrophobic bonds between neighbouring OSA groups allowed the formation of a network increasing the elastic modulus of the gels (Ortega-Ojeda et al., 2005; Tukomane and Varavinit, 2008). Hence, the addition of 0.5 to 1.5 wt% OSA starch to the lower concentration of wheat starch (15 wt%) increased the elastic modulus the gel possibly via the same OSA starch-OSA starch cross-linking mechanism. However, increasing the concentration of OSA starch to 2 wt% hindered the re-association of the starch molecules, possibly via steric hindrance dominated by the the bulky starch polymeric chains, which resulted in an elastic modulus similar to that of wheat starch without OSA substitution. At the higher concentration of wheat starch (20 wt%), OSA starch had probably little influence on the gels because the usual hydrogen bonds between wheat starch molecules were more numerous and dominated the gel strength.

Figure 3.3 demonstrates that the addition of OSA starch (0.5 to 2 wt%) affected the linear viscoelastic region (LVER) and limiting deformation value $\dot{\gamma}_L$ of starch gels, confirming that addition of hydrophobic groups might have an impact on sheared starch gel. Wheat starch gels at both 15 and 20 wt%, without OSA starch, had a similar $\dot{\gamma}_L$ ($p > 0.05$) of 10 and 3.2 % strain, respectively. The addition of over 1.5 wt% OSA starch to 15 and 20 wt% starch gels significantly increased $\dot{\gamma}_L$ to over 20 and 25 % strain ($p < 0.05$), respectively, even though their elastic modulus and complex viscosity was similar to their respective starch gel without OSA starch (Figure 3.2 A and

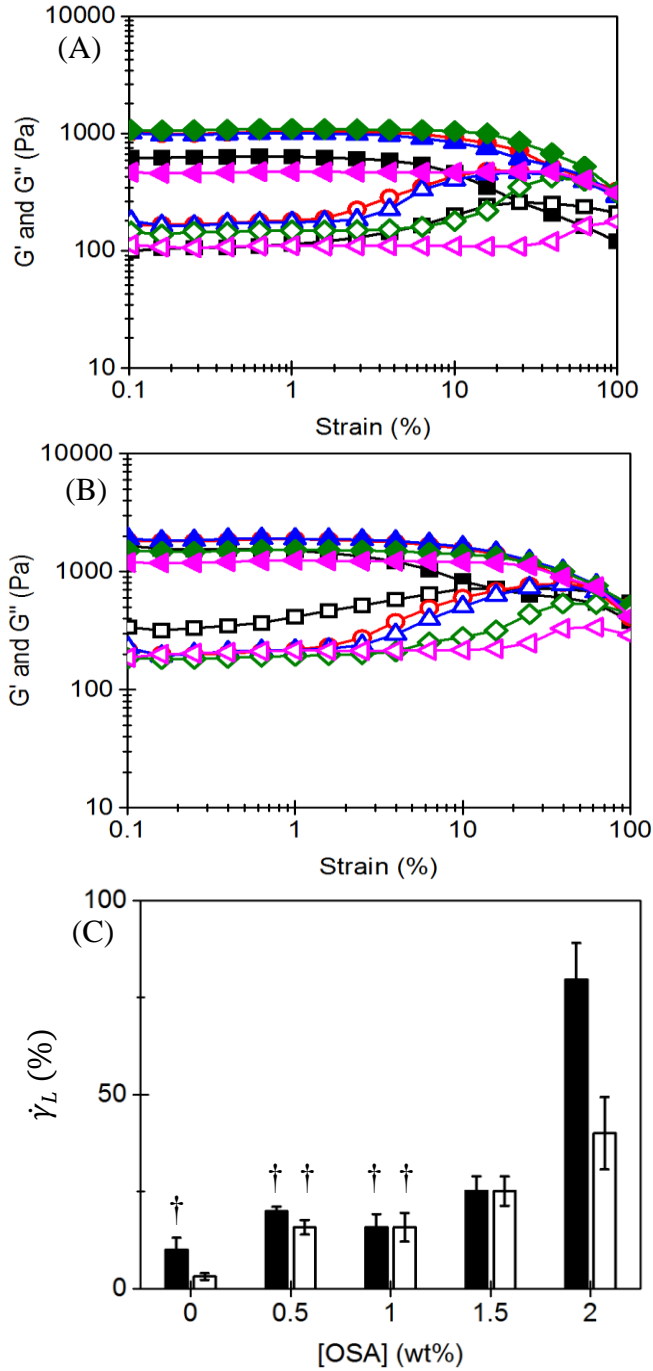


Figure 3.3 Elastic modulus (G' , filled symbols) and viscous modulus (G'' , empty symbols) as a function of strain of 15 wt% wheat starch gel (A) and 20 wt% wheat starch gel (B) prepared with different OSA starch concentrations (0 wt%, ■; 0.5 wt%, ●; 1 wt%, ▲; 1.5 wt%, ◆; 2 wt%, ▼). The limiting deformation value ($\dot{\gamma}_L$) of wheat starch gels at 15 wt% (black) and 20 wt% (white) is reported as a function of OSA concentration (C), samples with symbol (†) are not significantly different ($p > 0.05$) to wheat starch gel (15 or 20 wt%) without OSA starch.

Appendix A.1 A and B). At higher concentration of OSA starch (≥ 1.5 wt%), a denser network might have been formed due to OSA starch aggregation via hydrophobic interactions, which might have decreased the elastic modulus of the mixed gels but increased their flexibility as well as their LVER (Sweedman et al., 2013; Wang et al., 2015; Bhosale and Singhal, 2007). These OSA starch aggregates would have possibly allowed the gel network to absorb the energy applied during shearing and deform rather than fracture, for example (Torres et al., 2017; Dickinson, 2012). This reversible decrease in G' is representative of “weak” gel systems, which can undergo a progressive breakdown into smaller clusters with increasing strain. In comparison, “strong” gels under strain break down in an irreversible manner.

3.3.2 Droplet size of OSA-stabilised emulsions

Figure 3.4 A shows the oil droplet size distribution of 40 wt% sunflower oil emulsions stabilised by either 1 wt%, 2 wt% or 4 wt% OSA starch. At the low concentration of OSA starch (1 wt%), the droplet size distribution was bimodal and had a large d_{43} value with significant population of oil droplets in the region of 1 – 20 μm suggesting aggregation or coalescence. Increasing the concentration of OSA starch to 2 wt% led to a significant (90%) decrease of the d_{32} and d_{43} values, to 0.09 and 0.82 μm respectively (Figure 3.4 A). The significantly lower d_{32} value (0.09 μm) might suggest the formation of OSA starch aggregates in the unadsorbed phase. Previous authors have referred to such aggregates of OSA starch molecules as micelles, although the structures formed must be far more complex than conventional surfactant micelles. Krstonošić et al. (2011), Zhu et al. (2013) and Sweedman et al. (2014) reported critical micelle concentrations between 0.41 – 0.88 g L^{-1} . Therefore, at 2 wt% OSA starch, the formation of micelles is unlikely. The increased OSA starch concentration (from 1 to 2 wt%) might have allowed a faster adsorption of the OSA starch to the oil droplet. Furthermore, an increase in viscosity of the aqueous phase, due to the increase of OSA starch concentration, would limit any coalescence (as observed with the emulsion stabilised by 1 wt%) post homogenization and thus significantly reduced the oil droplet size (Nilsson and Bergenståhl, 2006).

Doubling the concentration of OSA starch further to 4 wt% showed a significant increase in the emulsion stability as the oil droplet size distribution became

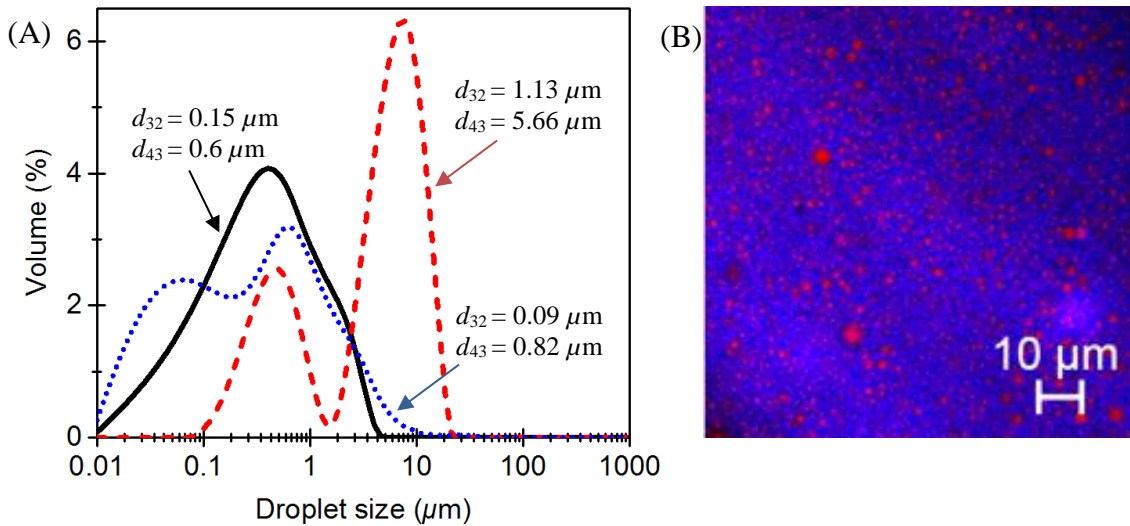


Figure 3.4 Droplet size distribution (A) indicating d_{32} and d_{43} values of 40 wt% oil-in-water emulsion stabilised by 1 wt% OSA (red dashed line), 2 wt% OSA (blue dotted line) and 4 wt% OSA (black full line) and CLSM micrograph (B) of 40 wt% oil-in-water emulsion stabilised by 4 wt% OSA, oil droplets in red stained using Nile Red and OSA starch in blue stained using Methylene Blue. Scale bar represents 10 μm.

monomodal and symmetrical. The CLSM image (Figure 3.4 B) further confirms that the oil droplets (in red) were uniformly distributed in agreement with the light scattering data (Figure 3.4 A). These results are in accordance with previous studies conducted on the stabilization properties of OSA starch (Sweedman et al., 2013; Tesch et al., 2002). Further studies are needed, focusing on kinetics of stability of OSA-starch stabilized emulsions. However, we note that most emulsions, if they exhibit the good stability shown here over 24 h, tend to be stable over much longer periods. Based on these results, further experiments were conducted using this optimized formulation (*i.e.*, 40 wt% oil, 4 wt% OSA starch).

3.3.3 Rheological properties of OSA starch-stabilised emulsion gels

The influence of different concentrations of OSA starch-stabilised emulsions on the rheology of the sheared wheat starch gels was recorded (Figure 3.5 A and B) over the same cooling and holding regime (from 80 to 25 °C followed by 66 min at 25 °C) as discussed for the previous experiments. As in the previous results, all samples showed “gel”-like signature from time 0 s since $G' \gg G''$ and they all had a similar

rheological behaviour irrespective of the wheat starch (15 or 20 wt%) or OSA starch-stabilised emulsion concentrations (5, 10, 15 or 20 wt%).

In contrast with the previous results (samples without added oil droplets) (Figure 3.2 A and B), the addition of OSA-stabilised emulsion had a significant impact on the final elastic modulus of the gels (Figure 3.5 A and B). The incorporation of the emulsions to 15 wt% starch gels led to an almost linear increase of the final G' (Figure 3.5 C), although 5 wt% oil appeared to be not sufficient enough to increase the final G' of 15 wt% starch gel significantly ($p > 0.05$). The addition of 5 wt% emulsion droplets and/or 0.26 wt% OSA starch did not contribute to significant strengthening of the gel matrix, probably because the OSA starch molecules were mainly adsorbed at the surface of the oil droplets and were not in excess to interact with the continuous phase (Dickinson and Chen, 1999). Also, the volume fraction of filler added was not high enough to significantly reinforce the matrix (Torres et al., 2016) .

At 20 wt% wheat starch, the emulsion droplets (5 to 20 wt%) significantly ($p < 0.05$) increased the final G' of the gels (Figure 3.5 B). The addition of 5 to 15 wt% oil provided an average of 50% increase in G' , whereas 20 wt% oil strengthened the gel matrix by approximately 70% (Figure 3.5 C). The oil droplet size was on average 0.1 μm , hence the Laplace pressure means such droplets can be considered effectively as solid particles (van Vliet, 1988). The increase in elastic modulus (G') points to the OSA-starch stabilized emulsion droplets acting as “active fillers” in the starch gel matrix (Dickinson and Chen, 1999; Torres et al., 2016; Torres et al., 2017). To our knowledge, this is the first study that reports the use of OSA starch-stabilized droplets as active fillers in starch gels. The binding of the filler (droplets) to the matrix (wheat starch gel) was no doubt due to the association between the wheat starch and OSA groups protruding from the surface of the oil droplets. Three types of interactions might have contributed to the filler-matrix association: (i) OSA groups adsorbed at the surface of oil droplets might have some hydrophobic groups oriented towards the aqueous phase allowing the formation of a hydrophobic network between neighbouring OSA groups absorbed on other oil droplets and OSA groups found in the continuous phase; (ii) hydroxyl groups on neighbouring wheat starch molecules might interact via hydrogen bonding, and (iii) some association between non-absorbed OSA starch molecules (via hydrogen bonding or hydrophobic interaction) may have also made a more minor contribution to the overall modulus – on the basis of the minor

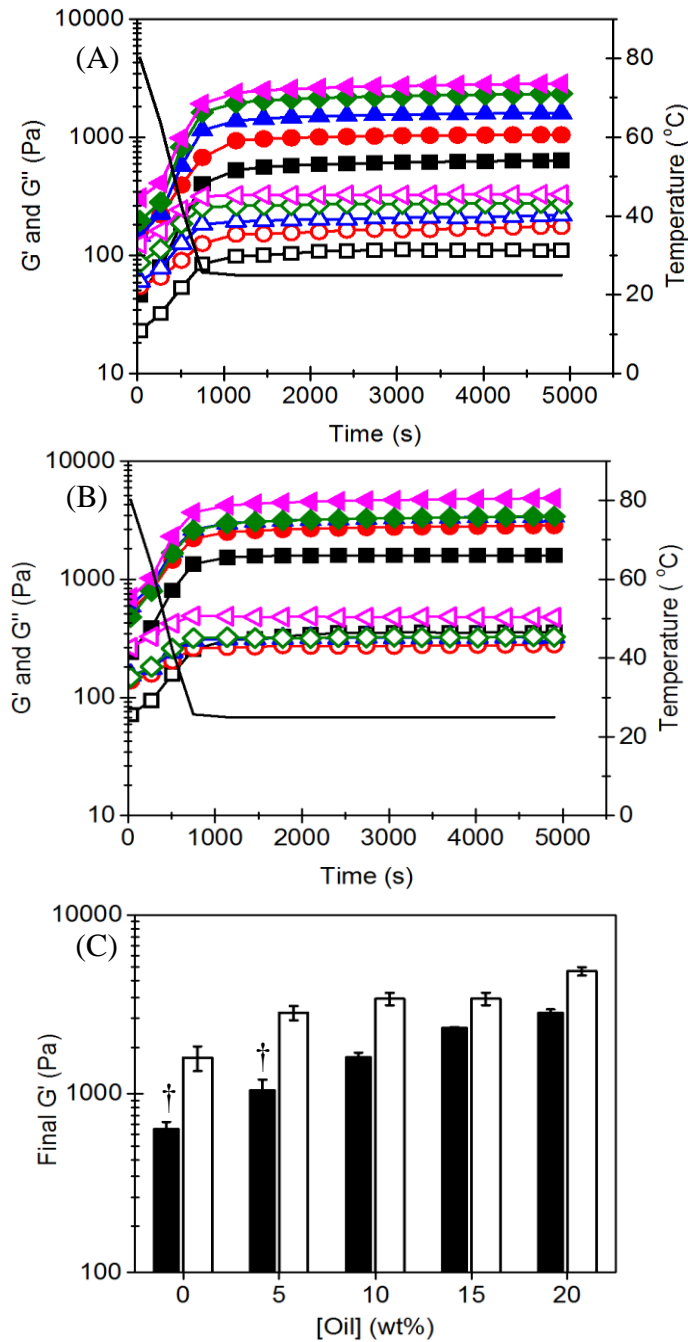


Figure 3.5 Elastic modulus (G' , filled symbols) and viscous modulus (G'' , empty symbols) as a function of time and temperature (full line) of 15 wt% wheat starch gel (A) and 20 wt% wheat starch gel (B) prepared using different oil fractions (0 wt%, ■; 5 wt%, ●; 10 wt%, ▲; 15 wt%, ◆; 20 wt%, ▲), at 1 Hz and 0.5 % strain. Final elastic modulus of wheat starch gels at 15 wt% (black) and 20 wt% (white) is shown as a function of oil concentration (C) measured at 25 °C, 1 Hz and 0.5 % strain, samples with symbol (†) are not significantly different ($p > 0.05$) to wheat starch gel (15 or 20 wt%) without oil droplets.

effect of OSA starch alone on the wheat starch gels described above (Sweedman et al., 2013; Singh et al., 2003; Bhosale and Singhal, 2007).

Similar rheological behaviour has been previously demonstrated using whey protein stabilised emulsion gels (20 wt% oil fraction), where the oil droplets were bound to the matrix via electrostatic, hydrogen bonding and hydrophobic interactions (Dickinson and Chen, 1999; Torres et al., 2017). However, no net charges were present in the OSA-stabilised emulsion (data not shown, ζ -potential = 0 ± 0.12 mV), suggesting electrostatic interactions were probably not involved in this case. For comparison purposes, the relative change in final G' was calculated, using $|\Delta G'| = |(G'_{(\text{emulsion gel})} - G'_{(\text{gel})}) / G'_{(\text{emulsion gel})}|$, for both whey protein and starch gels at 20 wt% oil. The incorporation of 20 wt% oil droplets with an average size of $0.1 \mu\text{m}$ into a whey protein gel matrix led to $\Delta G' \approx 98\%$ increase in the strength of the gel (Torres et al., 2017), whereas in the starch matrix gel $\Delta G' \approx 67\%$. The absence of strong electrostatic interactions in the starch emulsion gel might explain their significantly weaker elastic modulus as compared to whey protein emulsion gel at the same oil volume fraction and oil droplet size ($d_{32} = 0.1 \mu\text{m}$) (Dickinson, 2012).

Under strains 0.1 to 100%, the incorporation of OSA-stabilised oil droplets bound to the starch gel affected their linear viscoelastic region (LVER), as observed in Figure 3.6. Low amounts of emulsion (5 and 10 wt%) did not significantly affect the LVER or $\dot{\gamma}_L$ of 15 wt% wheat starch gels, again suggesting that the oil volume fraction or OSA starch concentration was not high enough to significantly interact with the wheat starch gel matrix. Increasing the oil concentration to 15 and 20 wt% gave a significant increase $\dot{\gamma}_L$ for both gels (Figure 3.6 A and B). For example, $\dot{\gamma}_L$ of 20 wt% starch gel without emulsion droplets was measured to be $3.2 \pm 0.85\%$ strain, whereas with the addition of 20 wt% oil $\dot{\gamma}_L$ increased to $31.5 \pm 3.7\%$ strain (Figure 3.6 C), *i.e.*, the gels were less brittle. Thus, although the filled starch emulsion gels were not as rigid, they may have the rheological advantage of being more flexible.

At the same time, it is seen that the LVER of the emulsion gels with 20 wt% oil was significantly shorter than the LVER of starch gels with the same freely added OSA starch concentration (2 wt%) (compare Figure 3.3 A and Figure 3.6 A). For example, for 15 wt% starch gel + 2 wt% of OSA starch, $\dot{\gamma}_L$ of the gel was $79.6 \pm 9.43\%$ strain and 15 wt% starch gel + 20 wt% emulsion gel $\dot{\gamma}_L$ was $31.8 \pm 3.71\%$ strain (Figure 3.3 A and Figure 3.6 A). Thus, oil droplets bound to wheat starch gel matrices may act as crack initiators weakening the emulsion gel under higher strain.

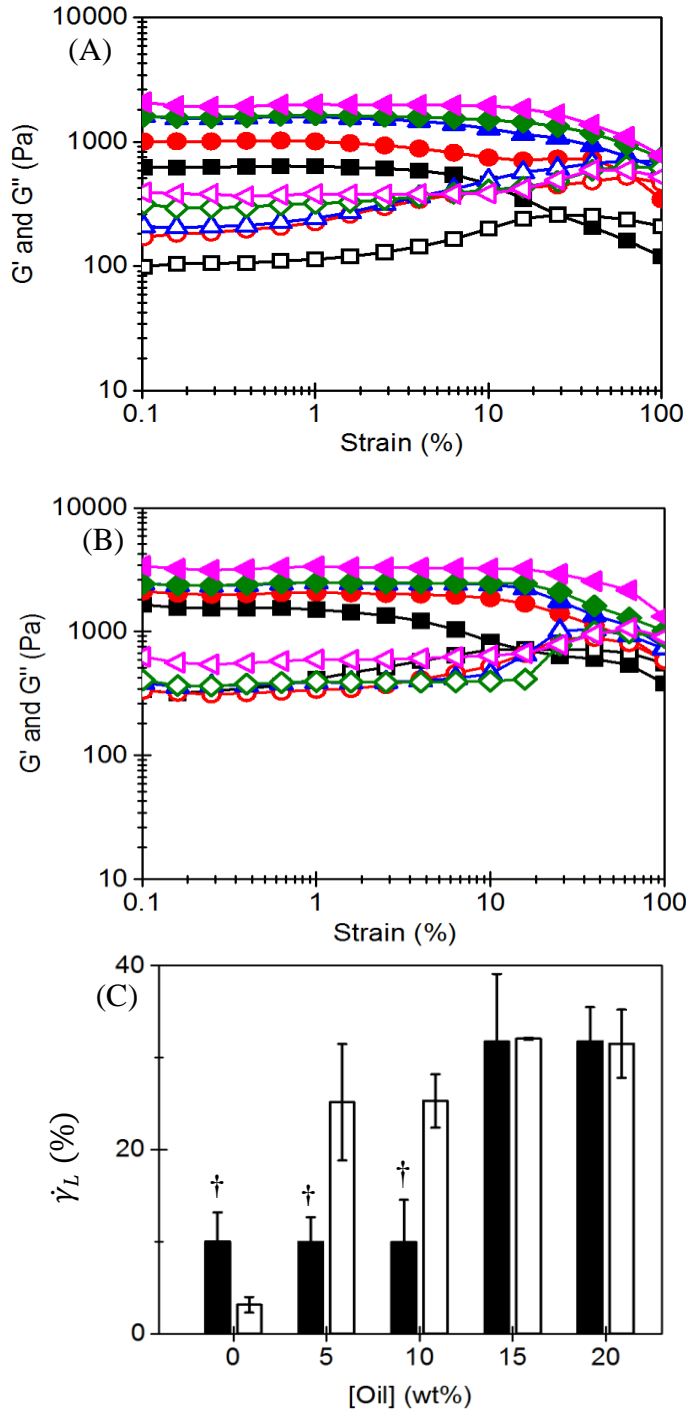


Figure 3.6 Elastic modulus (G' , filled symbols) and viscous modulus (G'' , empty symbols) as a function of strain of 15 wt% wheat starch gel (A) and 20 wt% wheat starch gel (B) prepared using different oil fractions (0 wt%, ■; 5 wt%, ●; 10 wt%, ▲; 15 wt%, ◆; 20 wt%, ▼). The limiting deformation value ($\dot{\gamma}_L$) of wheat starch gels at 15 wt% (black) and 20 wt% (white) is reported as a function of oil concentration (C), samples with symbol (\dagger) are not significantly different ($p > 0.05$) to wheat starch gel (15 or 20 wt%) without oil droplets.

3.3.4 Characteristics of starch emulsion microgel particles

Starch-based emulsion microgel particles were designed from the emulsion gels with oil fraction (5, 10 and 15 wt%) and the concentration of native wheat starch (15 and 20 wt%) and OSA starch (0.5, 1, 1.5 wt%).

The size of the emulsion microgel particles produced at different concentrations of wheat starch and oil were similar (Figure 3.7). At 5 – 10 wt% oil content, all three particle size distributions were monomodal, (1 – 10 μm) with similar d_{32} and d_{43} values (Figure 3.7 A, B and C) (note the d_{32} of encapsulated oil droplets was previously measured as around 0.1 μm). All the above suggests that the emulsion

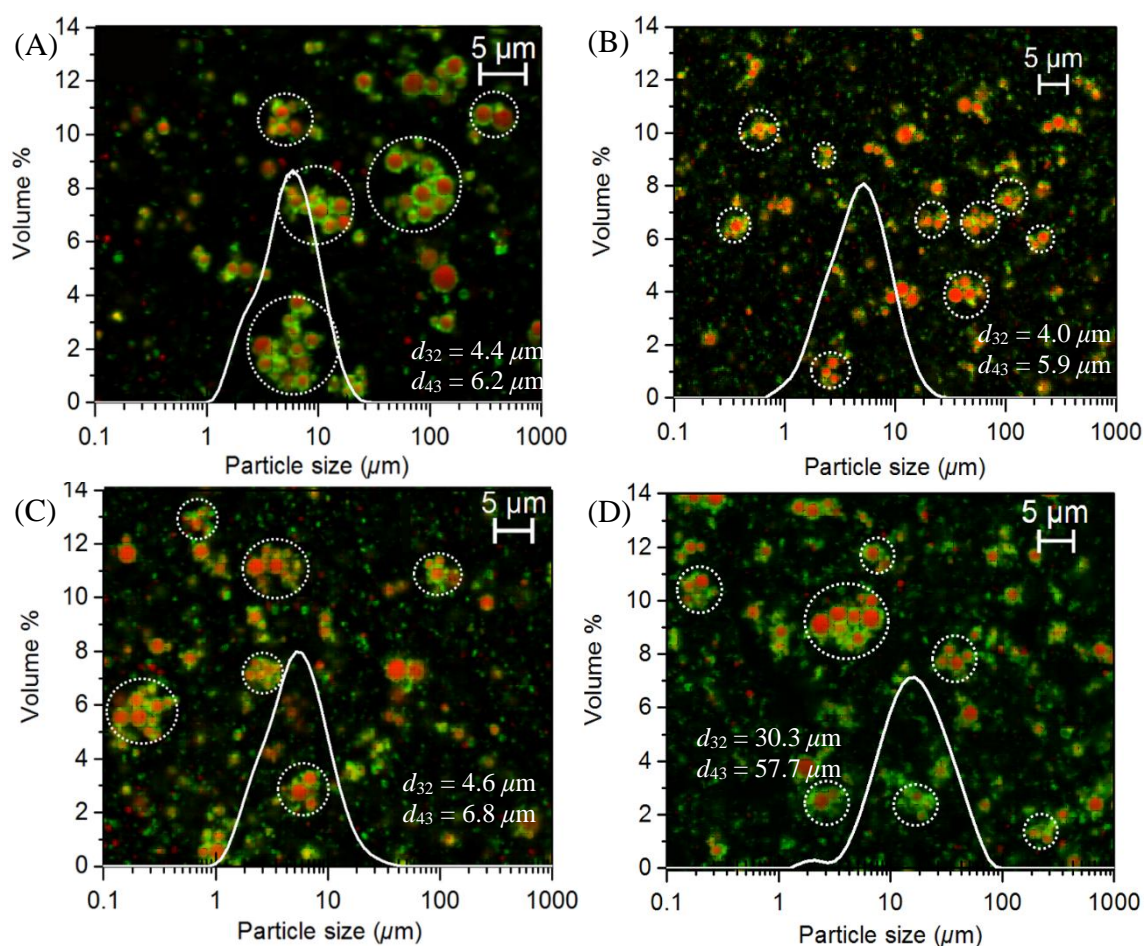


Figure 3.7 CLSM micrograph with superimposed droplet size distribution and d_{32} and d_{43} values of emulsion microgel particles produced at 15 wt% wheat starch + 5 wt% oil (A), 15 wt% wheat starch + 10 wt% oil (B), 20 wt% wheat starch + 10 wt% oil (C) and 20 wt% wheat starch + 15 wt% oil (D). Dotted circles highlight the emulsion microgel particles in the images. Wheat starch in green, stained with Nile Blue and oil droplets in red stained with Nile Red.

microgel particle formation process did not lead to significant destabilization and coalescence of the emulsion droplets but that most of the droplets were encapsulated into emulsion microgel particles.

Increasing the oil fraction to 15 wt% led to significantly larger particles with a d_{32} value of $30.3 \mu\text{m}$ (Figure 3.7D). As discussed previously, increasing the oil fraction to 15 wt%, significantly increased the critical strain of the emulsion gel (see Figure 3.6 C). The larger critical strain of the emulsion gel might have allowed the emulsion gel to deform more extensively under high pressure homogenization and fracture the gel into larger particles as compared to emulsion gels with a lower critical strain, which were more brittle and therefore might break down more randomly into smaller emulsion microgel particles (Dickinson, 2012; Torres et al., 2017; Moakes et al., 2015). The emulsion microgel particle morphology was polyhedral aggregates of emulsion droplets encapsulated into starch particles (see Figure 3.7). No significant variation in morphology was observed at the different concentrations of starch or percentage oil droplets. Most oil droplets (in red) seemed to be entrapped in a starch gel matrix (in green) and no free surface oil was observed after homogenization, suggesting little loss of droplets to the aqueous phase. However, increasing the concentration of wheat starch from 15 to 20 wt% led to a higher amount of matrix debris in dispersion as well as more structures where individual oil droplets (in red) were visibly surrounded by a thin layer of starch (Figure 3.7 C and D). At higher concentrations of wheat starch (20 wt%) and oil fraction (10 – 15 wt%), the final G' and critical strain of the emulsion gel was the highest, forming larger emulsion microgel particles (see above). During the first pass through the homogenizer, the higher starch concentration and oil fraction enabled the formation of large emulsion microgel particles where some were only loosely bound beneath the surface of the microgel particles. The second pass through the homogenizer might have disrupted such particles and released more individual oil droplets surrounded by fragments of the matrix (Dickinson, 2000; Malone and Appelqvist, 2003).

The cryo-SEM micrographs (Figure 3.8) indicates that emulsion microgel particles were of the order of $2 - 3 \mu\text{m}$, which is about 40 – 50% lower as compared to that of CLSM images (Figure 3.7). This might be due to the potential shrinkage during the cryo-SEM preparation procedure. Figure 3.8 A shows several emulsion microgel particles of similar sizes homogeneously distributed throughout the micrograph. Most

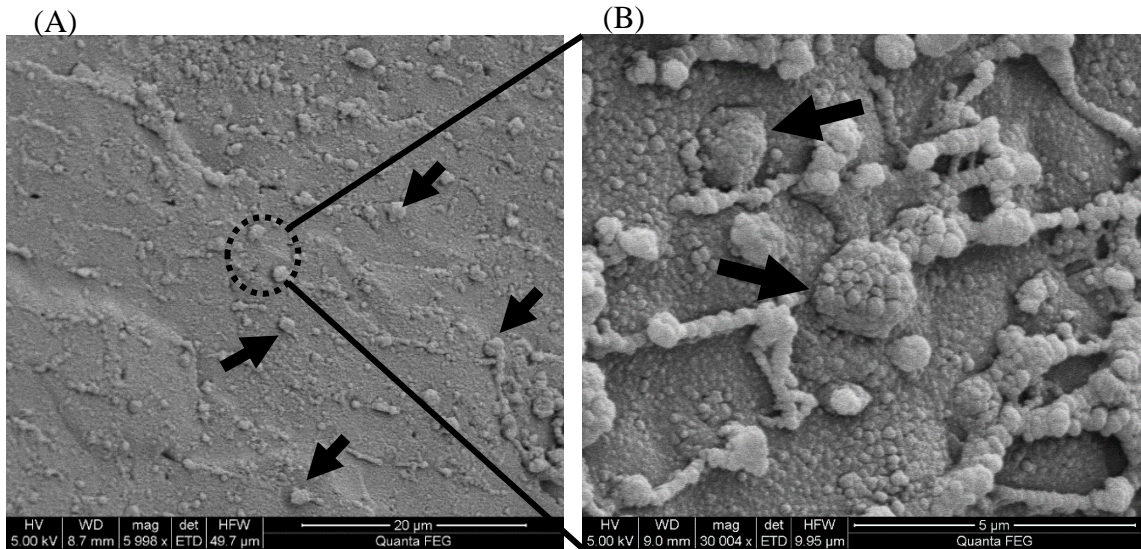


Figure 3.8 Cryo-SEM micrograph of starch emulsion microgel particles produced using 10 wt% OSA-stabilised emulsion encapsulated into 15 wt% wheat starch, scale bar represents 20 μm (A) and higher magnification image showing the external surface of the emulsion microgel particles, scale bar represents 5 μm (B). The arrows point to the individual emulsion microgel particles.

particles appeared to be spherical and did not seem to be significantly aggregated. At higher magnification (Figure 3.8 B), a few emulsion microgel particles seemed to have aggregated into linear chains, but this is assumed to be an artefact of the cryo-SEM preparation.

Higher magnification images (Figure 3.8 B) showed that the particles appeared to have a “raspberry-like” surface, which is assumed to be due to the underlying intact encapsulated oil droplets. It has been demonstrated that composite materials containing hydrophobic particles bound to a gel matrix tend to fracture adjacent to the particle surface (Dickinson, 2012; Langley and Green, 1989). Therefore, under shear, one might expect, the emulsion gel to break adjacent to the oil droplet surface, explaining the appearance of the emulsion microgel particle surface.

3.4 Conclusions

Findings from this study have demonstrated that OSA stabilised-emulsion droplets act as active fillers in a sheared wheat starch gel allowing the design of novel starch emulsion microgel particles *i.e.*, a soft solid network encapsulating several oil droplets into one particle via a facile top-down shearing approach. The emulsion droplets are firmly bound to the gel network, probably due to a combination of three types of associations: the OSA starch at the oil-water interface forming a hydrophobic network with neighbouring OSA starch-stabilized droplets; wheat starch macromolecules associating together via hydrogen bonding; minor hydrogen bonds forming between hydroxyl groups on OSA starch and wheat starch in the continuous phase.

Emulsion microgel particles with controlled sizes and mechanical properties can be produced from starch and OSA starch as long as there is a strong understanding of the interplay between the concentration of the wheat starch, surface active (OSA) starch, oil volume fraction, gelation kinetics and emulsion gel mechanical behaviour. The understanding of the different interactions occurring in the emulsion microgel particles might also be of great help to understand their control release properties in the following study. In a similar way, it is of great interest, to understand the interactions occurring in whey protein emulsion gels so that whey protein-based emulsion microgel particles could be designed. This is now discussed in the next chapter.

3.5 References

- Ballauff, M. and Lu, Y. 2007. "Smart" nanoparticles: Preparation, characterization and applications. *Polymer*. **48**(7), pp.1815-1823.
- Bao, J. et al. 2003. Physical Properties of Octenyl Succinic Anhydride Modified Rice, Wheat, and Potato Starches. *Journal of Agricultural and Food Chemistry*. **51**(8), pp.2283-2287.
- Beaulieu, L. et al. 2002. Elaboration and characterization of whey protein beads by an emulsification/cold gelation process: application for the protection of retinol. *Biomacromolecules*. **3**(2), pp.239-248.

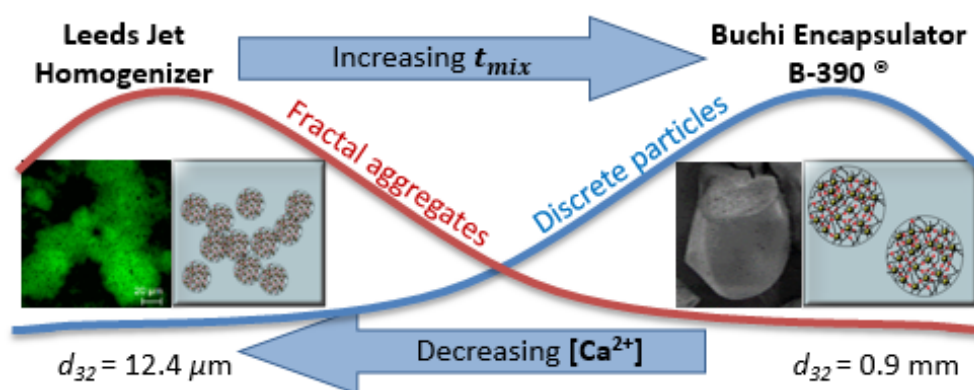
- Bhosale, R. and Singhal, R. 2007. Effect of octenylsuccinylation on physicochemical and functional properties of waxy maize and amaranth starches. *Carbohydrate Polymers*. **68**(3), pp.447-456.
- Dickinson, E. 2000. Structure and Rheology of Simulated Gels Formed from Aggregated Colloidal Particles. *Journal of Colloid and Interface Science*. **225**(1), pp.2-15.
- Dickinson, E. 2012. Emulsion gels: The structuring of soft solids with protein-stabilized oil droplets. *Food Hydrocolloids*. **28**(1), pp.224-241.
- Dickinson, E. and Chen, J.S. 1999. Heat-Set Whey Protein Emulsion Gels: Role of Active and Inactive Filler Particles. *Journal of Dispersion Science and Technology*. **20**(1-2), pp.197-213.
- Imai, E. et al. 1999. Effect of physical properties of food particles on the degree of graininess perceived in the mouth. *Journal of Texture Studies*. **30**(1), pp.59-88.
- Kaufman, R.C. et al. 2015. Development of a 96-well plate iodine binding assay for amylose content determination. *Carbohydrate Polymers*. **115**, pp.444-447.
- Krstonošić, V. et al. 2011. Micellar properties of OSA starch and interaction with xanthan gum in aqueous solution. *Food Hydrocolloids*. **25**(3), pp.361-367.
- Langley, K.R. and Green, M.L. 1989. Compression Strength and Fracture Properties of Model Particulate Food Composites in Relation to Their Microstructure and Particle-Matrix Interaction. *Journal of Texture Studies*. **20**(2), pp.191-207.
- Lu, T.-J. et al. 2008. Effect of granular characteristics on the viscoelastic properties of composites of amylose and waxy starches. *Food Hydrocolloids*. **22**(1), pp.164-173.
- Malone, M.E. and Appelqvist, I.A.M. 2003. Gelled emulsion particles for the controlled release of lipophilic volatiles during eating. *Journal of Controlled Release*. **90**(2), pp.227-241.
- McClements, D.J. 2015. Encapsulation, protection, and release of hydrophilic active components: Potential and limitations of colloidal delivery systems. *Advances in Colloid and Interface Science*. **219**, pp.27-53.
- Miles, M.J. et al. 1985. The roles of amylose and amylopectin in the gelation and retrogradation of starch. *Carbohydrate Research*. **135**(2), pp.271-281.
- Moakes, R.J.A. et al. 2015. Preparation and characterisation of whey protein fluid gels: The effects of shear and thermal history. *Food Hydrocolloids*. **45**, pp.227-235.

- Nilsson, L. and Bergenståhl, B. 2006. Adsorption of Hydrophobically Modified Starch at Oil/Water Interfaces during Emulsification. *Langmuir*. **22**(21), pp.8770-8776.
- Ortega-Ojeda, F.E. et al. 2005. Gel formation in mixtures of hydrophobically modified potato and high amylopectin potato starch. *Carbohydrate Polymers*. **59**(3), pp.313-327.
- Rosalina, I. and Bhattacharya, M. 2002. Dynamic rheological measurements and analysis of starch gels. *Carbohydrate Polymers*. **48**(2), pp.191-202.
- Singh, N. et al. 2003. Morphological, thermal and rheological properties of starches from different botanical sources. *Food Chemistry*. **81**(2), pp.219-231.
- Svegmark, K. and Hermansson, A.-M. 1991. Changes induced by shear and gel formation in the viscoelastic behaviour of potato, wheat and maize starch dispersions. *Carbohydrate Polymers*. **15**(2), pp.151-169.
- Sweedman, M.C. et al. 2014. Aggregate and emulsion properties of enzymatically-modified octenylsuccinylated waxy starches. *Carbohydrate Polymers*. **111**, pp.918-927.
- Sweedman, M.C. et al. 2013. Structure and physicochemical properties of octenyl succinic anhydride modified starches: A review. *Carbohydrate Polymers*. **92**(1), pp.905-920.
- Tesch, S. et al. 2002. Stabilization of emulsions by OSA starches. *Journal of Food Engineering*. **54**(2), pp.167-174.
- Teyssandier, F. et al. 2011. Sol-gel transition and gelatinization kinetics of wheat starch. *Carbohydrate Polymers*. **83**(2), pp.400-406.
- Thirathumthavorn, D. and Charoenrein, S. 2006. Thermal and pasting properties of native and acid-treated starches derivatized by 1-octenyl succinic anhydride. *Carbohydrate Polymers*. **66**(2), pp.258-265.
- Torres, O. et al. 2016. Emulsion microgel particles: Novel encapsulation strategy for lipophilic molecules. *Trends in Food Science & Technology*. **55**, pp.98-108.
- Torres, O. et al. 2017. Design of novel emulsion microgel particles of tuneable size. *Food Hydrocolloids*. **71**, pp.47-59.
- Tukomane, T. and Varavinit, S. 2008. Influence of Octenyl Succinate Rice Starch on Rheological Properties of Gelatinized Rice Starch before and after Retrogradation. *Starch - Stärke*. **60**(6), pp.298-304.

- van Vliet, T. 1988. Rheological properties of filled gels. Influence of filler matrix interaction. *Colloid and Polymer Science*. **266**(6), pp.518-524.
- Wang, S. et al. 2015. Starch Retrogradation: A Comprehensive Review. *Comprehensive Reviews in Food Science and Food Safety*. **14**(5), pp.568-585.
- Wei, J. et al. 2016. Tailor-made microgel particles: Synthesis and characterization. *Colloids and Surfaces A: Physicochemical and Engineering Aspects*. **489**, pp.122-127.
- Zhang, N. et al. 2013. Developing gelatin–starch blends for use as capsule materials. *Carbohydrate Polymers*. **92**(1), pp.455-461.
- Zhang, Z. et al. 2015. Designing hydrogel particles for controlled or targeted release of lipophilic bioactive agents in the gastrointestinal tract. *European Polymer Journal*. **72**, pp.698-716.
- Zhu, J. et al. 2013. Nano-structure of octenyl succinic anhydride modified starch micelle. *Food Hydrocolloids*. **32**(1), pp.1-8.

Chapter 4

Design of novel whey protein based-emulsion microgel particles of tuneable size³



Abstract

In this study, we designed a one-step solvent-free route to prepare emulsion microgel particles, *i.e.*, microgel particles containing several sub-micron sized emulsion droplets stabilised by heat-treated whey protein. The heat treatment conditions were optimized using aggregation kinetics via fluorimetry and dynamic light scattering. Emulsions were gelled and microgel particles were formed simultaneously via turbulent mixing with calcium ions using two specific processing routes (Extrusion and T-mixing). By varying the calcium ion concentration and mixing conditions, the optimal parameters to tune the size and structure of the resultant emulsion microgel particles were identified. Microscopy at various length scales (confocal laser scanning microscopy, scanning electron microscopy) and static light scattering measurements revealed a decrease in particle size (100 to 10 μm) with lower turbulent mixing time (ca. 1.2×10^{-5} s) and lower concentrations of calcium ions (0.1 – 0.02 M). Larger particle sizes (500-1000 μm) were achieved with an increase in the

³ Published as: Torres, O., Murray, B. and Sarkar, A. 2017. Design of novel emulsion microgel particles of tuneable size. *Food Hydrocolloids*. **71**(Supplement C), pp.47-59. DOI: <https://doi.org/10.1016/j.foodhyd.2017.04.029>

turbulent mixing time (ca. 4.3×10^{-2} s) and higher concentrations of calcium ions (1 – 1.4 M). Using gelation kinetics data (small deformation rheology) and theoretical considerations, creation of smaller sized emulsion microgel particles was explained by the increased flux of calcium ions to the denatured whey protein moieties coating the emulsion droplets, enabling faster gelation of the particle surfaces. These novel emulsion microgel particles of tuneable size formed as a result of complex interplay between calcium ion concentration, heat treatment of whey protein, gelation kinetics and mixing time, may find applications in food, pharmaceutical and personal care industries.

4.1 Introduction

Lipophilic active molecules such as fat soluble vitamins, flavourings, fatty acids and essential oils pose challenges when incorporated into food, pharmaceuticals or other soft matter applications due to their partial or complete water insolubility. Besides oxidizing rapidly, most of these compounds are difficult to deliver in physiology and are generally only partially absorbed by the skin or via the gastrointestinal tract. Thus, their physiological activity is most often partly or fully lost before reaching the targeted physiological site (McClements, 2015). Consequently, there is a huge need to protect these lipophilic compounds from environmental degradation and tailor their release at particular biological sites (Sung et al., 2015). A wide range of technologies have been developed to encapsulate oil-soluble molecules, such as emulsions, emulsion gels, liposomes, micelles, nanoparticles, etc (McClements, 2011). Each of these has its own specific advantages and disadvantages in terms of degree of protection, delivery, cost, regulatory status, ease of use, biodegradability and biocompatibility (McClements and Li, 2010). Among these, emulsion microgel particles are vehicles that have not been explored as widely.

Emulsion microgel particles are a relatively new class of soft solids (Torres et al., 2016). The particles have a similar structure to emulsion gels, although their physical characteristics and scales differ. In emulsion microgel particles, emulsion droplets are stabilised by an emulsifier and gelling agent that create a soft solid shell around several emulsion droplets, which are then incorporated into a continuous gel matrix (Ruffin et al., 2014; Zhang et al., 2015). This soft solid shell has been demonstrated to protect lipophilic compounds such as polyunsaturated fatty acids

against oxidation (Beaulieu et al., 2002; Augustin and Sanguansri, 2012; Velikov and Pelan, 2008). Additionally, the microgel particle allows swelling or de-swelling as a function of pH, ionic strength, temperature and enzymatic conditions via tuning the size and/or physicochemical properties (Ballauff and Lu, 2007; Wei et al., 2016). Hence, these particles have great potential for site-dependent release of lipophilic active compounds in a range of food, pharmaceutical, personal care and other soft material applications (Ching et al., 2016).

Whey protein isolate (WPI) is widely accepted for research and commercial applications and its versatility as an emulsifier and gelling agent is well recognized (Sarkar, Murray, et al., 2016). Under heat-treatment WPI undergoes conformational changes, exposing its hydrophobic and sulfhydryl groups allowing irreversible aggregation and gel formation under specific conditions of protein concentration, ionic strength and temperature (Roefs & Peppelman, 2001). On addition of calcium (Ca^{2+}) ions, heat treated WPI (HT-WPI) undergoes further aggregation via Ca^{2+} cross-linking of the negatively charged carboxylic groups on the WPI. Protein- Ca^{2+} -protein complexes are formed, reducing the negative charge on the protein (Bryant & McClements, 2000; Hongsprabhas, Barbut, & Marangoni, 1999; Phan-Xuan, et al., 2014).

Several technologies have been developed for the production of WPI stabilised emulsion microgel particles. For instance, multistep emulsion-templating allows the formation of emulsion particles via $\text{O}_1/\text{W}/\text{O}_2$ emulsions (Sung, et al., 2015). The WPI aqueous phase of the $\text{O}_1/\text{W}/\text{O}_2$ emulsion is typically gelled through heat treatment, forming (O_1/W) WPI stabilised emulsion microgel particles suspended in an external oil phase (O_2). The oil phase is then washed away with the use of organic solvents. Although this generates microgel particles of controlled size: the multiple processing steps causes the technique to be laborious; heat gelation renders it ineffective for the use of heat-sensitive compounds; the use of organic solvents limits its application in certain medical drugs and food products where biocompatibility is a key issue (Beaulieu, et al., 2002). An alternative multistep emulsion-templating method was designed by Egan, Jacquier, Rosenberg, and Rosenberg (2013). The aqueous WPI phase of the $\text{O}_1/\text{W}/\text{O}_2$ emulsion was gelled via a cold set technique. The external oil phase (O_2) was then washed away with surfactants rather than solvents. Although this technique allows the encapsulation of heat-sensitive compounds and does not require

the use of solvents, the multiple processing required still causes this method to be time consuming and laborious plus excess surfactant may need to be removed.

Extrusion technologies allowing cold external gelation of heat-treated WPI emulsion microgel particles have also been developed (Egan, et al., 2013). In this case, the heat-treated WPI stabilised emulsion was dropped into an ionic bath, allowing the gelation of the continuous phase, which entrapped oil droplets into microgel particles. Although this external gelation method was successful it produced large particles, of 1 – 2 mm in diameter, limiting their application in food systems. Other processing methods produce emulsion microgel particles by emulsifying the oil phase with WPI or sodium caseinate and gelling the emulsion into microgel particles with alginate or pectin (Ruffin, et al., 2014; Zhang, Zhang, & McClements, 2016). The use of several different biopolymers causes this technique to be not very cost effective. Also, thermodynamic incompatibility between the protein at the interface and the gelling biopolymer might result in uncontrolled release behaviour.

Thus, external gelation has considerable potential if it can be made facile, rapid and allow processing of clean emulsion microgel particles. Careful optimization of temperature, shear and WPI and Ca^{2+} concentration might also allow the tailoring of the size of emulsion microgel particles. The objective of this study was to design and characterize HT-WPI emulsion microgel particles of tailored sizes and examine the complex interplay between whey protein concentration, Ca^{2+} concentration ($[\text{Ca}^{2+}]$) and turbulent mixing conditions.

Commercial whey protein isolate was heat treated at different temperatures and times and its unfolding and aggregation rate were monitored using a fluorescent probe method and dynamic light scattering, respectively. The gelation kinetics of HT-WPI stabilised emulsions with different concentrations of Ca^{2+} ions were examined using small deformation shear rheology. These rheological experiments showed the effect of $[\text{Ca}^{2+}]$ on the type of gels formed. Finally, two different turbulent mixing processing techniques involving extrusion or T-mixing were tested, hypothesized to offer different mixing times. The emulsion microgel particles were examined using confocal laser scanning microscopy and scanning electron microscopy. Theoretical considerations, such as the Kolmogorov mixing time and the flux of Ca^{2+} ions to HT-WPI interfaces were used to explain the differences in particle size of emulsion microgel particles, obtained with both processing routes.

4.2 Materials and Methods

4.2.1 Materials

Whey protein isolate (WPI) powder containing 96.3 wt% protein (Molecular mass: 18.4 kDa) was a kind gift from Fonterra Limited (Auckland, New Zealand). Sunflower oil was purchased from Morrisons supermarket (UK). Calcium chloride, 8-aniline-1-naphthalenesulfonic acid (ANS), sodium hydroxide, hydrochloric acid, sodium chloride, hexane anhydrous, 95% were purchased from Sigma-Aldrich (Gillingham, UK). Silicone oil 350 CST was purchased from VWR international S.A.S (Fontenay-sous-Bois, France). All solutions were prepared with Milli-Q water having ionic purity of 18.2 MΩ·cm at 25 °C (Milli-Q apparatus, Millipore, Bedford, UK). Nile Red was purchased from Sigma-Aldrich (Steinheim, Germany). Dimethyl sulfoxide (DMSO) was purchased from Fluorochem (Hadfield, UK). All other chemicals were of analytical grade and purchased from Sigma-Aldrich unless otherwise specified.

4.2.2 Analysis of whey protein aggregation

4.2.2.1 ANS Fluorescence method

Different concentrations of WPI (9.6 and 12 wt%) were diluted into Milli-Q water at pH 7. 8-aniline-1-naphthalenesulfonic acid (ANS) (1 mg mL⁻¹) were dissolved into 0.1 M NaCl. Spectrofluorimetric measurements were made using a Fluorescence spectrophotometer (Perkin-Elmer, LS-3, Waltham, USA) following the method of Nyman and Apenten (1997). The ANS fluorescence measurements involved a fluorescence excitation wavelength of 280 nm and an emission wavelength of 470 nm. The final concentration of ANS was determined by fluorescent titration of 12 wt% WPI heated at 85 °C for 40 min. Increasing amounts of ANS stock solution were added to WPI samples (3 mL) in a quartz cuvette. Fluorescence emission intensity (ΔF) was recorded in relative fluorescence units (rfu). A graph of volume ANS (x-axis) vs ΔF provided a value for the maximum volume of ANS needed (150 μ L) as the curve reached a plateau (result not shown). The concentration of ANS was determined using Equation 4.1:

$$[\text{ANS}] = \frac{V_{\text{ANS}} \times C_{\text{ANS}}}{(V_{\text{ANS}} + V_{\text{WPI}})} \quad (4.1)$$

where, C_{ANS} is the concentration of ANS stock solution (3.2 mM), V_{WPI} is the volume of protein and V_{ANS} is the volume of ANS added to the protein solution. This final concentration of ANS (0.15 mM) was used for the subsequent measurement.

12 wt% and 9.6 wt% WPI solutions were heated at different temperatures (75, 80 or 85 °C) for different time periods (0, 8, 15, 30, 40, 50 min). Protein solutions were decanted into quartz cuvettes (3 mL) and ANS (150 μ L) was then added to each sample. The fluorescence emission intensity of each sample was recorded at the stated temperature.

The data was analysed using the Scatchard Equation 4.2,

$$\frac{LB}{LF} = \frac{nP}{Kd} - \frac{LB}{Kd} \quad (4.2)$$

where LB is the concentration of ANS bound to the protein, LF is the concentration of unbound ANS, n is the number of moles of ANS bound per mole of protein, P is the concentration of WPI and Kd is the dissociation constant for reaction: ANS + protein = complex.

The LB was determined from ΔF (the fluorescence measurements) using the conversion factor Q_c as given by Equation 4.3:

$$LB = \Delta F / Q_c \quad (4.3)$$

The conversion factor Q_c was obtained following the method from Nyman and Apenten (1997).

The LF was determined from $LF = [ANS] - LB$. The ratio LB/LF was then calculated and plotted against time using Equation 4.4:

$$Relative \frac{LB}{LF} = \frac{\left(\frac{LB}{LF}\right)_t}{\left(\frac{LB}{LF}\right)_f} \quad (4.4)$$

where $(LB/LF)_t$ is LB/LF at different times and $(LB/LF)_f$ the final value of LB/LF .

All measurements were repeated three times and mean values are reported.

4.2.2.2 Particle size of protein aggregates

The aggregation rate of the aforementioned 12 wt% and 9.6 wt% WPI solutions were measured at the different time-temperature treatments using dynamic light scattering (Zetasizer, Nano ZS series, Malvern Instruments, Worcestershire, UK).

Sizing of WPI particles was conducted based on a relative refractive index of 1.150 (*i.e.*, the ratio of the refractive index of WPI (1.53) to that of the aqueous phase at 1.33). The absorbance value of WPI particles was set at 0.001. Before analysis, samples were diluted to 0.1 wt% WPI with Milli-Q water and filtered through with a membrane of 0.45 μm (PTFE Syringe filters, Perkin Elmer, USA). One mL of solution was injected into a clean cuvette (PMMA, Brand GmbH, Wertheim, Germany). Particle size was presented as mean hydrodynamic diameter of five readings on duplicate samples.

4.2.3 Preparation of heat denatured whey protein-stabilised emulsion

Whey protein isolate (12 wt%) was dissolved in Milli-Q water and gently stirred (500 rpm) for 2 h using a magnetic stirrer to allow complete protein hydration. The solution was adjusted to pH 7 using 0.1 M NaOH or HCl. The suspension was then heat treated at 85 °C for 40 min in a water bath and cooled in cold water (10 °C) for 2 h to create heat denatured WPI (HT-WPI).

Sunflower oil was subsequently mixed with the HT-WPI solutions. The ratio of the aqueous phase to lipid phase in the emulsion was 80:20 (w/w), with a final HT-WPI concentration of 9.6 wt%. This solution was pre-emulsified with a high speed rotor-stator mixer (Silverson, L5M-A, UK) at 8,000 rpm for 5 min. The pre-emulsion was further homogenized in a laboratory scale two-stage valve high pressure homogenizer at 250/50 bar with three passes (Panda Plus, GEA Niro Soave, Parma, Italy). Sodium azide (0.02 wt%) was added as an antimicrobial agent to the emulsion samples stored for 24 h at 4 °C.

4.2.4 Zeta-potential

The ζ -potential of the emulsion droplets was determined using a particle electrophoresis instrument (Zetasizer, Nano ZS series, Malvern Instruments, Worcestershire, UK). The emulsion was diluted to 0.005 wt% droplet concentration using Milli-Q water. It was then added to a folded capillary cell (Model DTS 1070,

Malvern Instruments Ltd., Worcestershire, UK). The ζ -potential of the emulsion was measured ten times for each diluted sample.

4.2.5 Preparation of emulsion microgel particles

Emulsion microgel particles were produced using two different bottom-up techniques via Ca^{2+} -mediated external gelation: 1. Buchi Encapsulator[®] or 2. the Leeds jet homogenizer.

Table 4.1 illustrates the key processing conditions for both equipment and Figure 4.1 illustrates the formation method of emulsion microgel particles.

In the Buchi Encapsulator B-390[®], the HT-WPI stabilised emulsion was dropped through a 150 μm vibrating nozzle into a turbulently stirred solution ($\text{Re} > 10^4$) of Ca^{2+} ions (1 – 1.4 M). The Encapsulator nozzle was set to oscillate at a frequency of approximately 260 Hz, with a drive current amplitude of 3 A and generating a differential pressure of 418 mbar. All solutions were at ambient temperature (25 °C) at the time of the experiment. Throughout the “extrusion” process and for 30 min thereafter, the aqueous Ca^{2+} solution was stirred at 500 rpm using a 3 cm magnetic stirrer. The microgel particles were then filtered and washed three times using Milli-Q water to remove residual Ca^{2+} and stored at 4 °C before characterization. The second method involved the use of the Leeds Jet Homogenizer along the lines described by Pravinata et al. (2016). Briefly, the Leeds Jet Homogenizer has two separate chambers of different ratios (45:55 w/w were used in this case) connected via a thin capillary tubing to an outlet via a pinhole (0.5 mm diameter in this work). Essentially, it is a T-mixer capable of producing very high liquid velocities. A hydraulic ram pushes onto the pistons on top of both chambers forcing the liquids through the pinhole at high velocity, generating highly turbulent conditions depending on the pressure applied (100 – 400 bar) (Casanova and Higueta, 2011).

Table 4.1 Key processing conditions for Buchi Encapsulator B-390[®] and Leeds Jet homogenizer, respectively.

Parameters	Buchi Encapsulator B-390 [®]	Leeds Jet Homogenizer
[Ca^{2+}] (M)	1-1.4	0.02-0.1
Nozzle size (μm)	150	500
Pressure (bar)	0.4	250
Flow Rate (mL/sec)	5.6×10^{-2}	30
Reynolds number	4.7×10^4	7.6×10^4

In this work, HT-WPI stabilised emulsion was added to one chamber and CaCl₂ solution (0.02 – 0.1 M) to the other chamber. A pressure of 250 bar was employed (Table 4.1). The turbulent mixing resulted in the formation of emulsion microgel particles. The resulting particles were collected in a beaker and immediately diluted with Milli-Q water and stirred for 30 min at low speed to limit particle aggregation. The Reynolds number of the Jet Homogenizer was calculated using Equation 4.5:

$$\text{Re} = \rho v d / \eta \quad (4.5)$$

with ρ the solvent density (*i.e.*, water), v the maximum fluid velocity, d the diameter of the nozzle used with the Jet Homogenizer, η the dynamic viscosity of the solution at 20 °C.

In the case of the Jet Homogenizer, the velocity was calculated using the mean velocity of a fluid in a pipe Equation 4.6:

$$v = \frac{4q}{d^2\pi} \quad (4.6)$$

with q the volumetric flow rate and d the diameter of the nozzle.

In the case of the Encapsulator, the Reynolds number was calculate using the stirred vessel model Equation 4.7:

$$\text{Re} = \frac{\rho n d^2}{\eta} \quad (4.7)$$

with n the rotational speed of the magnetic agitator and d the diameter of the magnetic agitator.

4.2.6 Small deformation rheology

The dynamic oscillatory viscoelasticity of the HT-WPI and HT-WPI stabilized emulsion gels formed at different [Ca²⁺] were investigated at low strain and ambient temperature using a Kinexus Ultra, (Malvern Instruments) shear rheometer following the method from Sok et al. (2005) for Ca²⁺-induced cold gelation of whey protein. The gelation of the protein solution or protein stabilized emulsion were induced by adding different [Ca²⁺] ions solution and vortexing the solutions at 23 °C. A 40 mm cone-and-

plate geometry (model: CP4/40 SS017SS) was used for all the measurements. About 0.5 mL of sample (HT-WPI solution or HT-WPI-stabilized emulsion (20 wt% oil, 9.6 wt% HT-WPI)) was poured onto the sample plate and sealed with a thin layer of the 350 cst silicone oil to prevent evaporation.

The storage modulus (G') and the loss modulus (G'') were measured firstly on conducting a strain sweep between 0.01 and 100 % strain, at 1 Hz and 25 °C, to determine the linear viscoelastic region. The second test performed on the emulsion gel was the time sweep. This test was carried out in the linear viscoelastic region (0.5 % strain), 25 °C and 1 Hz. Three measurements were performed on individual samples for each of the aforementioned tests.

4.2.7 Particle size analysis of emulsion and emulsion microgel particles

Static light scattering was used to measure the particle size distribution of the emulsion droplets and emulsion microgel particles via a Malvern Mastersizer 3000E hydro, (Malvern Instruments, Worcestershire, UK). Samples were diluted in distilled water until the instrument gave an obscuration of 4 – 6%. Sizing of the emulsion oil droplets was conducted based on a relative refractive index of 1.097 (*i.e.*, the ratio of the refractive index of sunflower oil at 1.460 to that of the aqueous phase at 1.33). The absorbance value of the emulsion droplets was set to 0.001. Sizing of the emulsion microgel particles formed with Leeds Jet homogenizer was conducted based on a relative refractive index of 1.150 (*i.e.*, the ratio of the refractive index of WPI at 1.53 to that of the aqueous phase at 1.33). The absorbance value of the emulsion microgel particles was similarly set to 0.001.

Emulsion microgel particles formed using the Buchi Encapsulator B-390[®] were sized using image analysis of the digitized images captured via a Nikon SMZ-2T (Nikon, Japan) optical microscope, due to their larger sizes (> 500 μm). To achieve acceptable statistical errors ten images containing at least twelve emulsion microgel particles were analysed.

4.2.8 Microscopy

All emulsion microgel particles were imaged at various length scales via optical microscopy (Nikon, SMZ-2T, Japan), confocal laser scanning microscopy (CLSM) or scanning electron microscopy (SEM).

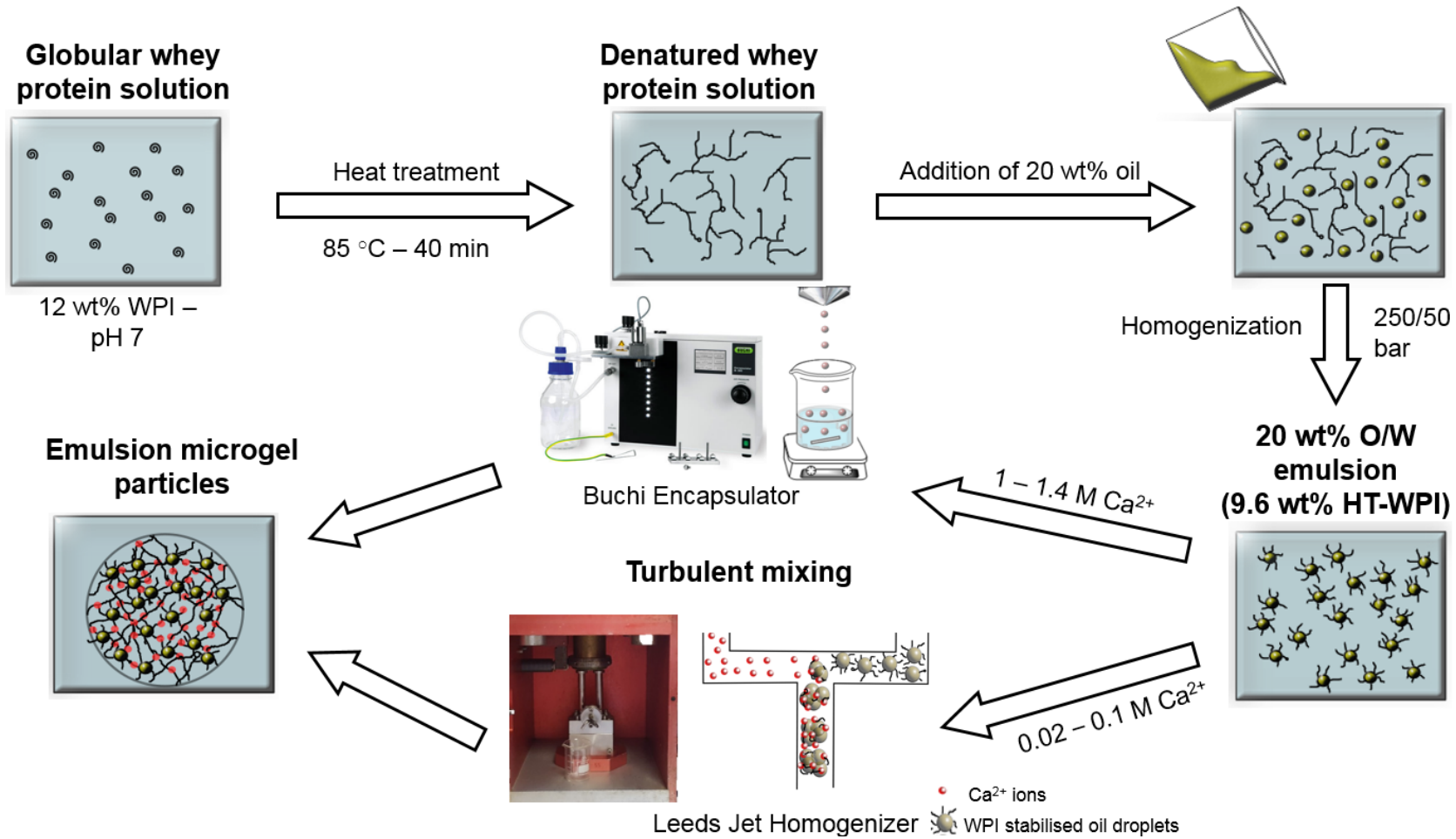


Figure 4.1 Schematic diagram of the formation of emulsion microgel particles using cold Ca^{2+} ion-induced gelation process

A Zeiss LSM 700 confocal microscope (Carl Zeiss MicroImaging GmbH, Jena, Germany) with a 10 – 40× magnification was used. Nile Red (1 mg mL⁻¹ in dimethyl sulfoxide, 1:100 v/v) was used to stain oil (argon laser with an excitation line at 488 nm) and Rhodamine B (0.5 mg mL⁻¹ in Milli-Q water, 1:100 v/v) was used to stain proteins (argon laser with an excitation line at 568 nm). The microgel particles were mixed with 10 μL of Nile Red (0.1% w/v) and 10 μL of Rhodamine B, stirred for 15 min and placed onto a microscope slide and covered with a cover slip before imaging.

A scanning electron microscope (JEOL 6390 A, JEOL, Japan) was also used to study the structural features of some particles modifying the method of Sarkar et al. (2016a). The emulsion microgel particles were dried in an oven at 37 °C for 72 h and subsequently washed with hexane removing all oil droplets. After removal of the oil, the intact or deliberately fractured particles were mounted onto a chrome coated steel plate with carbon double sided-tape and sputter coated with gold using a JEOL JFC-1600 Auto Fine Coater (JEOL Japan) for 200 s at 30 mA. The SEM images were then obtained at 10 – 20 kV.

4.2.9 Statistical analysis

Significant differences between samples were determined by one-way ANOVA and multiple comparison test with Tukey's adjustment performed using SPSS software (IBM, SPSS statistics, version 24) and the level of confidence was 95%.

4.3 Results and discussion

4.3.1 Denaturation and aggregation kinetics of HT-WPI solution

ANS fluorescence was used to examine the changes in hydrophobicity of WPI at different heat-treatments, since ANS fluorescence intensity increases when bound to nonpolar hydrophobic groups (Jeyarajah and Allen, 1994). WPI contains globular proteins with their hydrophobic and sulfhydryl groups tending to be buried in the interior of the protein structure. However, during heat-treatment, the WPI proteins unfold, exposing and activating their hydrophobic and sulfhydryl groups towards the outer surface of the protein (Moakes et al., 2015a; Wolz and Kulozik, 2015). Therefore, ANS fluorescence can be used to understand the extent to which WPI unfolds at different temperatures and times, initiating aggregation and subsequent

gelation (Das and Kinsella, 1990; Kim et al., 2005; Nyman and Apenten, 1997). The temperature at which WPI was heated had a significant effect on the unfolding rate of the protein, regardless of the protein concentration. It can be observed from Figure 4.2 A that on increasing the temperature by 10 °C (from 75 °C to 85 °C), the relative LB/LF ratio reached a plateau 25 min earlier, irrespective of WPI concentration. The faster unfolding of WPI with increase temperature has also been noticed by Das and Kinsella (1990). In the case of 9.6 wt% WPI, LB/LF reached a plateau at 85 °C after 15 min: approximately 87% ANS was observed to be bound to HT-WPI (Figure 4.2 B). Consequently, it is suggested that after 15 min at 85 °C, no more hydrophobic groups are available for ANS to bind to resulting in almost total unfolding of WPI, in agreement with previous studies (Kim et al., 2005). In comparison, at the lower temperature of 75 °C, LB/LF reached a plateau only after a longer exposure time of 40 min with 76% ANS bound to WPI (Figure 4.2 A and B). Thus, at 75 °C, the temperature was not high enough to unfold and denature the WPI fully. These results are in agreement with previous studies in the literature (Ruffin et al., 2014; Wolz and Kulozik, 2015) as well as circular dichroism results (see Appendix B.1).

The concentration of WPI also affected its denaturation and aggregation rate. As shown in Figure 4.2 B, lower WPI concentrations reached a higher LB/LF ratio at any given time and temperature. For instance, 9.6 wt% WPI heat-treated at 80 °C for 30 min had 93% ANS bound whereas, 12 wt% WPI heat-treated at 80 °C for 30 min only had 68% ANS bound. However, the ANS fluorescence method holds limitations.

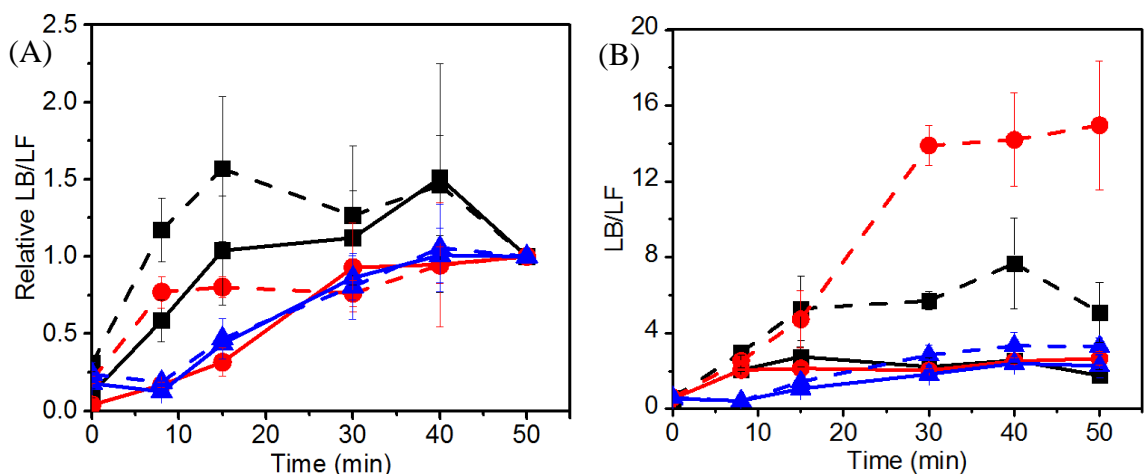


Figure 4.2 Influence of temperature (75 °C, ▲; 80 °C, ● and 85 °C, ■) on relative bound/ unbound ratio (A) and absolute bound/ unbound ratio (B) of ANS to whey protein. Solid and dashed lines indicate 12 wt% and 9.6 wt% WPI, respectively.

Under prolonged heat treatment WPI aggregates promptly, re-burying the exposed hydrophobic groups which might become inaccessible to ANS. This might reduce the fluorescence intensity of the sample. For that reason, dynamic light scattering, and circular dichroism results have been analysed in parallel to the ANS fluorescence measurements.

Analysing ANS results in connection with the aggregation rate of WPI at different times and temperature (Figure 4.3) highlighted that at higher concentrations, HT-WPI aggregated more easily (Wolz and Kulozik, 2015; Marangoni et al., 2000). As can be observed from dynamic light scattering results, before heat treatment the particle sizes at 12 wt% and 9.6 wt% WPI were similar, *i.e.*, 181 nm and 189 nm, respectively, clearly larger in size than the native constituent proteins of WPI. Eight min after heat treatment, the particle size at both concentrations decreased by approximately 75%. Such a decrease has also been noticed by previous authors (Ju and Kilara, 1998). At high concentration, WPI probably forms oligomers in solution prior to heating, due to its reduced solubility, increasing its particles size. With increasing temperature ($> 60\text{ }^{\circ}\text{C}$), the solubility of the WPI aggregates is likely to increase, allowing the dissociation of these oligomers into dimers and monomers, which increases WPI flexibility and mobility as well as decreases the size of the aggregates (Wijayanti et al., 2014; Zúñiga et al., 2010). Interestingly, for 12 wt% at 75 and 80 $^{\circ}\text{C}$, the particle size after 8 min only decreased

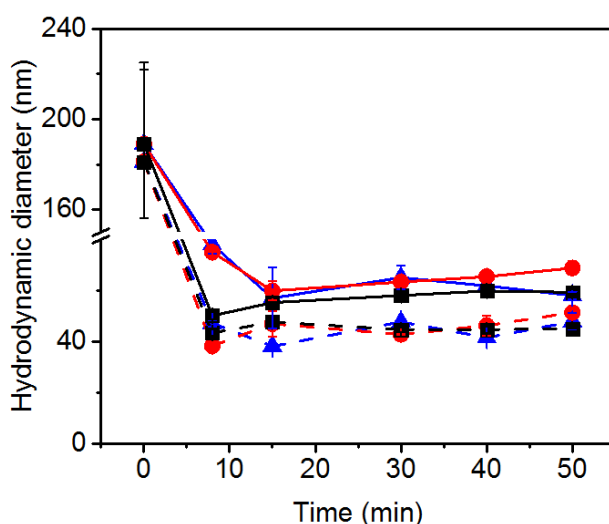


Figure 4.3 Mean hydrodynamic diameter (nm) of whey protein aggregates when subjected to temperature conditions (75 $^{\circ}\text{C}$, ▲; 80 $^{\circ}\text{C}$, ● and 85 $^{\circ}\text{C}$, ■). Solid and dashed lines indicate 12.5 wt% and 9.6 wt% WPI, respectively.

by approximately 60% (from 189 nm to 78 and 75 nm, respectively), whereas at 85 °C the particle size decreased by 75%. At high WPI concentration (*i.e.*, 12 wt%), a further 7 min at 80 °C were necessary to break down the oligomers into monomers and reduce WPI particle size by 75%. These results are in agreement with previous studies conducted by Das, et al. (1990). After 15 min of heat treatment, HT-WPI particle size slightly increased. For instance, at 85 °C, 9.6 wt% WPI particles size at 8 min measured 43 nm and after 15 min these measured 48 nm (into dimers and monomers, which increases WPI flexibility and mobility as well as decreases the size of the aggregates (Wijayanti et al., 2014; Zúñiga et al., 2010). Interestingly, for 12 wt% at 75 and 80 °C, the particle size after 8 min only decreased (Figure 4.3). As previously discussed, 87% ANS was found to be bound to HT-WPI after 15 min at 85 °C, suggesting almost total unfolding. This slight increase in particle size might therefore be explained by the exposure of the hydrophobic groups of the protein upon unfolding which might lead to protein-protein interactions (Beaulieu et al., 2002; Iametti et al., 1995; Jeyarajah and Allen, 1994), reinforced by subsequent disulphide and other types of cross-linking.

The concentration of WPI also affected the size of the HT-WPI aggregates. For instance, at 75 °C after 30 min, the particle size of 12 wt% WPI was 35% higher than for 9.6 wt%. This is probably explained by the fact that at higher WPI concentrations, the chances of hydrophobic and sulfhydryl groups from one protein colliding with groups of neighbouring proteins increases, resulting in larger sized particles at all heating times (Ju and Kilara, 1998; Barbut and Foegeding, 1993; Hongsprabhas and Barbut, 1997). Other non-covalent physical interactions, such as van der Waals attraction, hydrogen bonds and electrostatic attraction, contribute to a lesser extent to the aggregation of HT-WPI during heat-treatment (Roefs and Peppelman, 2001). Therefore, at 12 wt% WPI, HT-WPI might have aggregated completely after 15 min, concealing its hydrophobic and sulfhydryl groups on the inner surface of the protein. These buried hydrophobic groups would be inaccessible to ANS, leading to lower LB/LF ratios as compared to 9.6 wt% WPI (Iametti et al., 1995). These results suggested that the formation of cold set emulsion microgel particles would only occur if the initial concentration of WPI was high enough and WPI was largely unfolded and aggregated, allowing spontaneous gelation when contacting Ca^{2+} . Based on the above results, further experiments were conducted with an initial concentration of 12 wt% WPI heat-treated at 85 °C for 40 min.

4.3.2 Droplet size of HT-WPI stabilised emulsions

Figure 4.4 shows the droplet size distribution of the 20 wt% sunflower oil emulsion stabilised by 9.6 wt% HT-WPI. Droplet sizes ranged from 0.1 to 10 μm as expected from many other studies. The CLSM image (Figure 4.4) confirms this, showing a uniform size distribution of oil droplets. Additionally, the droplet size distribution was monomodal, narrow and symmetric, suggesting that the emulsion was well homogenized and stable. The emulsion droplets were not flocculated during the homogenization stage, as confirmed by the d_{43} value, which was below 0.5 μm and were anionic (-43 mV) as expected at pH 7.

4.3.3 Rheological properties of cold-set HT-WPI emulsion gels

The gelation of HT-WPI solutions and emulsions was induced by the addition of Ca^{2+} at different concentrations. Figure 4.5 shows the storage modulus (G') of the emulsion gels or protein gels (without oil droplets) at different concentrations of Ca^{2+} ions as a function of time and strain. For all systems, G' was significantly greater than G'' ($p < 0.05$), with $\tan \delta < 0.3$, which implied that the gels had an elastic behaviour. Therefore, in the following, only results for G' are presented and discussed. In comparison to cold set HT-WPI protein gels (without oil droplets), cold set HT-WPI emulsion gels were nearly two orders of magnitude stronger (Figure 4.5 A insert).

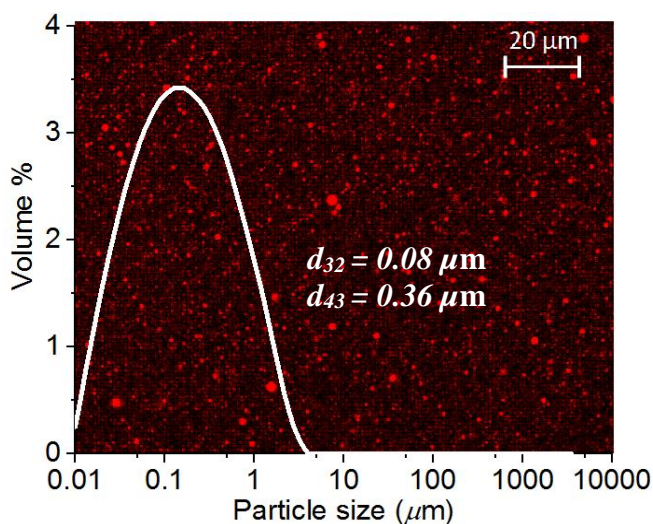


Figure 4.4 CLSM micrograph, superimposed droplet size distribution and d_{32} , d_{43} values of 20 wt% oil-in-water emulsion stabilised by 9.6 wt% HT-WPI at 25 °C and pH 7; oil droplets stained using Nile Red. Scale bar represents 20 μm .

Since the size of the oil droplets was on average $0.1 \mu\text{m}$, the interfacial tension and Laplace pressure means that these droplets can effectively be considered as solid particles (van Vliet, 1988). Additionally, the HT-WPI adsorbed at the surface of oil droplets may be considered as physically and chemically bound to the HT-WPI in the matrix, via electrostatic and hydrophobic interactions as well as hydrogen bonds. Hence, the oil droplets acted as “active” or “bound” fillers (Torres et al., 2016), increasing the strength of the gel.

As observed in Figure 4.5 A, all cold set emulsion gels had similar rheological behaviour irrespective of the $[\text{Ca}^{2+}]$ (0.02 to 1.4 M). On addition of Ca^{2+} , the emulsions gelled instantaneously, as shown by the storage modulus being above 3 kPa at time zero. Over time, all four emulsion gels became slightly stronger: after 1h 40 min, G' of all emulsion gels increased on average by 50%. This might be attributed to a gradual increase in the number density of Ca^{2+} -protein interactions (Marangoni et al., 2000). Understanding the structure of the emulsion gels with regard to varying $[\text{Ca}^{2+}]$ might give valuable insight on the mechanical strength of the emulsion gels. The rubber elasticity theory modified by Flory (Flory, 1953; Betz et al., 2012) for polymers allows a simplistic analysis of the structure of viscoelastic material via their elastic mechanical behaviour. At small deformations ($< 2\%$), the emulsion gels fully recovered to their original dimension in a prompt manner (Peppas et al., 2000) implying that these emulsion gels were almost perfectly elastic. Therefore, it was of interest to express the results in terms of the theoretical mesh size. The average mesh (or pore) size (ξ) of a cross-linked network is defined as the distance between two crosslinks or macromolecular chains (Peppas et al., 2000; Sarkar et al., 2015) and can be calculated using Equation 4.8:

$$\xi^3 = \frac{\kappa_B T}{G'} \quad (4.8)$$

where κ_B is the Boltzmann constant, T is the temperature and G' the storage modulus. However, it should be noted that whey protein gels are not cross-linked networked but rather particulate gels, hence the average mesh size calculation can only be used as an indication as to how the mesh size changes under strain.

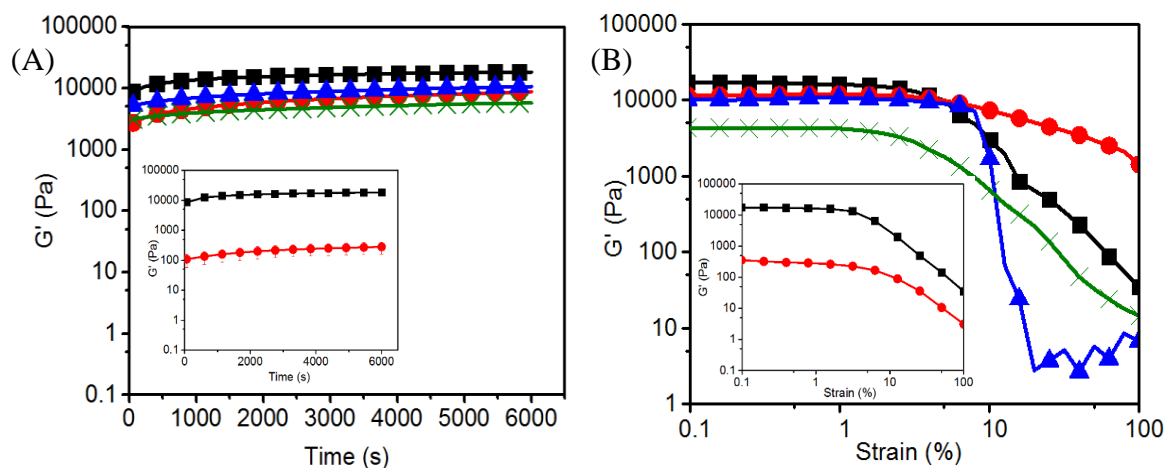


Figure 4.5 Storage modulus (G') as a function of time (A) and strain (B) of emulsion gel with 9.6 wt% HT-WPI and 20 wt% oil prepared using different concentration of Ca^{2+} ions (0.02 M, ●; 0.1 M, ■; 1 M, ▲; 1.4M, ×) and insert of emulsion gel (■) versus protein gel (●) at 0.1 M Ca^{2+} .

Table 4.2 highlights the impact of $[\text{Ca}^{2+}]$ on the storage modulus and mesh size of the cold set emulsion gels. For instance, 0.1 M Ca^{2+} ions significantly produced the strongest gel ($G' = 18.2$ kPa) and therefore the smallest calculated mesh size (6.1 nm), whereas 0.02, 1 and 1.4 M Ca^{2+} ions produced the weakest gels ($G' = 8.8, 10.6$ and 5.7 kPa, respectively), during a corresponding time period of 1 h 40 min. Thus, as expected from Equation 4.8 and the values of G' , calcium plays an important role in the type and strength of gels formed. Above and below 0.1 M Ca^{2+} , values of G' suggest coarser and more porous structures weakening the emulsion gel strength. However, the calculated mesh sizes of all the emulsion gels were nearly an order of magnitude smaller than the oil droplets size (> 80 nm), suggesting the droplets would probably not be able to diffuse out of the gel matrix and further explaining their action as “active” fillers. The chances of them leaking out during the emulsion microgel particles formation is also minimized although possible as the cross-linking of the WPI network is not fully complete (Table 4.2). Emulsion gels produced with 0.02 M Ca^{2+} had gel strengths similar to those formed with 1 M and 1.4 M Ca^{2+} . As explained by several authors, Ca^{2+} ions cross-link with negatively charged carboxylic groups on WPI via electrostatic interactions (Phan-Xuan et al., 2014). Understanding the minimum concentration of Ca^{2+} required to bind to every free carboxylic groups on WPI may provide further insight into the HT-WPI emulsion gelation. Assuming all the

Table 4.2 Final storage modulus (G') measurement at 25 °C and 1 Hz, and mesh size (ζ) and standard deviation for the various rheological measurements of HT-WPI emulsion gel at different $[Ca^{2+}]$; line containing mean with similar subscript letter are not significantly different ($p > 0.05$).

Parameter	$[Ca^{2+}]$ (M)			
	0.02	0.1	1	1.4
Final G' (kPa)	8.8 ± 1.6 ^{a,c}	18.2 ± 3.6 ^b	10.6 ± 0.3 ^{a,d}	5.7 ± 2.4 ^{c,d}
G' at 10% strain (kPa)	7.3 ± 2.2 ^a	3 ± 2.3 ^{a,b,c}	1.6 ± 0.3 ^{b,d}	0.7 ± 0.2 ^{c,d}
Initial ζ (nm)	7.8 ± 0.4 ^{a,b,c}	6.1 ± 0.4 ^{a,d}	7.2 ± 0.06 ^{b,d}	9.2 ± 1.2 ^c
ζ at 10% strain (nm)	8.3 ± 0.8 ^a	12.2 ± 3.3 ^{a,b}	13.5 ± 0.9 ^b	20.3 ± 1.3 ^c

WPI consists of β -lactoglobulin molecules, theoretically, this minimum $[Ca^{2+}]$ can be calculating from Equation 4.9: α

$$[Ca^{2+}] = \frac{n(COO^-)m(WPI)_i}{M_w} \frac{1}{2V} \quad (4.9)$$

where $n(COO^-)$ is the number of free carboxylic groups per β -lactoglobulin molecule, $m(WPI)_i$ is the mass of WPI, M_w is the molecular weight of β -lactoglobulin and V is the solution volume. In this study, the molecular weight of one β -lactoglobulin monomer (18.4 kDa) containing 28 free carboxylic groups (Alexander et al., 1989) was used, since on heat treatment above 60 °C, β -lactoglobulin dimers dissociate into monomers (Zúñiga et al., 2010). Note that this calculation assumes that all COO^- groups were available for binding, which clearly is an over estimate since some carboxylic groups may still be hidden within the protein structure and unavailable for binding. From previous studies, the HT-WPI monolayer surface coverage (Dickinson, 1998; Das and Kinsella, 1990) of droplets was estimated at 3 mg/m². Therefore, in this study, assuming that the total surface area of the 20 wt% oil emulsion was 1203 m² (calculated from the particle size distribution), we calculated that this surface was covered by 3.6 g of HT-WPI.

From Equation 4.9, we then calculated that the minimum $[Ca^{2+}]$ required to bind to all COO^- groups on the β -lactoglobulin molecules absorbed at the oil/water interface would be 0.03 M. On this basis, for the systems gelled at 0.02 M Ca^{2+} , there

was not enough Ca^{2+} and this insufficient amount led to slower gelation kinetics of HT-WPI, as well as the formation of a weaker emulsion gel ($G' = 8.8$ kPa). For systems gelled at 0.1 M Ca^{2+} and above, there would clearly be a significant excess of Ca^{2+} and bridging flocculation might have led to more coarse, porous and non-continuous aggregates, especially for emulsion gels produced at high $[\text{Ca}^{2+}]$ such as 1 and 1.4M. These coarser non-continuous aggregates would allow the disruption of the protein network reducing the emulsion gel strength, as seen with the theoretical mesh size calculations (Beaulieu et al., 2002; Sok et al., 2005; Westerik et al., 2015).

Figure 4.5 B demonstrates that all emulsion gels tested (0.02 – 1.4 M Ca^{2+}) had a similar linear viscoelastic region, ranging from 0.1 – 2.0% shear strain. With increasing strain, emulsion gels became weaker and their storage modulus decreased dramatically. Oil droplets probably acted as weakening points at larger strain ($> 10\%$), allowing the gels to collapse. These results are in accordance with previous studies (Chen and Dickinson, 1999; Dickinson, 2000). Additionally, the concentration of Ca^{2+} ions involved in the emulsion gel formation influenced their behaviour under small deformation. At low $[\text{Ca}^{2+}]$ (0.02 and 0.1 M), the structure of the gel was probably more fine stranded (Hongprabhas et al., 1999) and able to absorb the energy applied during shearing, as previously described by Dickinson (2000). For instance, at 0.02 M Ca^{2+} the theoretical initial mesh size is similar to the mesh size at 10% strain (Table 4.2) and the emulsion gel did not break down ($G' = 7.3$ kPa at 10% strain). Above this $[\text{Ca}^{2+}]$, the emulsion gels broke down readily above 10% strain ($G' < 5$ kPa). The theoretical mesh size of emulsion gels formed above 0.02 M Ca^{2+} doubled after 10% strain. For instance, the theoretical mesh size of emulsion gels formed at 1.4 M Ca^{2+} ions increased from 9.2 to 20.3 nm. Clearly, this emulsion gel was significantly weaker and less elastic and this could possibly be explained by its higher porosity. In coarser aggregates, zones of higher densities of cross-links act as crack initiators and increase the brittleness of gels (Kuhn et al., 2010).

4.3.4 Design of size-tuneable HT-WPI emulsion microgel particles

Two processing methods were used to form different sized and shaped emulsion microgel particles (Figure 4.6). The first method involved turbulent mixing of the emulsion and Ca^{2+} ions solution via the Leeds Jet Homogenizer at 250 bar and nozzle size 500 μm (Figure 4.6 A). Low concentrations of Ca^{2+} ions (0.02 to 0.1 M) were

chosen to create emulsion microgel particles due to the fact that at higher concentrations the gelation happened too quickly, blocking the homogenizer and nozzle. The Leeds Jet homogenizer produced small (around 20 μm) but highly aggregated microgel particles (Figure 4.6 A1). Some oil droplets could also be seen coating the surface of the particles due to the short residence time (Figure 4.6 A2). However, most oil droplets (in red) appeared to be entrapped within the HT-WPI matrix (Figure 4.6 A2) as is emphasized with Figure 4.6A3, where the protein matrix is in green and the oil droplets are in black. A statistical analysis of the amount of oil found at the surface of the emulsion microgel particles was carried out on Figure 4.6 A2 using ImageJ software (version 1.48r, National Institute of Health, Bethesda, USA). It should be noted however, that because the analysis was only conducted on one image, the accuracy of the statistical analysis might be limited. Further images should be analysed for a better approximation of the amount of oil found at the surface of the particles. A colour threshold was applied to segregate oil droplets found at the surface of the particles from oil droplets encapsulated inside the particles and particle analysis was conducted. The number of surface oil droplets, their area and diameter were determined as well as the area of the emulsion microgel particles. The total area represented by the surface oil droplets was only 9,100 μm^2 or 9% of the total area (98,900 μm^2) of the emulsion microgel particles. Although this is purely a two-dimensional analysis, through a 'cut' across the sample, it suggests that the majority of the oil droplets were effectively incorporated inside the emulsion microgel particles. Further measurements should be conducted for more accurate characterization of the efficiency of emulsion encapsulation. It should also be noted that the oil droplets observed at the surface of the particles tended to be significantly larger (around 4 μm) than the majority of the emulsion droplets entrapped – which appeared to have retained the original mean size (around 0.1 μm) prior to microgel particle formation (Figure 4.6 A3). Therefore, it may also be concluded that the formation process did not lead to significant destabilisation and coalescence of the emulsion droplets.

The second processing method involved extrusion of the emulsion via the Buchi Encapsulator[®] at low pressure (0.4 bar) with the smaller vibrating nozzle size (150 μm), as well as turbulent mixing of the Ca^{2+} ions solution (500 rpm stirrer speed; $\text{Re} = 4.7 \times 10^4$) (Figure 4.6 B). High concentrations of Ca^{2+} ions (1 – 1.4 M) were required for this method, because at lower concentrations diffusion of Ca^{2+} to the

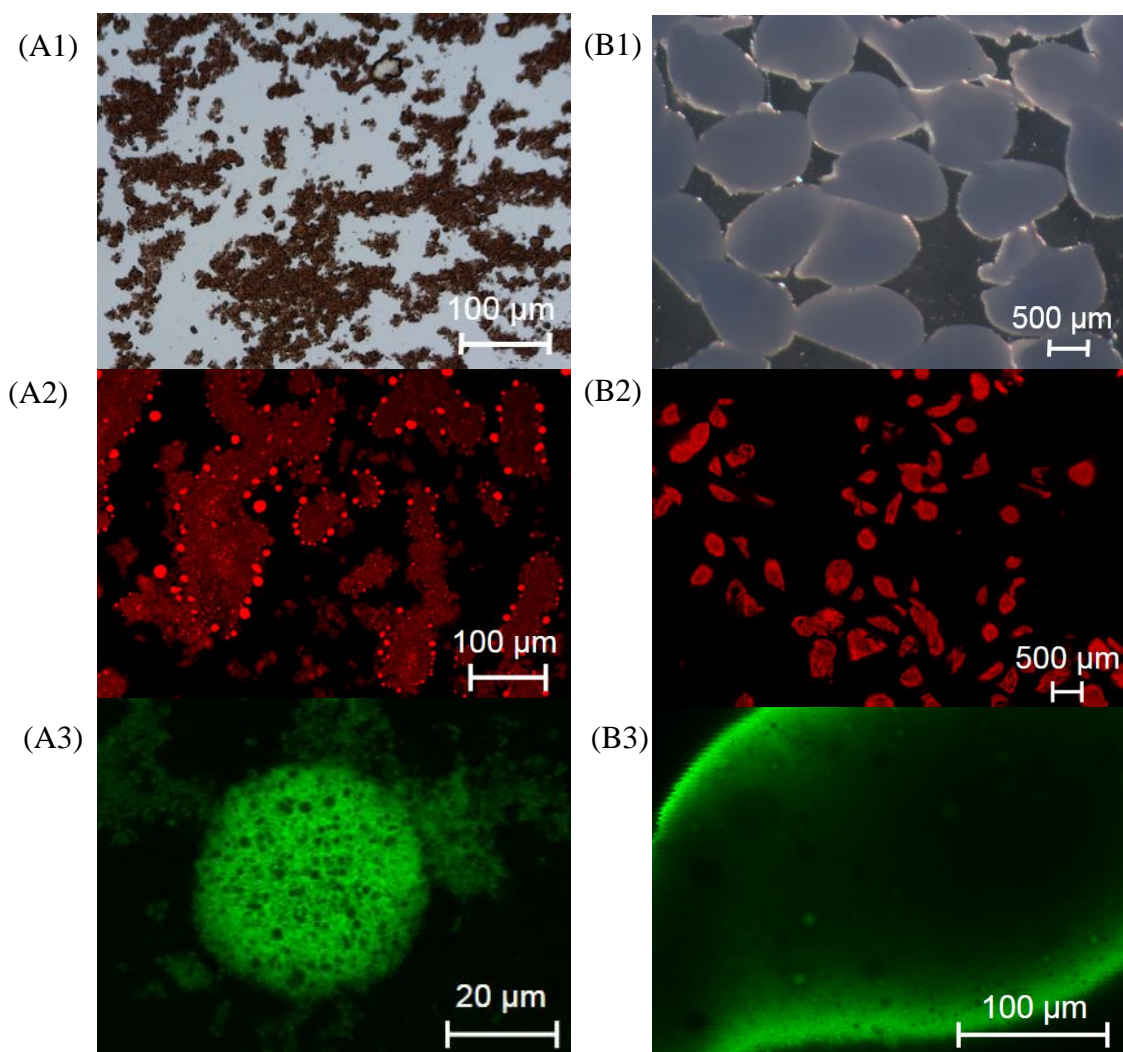


Figure 4.6 Micrographs of the emulsion microgel particles (9.6 wt% WPI, 20 wt% oil) produced with Leeds Jet Homogenizer (0.1 M Ca^{2+}) (A) and Buchi Encapsulator (1 M Ca^{2+}) (B) via optical microscope, 20 \times magnification (A1) and 1.5 \times magnification (B1) and CLSM (20 \times and 40 \times magnification) with the oil droplets stained in Nile Red (2) and the protein network stained in Rhodamine B (3).

droplets of HT-WPI was not fast enough to produce gelation of the droplets into coherent particles. The Encapsulator method produced large polyhedral particles ($< 1000 \mu\text{m}$) with a high internal oil volume fraction (Figure 4.6 B2). The protein network produced was well defined (Figure 4.6 B3) with no presence of surface oil. Dark spherical areas of around $10 \mu\text{m}$ can be observed on Figure 4.6 B3 which might suggest minor artefacts, since none can be depicting on Figure 4.6 B2.

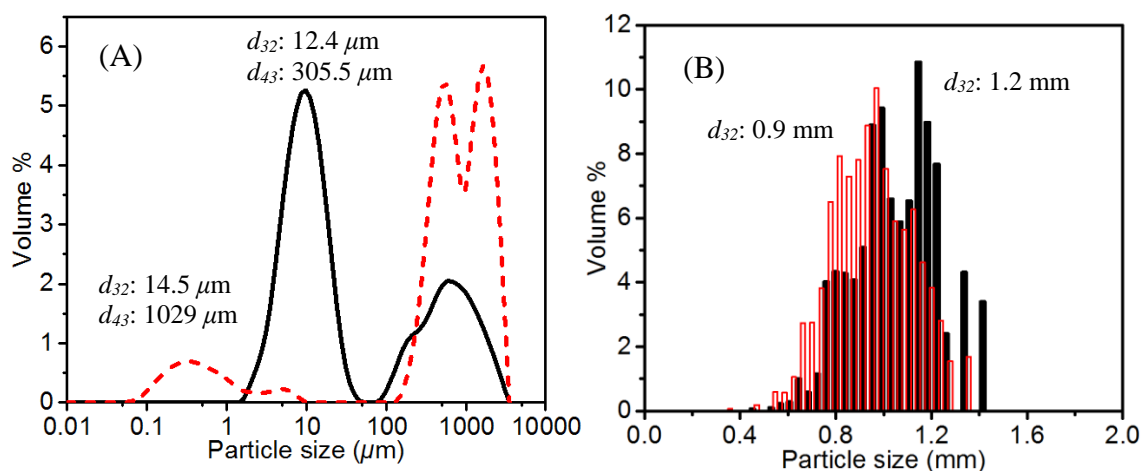


Figure 4.7 Particle size distribution of emulsion microgel particles formed with Leeds jet homogeniser (A) at 0.02 M (dashed red line) and 0.1 M (full black line) and with Buchi Encapsulator (B) at 1 M (empty) and 1.4 M (full) Ca^{2+} , respectively.

The encapsulated oil was around $0.1 \mu\text{m}$ suggesting effective encapsulation of the oil droplets.

More quantitative particle sizing was performed via static light scattering (Figure 4.7 A) and image analysis (Figure 4.7 B). Figure 4.7 A shows the emulsion microgel particle size distribution formed with the Leeds Jet Homogenizer. The particle size distribution was bimodal. In presence of 0.02 M Ca^{2+} ions, the first peak was approximately in the same region as the emulsion oil droplets (0.1 to $1 \mu\text{m}$), suggesting that some emulsion droplets had not been incorporated into microgel particles. Second and third peaks indicated particles in a higher size range (100 to $3000 \mu\text{m}$). The ratio between d_{32} and d_{43} at 0.02 M Ca^{2+} ions, suggested that most particles were aggregated and confocal microscopy confirmed the highly aggregated nature of the sample (Figure 4.8 A). As discussed previously, the minimum $[\text{Ca}^{2+}]$ required to bind to every free carboxylic group on HT-WPI adsorbed to oil droplets was $[\text{Ca}^{2+}]_{\text{min}} = 0.03 \text{ M}$.

Increasing the concentration of Ca^{2+} to 0.1 M led to smaller microgel particles with an 80% reduction in mean d_{43} value ($306 \mu\text{m}$). The first peak of the particle size distribution then shifted to 1 to $30 \mu\text{m}$ (Figure 4.7 A). This suggested that emulsion droplets that were not encapsulated into the emulsion microgel particles at 0.02 M Ca^{2+} were now immobilized into small microgel particles. Interestingly, it can be observed in Figure 4.8 B that some oil droplets (black) were individually stabilized by a layer

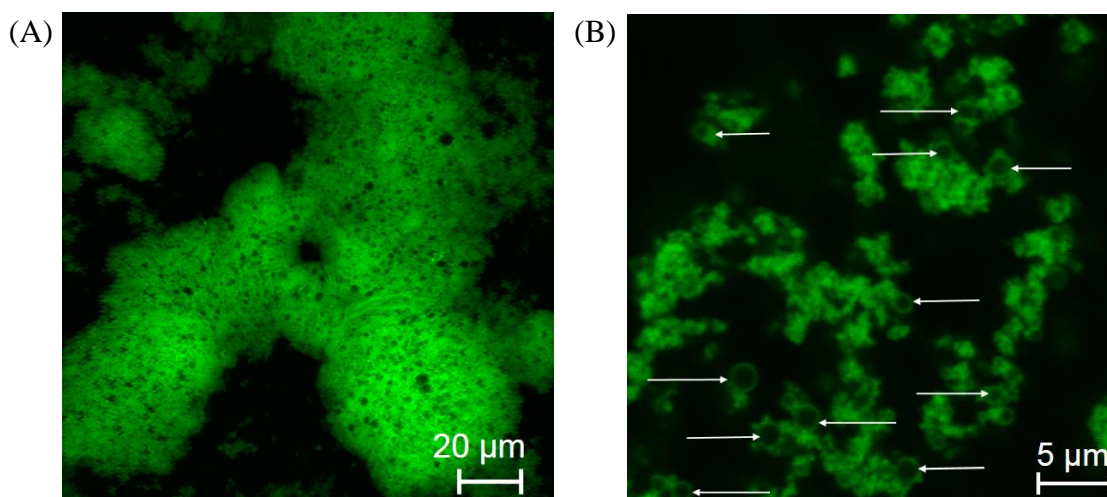


Figure 4.8 CLSM micrograph of emulsion microgel particles produced with Leeds jet homogenizer encapsulating several oil droplets at 0.02 M Ca^{2+} ions (A) and single emulsion droplet encapsulation at 0.1 M Ca^{2+} ions (B), protein network stained in green and black represents oil droplets or background.

of HT-WPI aggregates (green), forming particles of approximately 2 μm diameter. These singly encapsulated oil droplets can be compared to Pickering emulsions stabilized by whey protein microgels (Sarkar et al., 2016b). The second peak of the size distribution in the case of 0.1 M Ca^{2+} was approximately in the same region as the second peak for particles formed with 0.02 M Ca^{2+} , suggesting that some microgel particles remained aggregated. Previous experiments have reported such aggregation when using T-mixing devices (Casanova and Higuita, 2011). The highly turbulent mixing processes generated in T-mixers can lead to the precipitation of the emulsion and Ca^{2+} ions. This precipitation has been demonstrated to reduce particle surface charge, increasing electrostatic attraction and aggregation before gelation of the particles can be completed (Casanova and Higuita, 2011).

In comparison, emulsion microgel particles formed via the Encapsulator had a monomodal size distribution - though they were much larger – from 0.5 to 1 mm (Figure 4.7 B). The emulsion microgel particles produced at higher concentrations of Ca^{2+} (1.4 M) were 10% larger compared to those formed at 1 M (Figure 4.6 B1). As previously demonstrated by (Jeyarajah and Allen, 1994), the addition of salt to heat-treated WPI solution increases the hydrophobicity of the protein as well as its reactive SH content. SH groups found in proximity of Ca^{2+} ion cross-bridges might form additional covalent bonds more easily, strengthening the aggregation of WPI (Jeyarajah and Allen, 1994). Therefore, increasing the concentration from 1 to 1.4 M

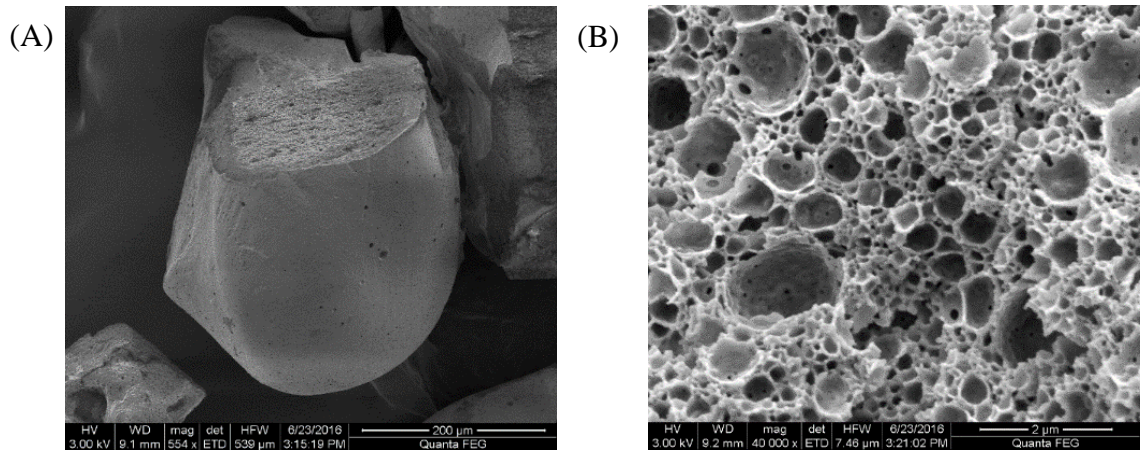


Figure 4.9 Scanning electron micrograph of hexane washed emulsion microgel particle (A) and inner distribution of oil droplets within an emulsion microgel particle (B) produced using a Buchi Encapsulator at 1 M Ca²⁺.

may enhance various protein-protein interactions resulting in further aggregation and larger particle sizes.

The SEM imaging allowed further understanding of the structure of the emulsion microgel particles as well as the oil distribution inside the particles. Preparation of the emulsion microgel particles for SEM resulted in some shrinkage of the particles. Prior to drying and washing, the particle size was between 0.5 to 1 mm. Upon drying the particle size seem to have reduced by 50% (Figure 4.9 A). However, no surface indentations could be noticed suggesting that drying did not induce uneven shrinkage of the particles. Therefore, particles should have retained their initial internal structure upon drying (Rosenberg & Lee, 2004). Figure 4.9 A shows the smooth exterior surface of an emulsion microgel particle produced with the Encapsulator. Small spherical voids could be found at the exterior surface which could be attributed to air bubbles entrapped at the surface prior to drying. The top of the particle was fractured to observe the interior distribution of the emulsion microgel particle. All oil droplets associated with the oil droplets within the microgel particle had been previously washed away with hexane. Figure 4.9 B shows the protein network (white) around the hollow pockets where the oil droplets previously resided (darker colour) (as observed by Beaulieu, et al., 2002; Chen, et al., 1999). The white protein layer noticed around the hollow pockets suggested that the oil droplets were physically bound to the WPI gel matrix, confirming the rheological results (Rosenberg, et al., 2004). The micrographs also indicated that the oil droplets were evenly distributed

throughout the WPI matrix. Some hollows had been distorted and did not retain their spherical shape upon drying of the particles. However, the sizes of the hollows were in the same size range of the original emulsion droplets (0.1 to 1 μm). These observations confirm very little oil droplet coalescence occurred during processing and hollows were left by oil droplets rather than pores of the protein gel (previously estimated at 7.9 nm).

In summary, the two methods produced different sized and shaped emulsion microgel particles. The Leeds Jet Homogenizer produced aggregated, but smaller (around 20 μm), particles whereas Buchi Encapsulator formed well defined emulsion microgel particles but of a much larger size (around 900 μm). In order to fully understand the reasons for the microstructural differences between the two systems, several theoretical aspects were considered regarding particle formation, such as pressure, flow velocity, Reynold number and $[\text{Ca}^{2+}]$.

The Leeds Jet Homogenizer is effectively a T-mixer in which the HT-WPI emulsion comes into contact with Ca^{2+} ions in a turbulent flow ($\text{Re} > 10^4$). The Buchi Encapsulator involved the extrusion of the HT-WPI stabilised emulsions through a nozzle at a transitional flow ($\text{Re} \approx 4 \times 10^3$) into a Ca^{2+} ions bath. However, the bath had stirring which provided turbulence ($\text{Re} > 10^4$). In the latter, since the gelation of the HT-WPI emulsion occurred as soon as the HT-WPI came into contact with Ca^{2+} ions, the flow influencing the particle size was assumed to be the shear rate in the Encapsulator bath. Thus, both systems effectively had turbulent flow, though their mixing dynamics differed significantly. We calculated theoretical mixing time in both methods using Kolmogorov (Peters et al., 2016; Kolmogorov, 1991) microscale theory of energy dissipation. Kolmogorov theory defines the mixing time shown by Equation 4.10:

$$t_{mix} = \left(\frac{\eta_k}{E_\varepsilon} \right)^{\frac{1}{2}} \quad (4.10)$$

where η_k is the kinematic viscosity of the solution and E_ε is the energy dissipation.

The emulsion behaved as a non-Newtonian shear-thinning fluid and its viscosity was estimated at the shear rate of the Jet Homogenizer and the Encapsulator. The shear rate of both instruments was defined by $\dot{\gamma} = 8v/d$ where v is the velocity of the emulsion and d the diameter of the pipe or stirrer bar. The energy dissipation

produced by the Leeds Jet Homogenizer at 250 bar has been previously calculated (Casanova, et al., 2011) and was found to be $E_\varepsilon = 3.1 \times 10^6 \text{ W kg}^{-1}$. Following Equation 4.10, the corresponding mixing time was $1.2 \times 10^{-5} \text{ s}$.

Regarding the Encapsulator, the energy dissipation was calculated following models developed for stirrer tanks using an impeller (Equation 4.11) (Hortsch and Weuster-Botz, 2010; Villermaux and Falk, 1994; Sánchez Pérez et al., 2006):

$$E_\varepsilon = \frac{P}{\rho V} \quad (4.11)$$

where V the solution volume, ρ the density of the solution (kg m^{-3}) and P is the power input given by Equation 4.12:

$$P = P_n \rho N^3 d^5 \quad (4.12)$$

where, P_n is the power number, ρ the density of the solution (kg m^{-3}), N the agitation speed (s^{-1}) and d the diameter of the stir bar (m).

The energy dissipation produced by the Encapsulator was thus calculated as $2.3 \times 10^{-1} \text{ W kg}^{-1}$, where the power number had previously been reported (Couper, 2005) for Reynolds numbers of the same order of magnitude ($P_n = 4$). Following Equation 4.10, the mixing time in the Encapsulator was therefore $4.3 \times 10^{-2} \text{ s}$. Consequently, it is proposed that the mixing time in the Leeds Jet Homogenizer was at least three orders of magnitude faster than that in the Encapsulator. This faster mixing time allowed emulsion microgel particles to form by reactive precipitation (Casanova and Higuita, 2011) and explains why considerably smaller emulsion microgel particles were formed compared to those formed with the Encapsulator, even at much higher $[\text{Ca}^{2+}]$ in the Encapsulator.

The above calculations do not take into account the different $[\text{Ca}^{2+}]$. Therefore, it was of interest to calculate the theoretical flux of Ca^{2+} ions to the WPI layer absorbed to the oil droplet surface. As a first approximation, the diffusive molecular flux of Ca^{2+} to the HT-WPI surface was calculated from Fick's first law (Equation 4.13):

$$J = 4\pi D_t R_i [\text{Ca}^{2+}] \quad (4.13)$$

where R_i is the radius of oil droplets, $[Ca^{2+}]$ the concentration of Ca^{2+} ions and D_t the turbulent diffusion (Deberdeev et al., 2013) coefficient given by $D_t = v \times d$ where, v is the velocity and d is the diameter of the nozzle or stir bar. Of course a key limitation of using Fick's first law is that it does not take into account the role of chaotic advection taking part during turbulent mixing (Nguyen, 2012). Further numerical simulation including the impact of chaotic advection might give additional understanding of the effect of turbulent mixing conditions on the formation of emulsion microgel particles.

Table 4.3 summarizes the flux of Ca^{2+} to HT-WPI (J) absorbed on the oil droplet surface depending on the $[Ca^{2+}]$ and turbulent diffusion coefficient (D_t). Noticeably, in both systems $[Ca^{2+}]$ did not affect the flux in the same manner. In the Jet Homogenizer, increasing $[Ca^{2+}]$ from 0.02 M to 0.1 M should increase the Ca^{2+} ions flux by a factor of ten, suggesting Ca^{2+} ions should bind to WPI more rapidly at 0.1 M, increasing the gelation kinetics. This was observed during measurement of the small deformation rheology (Figure 4.5 A). The increase in flux might also help explain the formation of individually encapsulated oil droplets in HT-WPI (Figure 4.8 B). At 0.1 M Ca^{2+} ions, the excess and high flux of Ca^{2+} ions to HT-WPI led to prompt gelation of WPI adsorbed at the oil-water interface and a higher probability of individually encapsulated oil droplets rather than emulsion microgel particles. Additionally, the lower flux of Ca^{2+} ions, as well as the insufficient amount of Ca^{2+} ions (0.02 M), led to slower gelation of HT-WPI resulting in a higher probability of fractal aggregates.

With regard to the Encapsulator, 1.4 M Ca^{2+} had a 30% faster flux than 1 M Ca^{2+} , leading to slightly faster gelation, in agreement with HT-WPI emulsion gelation kinetics (Figure 4.5 A). Therefore, emulsion microgel particles formed at 1.4 M Ca^{2+} should theoretically be smaller than the ones formed in presence of 1 M Ca^{2+} . However, high $[Ca^{2+}]$ led to larger emulsion microgel particles ($d_{32} = 1.2$ mm) as compared to lower $[Ca^{2+}]$ ($d_{32} = 0.9$ mm) even though the Ca^{2+} flux was significantly faster. As demonstrated by Hongsprabhas, et al., (1997) and Jeyarajah, et al., (1994) the addition of Ca^{2+} increases the hydrophobicity and sulfhydryl group reactivity of WPI, enhancing protein-protein interactions and aggregation through Ca^{2+} ion cross-linkage and covalent bonds (Beaulieu et al., 2002; Hongsprabhas and Barbut, 1997; Jeyarajah and Allen, 1994).

Overall, the main factor influencing the flux of Ca^{2+} is the turbulent diffusion coefficient, leading up to a 10 fold difference between both systems (Jet homogenizer and Encapsulator). The turbulent diffusion coefficient in the Jet Homogenizer ($D_t > 10 \text{ m}^2 \text{ s}^{-1}$) was three orders of magnitude larger than in the Encapsulator ($D_t > 10^{-2} \text{ m}^2 \text{ s}^{-1}$).

Table 4.3 Summary of the flux of Ca^{2+} ions to HT-WPI adsorbed at oil droplet surface as a function of different $[\text{Ca}^{2+}]$ and turbulent diffusion.

Parameters	Leeds Jet Homogenizer		Buchi Encapsulator B-390®	
D_t ($\text{m}^2 \text{ s}^{-1}$)	11.3		2.4×10^{-2}	
$[\text{Ca}^{2+}]$ (M)	0.02	0.1	1	1.4
J ($\text{mol m}^{-2} \text{ s}^{-1}$)	1.6×10^{-4}	7.8×10^{-4}	1.6×10^{-5}	2.3×10^{-5}

4.4 Conclusions

Findings from this study have demonstrated that emulsion microgel particles of tuneable size can be designed using simple bottom-up approaches and solvent-free turbulent mixing techniques. This is driven by the ability of heat-treated WPI to stabilise oil droplets as well as gel in presence of divalent cations, creating a soft solid network encapsulating several oil droplets into one particle. This study has also demonstrated the effect of different Ca^{2+} concentrations and turbulent mixing techniques on the gelation kinetics as well as their effect on particle size. Low $[\text{Ca}^{2+}]$ (0.02 to 0.1 M) in T-mixing devices allowed the formation of small (10 to 100 μm) aggregated emulsion microgel particles. High $[\text{Ca}^{2+}]$ (1 to 1.4 M) and extrusion stirrer mixing devices allowed the formation of large (500 to 1000 μm) non-aggregated emulsion microgel particles. These differences in size were explained by the fact that the T-mixer (Leeds Jet Homogenizer) allowed for more rapid flux of Ca^{2+} ions to HT-WPI, which in turn led to faster mixing times and faster gelation of HT-WPI stabilised emulsions. In comparison, the Encapsulator gave much slower mixing times and Ca^{2+} ions flux, leading to slower gelation of HT-WPI stabilized emulsions.

Similarly to the starch-based emulsion microgel particles developed in **Chapter 3**, stable whey protein-based emulsion microgel particles with tuneable sizes and mechanical properties can be produced via the understanding of the interplay

between concentration of WPI, heat treatment of WPI, $[Ca^{2+}]$, gelation kinetics and the mixing time. Thus, the understanding of both starch and whey protein-based emulsion microgel particles behaviour during *in vitro* oral or gastrointestinal processing is of great importance to appreciate their potential application in the food and pharmaceutical industries, which are covered in **Chapter 5** and **Chapter 6**.

4.5 References

- Alexander, L.J. et al. 1989. Complete sequence of the bovine beta-lactoglobulin cDNA. *Nucleic Acids Research*. **17**(16), p6739.
- Augustin, M.A. and Sanguansri, L. 2012. 2 - Challenges in developing delivery systems for food additives, nutraceuticals and dietary supplements A2 - Garti, Nissim. In: McClements, D.J. ed. *Encapsulation Technologies and Delivery Systems for Food Ingredients and Nutraceuticals*. Woodhead Publishing, pp.19-48.
- Ballauff, M. and Lu, Y. 2007. "Smart" nanoparticles: Preparation, characterization and applications. *Polymer*. **48**(7), pp.1815-1823.
- Barbut, S. and Foegeding, E.A. 1993. Ca^{2+} -Induced Gelation of Pre-heated Whey Protein Isolate. *Journal of Food Science*. **58**(4), pp.867-871.
- Beaulieu, L. et al. 2002. Elaboration and characterization of whey protein beads by an emulsification/cold gelation process: application for the protection of retinol. *Biomacromolecules*. **3**(2), pp.239-248.
- Betz, M. et al. 2012. Swelling behaviour, charge and mesh size of thermal protein hydrogels as influenced by pH during gelation. *Soft Matter*. **8**(8), pp.2477-2485.
- Casanova, H. and Higueta, L.P. 2011. Synthesis of calcium carbonate nanoparticles by reactive precipitation using a high pressure jet homogenizer. *Chemical Engineering Journal*. **175**, pp.569-578.
- Chen, J.S. and Dickinson, E. 1999. Effect of surface character of filler particles on rheology of heat-set whey protein emulsion gels. *Colloids and Surfaces B-Biointerfaces*. **12**(3-6), pp.373-381.
- Ching, S.H. et al. 2016. Rheology of emulsion-filled alginate microgel suspensions. *Food Research International*. **80**, pp.50-60.

- Das, K.P. and Kinsella, J.E. 1990. Effect of heat denaturation on the adsorption of β -lactoglobulin at the oil/water interface and on coalescence stability of emulsions. *Journal of Colloid and Interface Science*. **139**(2), pp.551-560.
- Deberdeev, R.Y. et al. 2013. *Fast Chemical Reactions in Turbulent Flows - Theory and Practice*. Shropshire, UK: Smithers Rapra Technology.
- Dickinson, E. 1998. Proteins at interfaces and in emulsions Stability, rheology and interactions. *Journal of the Chemical Society, Faraday Transactions*. **94**(12), pp.1657-1669.
- Dickinson, E. 2000. Structure and Rheology of Simulated Gels Formed from Aggregated Colloidal Particles. *Journal of Colloid and Interface Science*. **225**(1), pp.2-15.
- Flory, P.J. 1953. *Principles of Polymer chemistry*. Ithaca, NY: Cornell University Press.
- Hongsprabhas, P. and Barbut, S. 1997. Protein and salt effects on Ca^{2+} -induced cold gelation of whey protein isolate. *Journal of Food Science*. **62**(2), pp.382-385.
- Hongsprabhas, P. et al. 1999. The Structure of Cold-Set Whey Protein Isolate Gels Prepared With Ca^{++} . *LWT - Food Science and Technology*. **32**(4), pp.196-202.
- Hortsch, R. and Weuster-Botz, D. 2010. Power consumption and maximum energy dissipation in a milliliter-scale bioreactor. *Biotechnology Progress*. **26**(2), pp.595-599.
- Iametti, S. et al. 1995. Modifications of High-Order Structures upon Heating of β -Lactoglobulin: Dependence on the Protein Concentration. *Journal of Agricultural and Food Chemistry*. **43**(1), pp.53-58.
- James R. Couper, W.R.P., James R. Fair and Stanley M. Walas. 2005. Chapter 10 - Mixing and Agitation. *Chemical Process Equipment (Second Edition)*. Burlington: Gulf Professional Publishing, pp.277-328.
- Jeyarajah, S. and Allen, J.C. 1994. Calcium binding and salt-induced structural changes of native and preheated β -lactoglobulin. *Journal of Agricultural and Food Chemistry*. **42**(1), pp.80-85.
- Ju, Z.Y. and Kilara, A. 1998. Effects of preheating on properties of aggregates and of cold-set gels of whey protein isolate. *Journal of Agricultural and Food Chemistry*. **46**(9), pp.3604-3608.
- Kim, D.A. et al. 2005. Effect of thermal treatment on interfacial properties of β -lactoglobulin. *Journal of Colloid and Interface Science*. **285**(1), pp.100-109.

- Kolmogorov, A.N. 1991. Dissipation of Energy in the Locally Isotropic Turbulence. *Proceedings: Mathematical and Physical Sciences*. **434**(1890), pp.15-17.
- Kuhn, K.R. et al. 2010. Cold-set whey protein gels induced by calcium or sodium salt addition. *International Journal of Food Science & Technology*. **45**(2), pp.348-357.
- Marangoni, A.G. et al. 2000. On the structure of particulate gels—the case of salt-induced cold gelation of heat-denatured whey protein isolate. *Food Hydrocolloids*. **14**(1), pp.61-74.
- McClements, D.J. 2011. Edible nanoemulsions: fabrication, properties, and functional performance. *Soft Matter*. **7**(6), pp.2297-2316.
- McClements, D.J. 2015. Encapsulation, protection, and release of hydrophilic active components: Potential and limitations of colloidal delivery systems. *Advances in Colloid and Interface Science*. **219**, pp.27-53.
- McClements, D.J. and Li, Y. 2010. Structured emulsion-based delivery systems: controlling the digestion and release of lipophilic food components. *Adv Colloid Interface Sci*. **159**(2), pp.213-28.
- Moakes, R.J.A. et al. 2015a. Preparation and characterisation of whey protein fluid gels: The effects of shear and thermal history. *Food Hydrocolloids*. **45**, pp.227-235.
- Nguyen, N.-T. 2012. Chapter 6 - Micromixers based on chaotic advection. *Micromixers (Second Edition)*. Oxford: William Andrew Publishing, pp.195-238.
- Nyman, R. and Apenten, R.K.O. 1997. The Effect of Heat Treatment on Anilinonaphthalene-8-Sulphonate Binding to Rapeseed Albumin (Napin). *Journal of the Science of Food and Agriculture*. **74**(4), pp.485-489.
- Peppas, N.A. et al. 2000. Hydrogels in pharmaceutical formulations. *European Journal of Pharmaceutics and Biopharmaceutics*. **50**(1), pp.27-46.
- Peters, N. et al. 2016. Higher-order dissipation in the theory of homogeneous isotropic turbulence. *Journal of Fluid Mechanics*. **803**, pp.250-274.
- Phan-Xuan, T. et al. 2014. Heat induced formation of beta-lactoglobulin microgels driven by addition of calcium ions. *Food Hydrocolloids*. **34**, pp.227-235.
- Pravinata, L. et al. 2016. Preparation of alginate microgels in a simple one step process via the Leeds Jet Homogenizer. *Food Hydrocolloids*. **61**, pp.77-84.

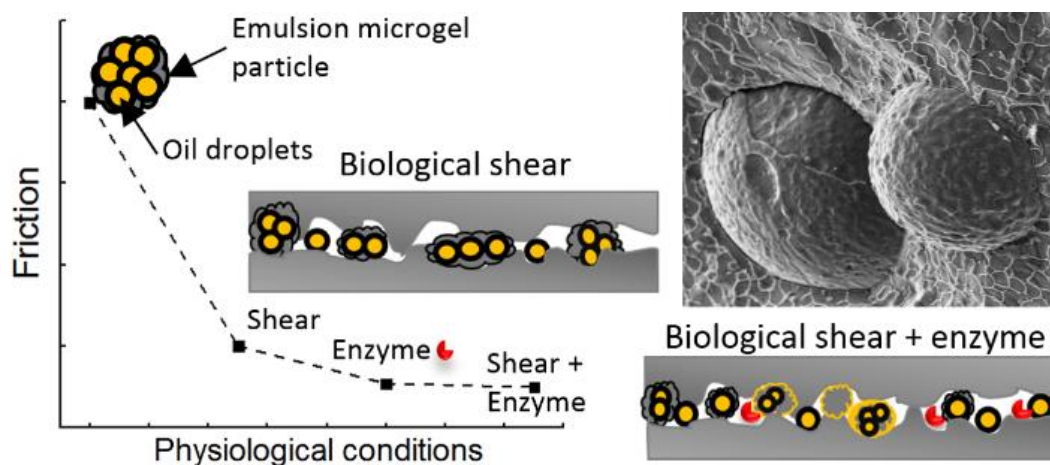
- Roefs, S.P.F.M. and Peppelman, H.A. 2001. Aggregation and gelation of whey proteins: Specific effect of divalent cations? In: Dickinson, E. and Miller, R. eds. *Food Colloids: Fundamentals of Formulation*. The Royal Society of Chemistry, pp.358-368.
- Ruffin, E. et al. 2014. The impact of whey protein preheating on the properties of emulsion gel bead. *Food Chemistry*. **151**, pp.324-332.
- Sánchez Pérez, J.A. et al. 2006. Shear rate in stirred tank and bubble column bioreactors. *Chemical Engineering Journal*. **124**(1–3), pp.1-5.
- Sarkar, A. et al. 2016a. Microstructure and long-term stability of spray dried emulsions with ultra-high oil content. *Food Hydrocolloids*. **52**, pp.857-867.
- Sarkar, A. et al. 2015. Impact of Protein Gel Porosity on the Digestion of Lipid Emulsions. *Journal of Agricultural and Food Chemistry*. **63**(40), pp.8829-8837.
- Sarkar, A. et al. 2016b. In vitro digestion of Pickering emulsions stabilized by soft whey protein microgel particles: influence of thermal treatment. *Soft Matter*. **12**(15), pp.3558-3569.
- Sok, L.V.L. et al. 2005. Cold gelation of β -lactoglobulin oil-in-water emulsions. *Food Hydrocolloids*. **19**(2), pp.269-278.
- Sung, M.R. et al. 2015. Fabrication, characterization and properties of filled hydrogel particles formed by the emulsion-template method. *Journal of Food Engineering*. **155**, pp.16-21.
- Torres, O. et al. 2016. Emulsion microgel particles: Novel encapsulation strategy for lipophilic molecules. *Trends in Food Science & Technology*. **55**, pp.98-108.
- van Vliet, T. 1988. Rheological properties of filled gels. Influence of filler matrix interaction. *Colloid and Polymer Science*. **266**(6), pp.518-524.
- Velikov, K.P. and Pelan, E. 2008. Colloidal delivery systems for micronutrients and nutraceuticals. *Soft Matter*. **4**(10), pp.1964-1980.
- Villiermaux, J. and Falk, L. 1994. A generalized mixing model for initial contacting of reactive fluids. *Chemical Engineering Science*. **49**(24), pp.5127-5140.
- Wei, J. et al. 2016. Tailor-made microgel particles: Synthesis and characterization. *Colloids and Surfaces A: Physicochemical and Engineering Aspects*. **489**, pp.122-127.

- Westerik, N. et al. 2015. The effect of calcium on the composition and physical properties of whey protein particles prepared using emulsification. *Food Chemistry*. **177**, pp.72-80.
- Wijayanti, H.B. et al. 2014. Stability of Whey Proteins during Thermal Processing: A Review. *Comprehensive Reviews in Food Science and Food Safety*. **13**(6), pp.1235-1251.
- Wolz, M. and Kulozik, U. 2015. Thermal denaturation kinetics of whey proteins at high protein concentrations. *International Dairy Journal*. **49**, pp.95-101.
- Zhang, Z. et al. 2015. Development of food-grade filled hydrogels for oral delivery of lipophilic active ingredients: pH-triggered release. *Food Hydrocolloids*. **44**, pp.345-352.
- Zúñiga, R.N. et al. 2010. Kinetics of Formation and Physicochemical Characterization of Thermally-Induced β -Lactoglobulin Aggregates. *Journal of Food Science*. **75**(5), pp.E261-E268.

**Oral to gastrointestinal digestion of
emulsion microgel particles**

Chapter 5

***In vitro* oral processing of starch-based emulsion microgel particles: from protection to lubrication performances⁴**



Abstract

Starch-based emulsion microgel particles with different starch (15 and 20 wt%) and oil contents (0 – 15 wt%), were synthesized and their lubrication performance under physiological conditions was investigated. Emulsion microgels were subjected to oral cavity mimicking conditions, *i.e.*, smooth hydrophobic polydimethylsiloxane ball-on-disc tribological tests, in the absence or presence of salivary enzyme (α -amylase). In the absence of enzyme, emulsion microgel particles (30 – 60 vol% particle content) conserved

⁴ Published as: Torres, O., Andablo-Reyes, E., Murray, B. S. and Sarkar, A. 2018. Emulsion microgel particles as high-performance bio-lubricant. *ACS Applied Materials & Interfaces*, **10**, 26893-26905. DOI: 10.1021/acsami.8b07883

the lubricating properties of emulsion droplets, providing considerably lower friction coefficients ($\mu \leq 0.1$) in the mixed lubrication regime compared to plain microgel particles (0 wt% oil). Upon addition of enzyme, the lubrication performance of emulsion microgel particles became strongly dependent on the particles' oil content. Microgel particles encapsulating 5 – 10 wt% oil showed a double plateau mixed lubrication regime having a lowest friction coefficient $\mu \sim 0.03$ and highest $\mu \sim 0.1$, the latter higher than with plain microgel particles. An oil content of 15 wt% was necessary for the microgel particles to lubricate similarly to the emulsion droplets, where both systems showed a normal mixed lubrication regime with $\mu \leq 0.03$. The observed trends in tribology, theoretical considerations and the combined results of rheology, light scattering and confocal fluorescence microscopy suggested that the mechanism behind the low friction coefficients was a synergistic enzyme- and shear-triggered release of the emulsion droplets, improving lubrication. The present work thus demonstrates experimentally and theoretically a novel bio-lubricant additive with stimuli-responsive properties capable of providing efficient boundary lubrication between soft polymeric surfaces. At the same time, the additive should provide an effective delivery vehicle for oil soluble ingredients in aqueous media. These findings demonstrate that emulsion microgel particles can be developed into multi-functional bio-lubricant additives for future use in numerous soft matter applications where both lubrication and controlled release of bioactives are essential.

5.1 Introduction

Bio-lubricants are in great demand to reduce friction between soft biological contacting surfaces, such as the eyes, the oral cavity, the gastrointestinal tract and joints, to prevent discomfort and wear of epithelial tissues and cartilage (Liu et al., 2014; Sterner et al., 2017; Timm et al., 2011; Røn et al., 2014; Røn et al., 2017). The use of submicron to micron sized particles (*e.g.*, microgels) as bio-lubricant additives has recently been a focal point in biomaterial science research due to their ability to reduce friction and wear in the boundary regime of sliding contact in biological areas, such as tongue-oral palate contacts, cartilage or eye blinking (Malone et al., 2003; Sterner et al., 2017; Sarkar et al.,

2017; Liu et al., 2014). In the food industry, the tribological behaviour of emulsions as compared to particles has also received a lot of attention due to the opportunity to understand and quantify differences in mouthfeel between full fat and low fat products. Therefore, tribology measurements have allowed to understand if lower fat content products could mimic the sensory properties of their full fat counter-part, which cannot be fully grasped using bulk rheology alone (Laguna et al., 2017). At low sliding speeds and contact pressures, these particles are able to enter the gap and reduce direct contact between the biological surfaces by acting as “true surface separators” by virtue of their rheological properties (Dou et al., 2016). The extent to which the friction reduces can be controlled by the particle properties, such as their size, volume fraction, surface roughness and mechanical response (Sarkar et al., 2017).

Oil-in-water emulsions are widely used as lubricants in pharmaceutical, personal care and food products. The lubrication properties of emulsions primarily arise from the oil droplets in the boundary regime, which is observed at the lowest entrainment speed where the friction force is independent of the entrainment speed and the load is supported predominantly by the asperity contact and surface adsorbed matter (Garrec and Norton, 2013; Sarkar et al., 2017). Whilst emulsions demonstrate lubrication properties for internal applications (in the form of medicine or food to coat the oral cavity, reduce friction and increase palatability (Batchelor et al., 2015; Stokes et al., 2013)), their instability to physicochemical and biochemical degradation (*e.g.*, light, temperature, shear, ionic and enzymatic activity) can lead to poor release of bioactive compounds and increased physiological oxidation of the oil droplets (Joyce et al., 2015; Porter et al., 2008; Simovic et al., 2012). Therefore, being able to tailor microstructures that combine high lubrication performances, protection of colloidal droplets against such physicochemical degradation and controlled release of bioactive compounds under either enzymatic- or mechanical shear- trigger is highly desirable. Nevertheless, most targeted release studies of bioactive material do not consider the effect of degradation caused by biological shear or enzymatic stresses.

Emulsion microgel particles are a new class of microgel particle where several oil droplets are trapped within a biopolymer hydrogel particle (Torres et al., 2016; Torres et al., 2017a; Torres et al., 2017b). In this study we demonstrate for the first time how, by

employing suitable novel biocompatible emulsion microgel particles, it is possible to provide protection to emulsion droplets combined with the desired lubrication under relevant physiological shear and/or enzymatic conditions. By engineering the appropriate biopolymer matrix, enzyme-triggered and/or mechanical shear-triggered release of the emulsion droplets can also be observed. To demonstrate the applied physiological performance of these emulsion microgel particles, the particles were subjected to internal environmental stress models (*i.e.*, oral mimicking tribological shear and enzymatic stress). A series of starch based emulsion microgel particles were produced at different starch (15 and 20 wt%) and sunflower oil (0 – 15 wt%) concentrations via a top down approach (Torres et al., 2017b). Starch was employed due to its known response to α -amylase in the oral cavity. The lubrication performance of the emulsion microgel particles was examined in the absence or presence of α -amylase using hydrophobic polydimethylsiloxane (PDMS) tribo-pairs (water contact angle 108 °), due to their resemblance to soft biological interfaces (Hamilton and Norton, 2016; Sarkar et al., 2017). For a better understanding of the lubrication mechanisms of the different samples, the theoretical drag force as well as the indentation of the different particles were calculated. The viscosity, particle size and microstructure of the microgel dispersions at various length scales were investigated before and after tribological shear in the absence or presence of α -amylase.

The results demonstrated that in conventional 40 wt% oil-in-water emulsions, the emulsion droplets coalesced releasing a thin oil film under shear and/or enzyme activity providing good lubrication properties. In comparison, the emulsion microgel particles (5-15 wt%) under tribological shear and enzyme activity led to the release of very few emulsion droplets improving lubrication without coalescence of the oil droplets. The noticeable stability of emulsion microgel particles offers immense potential for targeted release of emulsion droplets containing bio-active molecules at physiological sites (typically the small intestine) while reducing friction in aqueous biological environments that has wide potential soft matter industrial and biological applications in food, pharmaceutical and personal care industries. For instance during oral applications, emulsion microgel particles containing active compounds (such as nutraceuticals or pharmaceuticals) should provide the desirable creamy mouthfeel (Batchelor et al., 2015) without a high fat content and the destabilisation of the emulsion droplets, which occurs

in a conventional emulsion (de Wijk et al., 2006; Weenen et al., 2005). This protection might further allow for the bio-active molecules to be released at targeted physiological sites (Liu et al., 2014; Secret et al., 2014; Ravanfar et al., 2018; Xu et al., 2018; Xia et al., 2017; Sun et al., 2013; Nguyen et al., 2017).

5.2 Materials and Methods

5.2.1 Materials

Wheat native starch was purchased from Sigma-Aldrich (Gillingham, UK), commercial octenyl succinic anhydride (OSA) starch refined from waxy maize starch from Ingredion (Hamburg, Germany) was used as emulsifier and sunflower oil was obtained from Morrisons (UK) supermarket. α -Amylase from porcine pancreas Type VI-B (13 units.mg⁻¹) was obtained from Sigma-Aldrich and dissolved in pH 6.8 phosphate buffered saliva when used. All other chemicals were of Analytical grade and purchased from Sigma-Aldrich unless otherwise specified. All dispersions were prepared with Milli-Q water having a resistivity of not less than 18.2 M Ω ·cm at 25 °C (Milli-Q apparatus, Millipore, Bedford, UK).

5.2.2 Preparation of starch based emulsion microgel particles

Starch emulsion microgel particles at different concentrations of starch (15 – 20 wt%) and oil-in-water emulsions (0 – 15 wt%) were prepared using a top-down approach, as reported in **Chapter 3** (Torres et al., 2017b). Firstly, 40 wt% sunflower oil was emulsified with 4 wt% OSA starch. Secondly, starch pastes were formed by dispersing native wheat starch into Milli-Q water, heating at 80 °C for 40 minutes in a water bath and simultaneously sheared using a hand blender (Hand blender, XB986B, 170W, Argos, UK). Both starch pastes and emulsions were then mixed at different ratios to form emulsion gels. After cooling to 4 °C for three hours, the refrigerated starch and starch emulsion gels were passed twice through a high pressure homogenizer at 250/50 bar (Panda Plus, GEA Niro Soave, Parma, Italy). The resulting particles were collected in a beaker and immediately diluted in Milli-Q water (60:40 w/w, particles:MilliQ).

5.2.3 Preparation of model saliva (pH 6.8).

Phosphate buffer containing 75 U mL^{-1} α -amylase was prepared according to the composition used in previous literature (Minekus et al., 2014), mimicking the ionic composition and pH of saliva. The different samples were mixed gently with buffer (with or without α -amylase) in 1:1 w/w ratio for 15 minutes either in a beaker or directly in the pot of the tribometer, based on the oral processing protocol of the standardized static *in vitro* digestion method (Minekus et al., 2014).

5.2.4 Particle size analysis

The particle size distributions of the emulsion droplets and emulsion microgel particles were measured via a Malvern Mastersizer 3000E Hydro, (Malvern Instruments, Worcestershire, UK) using refractive indices of the emulsion droplets, starch microgel particles and aqueous phase of 1.46, 1.50 and 1.33, respectively.

5.2.5 Shear rheology

Rheological characterization was performed using a Kinexus ultra rheometer (Malvern Instruments Ltd, Worcestershire, UK) with a cone and plate geometry (\emptyset 40 mm, model: CP4/40 SS017SS). In order to prevent sample evaporation, in addition to the use of an adiabatic cover, the rim of the geometry was sealed with a thin layer of 350 cst silicone oil. Flow curves were obtained from the different samples before and after dilution (1:1 w/w) with buffer (with and without α -amylase) as a function of shear rate, ranging from $0.01 - 1000 \text{ s}^{-1}$ at $37 \text{ }^\circ\text{C}$.

5.2.6 Tribology

The lubrication performance of the emulsions, starch microgel particles (*i.e.*, without oil droplets) and starch emulsion microgel particles was assessed using a Mini Traction Machine (MTM2, PCS instruments, UK) following the methods outlined in previous studies (Laguna et al., 2017; Sarkar et al., 2017). The tribo-pairs used for this study consisted of a ball (\emptyset 19 mm) and plate (\emptyset 46 mm) made of hydrophobic polydimethylsiloxane (PDMS, Sylgard, Dow Corning, USA), each element having a surface roughness of $(R_a) < 50 \text{ nm}$ and Young's modulus of 2.8 MPa. All tests were

performed at constant normal load (W) of 2 N, equivalent to a maximum Hertzian contact pressure (P_{max}) of 100 kPa and contact radius of 2 mm. The friction coefficient (μ), defined as the ratio between the friction force and normal load, was measured as a function of entrainment speed (\bar{U}) swept between 1 and 500 mm s⁻¹ in both descending and ascending directions. Only data obtained from entrainment speed sweeps descending from 500 mm s⁻¹ to 2 mm s⁻¹ are reported, as the Stribeck curves showed negligible hysteresis. The sliding to rolling ratio, defined as $SRR = |U' - U''|/\bar{U}$ was kept at a constant value of 0.5, where U' and U'' are the ball and disc speeds, respectively, and the entrainment speed is defined as $\bar{U} = \frac{1}{2}(U' + U'')$. Prior to each test, the surfaces were cleaned with acetone and rinsed with Milli-Q water. One ball-and-disk pair was used each time for an individual experiment and then discarded. Tests were performed under isothermal conditions at 37 ± 1 °C, aiming to mimic human oral conditions. The mean value of three measurements for each sample was used to plot the Stribeck curve.

5.2.7 Confocal scanning laser microscopy (CLSM)

The microstructure of the OSA starch-stabilized emulsion and the emulsion microgel particles (15 wt% starch – 15 wt% oil) at time 0 s and 60 s after incorporating buffer with α -amylase (at 37 °C), was studied via a Zeiss LSM 880 confocal microscope (Carl Zeiss MicroImaging GmbH, Jena, Germany), at a 40 \times magnification. The samples were stained following the methods from **Chapter 3** (Torres et al., 2017b).

5.2.8 Cryo-scanning electron microscopy (cryo-SEM)

A cryo-scanning electron microscope (FEI Quanta 200F FEG ESEM, Japan), equipped with a Quorum PolarPrep 2000 cryo-system was used to study the structural features of the emulsion microgel particles following the methods used in **Chapter 3** (Torres et al., 2017b).

5.3 Results and discussion

5.3.1 Morphological characterization of emulsion microgel particles by cryo-SEM.

Cryo-scanning electron micrographs of the emulsion microgel particles at various magnifications are presented in Figure 5.1. The particles appeared to be roughly spherical with an average diameter of $20\ \mu\text{m}$. Their rough surface has been previously assumed to be the underlying intact encapsulated oil droplets (**Chapter 3** (Torres et al., 2017b)), which might impact the tribological performance of the particles. Under higher magnification, the internal structure of a fragmented particle can be observed (Figure 5.1 B), where spherical particles of $0.1 - 1\ \mu\text{m}$ can be seen. This size range is consistent with the size distribution of OSA starch-stabilized emulsion, which had an average Sauter mean diameter d_{32} of $0.16 \pm 0.004\ \mu\text{m}$, similar to the value obtained in previous studies (Sweedman et al., 2014; Tesch et al., 2002; Torres et al., 2017b).

5.3.2 Rheological characterization.

The viscosities of the emulsion and emulsion microgel particles before and after tribological shear were measured to check how shear affected the samples. The Newtonian curve of sunflower oil with a viscosity of approximately $0.04\ \text{Pa s}$ was introduced for

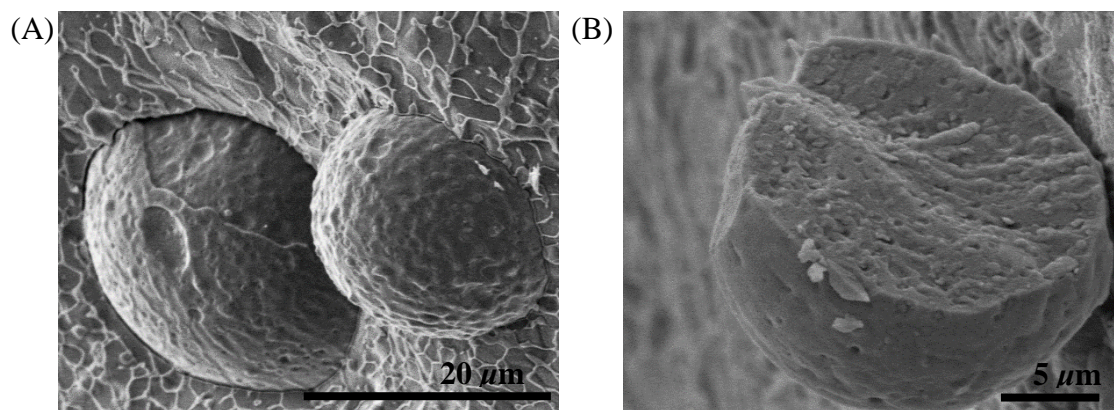


Figure 5.1 (A) Cryo-SEM micrograph of the external structure and (B) internal structure of starch emulsion microgel particles (15 wt% starch – 10 wt% oil), respectively. Scale bar represents 20 and $5\ \mu\text{m}$, respectively.

comparison. The viscosity of the emulsion in the absence of buffer and α -amylase decreased with increasing shear rate (Figure 5.2 A), *i.e.*, the emulsion exhibited typical shear thinning of a weakly flocculated system (Anvari and Joyner, 2017). Viscosity measurements of the emulsion *after* tribological shear (without buffer or α -amylase) indicated, on average, a 50% increase in viscosity over the shear rate range, suggesting an increase in droplet aggregation. Depletion flocculation due to non-absorbed OSA starch possibly contributed to this increased droplet aggregation (Dickinson, 2017).

The 1:1 dilution of the emulsion with buffer (without α -amylase) led to a 100 fold decrease in viscosity, over the same shear rate range showing further evidence of weak flocculation at the higher volume fraction (40 wt% oil), but largely absent at 20 wt% oil. Additionally, for the latter, a high shear rate viscosity plateau of approximately 0.04 Pa s can be observed at shear rates $> 1 \text{ s}^{-1}$, where shear-induced forces reach a balance and the average inter-particle structures are highly reduced in extent or completely absent.

Emulsions in the presence of buffer and α -amylase showed a more pronounced shear thinning behaviour compared to emulsions diluted only with buffer. This is consistent with flocculation due to decreased steric stabilization induced by the addition of α -amylase to the OSA starch-stabilized emulsion, which is expected to hydrolyse the OSA starch chains adsorbed at the oil droplet surface (de Wijk et al., 2004; Dickinson, 2017; Dresselhuis et al., 2008). The high shear rate viscosity plateau is observed to start approximately at the same shear rate and have a similar value to the emulsion without α -amylase, showing that both systems have a very similar state of dispersion in this limit, probably with few particle clusters surviving. Regarding the emulsion microgel particles, only the viscosity measurements obtained with 15 wt% starch particles at different oil concentrations are shown in Figure 5.2 B to Figure 5.2 D. The measurements obtained at 20 wt% starch are reported in Appendix C.1, since they followed very similar trends. However, emulsion microgel particles produced at 20 wt% starch had in average a viscosity 50% higher than the particles produced at 15 wt% starch.

In Figure 5.2 B, it is seen that emulsion microgel particle suspensions exhibited very similar flow curves in shape and absolute values of viscosity compared to non-diluted emulsions, despite the higher solids content - approximately double the former. This

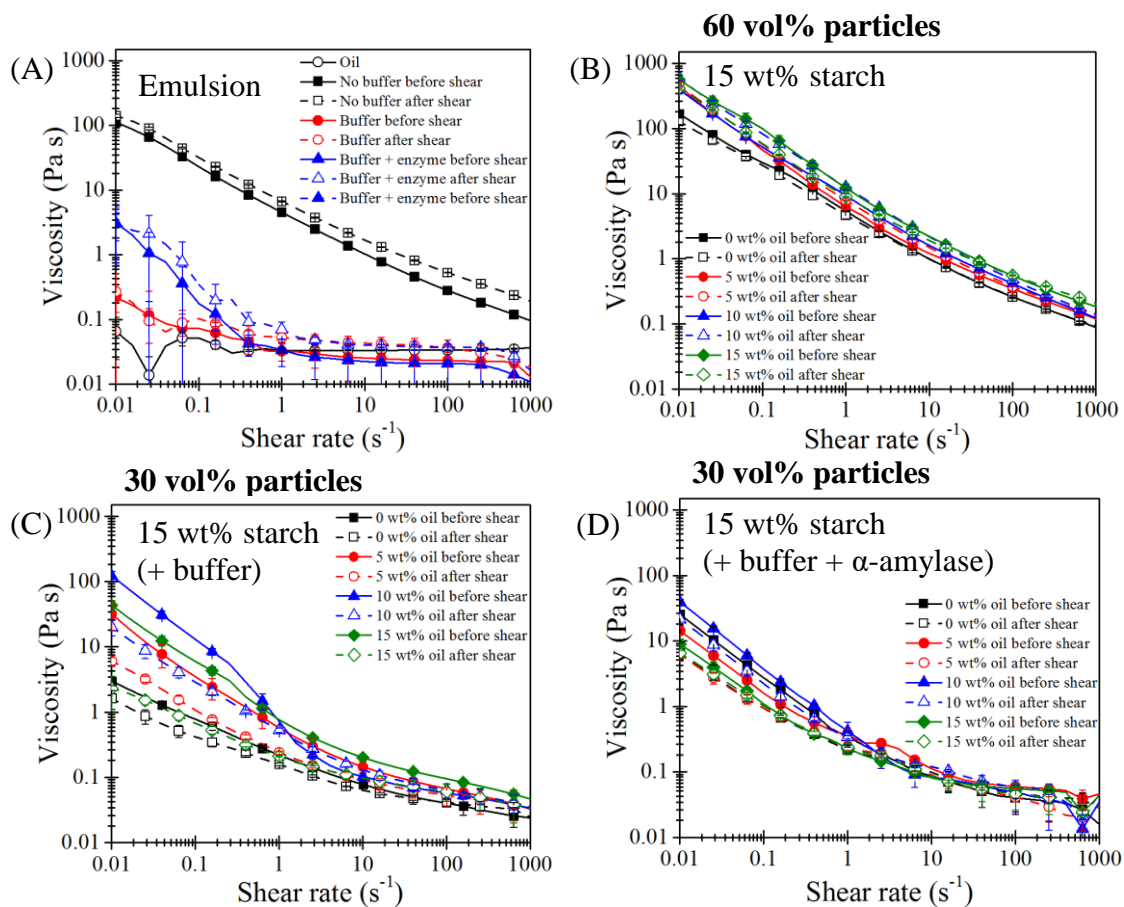


Figure 5.2 (A) Viscosity versus shear rate of the oil-in-water emulsion at 37 °C before and after tribological shear in the absence or presence of buffer and α -amylase; viscosity versus shear rate of the emulsion microgel particles (15 wt% starch) at different concentrations of oil at 37 °C, before and after tribological shear in the absence of buffer (B); in the presence of buffer (C) and α -amylase (D), respectively.

might be related to the relatively low elastic modulus of microgel particles which has been reported to have a large effect in the rheology of this type of system (Adams et al., 2004). This assumption is strengthened by the influence of increasing oil content of the emulsion microgel particles, which significantly increased the viscosity values. For instance, at 40 s⁻¹ the viscosities of the emulsion microgel particles produced with 0, 5, 10 and 15 wt% oil were, 0.42, 0.56, 0.70 and 0.94 ± 0.05 Pa s, respectively. Thus, encapsulating over 5 wt% oil significantly increased the viscosity of the starch particle dispersions ($p < 0.05$). It is also seen that tribological shear did not significantly affect the

rheological properties of the suspensions (Figure 5.2 B). The dilution of the emulsion microgel particles in buffer (50:50 w/w) did not affect the shear thinning behaviour of the samples (Figure 5.2 C) but, the viscosity of all samples decreased on average by one order of magnitude, in line with previous studies on the effect of microgel particle volume fraction on viscosity (Ching et al., 2016; Sarkar et al., 2017). A non-monotonic relationship between shear viscosity and emulsion microgel particle oil content can also be observed due to the relatively broader size distribution of emulsion microgel particles with 15% oil content compared to systems with lower oil concentrations. At lower volume fractions, particles are well separated, allowing the continuous phase to flow in between them (Mueller et al., 2009). The tribological shear applied to the emulsion microgel particles further decreased the viscosity of all the samples, suggesting that the shear further separated or damaged the aggregated emulsion microgel particles.

The addition of α -amylase to the emulsion microgel particles did not affect their shear thinning behaviour – their viscosity values were similar to the emulsion microgel particles diluted with buffer without α -amylase (Figure 5.2 D). Interestingly, however, in contrast to the systems diluted with buffer, when α -amylase was present as well, tribological shear seemed to have *less* effect in reducing the viscosities, so that all the flow curves before and after shear were closer (Figure 5.2 D). The reasons for this are not clear, but the rheology of partly enzyme degraded microgel particles and the starch fragments released, is not expected to be simple. Nevertheless, it is necessary to make these measurements to aid interpretation of the subsequent studies described in the next section.

5.3.3 Tribological properties of the emulsion.

Figure 5.3 A shows the friction coefficient of the OSA-stabilized emulsion under different conditions as a function of entrainment speed. Sunflower oil and buffer without α -amylase were also measured for comparison purposes.

Previously, it has been reported that under normal circumstances three tribological regimes can be observed (Alazemi et al., 2015; Sarkar et al., 2017; Stokes et al., 2013). At low entrainment speed the PDMS ball and disc are in contact with each other, excluding the sample from the contact area, resulting in a high friction coefficient. This condition is

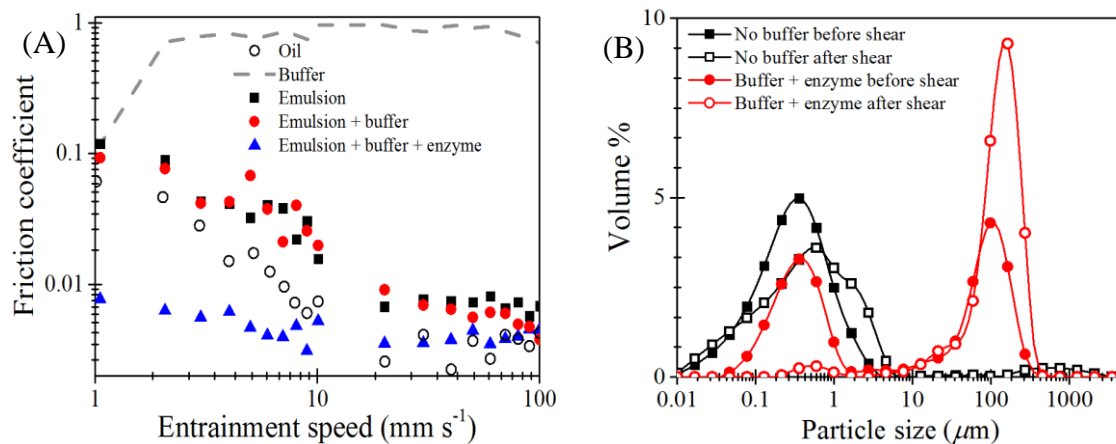


Figure 5.3 (A) Coefficient of friction as function of entrainment speed for sunflower oil, buffer without α -amylase and OSA starch stabilized emulsion in absence or presence of buffer and/or α -amylase subjected to a normal load of 2 N and at 37 °C; (B) Particle size distribution of the OSA starch stabilised-emulsion (40 wt% oil) with and without α -amylase before and after being subjected to tribological shear.

known as the boundary regime. As the entrainment speed increases, sample is entrained in between the ball and disc, forming a monolayer that decreases the friction: the mixed regime (the amount of entrainment will mainly depend on the size of the particles as compared to the size of the gap between the ball and disc). As the speed increases further, the amount of sample entering the contact area increases, pushing the ball and disc further apart reducing the friction further until the hydrodynamic regime is reached, where bulk properties rather than surface properties dominate. Since this study aims to understand biological surfaces relevant to oral applications, only the boundary and mixed regime will be discussed in detail. However, data in the hydrodynamic regime can be found in Appendix C.2.

In Figure 5.3 A, the contacts lubricated with buffer worked only in the boundary lubrication regime, with high friction coefficient values $\mu \sim 0.7$ for the whole range of entrainment speeds, showing practically no penetration of the lubricant into the contact area. In comparison to the buffer, a significantly different behaviour was displayed when lubricated with either the emulsion containing 40 wt% (no added buffer) or 20 wt% oil (with added buffer). The contacts exhibited the characteristics of working in the mixed lubrication regime with values of friction coefficient remarkably lower than that of the

buffer (see Appendix C.3 for statistical analysis) and decreasing from 0.1 to approximately 0.007 with increasing entrainment speed. Comparing the Stribeck curves obtained for emulsions and sunflower oil, both systems provided very similar lubricating properties (Appendix C.3). This has been observed in previous studies, where the dispersed phase of an emulsion had a viscosity at least four times larger than the that of the continuous phase (de Vicente et al., 2006), similar to the case of the systems studied here. However, the emulsion without added buffer (40 wt% oil) plateaued at a low friction coefficient ($\bar{U} > 50 \text{ mm s}^{-1}$, $\mu = 0.007 \pm 0.004$) whereas the emulsion diluted with buffer (20 wt% oil) clearly reached its elastohydrodynamic regime ($\bar{U} > 100 \text{ mm s}^{-1}$) (Appendix C.2). At high entrainment speeds, the lubrication mechanism of the emulsion diluted with buffer might be controlled by sunflower oil, as compared to the emulsion without buffer, which might be controlled by the emulsion droplets. These different mechanisms will be discussed in more detail further on.

In parallel, the droplet size distribution of the undiluted emulsion before and after tribological shear was also examined (Figure 5.3 B). The oil droplet size distribution before shear was monomodal and narrow, with a mean droplet size $d_{32} = 0.16 \pm 0.004 \mu\text{m}$. After shearing, the size distribution of the oil droplets became wider and more skewed towards higher diameters values, although the mean droplet size remained at $d_{32} = 0.16 \pm 0.021 \mu\text{m}$. Under tribological shear the oil droplets might be pressed together to enter the thin contact zone, leading to minor oil droplet aggregation (Dedinaite et al., 2010). To recall, an increase in viscosity of the emulsion was observed, which can be related to such shear induced aggregation (Figure 5.2 A). The addition of buffer + α -amylase to the emulsion decreased the friction coefficient values compared to sunflower oil, suggesting the destabilization of the emulsions. OSA starch adsorbed at the oil-water interface might be expected to be hydrolysed, leading to oil droplet destabilization, as described above in the rheology section. In addition, the oil droplet size distribution became bimodal on addition of α -amylase before being subjected to tribological shear (Figure 5.3 B). Interestingly, the oil droplet size distribution with α -amylase reverted to a monomodal distribution at the higher end of the particle size range (*i.e.*, $100 \mu\text{m}$), after shearing. This drastic increase in size also suggested that the tribological shear enhanced the destabilization and coalescence of the emulsions in contact with α -amylase, at least

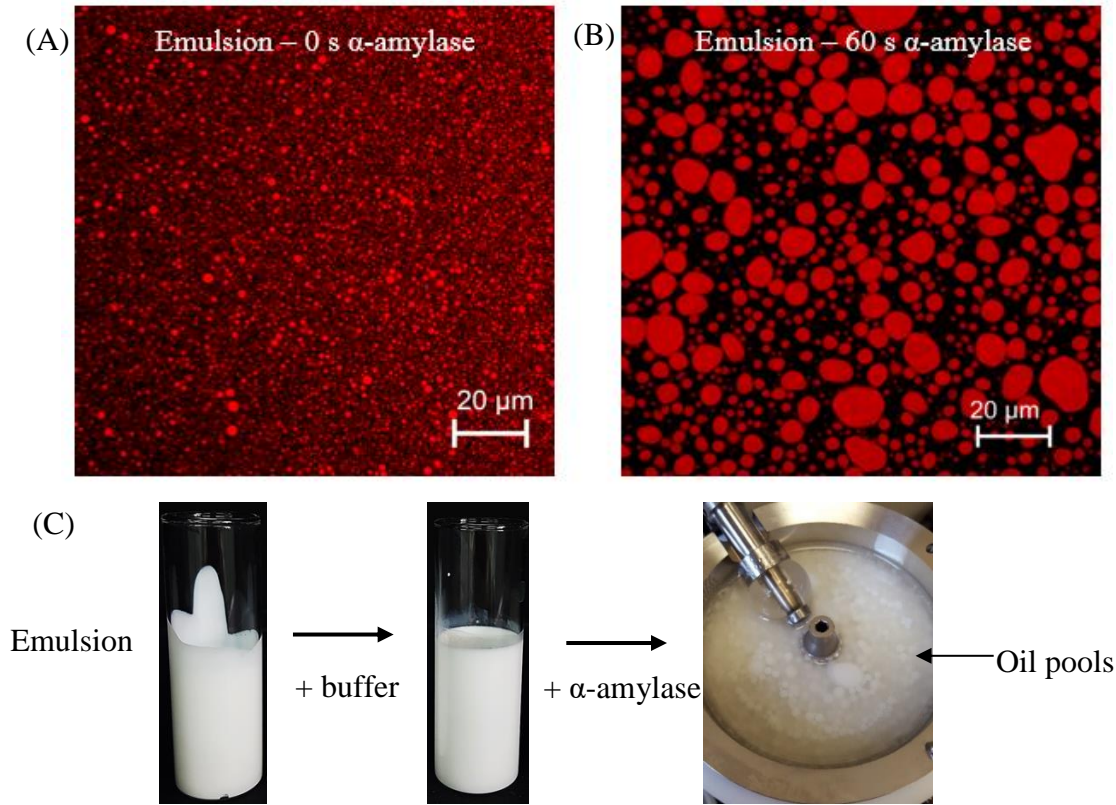


Figure 5.4 Confocal fluorescence images of the emulsion 0 s (A), 60 s (B) after the addition of α -amylase before tribological shear ($\lambda = 488$ nm, oil droplets); (C) photographs of the emulsions in the absence or presence of buffer and/or α -amylase in the tribometer.

for the smaller emulsion droplets, confirmed by visual observations as shown in Figure 5.4 C.

The microstructure of the OSA starch-stabilized emulsions at 0 and 60 s after adding α -amylase (at 37 °C) was investigated *in-situ* via confocal fluorescence microscopy (Figure 5.4 A and B). Without enzymes, the oil droplets were uniformly distributed (Figure 5.4 A). After 60 s with enzyme, much larger oil droplets were observable and the system was polydisperse (Figure 5.4 B), in agreement with the light scattering results. These results are also in accordance with previous studies (Dresselhuis et al., 2008). In summary, it seems possible to mimic the lubrication properties of sunflower oil using oil-in-water emulsions when subjecting them to oral processing conditions relevant to the operating conditions in the mouth.

5.3.4 Tribological properties of the emulsion microgel particles.

To recapitulate, in spite of the good lubrication properties of a 40 wt% oil-in-water emulsion, due to the oil droplet coalescence induced by the shear + α -amylase activity, this poor emulsion stability and therefore poor controlled release would be of great concern in many applications, such as liquid medicines. To overcome this drawback, the encapsulation of the emulsion droplets into starch microgel particles might allow better stability and controlled release than the emulsion itself, without compromising lubrication even at much lower oil content.

The tribological properties of the starch emulsion microgel particles (15 and 20 wt% starch; 0 – 15 wt% oil) were investigated for $1 < \bar{U} < 100 \text{ mm s}^{-1}$ under the same conditions as above (Figure 5.5). Results at $\bar{U} > 100 \text{ mm s}^{-1}$ can be found in Appendix C.4. Corresponding Stribeck curves of the emulsion, previously shown in Figure 5.3, are also shown in Figure 5.5 in order to aid comparison.

Starch microgel particles without oil droplets (15 and 20 wt% starch – 0 wt% oil), displayed significant differences in friction coefficient and in the limit of their boundary region (Figure 5.5 A and B and Appendix C.7). 15 wt% starch particles had a friction coefficient of 0.460 ± 0.068 at $\bar{U} = 3 \text{ mm s}^{-1}$ and 0.093 ± 0.014 at $\bar{U} = 50 \text{ mm s}^{-1}$ and entered the mixed regime $> 10 \text{ mm s}^{-1}$. In comparison, 20 wt% starch particles had a friction coefficient of 0.166 ± 0.028 at $\bar{U} = 3 \text{ mm s}^{-1}$ and 0.011 ± 0.002 at $\bar{U} = 50 \text{ mm s}^{-1}$ and entered the mixed regime $< 5 \text{ mm s}^{-1}$. Assuming that the starch microgel particles have the same elastic modulus as the starch gel, the particles would have an elastic modulus of $G' = 640 \text{ Pa}$ (**Chapter 3** (Torres et al., 2017b)) and behave as flexible and deformable soft solids. Therefore, at low entrainment speed ($\bar{U} \leq 10 \text{ mm s}^{-1}$), 15 wt% starch particles might enter the thin ball and disc gap and flatten out (Chojnicka et al., 2008) (Figure 5.5 A). Such particles would not be capable of supporting the load, which would increase the contact area causing an increase in the friction coefficient. This effect has previously been described as resulting from a sliding motion of the sample, retarding the onset of the mixed regime (Chojnicka et al., 2008). Increasing the starch concentration to 20 wt% resulted in harder and less deformable particles ($G' = 1600 \text{ Pa}$, **Chapter 3** (Torres et al., 2017b)), which would only enter the contact zone when the gap between the ball and disc reached the size of the particles (Fernández Farrés and Norton, 2015). As

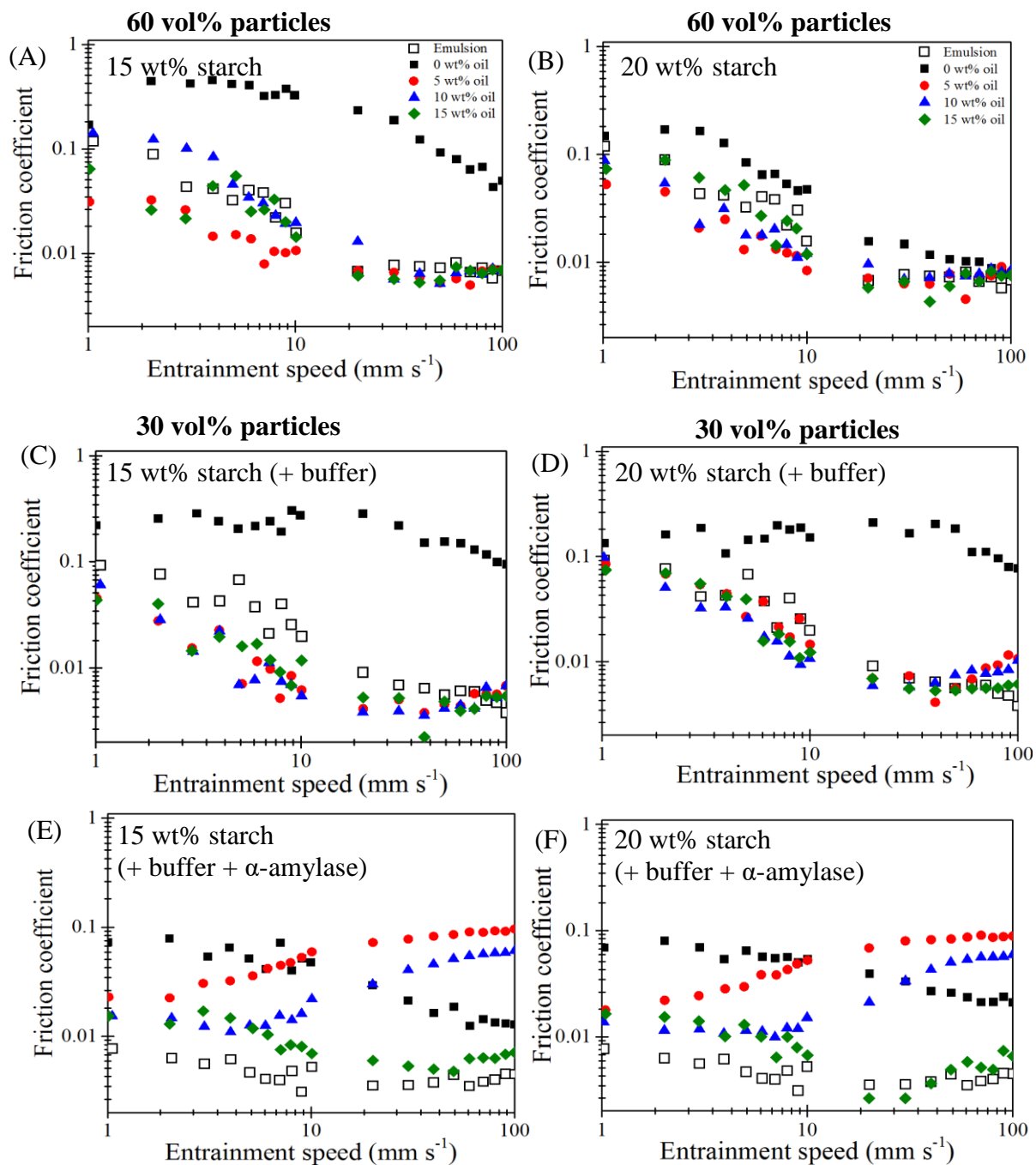


Figure 5.5 Coefficient of friction as function of entrainment speed of starch microgel particles encapsulating different oil contents measured at 2 N and 37 °C in absence of buffer and α -amylase (A and B); in presence of buffer (50:50 w/w) without α -amylase (C and D); in the presence of buffer (50:50 w/w) with α -amylase (E and F). Controls are the OSA-stabilised emulsion under the same conditions.

soon as such particles entered the contact zone these harder particles would be able to act as surface separators by carrying some part of the load, fast-tracking the onset of the mixed regime (Liu et al., 2016). Of course the difference in G' between the two particle types is less than a factor of 3, but any other explanation alludes us at present.

The encapsulation of oil droplets (5 – 15 wt% oil) into the starch particles led to similar friction coefficient values as compared to the emulsion (without buffer). The encapsulation of a small amount of oil thus seemed to allow the starch particles to have emulsion-like friction properties with negligible influence of the starch particles themselves. Similar results have previously been reported with the use of fluid gels (Hamilton and Norton, 2016). However, increasing the oil content further did not seem to significantly influence the friction coefficient values (see Appendix C.5 and C.6 for statistical analysis). The 1:1 dilution of the particles by buffer mainly influenced the friction properties of the starch particles without oil droplets, whereas the friction measurements of all the emulsion microgel particles did not seem to be affected by this dilution (Figure 5.5 C and D and Appendix C.7 and C.8). Both types of microgel particles behaved in a similar manner, with high friction ($\mu > 0.2$) in the boundary regime ($\bar{U} \leq 50 \text{ mm s}^{-1}$) and a decreased friction in the mixed regime ($50 \leq \bar{U} \leq 100 \text{ mm s}^{-1}$). Previous studies have demonstrated that the volume fraction of particles influences the friction coefficient in the boundary regime (Garrec and Norton, 2013; Sarkar et al., 2017). A low volume fraction of particles increases the friction coefficient, since less particles can be entrained into the contact zone, as compared to a high volume fraction of particles.

The addition of α -amylase drastically affected the friction properties of the different samples (Figure 5.5 E and F). Both starch particles without oil droplets (15 and 20 wt% starch) only displayed a mixed regime throughout the entrainment speed ($1 \leq \bar{U} \leq 100 \text{ mm s}^{-1}$). A significant reduction in friction coefficient compared to that with the diluted starch particles without α -amylase was also noticeable above $\bar{U} \geq 50 \text{ mm s}^{-1}$ (see Appendix C.8 for statistical analysis). For example, at $\bar{U} = 50 \text{ mm s}^{-1}$, 15 wt% starch particles in buffer without α -amylase $\mu = 0.156 \pm 0.015$, whereas, with α -amylase $\mu = 0.019 \pm 0.006$. This reduction in the friction coefficient might be explained by the degradation of the starch particles via the α -amylase into smaller microgel particles ($d_{32} = 18.5 \pm 1.6 \mu\text{m}$) as compared to the initial starch particles ($d_{32} = 39.9 \pm 1.1 \mu\text{m}$) (Figure 5.6).

Smaller particles can obviously more easily enter the tribo-pairs gap, separating the ball and disc at a lower entrainment speed and hence reducing the friction coefficient at a lower speed (Anvari and Joyner, 2017; Hamilton and Norton, 2016).

In the case of the emulsion microgel particles in the presence of α -amylase, at low entrainment speed ($1 \leq \bar{U} \leq 10 \text{ mm s}^{-1}$), their friction coefficient decreased below the values of the emulsion in buffer but were still above the value for the emulsion with α -amylase (Compare Figure 5.5 E and F to Figure 5.3 A). For example at $\bar{U} = 3 \text{ mm s}^{-1}$, the emulsion had a friction coefficient of $\mu = 0.0056 \pm 0.001$ and 15 wt% starch with 5 wt% oil $\mu = 0.016 \pm 0.008$. The higher friction coefficient of the emulsion microgel particles as compared to the emulsion with α -amylase suggested that the α -amylase started digesting the starch particle shell, allowing some stable oil droplets to be released in the continuous phase. Some degraded starch particles might also aid the reduction in friction by reducing the contact area further. However, any oil droplets released from the emulsion microgel particles did not appear to coalesce during the tribology measurements, no free oil could be observed (Figure 5.6 C). This is very different from the emulsion on its own, where phase separation was evident (Figure 5.4). Possibly the α -amylase activity was saturated by the starch shell, so that the OSA starch adsorbed at the oil interface was not significantly digested.

Additionally, it is worth noting that in the presence of enzymes, the oil concentration did seem to affect the friction values. For example, at $\bar{U} = 50 \text{ mm s}^{-1}$ the friction coefficient of 20 wt% starch particle with 5 wt%, 10 wt % and 15 wt% oil were 0.083 ± 0.003 , 0.050 ± 0.001 and 0.005 ± 0.001 , respectively (see Appendix C.8 for statistical analysis). By increasing the entrainment speed ($\bar{U} \geq 10 \text{ mm s}^{-1}$), the friction values of the emulsion microgel particles produced at 5 and 10 wt% oil increased, which might indicate jamming of the samples around the ball and disc contact zone (Fernández Farrés and Norton, 2015; de Vicente et al., 2005). Since the emulsion microgel particles do slightly break down under the effect of shear and enzyme hydrolysis (see below), some empty and/or smaller starch emulsion microgel particles might aggregate and build-up around the contact zone. This build-up of aggregated particles would prevent the entrainment of the sample (Timm et al., 2011), increasing the friction, until the entrainment speed reached 100 mm s^{-1} . In comparison, the emulsion microgel particles

with 15 wt% oil showed a decrease in friction between 10 to 100 mm s⁻¹. However, as the entrainment speed increased further ($\bar{U} \geq 100$ mm s⁻¹), the elasto-hydrodynamic regime was reached (Appendix C.3). The higher filler to matrix ratio might have produced a thinner and more brittle starch shell around the oil droplets, allowing for a higher oil content to be released between the gap, under tribological shear. Under the mixed regime this would have prevented the jamming of the particles at the contact zone, reducing the friction coefficient.

Further evidence for the explanation given above was obtained by measuring the particle size distribution (PSD) of the systems before and after tribological shear, combined with microscopic imaging described below.

5.3.5 Particle size distribution (PSD) before and after tribological shear.

The PSDs of 15 wt% and 20 wt% starch microgel particles were similar, hence only the results obtained for 15 wt% starch particles are presented, in Figure 5.6 (the results obtained for 20 wt% starch particles can be found in the supporting information (Appendix C.9)). Additionally, because essentially the same behaviour was observed for 15 wt% starch emulsion microgel particles with 5, 10 and 15 wt% oil encapsulated, for clarity only results for 5 and 15 wt% oil are shown. In the absence of α -amylase before tribological shear all samples had a monomodal particle size distribution, ranging in size between 10 and 100 μ m (Figure 5.6 A). After tribological shear, the PSDs of all the samples were similar, although shifted to smaller sizes, between 5 and 60 μ m. It is worth noting that the shift in PSD was greater for the starch microgel particles without oil droplets compared to those containing oil droplets. Possibly, this was due to the oil droplets strengthening the microgel particles as an active filler (Torres et al., 2017b). The PSD changes also fit in with the proposed explanation of the viscosity changes described earlier, in terms of breakup of aggregates with increasing shear rate.

In the presence of α -amylase Figure 5.6 B shows that the main effect of tribological shear was to produce a much broader PSD than in the absence of amylase for all the microgel particles. Thus the enzyme activity seemed to enhance the production of both

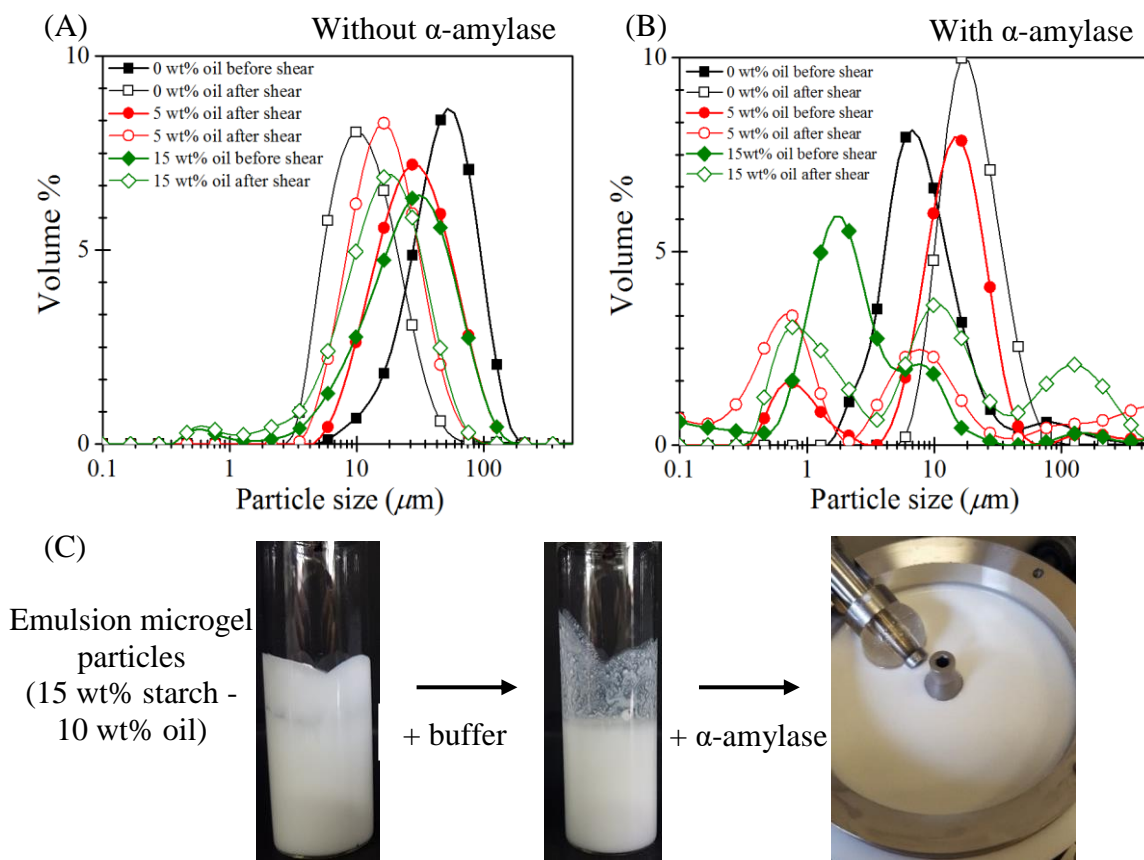


Figure 5.6 Particle size distribution of 15 wt% starch particles encapsulating different oil concentrations before or after being sheared by the tribometer in the absence (A) or presence of α -amylase (B); (C) photographs of the emulsion microgel particles after tribology in the absence or presence of buffer and/or α -amylase.

smaller fragments and larger clusters (0.1 to 100 μm), in line with previous studies (de Wijk et al., 2004). However, there was no evidence of coalescence (Figure 5.6 C) so that larger particles in the PSD are more likely to be aggregates of microgel materials than large oil droplets.

5.3.6 Morphology of the emulsion and emulsion microgel particles.

CLSM observations on the emulsion microgel particles (15 wt% starch – 10 wt% oil) illustrated in Figure 5.7, suggest that most oil droplets (red) were completely

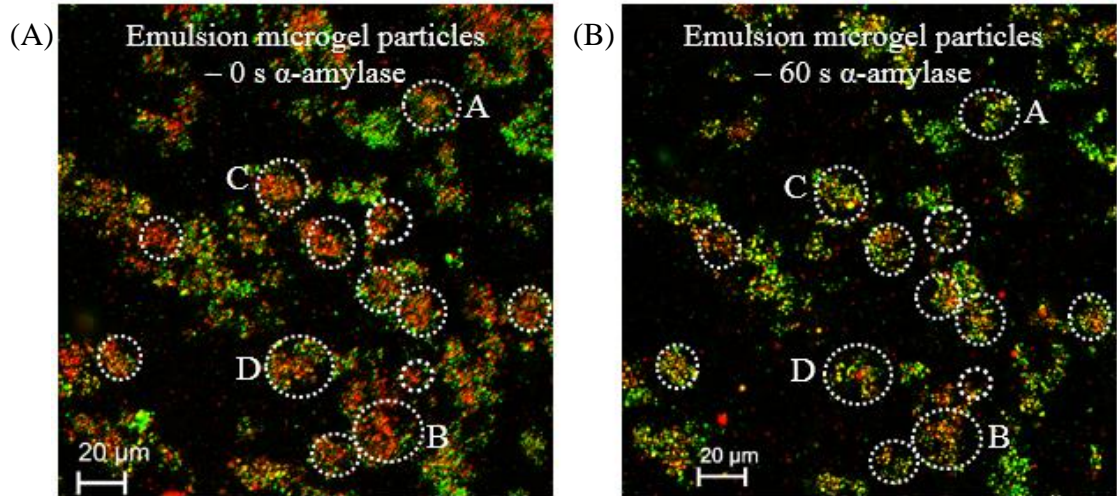


Figure 5.7 Confocal fluorescence images of the emulsion microgel particles 0 s (A) and 60 s (B) after the addition of α -amylase ($\lambda = 488$ nm, oil droplets and 639 nm, starch shell), scale bar represents 20 μ m.

entrapped in the starch gel matrix (green) at time 0 s. In Figure 5.7 A, dotted lines have been added surrounding typical microgel regions (A – D) before the addition of enzyme. After 60 s with enzyme the same regions became smaller and less red, *i.e.*, lower in oil content, suggesting their degradation and release of oil droplets (Figure 5.7 B). However, no coalescence of the oil droplets can be observed in Figure 5.7 A and B, confirming the previous observations that emulsion stability was not compromised when these were embedded in the emulsion microgel particles (Figure 5.6).

5.3.7 Lubrication mechanism of emulsion microgel particles.

In order to understand the physical properties of the lubricant partially separating the contact surfaces a mechanical analysis of the emulsion droplets, starch and emulsion microgel particles in the contact area was introduced.

From the Hertz theory (Tatara, 1991) of contact points, the radius of contact α_H and the indentation of the contact δ can be obtained. To establish the relative indentation of emulsion droplets or particles, the normal load supported by the lubricant (W_L) and by

an individual emulsion droplet or particle (W_p) as well as the reduced elastic modulus of contacts formed by the particles and the PDMS contact surfaces (E^*), were analysed (see Appendix C.5 and Figure 5.3 A and Figure 5.5). The number of particles (n_p) of radius R , forming a monolayer, inside the contact with an effective fraction of particles (ϕ_p) covering the contact area (a_{TP}) were also estimated (see Appendix C.10). Hence, the relative indentation for a monolayer of particles of a Poisson ratio ν , in the radius of contact (a_H) can be expressed as (Equation 5.1):

$$\frac{\delta}{R} = \left(\frac{a_H}{R}\right)^2 - \frac{4}{3\pi(1-\nu^2)} \left(\frac{a_H}{R}\right)^3 f\left(\frac{a_H}{R}\right) \quad (5.1)$$

where the ratio a_H/R is independent of R and relates the relative indentation to the fraction of surface covered by particles ϕ_p (Equation 5.2):

$$\frac{a_H}{R} = \left(\frac{3W_L}{4\phi_p E^* a_{TP}^2}\right)^{1/3} \quad (5.2)$$

In order to understand if such emulsion droplets could be dragged into the contact zone the entrainment force on the particles at the vicinity of the contact was also estimated using the Stokes drag equation 5.3:

$$F_d = 6\pi R \eta \bar{U}, \quad (5.3)$$

where, η and \bar{U} are the bulk viscosity and the entrainment speed, respectively. For particles to be entrained into the contact zone, the drag force (F_d) should be larger than the load applied to one particle (W_p).

Based on the experimental and theoretical results we have summarized the relative indentation and drag force of the emulsion, emulsion in buffer, 60 vol% starch particles produced at 15 and 20 wt% starch, 60 and 30 vol% emulsion microgel particles produced with 20 wt% starch and 10 wt% oil in Table 5.1. Due to the similarities of the other lubricants, their relative indentations and drag forces are not displayed. For both emulsions

(before and after dilution in buffer), at an entrainment speed of 3 mm s^{-1} (Figure 5.3 A), 86% of the load was calculated to be supported by the emulsion droplets, with $\mu = 0.1$ and $\mu_B = 0.7$. Therefore, at a Hertz contact radius of 2.07 mm, for 20% fraction of emulsion droplets covering the contact surface (ϕ_p) and W_p estimated at $1.3 \cdot 10^{-8} \text{ N}$, the relative indentation of the emulsion droplets was calculated as 0.72 (Table 5.1). This implies that, on entering the ball and disc contact zone, an emulsion droplet of radius $0.08 \text{ }\mu\text{m}$ would compress to an elliptical shape of a height of $\sim 0.05 \text{ }\mu\text{m}$. The surface roughness of PDMS being (R_a) $\leq 50 \text{ nm}$, the compressed emulsion droplets might also enter the asperities of PDMS whilst still supporting 86% of the load resulting in the decrease in friction coefficient. However, due to the viscosity difference between the emulsion and the emulsion + buffer, the drag force necessary to entrain the emulsion droplets differed.

Before dilution, the high viscosity of the emulsion at low shear ($\eta > 100 \text{ Pa s}$) led to a large drag force ($F_d > W_p$) as compared to the load applied to each emulsion droplets. The emulsion droplets would be entrained in between the tribo-pair via a sliding mechanism. The dilution of the emulsion with buffer reduced the viscosity ($\eta = 0.2 \text{ Pa s}$) of the emulsion as well as the volume fraction of oil entrained in between the tribo-pairs. Although the friction coefficient obtained for the diluted emulsion did not differ from the initial emulsion at $\bar{U} = 3 \text{ mm s}^{-1}$, the low viscosity of the emulsion in buffer leads to a lower drag force with $F_d < W_p$, predicting emulsion droplets of $0.08 \text{ }\mu\text{m}$ radius would not be entrained (Table 5.1). However, smaller emulsion droplets are also present that might be entrained and aggregate there, as suggested by the light scattering results (Figure 5.3 B). By aggregating the emulsion droplets would then be able to support the load and reduce the friction coefficient. Figure 5.8 A and B attempts to illustrate the lubrication mechanism of the emulsion droplets at $\bar{U} = 3 \text{ mm s}^{-1}$. It should be noted, that the hydrodynamic regime obtained with the diluted emulsion, resembling sunflower oil alone (Appendix C.2), might be explained by the coalescence of these aggregating emulsion droplets sliding inside the contact zone at high entrainment speed.

The presence of α -amylase dramatically changed the lubrication properties of the emulsion, although its bulk viscosity remained similar to the diluted emulsion without enzyme. As suggested earlier the OSA starch might have been hydrolysed and detached

Table 5.1 Relative indentation and drag force calculations of the emulsion droplets of radius $0.08 \mu\text{m}$ and particles of radius $15 \mu\text{m}$ at $\bar{U} = 3 \text{ mm s}^{-1}$ and $\phi_p = 20\%$.

Lubricant type	W_L (%)	$\frac{\delta}{R^*}$	η at 0.01 s^{-1} (Pa s)	W_p (N)	F_d (N)
Emulsion (40 wt% oil)	86	0.72	100	$1.3 \cdot 10^{-8}$	$4.5 \cdot 10^{-6}$
Emulsion + buffer (20 wt% oil)	86	0.72	0.1	$1.3 \cdot 10^{-8}$	$9.1 \cdot 10^{-9}$
15 wt% starch particles (60 vol%)	29	18.7	100	$1.5 \cdot 10^{-4}$	$8.5 \cdot 10^{-4}$
20 wt% starch particles (60 vol%)	71	18.7	1000	$3.7 \cdot 10^{-4}$	$8.5 \cdot 10^{-3}$
Emulsion microgel particles (60 vol%)	86	12.7	500	$4.5 \cdot 10^{-4}$	$4.5 \cdot 10^{-3}$
Emulsion microgel particles (30 vol%)	86	12.7	200	$4.5 \cdot 10^{-4}$	$1.7 \cdot 10^{-3}$

from the oil droplet surfaces, leading to their coalescence and the formation of an oil film (Figure 5.8 C) where the oil dominates the friction. It has also been suggested that surfactant molecules can absorb onto the PDMS surfaces preventing contact between the ball and disc at low entrainment speeds (Liu et al., 2016). Since OSA starch is amphiphilic, some surface active fragments might desorb from the oil droplets and adsorb to the ball and disc, separating the surfaces further compared to sunflower oil, in accordance with previous studies (Pradal and Stokes, 2016; Dickinson, 2017; Dresselhuis et al., 2008).

In comparison, starch micorgel particles had significantly larger ($p < 0.05$) friction coefficient values than the emulsion, depending on both the concentration of starch (*i.e.*, 15 wt% or 20 wt%) used to form the particles and the volume fraction of particles (*i.e.*, 60 vol% or 30 vol%) in solution. Since the friction coefficient of 15 and 20 wt% starch particles + buffer had similar friction values, it can be assumed that 30 vol% of particles had very limited lubrication properties in the boundary region, probably due to the low viscosity. At higher volume fraction (*i.e.*, 60 vol% particles), the concentration of starch influenced the lubrication behaviour of the particles. At 15 wt% starch, only 29% of the

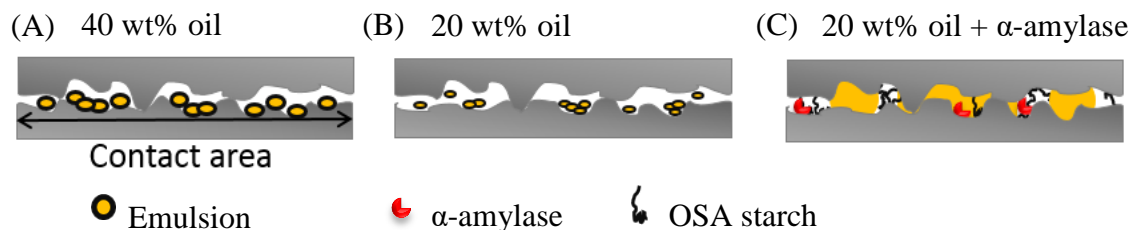


Figure 5.8 Schematic representation of OSA starch stabilized oil-in-water emulsion in the mixed regime of a tribometer in the absence (A) or presence of buffer without (B) and with α -amylase (C).

load is predicted to be supported by the starch particles, whereas at 20 wt% starch 71% of the load should be supported by the particles (Table 5.1). The relative indentation of the starch particles being larger than 1 suggests that on entering the contact zone both particle types would be deformed and destroyed. The light scattering results suggest that the particles formed from 15 wt% starch were broken down more easily during tribological shear compared to the 20 wt% starch particles (compare Figure 5.6 A and Appendix C.9 A). Their differences in lubrication might therefore be explained by their differences in viscosity, so that the viscosity of the 20 wt% starch particles dispersion lead to a higher drag force, allowing the particles to be entrained and deformed, decreasing the friction via load bearing (Figure 5.9 B).

Likewise the addition of α -amylase to the starch particles decreased the friction coefficient of both starch particles (15 and 20 wt%) due to the limited hydrolysis of the starch microgel particles (Figure 5.9 C) – under the action of α -amylase the particles might lose their structure and be entrained more easily at low speed.

The starch microgel particles with encapsulated oil droplets (Figure 5.9 C and E) gave a similar decrease of friction, compared to the emulsion, at both volume fractions (60 and 30 vol%). The oil droplets acted as active fillers and strengthened the emulsion gel so that the emulsion microgel particles were more rigid (see section 5.3.4 and **Chapter 3** (Torres et al., 2017b)). At $\bar{U} = 3 \text{ mm s}^{-1}$ the emulsion microgel particles before and after dilution gave a similar friction coefficient to the emulsion droplets, which implied that 86% of the load was supported by the emulsion microgel particles. However, regarding

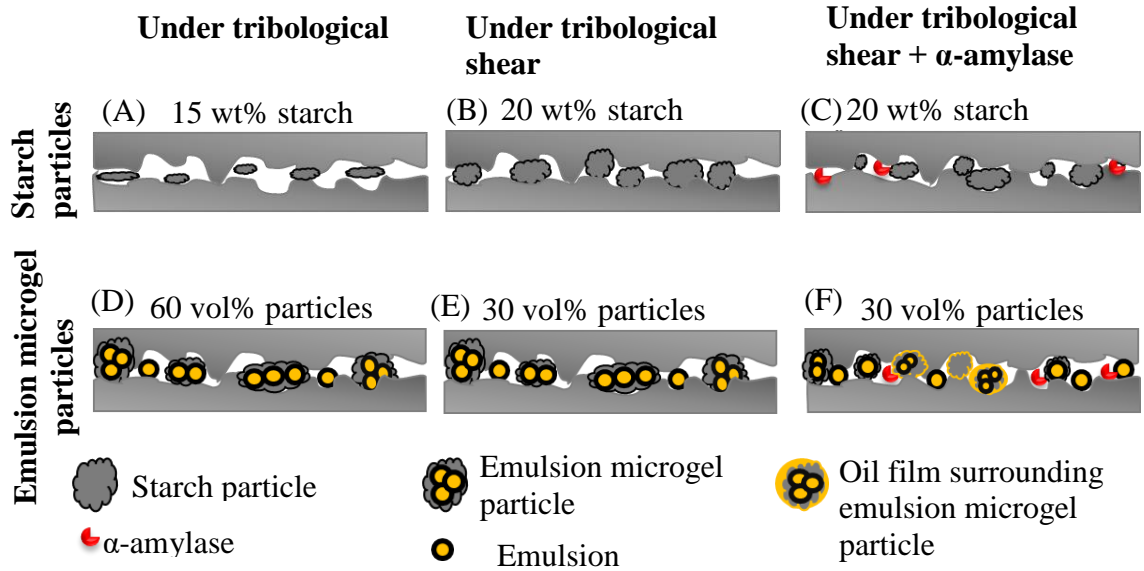


Figure 5.9 Schematic representation of native starch particles in the mixed regime of a tribometer at low (A) and high (B) starch concentration in the absence or presence α -amylase (C); schematic representation of starch based emulsion microgel particles at low (D) or high (E) particle volume fraction without or with α -amylase (F).

the relative indentation, this was estimated at 12.7 and the drag force was estimated high enough to entrain the emulsion microgel particles in the contact zone (Table 5.1). Similarly to the 20 wt% starch particles, on entering the contact zone the emulsion microgel particles should therefore become highly compressed and deformed, probably allowing some emulsion droplets to be released in the continuous phase. However, due to the emulsion droplets acting as active fillers it is possible that on entering the contact zone the microgel particles would compress until the modulus of the microgel particles approaches the modulus of the encapsulated emulsion droplets allowing the system to support the load rather than completely breaking down. This mechanism would also explain the smaller shift in particle size after tribological shear, compared to the larger shift in particle size observed for the unfilled microgel particles (Figure 5.6 A).

When α -amylase was added to the emulsion microgel particles, it is proposed that starch microgel particle fragments are produced as well as emulsion microgel particles surrounded by an oil film (Figure 5.9 F), due to the small amount of emulsion breakdown.

The OSA starch adsorbed at the surface of the oil droplets largely remains intact and the encapsulated emulsion droplets are able to diffuse into the continuous phase, where they are mostly stable. The released emulsion droplets thus enhance the lubrication of the filled microgel particles via the dual action of the few emulsion droplets released and the smaller sized emulsion microgel particles, mimicking the lubrication of the emulsion in the mixed region.

5.4 Conclusions

Emulsion microgel particles with stimuli-responsiveness to physiological enzyme and shear were proposed and have been realised creating a novel bio-lubricant additive. In response to tribological shear and enzyme activity, some emulsion droplets entrapped in the starch microgel particles are released and improved oral lubrication. Based on confocal fluorescence microscopy, these oil droplets are still stabilised by an adhering OSA starch layer and residual microgel material. Thus, the encapsulation of emulsion droplets into these emulsion microgel particles protected them throughout the oral processing so that their potential lubrication properties were not lost. This shear and enzyme-responsive emulsion microgel particle might reduce the degradation of lipophilic compounds in presence of harsh physiological environment (*i.e.*, biological shear such as mastication or gastric motility, biological enzymes, acidic conditions). For instance, the starch microgel particle should further protect the lipophilic bio-active during gastric conditions whilst degrade in the small intestine. Where further contact with α -amylase will allow the destabilisation of the emulsion droplets for increased bio-accessibility of oil-soluble bio-active compounds.

By modifying the biopolymer used to form the emulsion microgel particles, it is expected that further targeted release might be achievable. Hence, in the next chapter (**Chapter 6**) targeted release in the gastrointestinal regime was investigated with the use of whey protein-based emulsion microgel particles, the latter being relatively stable in the oral phase.

5.5 References

- Adams, S. et al. 2004. Influence of particle modulus on the rheological properties of agar microgel suspensions. *Journal of Rheology*. **48**(6), pp.1195-1213.
- Alazemi, A.A. et al. 2015. Ultrasoother Submicrometer Carbon Spheres as Lubricant Additives for Friction and Wear Reduction. *ACS Applied Materials & Interfaces*. **7**(9), pp.5514-5521.
- Anvari, M. and Joyner, H.S. 2017. Effect of formulation on structure-function relationships of concentrated emulsions: Rheological, tribological, and microstructural characterization. *Food Hydrocolloids*. **72**(Supplement C), pp.11-26.
- Batchelor, H. et al. 2015. The application of tribology in assessing texture perception of oral liquid medicines. *International Journal of Pharmaceutics*. **479**(2), pp.277-281.
- Ching, S.H. et al. 2016. Rheology of emulsion-filled alginate microgel suspensions. *Food Research International*. **80**, pp.50-60.
- Chojnicka, A. et al. 2008. Lubrication Properties of Protein Aggregate Dispersions in a Soft Contact. *Journal of Agricultural and Food Chemistry*. **56**(4), pp.1274-1282.
- de Vicente, J. et al. 2006. Viscosity Ratio Effect in the Emulsion Lubrication of Soft EHL Contact. *Journal of Tribology*. **128**(4), pp.795-800.
- de Vicente, J. et al. 2005. Lubrication properties of non-adsorbing polymer solutions in soft elastohydrodynamic (EHD) contacts. *Tribology International*. **38**(5), pp.515-526.
- de Wijk, R.A. et al. 2004. The role of α -amylase in the perception of oral texture and flavour in custards. *Physiology & Behavior*. **83**(1), pp.81-91.
- de Wijk, R.A. et al. 2006. Perceived creaminess of semi-solid foods. *Trends in Food Science & Technology*. **17**(8), pp.412-422.
- Dedinaite, A. et al. 2010. Lubrication by organized soft matter. *Soft Matter*. **6**(7), pp.1520-1526.
- Dickinson, E. 2017. On the road to understanding and control of creaminess perception in food colloids. *Food Hydrocolloids*. **77**, pp.372-385

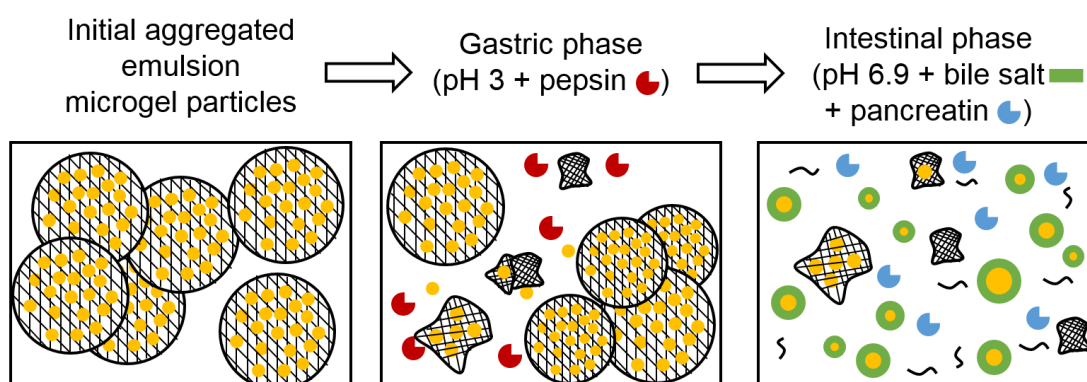
- Dou, X. et al. 2016. Self-dispersed crumpled graphene balls in oil for friction and wear reduction. *Proceedings of the National Academy of Sciences*. **113**(6), pp.1528-1533.
- Dresselhuis, D.M. et al. 2008. The occurrence of in-mouth coalescence of emulsion droplets in relation to perception of fat. *Food Hydrocolloids*. **22**(6), pp.1170-1183.
- Fernández Farrés, I. and Norton, I.T. 2015. The influence of co-solutes on tribology of agar fluid gels. *Food Hydrocolloids*. **45**(Supplement C), pp.186-195.
- Garrec, D.A. and Norton, I.T. 2013. Kappa carrageenan fluid gel material properties. Part 2: Tribology. *Food Hydrocolloids*. **33**(1), pp.160-167.
- Hamilton, I.E. and Norton, I.T. 2016. Modification to the lubrication properties of xanthan gum fluid gels as a result of sunflower oil and triglyceride stabilised water in oil emulsion addition. *Food Hydrocolloids*. **55**, pp.220-227.
- Joyce, P. et al. 2015. Bioactive Hybrid Particles from Poly(d,l-lactide-co-glycolide) Nanoparticle Stabilized Lipid Droplets. *ACS Applied Materials & Interfaces*. **7**(31), pp.17460-17470.
- Laguna, L. et al. 2017. Relating rheology and tribology of commercial dairy colloids to sensory perception. *Food & Function*. **8**(2), pp.563-573.
- Liu, G. et al. 2014. Hairy Polyelectrolyte Brushes-Grafted Thermosensitive Microgels as Artificial Synovial Fluid for Simultaneous Biomimetic Lubrication and Arthritis Treatment. *ACS Applied Materials & Interfaces*. **6**(22), pp.20452-20463.
- Liu, K. et al. 2016. Evidence for ball-bearing mechanism of microparticulated whey protein as fat replacer in liquid and semi-solid multi-component model foods. *Food Hydrocolloids*. **52**(Supplement C), pp.403-414.
- Malone, M.E. et al. 2003. Oral behaviour of food hydrocolloids and emulsions. Part 1. Lubrication and deposition considerations. *Food Hydrocolloids*. **17**(6), pp.763-773.
- Minekus, M. et al. 2014. A standardised static in vitro digestion method suitable for food - an international consensus. *Food & Function*. **5**(6), pp.1113-1124.
- Mueller, S. et al. 2009. The rheology of suspensions of solid particles. *Proceedings of the Royal Society A: Mathematical, Physical and Engineering Science*. **466**(2116), pp.1201-1228.

- Nguyen, C.T.H. et al. 2017. Bifunctional Succinylated ϵ -Polylysine-Coated Mesoporous Silica Nanoparticles for pH-Responsive and Intracellular Drug Delivery Targeting the Colon. *ACS Applied Materials & Interfaces*. **9**(11), pp.9470-9483.
- Porter, C.J.H. et al. 2008. Enhancing intestinal drug solubilisation using lipid-based delivery systems. *Advanced Drug Delivery Reviews*. **60**(6), pp.673-691.
- Pradal, C. and Stokes, J.R. 2016. Oral tribology: bridging the gap between physical measurements and sensory experience. *Current Opinion in Food Science*. **9**(Supplement C), pp.34-41.
- Ravanfar, R. et al. 2018. Controlling the Release from Enzyme-Responsive Microcapsules with a Smart Natural Shell. *ACS Applied Materials & Interfaces*. **10**(6), pp.6046-6053.
- Røn, T. et al. 2014. Lubrication of Soft and Hard Interfaces With Thermo-Responsive F127 Hydrogel. *Polymer*. **55**(22), pp.5708-5717
- Røn, T. et al. 2017. Gastric mucus and mucuslike hydrogels: Thin film lubricating properties at soft interfaces. *Biointerphases*. **12**(5), p051001.
- Sarkar, A. et al. 2017. Aqueous Lubrication, Structure and Rheological Properties of Whey Protein Microgel Particles. *Langmuir*. **33**(51), pp. 14699-14708
- Secret, E. et al. 2014. Enzyme-Responsive Hydrogel Microparticles for Pulmonary Drug Delivery. *ACS Applied Materials & Interfaces*. **6**(13), pp.10313-10321.
- Simovic, S. et al. 2012. Assembling nanoparticle coatings to improve the drug delivery performance of lipid based colloids. *Nanoscale*. **4**(4), pp.1220-1230.
- Sterner, O. et al. 2017. Reducing Friction in the Eye: A Comparative Study of Lubrication by Surface-Anchored Synthetic and Natural Ocular Mucin Analogues. *ACS Applied Materials & Interfaces*. **9**(23), pp.20150-20160.
- Stokes, J.R. et al. 2013. Oral processing, texture and mouthfeel: From rheology to tribology and beyond. *Current Opinion in Colloid & Interface Science*. **18**(4), pp.349-359.
- Sun, L. et al. 2013. Novel Chitosan-Functionalized Spherical Nanosilica Matrix As an Oral Sustained Drug Delivery System for Poorly Water-Soluble Drug Carvedilol. *ACS Applied Materials & Interfaces*. **5**(1), pp.103-113.

- Sweedman, M.C. et al. 2014. Aggregate and emulsion properties of enzymatically-modified octenylsuccinylated waxy starches. *Carbohydrate Polymers*. **111**, pp.918-927.
- Tatara, Y. 1991. On Compression of Rubber Elastic Sphere Over a Large Range of Displacements—Part 1: Theoretical Study. *Journal of Engineering Materials and Technology*. **113**(3), pp.285-291.
- Tesch, S. et al. 2002. Stabilization of emulsions by OSA starches. *Journal of Food Engineering*. **54**(2), pp.167-174.
- Timm, K. et al. 2011. Particulate lubricants in cosmetic applications. *Tribology International*. **44**(12), pp.1695-1703.
- Torres, O. et al. 2016. Emulsion microgel particles: Novel encapsulation strategy for lipophilic molecules. *Trends in Food Science & Technology*. **55**(Supplement C), pp.98-108.
- Torres, O. et al. 2017a. Design of novel emulsion microgel particles of tuneable size. *Food Hydrocolloids*. **71**(Supplement C), pp.47-59.
- Torres, O. et al. 2017b. Novel starch based emulsion gels and emulsion microgel particles: Design, structure and rheology. *Carbohydrate Polymers*. **178**, pp.86-94.
- Weenen, H. et al. 2005. Sensory sub-attributes of creamy mouthfeel in commercial mayonnaises, custard desserts and sauces. *Food Quality and Preference*. **16**(2), pp.163-170.
- Xia, F. et al. 2017. Size-Dependent Translocation of Nanoemulsions via Oral Delivery. *ACS Applied Materials & Interfaces*. **9**(26), pp.21660-21672.
- Xu, Y. et al. 2018. Novel Solid Lipid Nanoparticle with Endosomal Escape Function for Oral Delivery of Insulin. *ACS Applied Materials & Interfaces*. **10**(11), pp.9315-9324.

Chapter 6

Whey protein-based emulsion microgel particles for targeted intestinal release of lipophilic components⁵



Abstract

Whey protein based emulsion microgel particles (9.6 wt% whey protein – 20 wt% sunflower oil) were produced via cold set precipitation using calcium ions (0.1 M) and their behaviour under *in vitro* gastrointestinal digestion was investigated with conventional oil-in-water emulsions (9.6 wt% whey protein – 20 wt% sunflower oil) as a control. The droplet size distribution, zeta-potential, microstructure and hydrolysis of interfacial whey protein during *in vitro* gastric digestion and free fatty acid release during *in vitro* intestinal digestion were compared for both samples. During *in vitro* gastric digestion, emulsions flocculated and coalesced ($d_{32} \sim 0.13 \mu\text{m}$ to $\sim 12 \mu\text{m}$ after 120 min) due to pepsinolysis of the adsorbed protein layer, as evidenced by SDS-PAGE (sodium dodecyl sulphate polyacrylamide gel electrophoresis). This destabilisation led to uncontrolled and limited release of free

⁵ Published as: Torres, O., Murray, B. and Sarkar, A. 2019. Overcoming *in vitro* gastric destabilisation of emulsion droplets using emulsion microgel particles for targeted intestinal release of fatty acids. *Food Hydrocolloids*. **89**, pp.523-533. DOI: <https://doi.org/10.1016/j.foodhyd.2018.11.010>

fatty acids (44 % FFA) during subsequent intestinal digestion, largely due to the reduction in interfacial area. In comparison, emulsion microgel particles were noticeably more stable during *in vitro* gastric digestion, with only a slight decrease in particle size ($d_{32} \sim 50 \mu\text{m}$ to $\sim 20 \mu\text{m}$ after 120 min). The protection of emulsion droplets against gastric coalescence in emulsion microgel particles was controlled by physicochemical interactions between calcium ions and whey protein in the particles, limiting both pepsin-diffusion and cleavage at the pepsin active site. Under subsequent *in vitro* intestinal digestion, the microgel particles degraded due to the action of intestinal proteases, releasing fine emulsion droplets, which then gave significantly higher release of free fatty acids (54 % FFA).

6.1 Introduction

Lipophilic bio-active molecules, such as fat soluble vitamins, fatty acids, essential oils and drugs pose substantial challenges when incorporated into food, pharmaceuticals and other soft matter applications. Most of these lipophilic compounds are difficult to deliver to physiological sites (*i.e.*, via the intestinal phase) due to the physical instability, during gastrointestinal transit, of the oil phases in which they are solubilized (Golding & Wooster, 2010; Parada & Aguilera, 2007). Oil-in-water (O/W) emulsions stabilized by protein or surfactant have been commonly used to encapsulate and stabilise lipophilic molecules (Araiza-Calahorra et al., 2018; McClements et al., 2007). Nevertheless, their limited stability during gastric digestion, due to flocculation and coalescence of the oil droplets – largely attributed to pepsinolysis or harsh acidic/ ionic environments, leads to inadequate release of lipophilic molecules during subsequent intestinal digestion (Golding and Wooster, 2010; Hur et al., 2009; Sarkar et al., 2010a; Sarkar et al., 2009; Singh and Sarkar, 2011). Therefore, a strong emphasis has been placed on developing delivery systems that can protect the droplets in the gastric phase and then release the bio-actives molecules at specific locations during intestinal digestion (McClements, 2017; McClements et al., 2008; Matalanis and McClements, 2013).

In this direction of research, many authors have investigated manipulating the interface of droplets to restrict pepsinolysis of proteinaceous stabilizing layers by creating a more tortuous path for pepsin to reach the interface, for example by coating

the adsorbed protein with several layers (*i.e.*, layer by layer technique) of other material(s). In this fashion, gastric stability of emulsion droplets has been achieved by coating protein-stabilized droplets with a variety of non-digestible dietary fibres (Beysseriat, Decker, & McClements, 2006; Meshulam & Lesmes, 2014) and/or particles (Liu & Tang, 2016; Sarkar, Ademuyiwa, et al., 2018; Sarkar, Li, Cray, & Boxall, 2018; Sarkar, Zhang, Murray, Russell, & Boxal, 2017; Shao & Tang, 2016). The second strategy used in literature involves encapsulating emulsion droplets within a gel.

Emulsion gels have shown some success in providing gastric stability, attributed to the inhibition of diffusion of pepsin to the surface of emulsion droplets within the gel, largely controlled by the rheology/ microstructure of the gel matrix (Guo et al., 2017; Guo et al., 2014; Sarkar et al., 2015a). An alternative strategy is to embed the emulsion droplets into gelled particles: “emulsion microgel particles”.

Emulsion microgel particles are a relatively new class of “smart” soft solid vehicles where several emulsion droplets are encapsulated within a biopolymer hydrogel particle (Torres et al., 2016; Torres et al., 2017a; Torres et al., 2017b; Torres et al., 2018). This structure offers several advantages over conventional O/W emulsions. The soft solid shell encapsulating the emulsion droplets can protect lipophilic bio-actives against oxidation and offers the opportunity to tune its physicochemical properties as a function of environmental conditions (*e.g.*, swell or de-swell as a function of pH, ionic strength, temperature and enzymatic condition), allowing the protection or release of the lipophilic constituents (Beaulieu et al., 2002; Gunasekaran et al., 2007; Torres et al., 2016; Matalanis et al., 2012). Thus, emulsion microgel particles might enable targeted release of bio-active molecules at the different stages of digestion. Previous studies using different types of emulsifiers (*e.g.*, protein) and gelling agents (*e.g.*, alginate, κ -carrageenan, starch, gelatine, casein) to form emulsion-filled hydrogel particles have already started to examine the digestion and release mechanisms of the encapsulated emulsion droplets. (Mun et al., 2015; Ozturk et al., 2015; Tangsrianugul et al., 2015; Zhang et al., 2016; Corstens et al., 2017; van Leusden et al., 2018). Surface erosion of the gel particles during gastric digestion was perceived as the main degradation mechanism for digestible gel matrices (*e.g.*, casein and gelatine). Whilst, the stable gel matrices during gastric environment should be good candidates for the formation of resistant emulsion microgel particles, the possible thermodynamic incompatibility between different hydrocolloids forming the particles

might lead to uncontrolled swelling and diffusion of the lipophilic material (McClements, 2017). Therefore, engineering emulsion microgel particles from a single hydrocolloid (used as both the gelling agent and emulsifier), where the droplets are strongly linked by their adsorbed layer to the surrounding gel, is more likely to prevent any uncontrolled destabilisation due to possible thermodynamic incompatibility, etc. Of course, using a suspension of microgel particles as the carrier of the droplets will be far more versatile, in terms of technological usage, than macroscopic pieces of filled gel.

Whey protein, primarily composed of β -lactoglobulin, has been demonstrated to limit pepsinolysis, due to its globular structure (Nacer S et al., 2004). Additionally, from **Chapter 4**, whey protein forms cold-set microgel particles and emulsion microgel particles, of around 30 μm size, via the addition of calcium (Ca^{2+}) ions to a preheated whey protein suspension and whey protein-stabilized O/W emulsion. Hence, whey protein can be used as emulsifier and gelling agent to produce emulsion microgel particles with actively bound emulsion droplets. Cold set gelation of whey protein with Ca^{2+} results from the formation of a network between Ca^{2+} and free carboxylic groups found on the acidic amino groups (*i.e.*, aspartic acid and glutamic acid) of the main protein after their exposure on unfolding due to pre-heating (Egan et al., 2013; Torres et al., 2017a).

However, to our knowledge no study has yet investigated the digestion mechanism of encapsulated emulsion droplets using only one biopolymer as both emulsifier and gelling agent, nor has the behaviour of whey protein based emulsion microgel particles during *in vitro* gastrointestinal digestion been investigated.

The hypothesis behind this study is that encapsulating whey protein stabilized O/W emulsion droplets into whey protein microgel particles will protect the fine emulsion droplets from gastric flocculation and coalescence. Such gastric stability will allow more efficient release of free fatty acids from the smaller emulsion droplets (higher interfacial area) during lipolysis. The first stage of this study was therefore to develop the encapsulation of the droplets into microgel particles and demonstrate their enhanced stability under *in vitro* gastric conditions. Secondly, the rate of lipolysis under subsequent *in vitro* intestinal conditions was measured, using the original O/W emulsion (9.6 wt% WPI – 20 wt% oil) as a control. A combination of particle size characterization, zeta-potential measurements, confocal microscopic imaging, electrophoresis (SDS-PAGE) of the interfacial protein before and after *in vitro* gastric

digestion as well as pH-STAT based free fatty acid release measurements during *in vitro* intestinal digestion (pre- or post-gastric digestion) were used in this chapter.

6.2 Materials and Methods

6.2.1 2.1 Materials

Whey protein isolate (WPI) powder containing 96.3 wt% protein (Molecular mass: 18.4 kDa) was a kind gift from Fonterra Limited (Auckland, New Zealand). Sunflower oil was purchased from Morrisons supermarket (UK). Porcine pepsin (P7000, 526 U mg⁻¹ using haemoglobin as a substrate), porcine pancreatin (P7545, 8 ×USP and trypsin activity of 6.48 U mg⁻¹ using TAME, *N-p*-Tosyl-L-arginine methyl ester hydrochloride, as a substrate) and porcine bile extract B8631 (total bile salt content 49 wt% with 10 – 15% glycodeoxycholic acid, 3 – 9% taurodeoxycholic acid, 0.5 – 7% deoxycholic acid, 5 wt% phospholipids) were purchased from Sigma-Aldrich Company Ltd, Dorset, UK. All solutions were prepared with Milli-Q water having resistivity of 18.2 MΩ cm at 25 °C (Milli-Q apparatus, Millipore, Bedford, UK). Nile Red and Rhodamine B were purchased from Sigma-Aldrich (Steinheim, Germany). Dimethyl sulfoxide (DMSO) was purchased from Fluorochem (Hadfield, UK). All other chemicals were of analytical grade and purchased from Sigma-Aldrich unless otherwise specified.

6.2.2 Preparation of whey protein based emulsion microgel particles

Whey protein emulsion microgel particles were prepared using a bottom-up approach, as per **Chapter 4** (Torres et al., 2017a). Briefly, 20 wt% sunflower oil was emulsified with 12 wt% WPI that has been previously heat-treated at 85 °C for 40 min at pH 7 (final concentration of WPI in the emulsion: 9.6 wt%). Secondly, the heat-treated WPI-stabilised emulsion was mixed with a solution of 0.1 M calcium chloride (at a ratio of 45:55) and passed once through the Leeds Jet Homogenizer at a pressure of 250 bar. The resulting particles were collected in a beaker and immediately diluted with Milli-Q water to 50 wt% and stirred for 30 min at low speed to limit particle aggregation. Sodium azide (0.02 wt%) was added as an antimicrobial agent to the samples stored for 24 h at 4 °C. For control purposes, whey protein microgel particles

(without oil) were also prepared using the same procedure and final concentration of whey protein (9.6 wt%).

6.2.3 Static *in vitro* gastric and intestinal digestion

The different samples (WPI microgel particles, emulsion and emulsion microgel particles) were digested by subjecting them to simulated gastric fluid (SGF) mimicking fasted conditions of the stomach or simulated intestinal fluid (SIF) or sequential simulated gastric and intestinal fluids (SGF + SIF) using the slightly adapted digestion protocol of Minekus et al. (2014) and Sarkar et al. (2016a) and Mat et al. (2016). Ten mL of each sample were incubated for 2 hours at pH 3 with 7.5 mL of SGF composed of 6.9 mM KCl, 0.9 KH₂PO₄, 72.2 mM NaCl, 0.1 mM MgCl₂(H₂O)₆, 0.5 mM (NH₄)₂CO₃, 5 μ L CaCl₂ at 0.3 M, 1.6 mL pepsin (at 2000 U mL⁻¹ in the final chyme) and 0.695 μ L water. After 2 hours of incubation the pH of the sample + SGF (20 mL) was adjusted to pH 6.8 with 1 M NaOH and mixed with 11 mL of SIF. The SIF after gastric digestion (SGF + SIF) at pH 6.8 contained 6.8 mM KCl, 0.8 mM KH₂PO₄, 123.4 mM NaCl, 0.33 mM MgCl₂(H₂O)₆, 40 μ L CaCl₂.H₂O at 0.3 M, 2.5 mL bile salts at 160 mM, 1.31 mL water and 5 mL pancreatin solution at 800 U mL⁻¹ (to obtain a final activity of 100 U mL⁻¹ based on trypsin activity). In a separate experiment, the different samples were mixed in SIF in the absence of any pre-gastric digestion. Samples (2 mL) were mixed with 15 mL of SIF (4.7 mM KCl, 0.6 mM KH₂PO₄, 85.7 mM NaCl, 0.8 mM MgCl₂(H₂O)₆), 20 mL bile salts at 25 mM, 10 mL CaCl₂ at 1.5 mM, 2 mL water and 1 mL pancreatin solution at 5000 U mL⁻¹ (to obtain a final activity of 100 U mL⁻¹ based on trypsin activity). The *in vitro* intestinal digestion was carried out over 3 hours at pH 6.8 and 37 °C.

Aliquots were collected at different time points throughout the course of *in vitro* digestions (SGF, SIF and SGF + SIF) and were characterized. To stop pepsin activity at specific time points, 0.2 M sodium bicarbonate at pH 7 was added to the samples. The pancreatin activity was stopped by adding 1 mM of 4-(2-aminoethyl) benzenesulfonyl fluoride hydrochloride (Pefabloc©) at appropriate time points.

6.2.4 Particle size measurements

Static light scattering was used to measure the size distribution of the emulsion droplets and emulsion microgel particles undergoing *in vitro* digestion (at 0, 5, 60, 120 min during gastric digestion; at 0, 30, 180 min during intestinal digestion; and at 0, 30,

180 min after gastric and during intestinal digestion) using a Malvern Mastersizer 3000E hydro, (Malvern Instruments, Worcestershire, UK). Samples were diluted in distilled water until the instrument gave an obscuration of 4 to 6%. Sizing of the emulsion oil droplets was conducted based on a relative refractive index of 1.097 (*i.e.*, the ratio of the refractive index of sunflower oil at 1.460 to that of the aqueous phase at 1.33). The absorbance value of the emulsion droplets was set to 0.001. Sizing of the emulsion microgel particles was conducted based on a relative refractive index of 1.150 (*i.e.*, the ratio of the refractive index of WPI at 1.53 to that of the aqueous phase at 1.33). The absorbance value of the emulsion microgel particles was similarly set to 0.001.

6.2.5 ζ -potential measurements

The ζ -potential of the emulsion droplets and emulsion microgel particles undergoing *in vitro* digestion was determined using a particle electrophoresis instrument (Zetasizer, Nano ZS series, Malvern Instruments, Worcestershire, UK). The emulsion and emulsion microgel particles were diluted to 0.005 wt% droplet concentration. The diluted sample was then added to a folded capillary cell (Model DTS 1070, Malvern Instruments Ltd., Worcestershire, UK). The ζ -potential of the emulsion was measured ten times for each diluted sample.

6.2.6 Analysis of peptic hydrolysis of interfacial proteins

The protein composition at the interface of the emulsion droplets or encapsulated within whey protein microgel particles before and after *in vitro* gastric hydrolysis by pepsin was determined by analysing the cream phase using sodium dodecyl sulphate polyacrylamide gel electrophoresis (SDS-PAGE) under reducing conditions (Sarkar et al., 2016a; Sarkar et al., 2018a). For control purposes the protein compositions of 9.6 wt% WPI solution and whey protein microgel particles without any oil droplets were also determined. The different samples before and after *in vitro* gastric digestion were centrifuged for 40 min at 14,500 g and 20 °C. The cream layer of the emulsion and emulsion microgel particles was carefully removed, dispersed in Milli-Q water (to obtain an approximated final concentration of WPI of 0.192 wt% to ensure appropriate protein concentrations in the loaded gel) and centrifuged again for 40 min at 14500 g and 20 °C. Approximately, 65 μ L of cream layer was carefully collected and mixed with 25 μ L of SDS sample buffer (62.5 mM Tris-HCl, pH 6.8, 2%

SDS, 25% glycerol, 0.01% bromophenol blue) and 10 μL of dithiothreitol (DTT, of a final concentration of 50 mM) and heat treated at 95 $^{\circ}\text{C}$ for 5 min. The SDS-PAGE was carried out by loading 5 μL of standard protein marker and 10 μL of sample into gels previously prepared on a Mini-PROTEAN II system (Bio-Rad Laboratories, Richmond, CA, USA). The resolving gel contained 16% acrylamide and the stacking gel was made up of 4% acrylamide. The SDS-PAGE ran for 60 min at 100 V. After running, the gel was rinsed in Milli-Q water and stained for 2 h with 90% Proto-Blue Safe Colloidal Coomassie G-250 stain and 10% ethanol solution. The gel was destained in Milli-Q water overnight and scanned and analysed using a Gel DocTM XR+ System (Bio-Rad Laboratories, Richmond, CA, USA). Each band within the lanes was selected automatically by the software to cover the whole band. Background intensity was subtracted after scanning an empty lane.

6.2.7 Analysis of free fatty acid release after *in vitro* intestinal digestion

The free fatty acid release from the emulsion and emulsion microgel particles was analysed during the *in vitro* intestinal digestion without or with *in vitro* gastric digestion, the latter subsequently described as sequential digestion. The *in vitro* intestinal digestion was carried out over 1 hour whilst maintaining the pH at 6.8 by the addition of 0.05 M NaOH using a pH-STAT (TIM 854, Radiometer). The volume of 0.05 M NaOH added to the samples was used to calculate the concentration of free fatty acid (FFA) generated in the reaction vessel during digestion of the emulsified or encapsulated lipids. The percentage of FFA released was calculated, taking into account the auto-digestion of pancreatic juice (assuming the generation of 2 FFAs per triacylglycerol molecule by the action of lipase action) using Equation (6.1) (Sarkar et al., 2016a):

$$\%FFA = 100 \times \left(\frac{V_{NaOH} M_{NaOH} M_{WLipid}}{2 \times w_{Lipid}} \right) \quad (6.1)$$

where V_{NaOH} is the volume (mL) of sodium hydroxide, M_{NaOH} is the molarity of sodium hydroxide (0.05 M), M_{WLipid} is the average molecular weight of sunflower oil (0.880 kg mol^{-1}) and w_{Lipid} is the weight of lipid initially present in the reaction vessel.

The kinetics of the FFA released from the emulsion or emulsion microgel particle was analysed using a nonlinear regression model Equation (6.2):

$$\Phi(t) = \Phi_{max} + (\Phi_0 - \Phi_{max})\exp(-kt) \quad (6.2)$$

where $\Phi(t)$ is the amount of FFA released over time in the *in-vitro* intestinal digestion, Φ_{max} is the maximum FFA released that can be obtained during the simulated intestinal digestion, Φ_0 is the amount of FFA released at time 0 min during the *in vitro* intestinal digestion, k is the digestion rate constant and t is the time in during the simulated intestinal digestion. At the start of the simulated intestinal digestion ($t = 0$ min), it was assumed that no FFA were released, resulting in $\Phi_0 = 0$. Therefore Equation 6.2 can be simplified into Equation 6.3 (Sarkar et al., 2016b):

$$\Phi(t) = \Phi_{max}(1 - \exp(-kt)) \quad (6.3)$$

The FFA versus digestion time resulting from the lipolysis reaction can then be characterised using quantitative terms, such as Φ_{max} and k , by fitting Equation 6.3 to the experimental data and finding the values that minimize the difference between the experimental data and the model.

6.2.8 Confocal scanning laser microscopy

Emulsion microgel particles undergoing *in vitro* digestion were imaged using a confocal laser scanning microscope (CLSM). A Zeiss LSM 700 CLSM (Carl Zeiss MicroImaging GmbH, Jena, Germany) with a 40 \times magnification was used. Nile Red (1 mg mL⁻¹ in dimethyl sulfoxide, 1:100 v/v) was used to stain oil (argon laser with an excitation line at 488 nm) and Rhodamine B (0.5 mg mL⁻¹ in Milli-Q water, 1:100 v/v) was used to stain proteins (argon laser with an excitation line at 568 nm). The emulsion and emulsion microgel particles were mixed with 10 μ L of Nile Red (0.1% w/v) and 10 μ L of Rhodamine B, stirred for 15 min and placed onto a microscope slide and covered with a cover slip before imaging.

6.2.9 Statistical analysis

Significant differences between samples were determined by one-way ANOVA and multiple comparison test with Tukey's adjustment performed using SPSS software (IBM, SPSS statistics, version 24) and the level of confidence was 95%.

6.3 Results and Discussion

6.3.1 *In vitro* gastric digestion of emulsion microgel particles

Figure 6.1 A and B highlight the particle size distribution of both the whey protein stabilised-emulsion and emulsion microgel particles undergoing either a change of pH (*i.e.*, from pH 7 to pH 3) or undergoing simulated gastric digestion over time in presence of pepsin (*i.e.*, 5, 60, 120 min). At pH 7 and in absence of SGF, the majority of the emulsion droplets were in the range of 0.01 – 5 μm , with $d_{32} = 0.13 \mu\text{m}$ and $d_{43} = 0.76 \mu\text{m}$. The emulsion droplets were negatively charged with a ζ -potential of -47.5 mV (Figure 6.2 A) and the emulsion appeared to consist of uniformly dispersed droplets as observed via CLSM (Figure 6.1 C). The decrease of pH to pH 3 in the presence of SGF without pepsin led to the expected charge reversal of emulsion droplets due to the protonation of the ionisable groups. The ζ -potential did not reach high magnitudes at pH 3 ($+32.2 \text{ mV}$) owing to some degree of electrostatic screening of WPI by SGF ions (Zhang et al., 2017; Sarkar et al., 2010a) (Figure 6.2 A), meanwhile such charge screening effects did not influence the droplet size distribution (Figure 6.1 A).

In the presence of SGF containing pepsin, emulsions underwent a drastic increase in droplet size, ranging from 3 to 800 μm , suggesting flocculation or even coalescence of droplets, possibly due to the hydrolysis of the interfacial protein by pepsin (Singh et al., 2009). CLSM images of the emulsion + SGF after 120 min provided further evidence of the flocculation of the droplets (Figure 6.1 D), where large flocs of emulsion droplets of $>10 \mu\text{m}$ can be observed. A few much larger droplets are also noticeable, suggestive of coalescence during the simulated gastric digestion, as observed in previous studies (Macierzanka et al., 2009; Golding and Wooster, 2010; Sarkar et al., 2010a; Sarkar et al., 2009; Singh and Sarkar, 2011).

Shifting the focus to emulsion microgel particles at pH 7 in the absence of SGF, the particles ranged in size from 3 to 1000 μm with $d_{32} = 57 \mu\text{m}$ and $d_{43} = 206 \mu\text{m}$ (Figure 6.1 B) and a ζ -potential of -21.2 mV (Figure 6.2 B). This suggests that the fine emulsion droplets were clustered into discrete emulsion microgel particles (Figure 6.2 B), in accordance with **Chapter 4** (Torres et al., 2017a). From CLSM images it is noticeable that all the emulsion droplets (stained in red) are encapsulated within the WPI matrix (stained in green) with no significant free or coalesced oil droplets (Figure 6.1 E). The change in pH from pH 7 to pH 3 did not affect the emulsion microgel

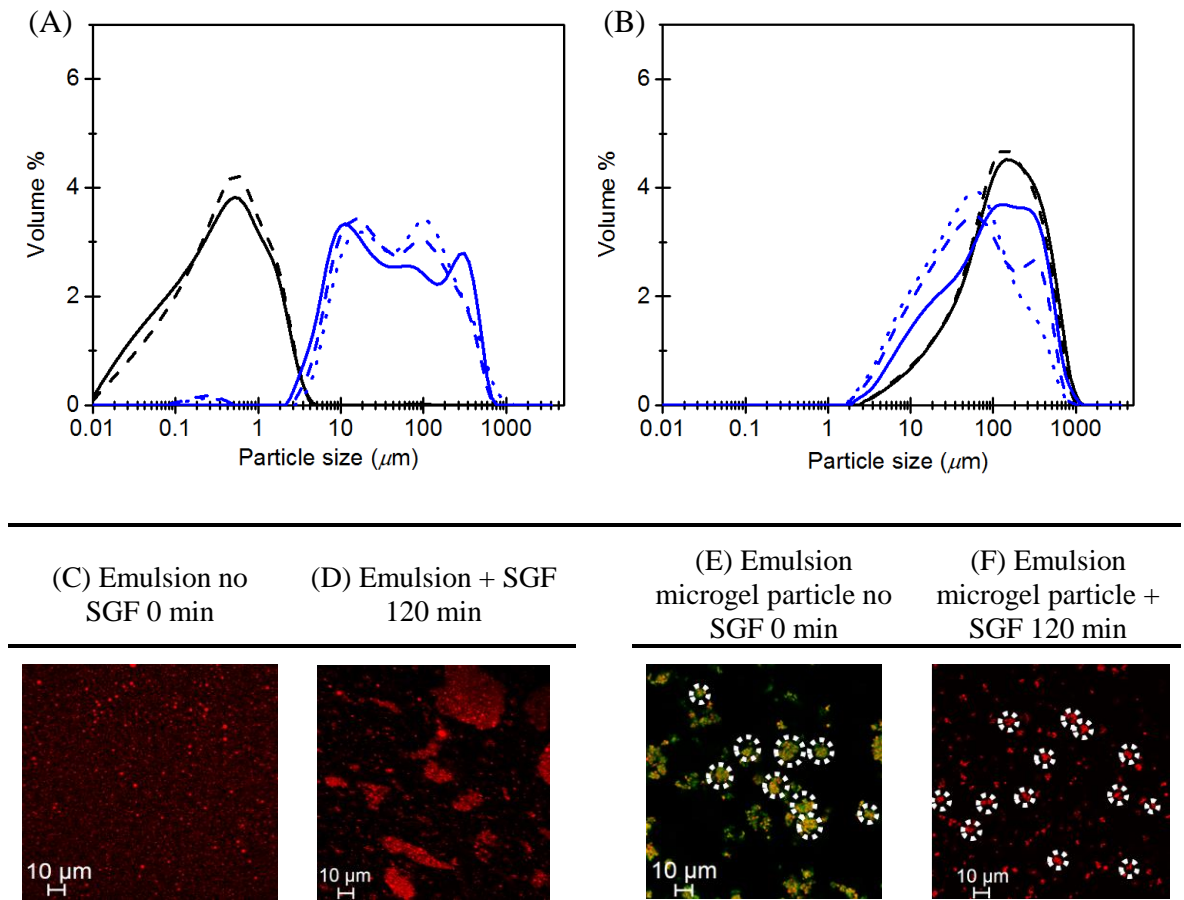


Figure 6.1 Emulsion (A) and emulsion microgel particle (B) size distribution (black full line: before digestion, black dashed line: in buffer pH 3; after *in vitro* gastric digestion blue full line: 5 min, blue dashed line: 60 min, blue dotted line: 120 min) and confocal microstructure of emulsion droplets (C and D) and emulsion microgel particles (E and F) under *in vitro* gastric digestion over time (oil droplets stained in red by Nile Red and protein matrix stained in green by Rhodamine B in Figure E only whereas only oil droplets stained in red by Nile Red in Figure C, D and F).

particle size distribution, although the ζ -potential became positive (+22.2 mV) due to the protonation of the WPI (Figure 6.2 B) (Zhang et al., 2017). Interestingly, even in presence of pepsin in the SGF, the particle size distribution of the emulsion microgel particles decreased only slightly, in contrast to the emulsion droplets. After 120 min of residence in SGF + pepsin, the emulsion microgel particle size decreased to $d_{32} = 22 \mu\text{m}$ and $d_{43} = 96 \mu\text{m}$, reflecting the changes observed in the CLSM images (Figure 6.1 F). Note that there was no evidence of large emulsion droplets (*i.e.*, no

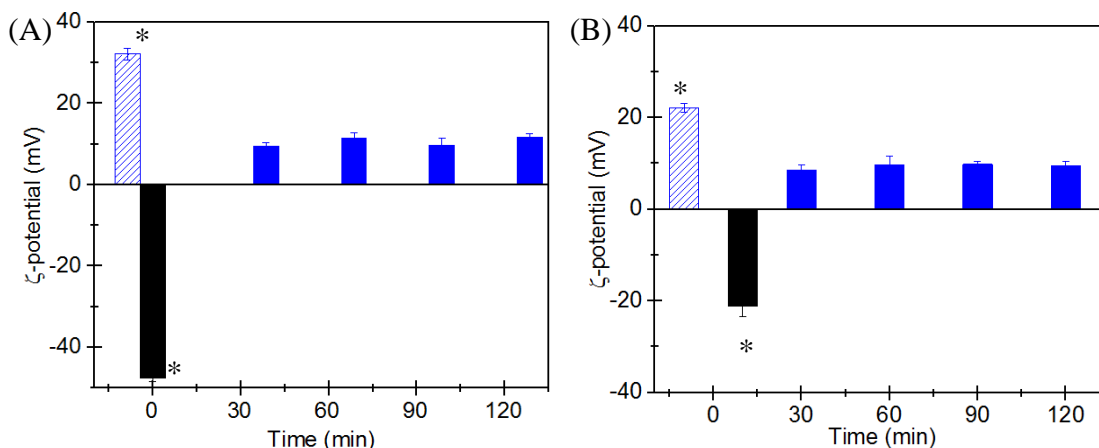


Figure 6.2 Zeta-potential of 9.6 wt% WPI stabilized emulsion (A) and emulsion microgel particles (B) at pH 7 (black) and pH 3 (blue slashed) and under in vitro gastric digestion (blue). Error bars represent standard deviations, mean with symbol (*) are statistically different at a level of $p < 0.05$ to all other samples.

coalescence) or significant release of droplets from the microgel particles, based on the particle size distribution data or the CLSM images. The ζ -potential data also remained fairly constant (Figure 6.2 B). Therefore, at this early stage, it can be speculated that the decrease in size of the emulsion microgel particles (Figure 6.1 B) is probably due to pepsin. The enzyme might be rupturing the protein network on the outside of the microgel particles, eroding them slightly, rather than degrading the interfacial protein of individual emulsion droplets, which would be expected to produce coalescence. The surface erosion of the microgel particles, rather than their degradation, was further confirmed by the analysis of microgel particles (for information on particles without any emulsion droplet, see Appendix D.1 and D.2).

In order to better understand the gastric stability of WPI stabilised-emulsion and emulsion microgel particles towards pepsinolysis, the hydrolysis patterns of the adsorbed protein phase (*i.e.*, the cream layer) from the emulsion and the emulsion microgel particles are presented in Figure 6.3. As controls, an aqueous dispersion of 9.6 wt% whey protein and whey protein microgel particles (without any encapsulated emulsion droplets) were also analysed. In agreement with findings elsewhere, whey protein, composed primarily of β -lactoglobulin (18.4 kDa) and α -lactalbumin (14 kDa), is resistant to pepsin-induced digestion owing to their globular conformation (Guo et al., 1995; Macierzanka et al., 2009). From Figure 6.3 A and B (lines a and a'), 51% of α -lactoglobulin and 92% of β -lactoglobulin (estimated via densitometry)

remained after digestion in SGF for 120 min as compared to the non-digested whey protein solution. Due to the globular nature of β -lactoglobulin, pepsin has very limited access to the carboxyl side of the aromatic amino acid buried inside the β -lactoglobulin dimers (Guo et al., 1995; Luo et al., 2017; Nacer S et al., 2004).

The formation of whey protein microgel particles via a process of heat treatment and Ca^{2+} – induced gelation under turbulent flow conditions, as discussed in **Chapter 4** (Torres et al., 2017a) – led to WPI particles slightly less resilient towards digestion (Figure 6.3A and B, lines b and b'). After 120 min in SGF, α -lactalbumin and β -lactoglobulin were broken down into peptides with $M_w < 10$ kD, although considerable quantities of intact α -lactalbumin (45%) and β -lactoglobulin (70%) remained. This is most obviously explained by the heat treatment, causing some unfolding of β -lactoglobulin, enhancing the digestibility of WPI (Mackie and Macierzanka, 2010; Beaulieu et al., 2002). From a previous study, heat treating whey protein at 85 °C for 40 min has been estimated to lead to protein denaturation by over 85% (Torres, Murray, & Sarkar, 2017). However, the cross-linking of whey protein with Ca^{2+} might have created a network around the aromatic amino acids of β -lactoglobulin, limiting the access to pepsin and slowing down pepsinolysis.

In the case of whey protein stabilised-emulsion (previously heat treated), α -lactalbumin and β -lactoglobulin in the adsorbed phase also appeared to break down into peptides although approximately 42% and 75% of the intact protein remained, respectively (Figure 6.3A and B, lines c and c'). Previous studies have shown that

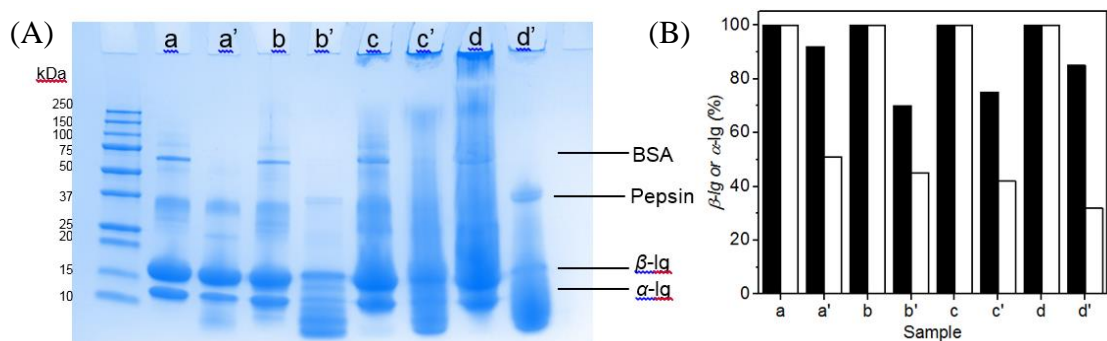


Figure 6.3 SDS-PAGE pattern before and after *in vitro* gastric digestion (A) of 9.6 wt% native WPI solution (a and a'), 9.6 wt% WPI microgel particles (b and b'), 9.6 wt% interfacial WPI stabilised emulsion (c and c') and 9.6 wt% WPI emulsion microgel particles (d and d') and relative quantification (B) of intact β - (black) and α -lactalbumin (white) bands by densitometric analysis of the gel.

alongside heat treatment, emulsification also unfolds the secondary structure of β -lactoglobulin at the oil droplet interface, which would increase the accessibility of pepsin towards the polypeptide chains (Macierzanka et al., 2009; Mackie and Macierzanka, 2010; Sarkar et al., 2009). However, due to the acidic conditions in the gastric phase, increased internal hydrogen bonding can occur between two carboxyl groups or one carboxyl group and one amine group limiting the accessibility to pepsin (Nacer S et al., 2004; Reddy et al., 1988). The large flocs observed during simulated gastric digestion (Figure 6.1 D) also suggested the formation of a coarse network which might further protect the protein from pepsinolysis.

In the case of the whey protein emulsion microgel particles, a considerable amount of interfacial material remained in the stacking gel. The emulsion microgel particle aggregates were possibly too large (> 250 kDa) to enter the resolving gel (Figure 6.3 A line d). The hydrolysis pattern of the emulsion microgel particles was similar to that of the whey protein microgel particles alone and the emulsion alone (Figure 6.3B, lines b', c' and d'), although slightly more intact β -lactoglobulin remained (85%) after 120 min of *in vitro* gastric digestion. However, it should be noted that due to smearing of the bands, the exact amount of intact protein remaining after digestion might not have been accurately assessed via densitometry. A potential cause of this lower pepsinolysis of the emulsion microgel particles might be related to the mesh size of the emulsion microgel particles (Beaulieu et al., 2002; Gunasekaran et al., 2007; Sarkar et al., 2015b). From **Chapter 4**, it was suggested that the theoretical mesh size of WPI microgel particles and WPI emulsion microgel particles is related to the elastic modulus of the gel network as well as the interfacial tension and emulsion droplet size of the encapsulated emulsion droplets. From the rubber elasticity theory modified by Flory the mesh size of the model whey protein gel can be calculated, via Equation 1:

$$\xi^3 = \frac{\kappa_B T}{G'_m} \quad (1)$$

where κ_B is the Boltzmann constant, T is the temperature and G'_m the storage modulus of the starch gel.

The estimation of the mesh size of an emulsion gel can be achieved using the Palierne model (Bousmina, 1999; Palierne, 1990, 1991), which takes into account the interfacial tension, the oil droplet size and the oil content in the emulsion (Equation 2):

$$G_b^*(\omega) = G_m^*(\omega) \frac{1+3\phi H(\omega)}{1-2\phi H(\omega)} \quad (2)$$

$$\text{where } H(\omega) = \frac{4(\alpha/R)[2G_m^*(\omega)+5G_d^*(\omega)]+[G_d^*(\omega)-G_m^*(\omega)][16G_m^*(\omega)+19G_d^*(\omega)]}{40(\alpha/R)[G_m^*(\omega)+G_d^*(\omega)]+[2G_d^*(\omega)+3G_m^*(\omega)][16G_m^*(\omega)+19G_d^*(\omega)]}$$

with, ϕ the concentration of oil, R the average radius of the emulsion droplets, α the interfacial tension of the OSA starch, ω the frequency, G_m^* , G_d^* and G_b^* the complex shear moduli of the matrix, the emulsion droplets and the emulsion gel, respectively.

Therefore, from Equation 1 the mesh size of the whey protein gel was estimated to be 24.5 nm, whilst from Equation 2 the mesh size of the emulsion gel was estimated to be 6.6 nm (Torres, Murray, et al., 2017). However, it should be recognized that the mesh size for the filled microgel particles could be misleading. The concentration of protein is the same for both microgel particles the overall modulus of the filled gelled phase does not necessarily translate to the equivalent modulus of an unfilled gel. However, the local structure of the protein gel in the vicinity of the surface of the droplets is likely to be affected, since the protein on the surface of the droplets is apparently actively bound to the bulk gel matrix (Dickinson, 2012; Dickinson & Chen, 1999). More importantly, the model used assumes the droplets are randomly distributed throughout the protein gel phase. We have little evidence that is not the case, but some droplet aggregates are seen and if some aggregates extend to form strands within some microgel particles, possibly even a secondary network, then this could have even larger effects on their overall modulus, making the calculation increasingly invalid. Unfortunately, no such models seem to exist for dealing with such complexity and so we believe it is still worth stating the values calculated, recognizing the system may be considerably more complex than the calculation implies.

The radius of gyration of pepsin is ca. 2.3 nm (Amsden, 1998), so pepsin would more easily diffuse into the larger WPI microgel particle pores, resulting in a higher digestibility. In the case of the emulsion microgel particles, pepsin might only be able to digest a thin layer of WPI at the surface of the particles (Luo et al., 2015; Luo et al., 2017). The tortuous network of the droplets within the emulsion microgel particles might also hinder pepsin reaching the interfacial whey protein of all the emulsion droplets. This would explain the decrease in size of the emulsion microgel particles rather than the release and coalescence of free oil droplets.

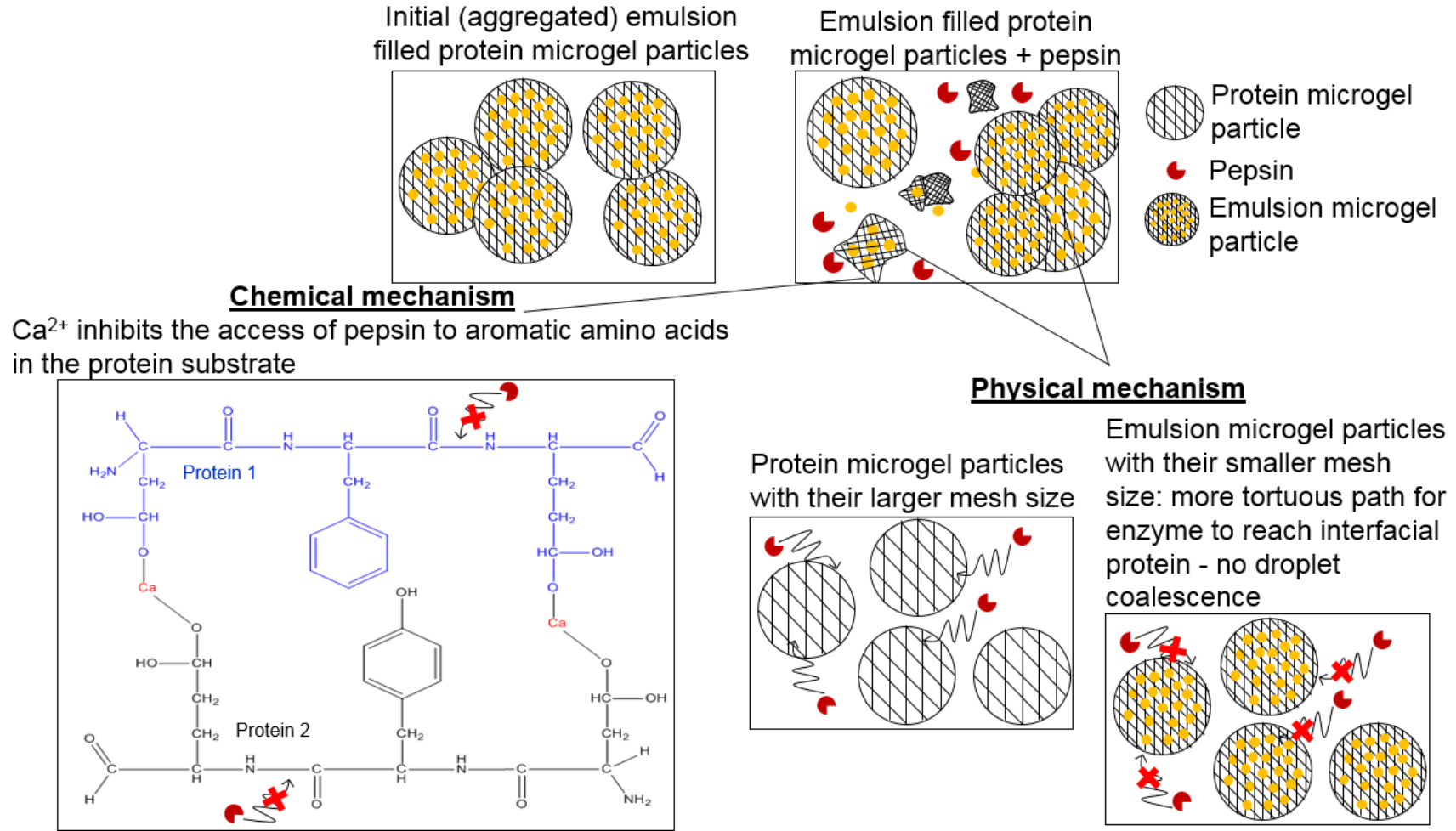


Figure 6.4 Schematic diagram of the protective properties of emulsion microgel particles against complete *in vitro* gastric digestion by pepsin.

Therefore, we propose that the protection of the emulsion microgel particles from complete pepsinolysis was possibly caused by the chemical and/or physical mechanisms depicted in Figure 6.4. The key chemical mechanisms might be: (i) the binding of calcium ions to whey protein limiting the access to the active sites of pepsin, (ii) the increased internal hydrogen bonding at acidic pH, both of which would restrict the diffusion of pepsin to the aromatic amino acid. On the other hand, the physical mechanism might be that (iii) the small mesh size of the particles would inhibit or slow down the diffusion of pepsin inside the emulsion microgel particles.

6.3.2 *In vitro* intestinal digestion of emulsion microgel particles

Simulated intestinal digestion of the emulsion and emulsion microgel particles were carried out using two conditions, one without simulated gastric pre-digestion and another post simulated gastric digestion, *i.e.*, sequential gastric-to-intestinal digestion, to understand the distinctive influence of the simulated gastric and intestinal regimes. Figure 6.5 shows the particle size distribution and representative CLSM images of the emulsion and emulsion microgel particles undergoing *in vitro* intestinal digestion with or without the *in vitro* gastric pre-digestion step. Without the pre-gastric digestion, 30 min was enough to destabilise the emulsion. The emulsion droplets became polydisperse, with prominent peaks at about 100 – 1000 μm , suggesting coalescence and confirmed by the CLSM images. The substantial decrease of the ζ -potential from -47.5 ± 0.9 mV before *in vitro* intestinal digestion, to -78.2 ± 1.1 and -91.3 ± 4.4 mV 30 min and 180 min after *in vitro* intestinal digestion, respectively, corroborates the emulsion droplet destabilization (Figure 6.6 A). During the *in vitro* intestinal digestion, bile salts will displace the WPI from the interface allowing access to lipase. The lipolysis of the oil droplets will produce free fatty acids, as well as mono- and diglycerides, which are negatively charged surface active digestion products, resulting in the decrease of the ζ -potential of the emulsion (Mackie and Macierzanka, 2010; Torcello-Gomez et al., 2011; Sarkar et al., 2010c; Sarkar et al., 2010b; Sarkar et al., 2016b).

The emulsion undergoing *in vitro* intestinal digestion post-gastric digestion behaved differently. The emulsion droplet size distribution at both 30 and 180 min showed polydispersity with a prominent peak ranging between 1 and 50 μm (Figure

6.5). Additionally, the ζ -potential of the emulsion was stable over time, at around -40 mV (Figure 6.6 A). The flocculation of the emulsion droplets in the SGF might have delayed the displacement of whey protein from the interface by bile salts. Additionally, the flocculation and coalescence of the oil droplets in the gastric regime decreases the interfacial area, which would reduce the lipolysis kinetics (Torcello-Gomez et al., 2011).

For the emulsion microgel particles, the *in vitro* intestinal digestion without any pre-gastric digestion led to some release of the emulsion droplets, as observed by the peak ranging from 0.01 to 1 μm after both 30 and 180 min in Figure 6.5 E and F. From the CLSM images, the released emulsion droplets after 30 min did not seem to have coalesced, no large oil droplets are noticeable (Figure 6.5 E). Interestingly, after 180 min the particle size distribution of the emulsion microgel particles did not appear to have changed significantly, although due to the polydispersity of the sample, a few large droplets were evident from the CLSM micrographs (Figure 6.5 F). The ζ -potential measurements showed an initial net decrease in the ζ -potential from -21.2 ± 2.2 to -52.9 ± 2.4 mV at time 0 and 30 min, respectively (Figure 6.6 B). Over the next 180 min, the ζ -potential stabilized at an average value of -47.8 ± 2.1 mV. At intestinal pH (pH 6.8) and ionic strength, the deprotonation of the carboxyl groups of β -lactoglobulin drastically increased ($p < 0.05$) the net negative charge of the emulsion microgel particles, hence contributing to higher repulsive forces. This electrostatic repulsion might have led to the swelling of the particles, which might allow the release of emulsion droplets (van Leusden et al., 2018; Beaulieu et al., 2002). The swelling of the microgel particles was particularly noticeable by the particle size change of the whey protein microgel particles (containing no oil) over the intestinal digestion time (see Appendix D.3 and D.2). The increase of the particle size might also result from the aggregation of fragmented particles during intestinal digestion. Additionally, the large decrease in ζ -potential might also suggest surface erosion and destabilisation of the whey protein microgel particles by the trypsin in pancreatin, allowing the release of the emulsion droplets, which had a ζ -potential of -47.5 mV (Figure 6.2 A) (see Appendix D.4 for particles without oil droplets showing no noticeable change). The stability of the ζ -potential over the next 180 min suggested that pancreatin did not significantly hydrolyse further the interfacial protein on the emulsion droplets. In contrast, the behaviour of emulsion microgel particles during *in vitro* intestinal digestion post-gastric digestion differed. It is noticeable from Figure 6.5 G that, after

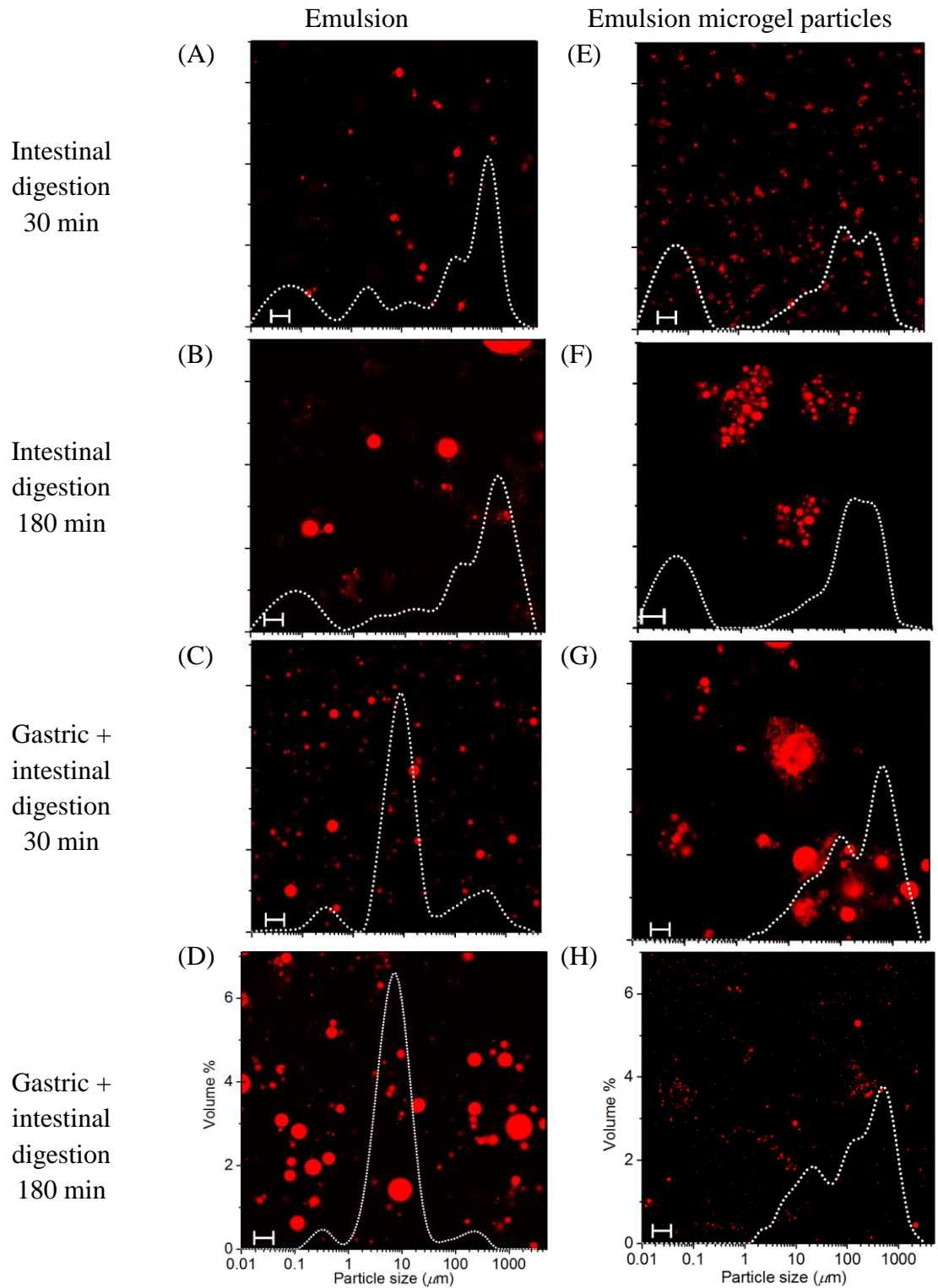


Figure 6.5 Confocal micrograph with superimposed particle size distribution of 9.6 wt% WPI stabilized emulsion and 9.6 wt% WPI based emulsion microgel particles under intestinal and sequential gastric + intestinal static *in vitro* digestion after 30 and 180 min, scale bar represents 10 μm .

30 min, all the microgel particles were hydrolysed, releasing their emulsion droplets, which subsequently coalesced. After 180 min, fewer and smaller oil droplets can be observed in the CLSM micrographs suggesting almost complete lipolysis of the oil droplets. However, it should be noted that large coalesced oil droplets might still be present, as depicted by the light scattering results (Figure 6.5 H), which might have migrated to the top of the microscopic slide due to density gradient and were not captured during imaging. The ζ -potential after 180 min slightly decreased to -26.0 ± 1.3 mV.

To assess the impact of emulsion droplet encapsulation in microgel particles, the free fatty acid (FFA) release during intestinal digestion was monitored via a pH-STAT titration measurement (at 37 °C) (Figure 6.7). The experimental data was fitted with a nonlinear regression mathematical model (Equation 6.3) and the corresponding fitting parameters (the rate constant, k , and the maximum FFA release, Φ_{\max}) are also reported in Figure 6.7. It should be noted that this may not be the best model for the initial part of the digestion, since this model assumes individual emulsion droplets rather than clustered droplets. However, the fitting still gives some indication of the effects on the rate constant.

For control purposes, the FFA release of both emulsion and emulsion microgel particles pre-gastric digestion was also assessed and reported in the appendix

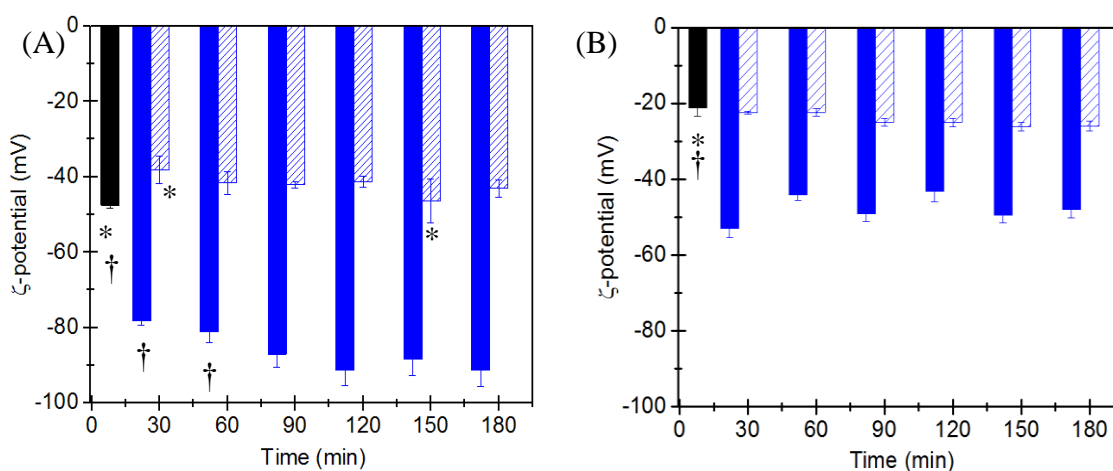


Figure 6.6 Zeta-potential of 9.6 wt% WPI stabilized emulsion (A) and emulsion microgel particles (B) at pH 7 (black) and under intestinal *in-vitro* digestion (blue) and under *in-vitro* gastric + intestinal digestion (blue slashed), mean with symbol (*, †) are statistically different at a level of $p < 0.05$ to all other samples undergoing the same digestion conditions.

(Appendix D.5). As a general trend, both pre-gastric digested emulsions and emulsion microgel particles showed a steep increase in the percentage of FFA release but this stabilised after 30 min. The total amount of FFA released as well as the rate constant and half time of both emulsion and emulsion microgel particles were not significantly different ($p > 0.05$). After 60 min of *in vitro* intestinal digestion, the emulsion generated a FFA release of $54.9 \pm 3.7\%$, whilst the emulsion microgel particles generated a release of $60.5 \pm 3.2\%$ FFA (Figure 6.7 A). Therefore, it can be assumed that after the full 3 hours of intestinal digestion all the FFA (66.66%) would have been released from both the emulsion and emulsion microgel particles. During the intestinal digestion, lipolysis of the emulsion droplets only occurs after bile salts displace the emulsifier from the oil-in-water interface. Previous studies have demonstrated that bile salts displace protein via an orogenic displacement process involving the nucleation of bile salt domains at weak points within the protein network film (Mackie et al., 2000). Subsequently, lipase-colipase complexes are able to adsorb to the oil interface to initiate the hydrolysis of the emulsion droplets.

In O/W emulsions, bile salts generally rapidly displace WPI from the interface permitting lipase to adsorb and release FFAs (Maldonado-Valderrama et al., 2008; Sarkar et al., 2010b; Singh and Sarkar, 2011). Such results are in accordance with the sharp decrease in ζ -potential data (< -75 mV) obtained in the first 30 min of the pre-gastric *in vitro* intestinal digestion. In the emulsion microgel particles a limited or delayed lipolysis might have been expected. However, the swelling capacity of the whey protein microgel particles at pH 6.8 might have allowed relatively easy diffusion of trypsin and chymotrypsin into the particles, which would then hydrolyse the whey protein and break up the protein gel network that previously immobilized the droplets. Free emulsion droplets could then diffuse out of the swollen and fragmenting microgel particles into the continuous phase. Lipase and bile salts might also be able to diffuse into the microgel particles to reach the oil-water interface initiating the lipolysis of the emulsion droplets. The bile salts, as well as displacing the interfacial protein, have also been demonstrated to destabilise the tertiary structure of β -lactoglobulin, accelerating its proteolysis by both trypsin and chymotrypsin (Reddy et al., 1988; Gass et al., 2007). This whey protein breakdown might further aid dissolution of the WPI microgel particles and allow lipase to access the emulsion droplet interface, as well as releasing emulsion droplets into the aqueous phase for lipase to hydrolyse.

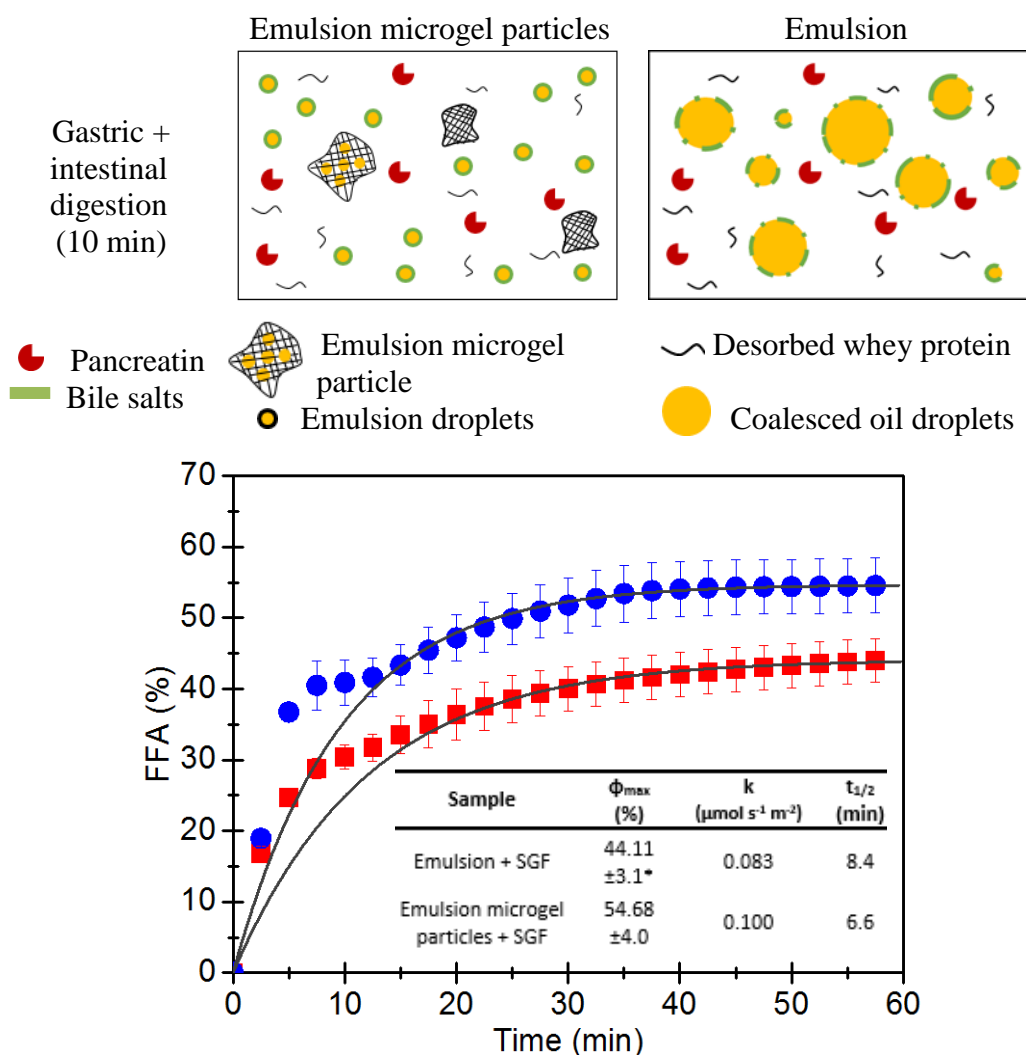


Figure 6.7 Free fatty acid release during *in vitro* intestinal digestion (post-gastric digestion) over time and release schematics of 9.6 wt% WPI stabilised emulsion (■) and 9.6 wt% WPI emulsion microgel particles (●) and mathematical modelling fit (grey line). Maximum free fatty acid release (Φ_{\max} , %), rate constant after 60 min (k , $\mu\text{mol s}^{-1} \text{m}^{-2}$) of *in vitro* intestinal digestion of different samples in the inset table (* mean statistical different at a level of $p < 0.05$)

From Figure 6.7, it is noticeable that the emulsion post-gastric digestion had a significantly lower ($p < 0.05$) release of FFA after 60 min with $\Phi_{\max} = 44.1 \pm 3.1\%$, as compared to the FFA release from emulsion pre-gastric digestion ($\Phi_{\max} = 54.9 \pm 3.7\%$, Appendix D.5). The oil droplet coalescence during the *in vitro* gastric digestion (Figure 6.5) might have affected the FFA release. Without pre-gastric digestion, the emulsion

droplets coming into contact with the simulated intestinal phase had a size ranging from 0.1 to 5 μm , whereas post-gastric digestion these were nearly 10 times larger (compare Figure 6.1 A to 6.5). As mentioned above, the rate of lipolysis is inversely proportional to the oil droplet size, since with larger oil droplets a lower number of triacylglycerol molecules are exposed to lipase (Golding and Wooster, 2010; Mackie et al., 2000; Singh et al., 2009). Additionally, flocculation of WPI during the *in vitro* gastric digestion (as seen in Figure 6.1 A and D), which appeared to form a network of aggregated WPI around the emulsion droplets, might have slightly restrained the diffusion of bile salts and lipase to the oil droplet interface.

In comparison, encapsulating the emulsion droplets into whey protein microgel particles allowed a similar FFA release to the emulsion and emulsion microgel particle pre-gastric digestion (compare Figure 6.7 and Appendix D.5). As observed during the simulated gastric phase, the emulsion droplets seemed to have been protected from any flocculation and/or coalescence. Thus, during the simulated intestinal phase, the swelling and breakdown of the microgel particles through the action of pH, bile salts and proteolysis allows the release of the fine encapsulated emulsion droplets which can be readily hydrolysed. These results suggest that encapsulating the emulsion droplets into whey protein microgel particles protects them from degradation, uncontrolled flocculation and coalescence in the gastric regime, enabling a more complete release of FFA during subsequent intestinal digestion.

6.4 Conclusions

This study has shown that whey protein based emulsion microgel particles have the ability to protect and target the release of emulsion droplets at a desired physiological site. Under *in vitro* gastric conditions (*i.e.*, acidic pH and in the presence of endoprotease (pepsin)), non-encapsulated emulsion droplets were destabilised and coalesced in an uncontrolled manner. In comparison, encapsulating the emulsion droplets into whey protein microgel particles protected the emulsion droplets from flocculation and coalescence. The formation of a network between calcium ions and the carboxylic groups of whey protein possibly protected the aromatic amino acids of the protein from the cleavage by pepsin, hindering the proteolysis of the emulsion microgel particles. Also the tighter network density and henceforth the smaller mesh

size of the microgel particles also possibly prevented the enzyme from diffusing to the surface of the emulsion droplets, limiting pepsinolysis of the interfacial protein. Under *in vitro* intestinal conditions the whey protein microgel particles swelled and disintegrated due to the combined action of pH, bile salts and proteolysis allowing the full release of the free fatty acids from the emulsion droplets. Thus, emulsion microgel particles might also have applications for encapsulation of lipophilic bioactive material that needs stability in the gastric phase but complete release in the intestinal phase.

6.5 References

- Amsden, B. 1998. Solute Diffusion within Hydrogels. Mechanisms and Models. *Macromolecules*. **31**(23), pp.8382-8395.
- Araiza-Calahorra, A. et al. 2018. Recent advances in emulsion-based delivery approaches for curcumin: From encapsulation to bioaccessibility. *Trends in Food Science & Technology*. **71**, pp.155-169.
- Beaulieu, L. et al. 2002. Elaboration and characterization of whey protein beads by an emulsification/cold gelation process: application for the protection of retinol. *Biomacromolecules*. **3**(2), pp.239-248.
- Beysseriat, M. et al. 2006. Preliminary study of the influence of dietary fiber on the properties of oil-in-water emulsions passing through an *in vitro* human digestion model. *Food Hydrocolloids*. **20**(6), pp.800-809.
- Corstens, M.N. et al. 2017. Emulsion-alginate beads designed to control *in vitro* intestinal lipolysis: Towards appetite control. *Journal of Functional Foods*. **34**, pp.319-328.
- Dickinson, E. 2012. Emulsion gels: The structuring of soft solids with protein-stabilized oil droplets. *Food Hydrocolloids*. **28**(1), pp.224-241.
- Dickinson, E. and Chen, J.S. 1999. Heat-Set Whey Protein Emulsion Gels: Role of Active and Inactive Filler Particles. *Journal of Dispersion Science and Technology*. **20**(1-2), pp.197-213.
- Egan, T. et al. 2013. Cold-set whey protein microgels for the stable immobilization of lipids. *Food Hydrocolloids*. **31**(2), pp.317-324.
- Gass, J. et al. 2007. Enhancement of Dietary Protein Digestion by Conjugated Bile Acids. *Gastroenterology*. **133**(1), pp.16-23.

- Golding, M. and Wooster, T.J. 2010. The influence of emulsion structure and stability on lipid digestion. *Current Opinion in Colloid & Interface Science*. **15**(1), pp.90-101.
- Gunasekaran, S. et al. 2007. Use of whey proteins for encapsulation and controlled delivery applications. *Journal of Food Engineering*. **83**(1), pp.31-40.
- Guo, M.R. et al. 1995. Susceptibility of β -Lactoglobulin and Sodium Caseinate to Proteolysis by Pepsin and Trypsin. *Journal of Dairy Science*. **78**(11), pp.2336-2344.
- Guo, Q. et al. 2017. Role of gel structure in controlling in vitro intestinal lipid digestion in whey protein emulsion gels. *Food Hydrocolloids*. **69**, pp.264-272.
- Guo, Q. et al. 2014. Effect of gel structure on the gastric digestion of whey protein emulsion gels. *Soft Matter*. **10**(8), pp.1214-1223.
- Hur, S.J. et al. 2009. Influence of initial emulsifier type on microstructural changes occurring in emulsified lipids during in vitro digestion. *Food Chemistry*. **114**(1), pp.253-262.
- Luo, Q. et al. 2015. Digestion of protein and protein gels in simulated gastric environment. *LWT - Food Science and Technology*. **63**(1), pp.161-168.
- Luo, Q. et al. 2017. Pepsin diffusivity in whey protein gels and its effect on gastric digestion. *Food Hydrocolloids*. **66**, pp.318-325.
- Macierzanka, A. et al. 2009. Emulsification alters simulated gastrointestinal proteolysis of [small beta]-casein and [small beta]-lactoglobulin. *Soft Matter*. **5**(3), pp.538-550.
- Mackie, A. and Macierzanka, A. 2010. Colloidal aspects of protein digestion. *Current Opinion in Colloid & Interface Science*. **15**(1), pp.102-108.
- Mackie, A.R. et al. 2000. Orogenic Displacement of Protein from the Oil/Water Interface. *Langmuir*. **16**(5), pp.2242-2247.
- Maldonado-Valderrama, J. et al. 2008. Interfacial Characterization of β -Lactoglobulin Networks: Displacement by Bile Salts. *Langmuir*. **24**(13), pp.6759-6767.
- Mat, D.J.L. et al. 2016. In vitro digestion of foods using pH-stat and the INFOGEST protocol: Impact of matrix structure on digestion kinetics of macronutrients, proteins and lipids. *Food Research International*. **88**, pp.226-233.
- Matalanis, A. et al. 2012. Inhibition of lipid oxidation by encapsulation of emulsion droplets within hydrogel microspheres. *Food Chemistry*. **132**(2), pp.766-772.

- Matalanis, A. and McClements, D.J. 2013. Hydrogel microspheres for encapsulation of lipophilic components: Optimization of fabrication & performance. *Food Hydrocolloids*. **31**(1), pp.15-25.
- McClements, D.J. 2017. Designing biopolymer microgels to encapsulate, protect and deliver bioactive components: Physicochemical aspects. *Advances in Colloid and Interface Science*. **240**, pp.31-59.
- McClements, D.J. et al. 2008. Controlling Lipid Bioavailability through Physicochemical and Structural Approaches. *Critical Reviews in Food Science and Nutrition*. **49**(1), pp.48-67.
- McClements, D.J. et al. 2007. Emulsion-Based Delivery Systems for Lipophilic Bioactive Components. *Journal of Food Science*. **72**(8), pp.R109-R124.
- Meshulam, D. and Lesmes, U. 2014. Responsiveness of emulsions stabilized by lactoferrin nano-particles to simulated intestinal conditions. *Food & Function*. **5**(1), pp.65-73.
- Minekus, M. et al. 2014. A standardised static in vitro digestion method suitable for food - an international consensus. *Food & Function*. **5**(6), pp.1113-1124.
- Mun, S. et al. 2015. Control of lipid digestion and nutraceutical bioaccessibility using starch-based filled hydrogels: Influence of starch and surfactant type. *Food Hydrocolloids*. **44**, pp.380-389.
- Nacer S, A. et al. 2004. Interactions between β -Lactoglobulin and Pectins during in Vitro Gastric Hydrolysis. *Journal of Agricultural and Food Chemistry*. **52**(2), pp.355-360.
- Ozturk, B. et al. 2015. Formation and stabilization of nanoemulsion-based vitamin E delivery systems using natural biopolymers: Whey protein isolate and gum arabic. *Food Chemistry*. **188**, pp.256-263.
- Reddy, I.M. et al. 1988. Structural and conformational basis of the resistance of β -lactoglobulin to peptic and chymotryptic digestion. *Journal of Agricultural and Food Chemistry*. **36**(4), pp.737-741.
- Sarkar, A. et al. 2018a. Pickering emulsions co-stabilized by composite protein/polysaccharide particle-particle interfaces: Impact on in vitro gastric stability. *Food Hydrocolloids*. **84**, pp.282-291.
- Sarkar, A. et al. 2010a. Properties of oil-in-water emulsions stabilized by β -lactoglobulin in simulated gastric fluid as influenced by ionic strength and presence of mucin. *Food Hydrocolloids*. **24**(5), pp.534-541.

- Sarkar, A. et al. 2009. Behaviour of an oil-in-water emulsion stabilized by β -lactoglobulin in an in vitro gastric model. *Food Hydrocolloids*. **23**(6), pp.1563-1569.
- Sarkar, A. et al. 2010b. Interactions of milk protein-stabilized oil-in-water emulsions with bile salts in a simulated upper intestinal model. *Food Hydrocolloids*. **24**(2), pp.142-151.
- Sarkar, A. et al. 2010c. Pancreatin-induced coalescence of oil-in-water emulsions in an in vitro duodenal model. *International Dairy Journal*. **20**(9), pp.589-597.
- Sarkar, A. et al. 2015a. Impact of Protein Gel Porosity on the Digestion of Lipid Emulsions. *Journal of Agricultural and Food Chemistry*. **63**(40), pp.8829-8837.
- Sarkar, A. et al. 2015b. Impact of Protein Gel Porosity on the Digestion of Lipid Emulsions. *Journal of Agricultural and Food Chemistry*. **63**(40), pp.8829-8837.
- Sarkar, A. et al. 2018b. Composite whey protein–cellulose nanocrystals at oil-water interface: Towards delaying lipid digestion. *Food Hydrocolloids*. **77**, pp.436-444.
- Sarkar, A. et al. 2016a. In vitro digestion of Pickering emulsions stabilized by soft whey protein microgel particles: influence of thermal treatment. *Soft Matter*. **12**(15), pp.3558-3569.
- Sarkar, A. et al. 2016b. On the role of bile salts in the digestion of emulsified lipids. *Food Hydrocolloids*. **60**, pp.77-84.
- Sarkar, A. et al. 2017. Modulating in vitro gastric digestion of emulsions using composite whey protein-cellulose nanocrystal interfaces. *Colloids and Surfaces B: Biointerfaces*. **158**, pp.137-146.
- Singh, H. and Sarkar, A. 2011. Behaviour of protein-stabilised emulsions under various physiological conditions. *Advances in Colloid and Interface Science*. **165**(1), pp.47-57.
- Singh, H. et al. 2009. Structuring food emulsions in the gastrointestinal tract to modify lipid digestion. *Progress in Lipid Research*. **48**(2), pp.92-100.
- Tangsrinugul, N. et al. 2015. Simulated gastrointestinal fate of lipids encapsulated in starch hydrogels: Impact of normal and high amylose corn starch. *Food Research International*. **78**, pp.79-87.

- Torcello-Gomez, A. et al. 2011. Physicochemical properties and digestibility of emulsified lipids in simulated intestinal fluids: influence of interfacial characteristics. *Soft Matter*. **7**(13), pp.6167-6177.
- Torres, O. et al. 2016. Emulsion microgel particles: Novel encapsulation strategy for lipophilic molecules. *Trends in Food Science & Technology*. **55**, pp.98-108.
- Torres, O. et al. 2017a. Design of novel emulsion microgel particles of tuneable size. *Food Hydrocolloids*. **71**, pp.47-59.
- Torres, O. et al. 2018. Emulsion microgel particles as high performance bio-lubricants. *ACS Applied Materials & Interfaces*. **10**(32), pp. 26893-26905
- Torres, O. et al. 2017b. Novel starch based emulsion gels and emulsion microgel particles: Design, structure and rheology. *Carbohydrate Polymers*. **178**, pp.86-94.
- van Leusden, P. et al. 2018. Lipase diffusion in oil-filled, alginate micro- and macrobeads. *Food Hydrocolloids*. **85**, pp.242-247.
- Zhang, Z. et al. 2016. Encapsulation of β -carotene in alginate-based hydrogel beads: Impact on physicochemical stability and bioaccessibility. *Food Hydrocolloids*. **61**, pp.1-10.
- Zhang, Z. et al. 2017. Control of protein digestion under simulated gastrointestinal conditions using biopolymer microgels. *Food Research International*. **100**, pp.86-94.

Chapter 7

General Discussion

7.1 Introduction

The design of novel encapsulation strategies for lipophilic molecules is essential to target and control the delivery of the compound at specific physiological sites. A wide range of encapsulation technologies are available in literature to encapsulate lipophilic compounds ranging from conventional emulsions, liposomes, vesicles and other various nanostructures. Based on the perceived knowledge gap from the literature (**Chapter 2**), a novel encapsulation strategy was developed in this thesis, which targets the delivery of lipophilic molecules. This strategy involves engineering smart particles that can alter their network structure, swelling behaviour, permeability or mechanical strength in response to internal physiological stimuli (*e.g.*, change in pH, ionic strength, temperature, mechanical shear, enzymatic action, etc.).

The specific aim of this thesis was to engineer novel soft emulsion microgel particles with controlled release properties at specific physiological sites, such as oral or gastrointestinal (Figure 7.1), by unravelling the interactions between emulsion droplets (*i.e.*, filler) and the encapsulation material (*i.e.*, the matrix particle). Two particles were developed: starch emulsion microgel particles via a top-down approach and heat-treated whey protein emulsion microgel particles via bottom-up approach. The unique design of these emulsion microgel particles, developed in this PhD, was that both the emulsifying agent and the matrix material were composed of the same biopolymer without the need of additional hydrocolloids. In other words, in the case of whey protein emulsion microgel particle, whey protein was used as the emulsifying agent for the oil droplets as well as the gel matrix forming the microgel particle, which also holds true for the starch emulsion microgel particles.

In view of the above, the oil content, particle size, filler to matrix ratio and matrix polymer properties were taken into account in the design principles to create

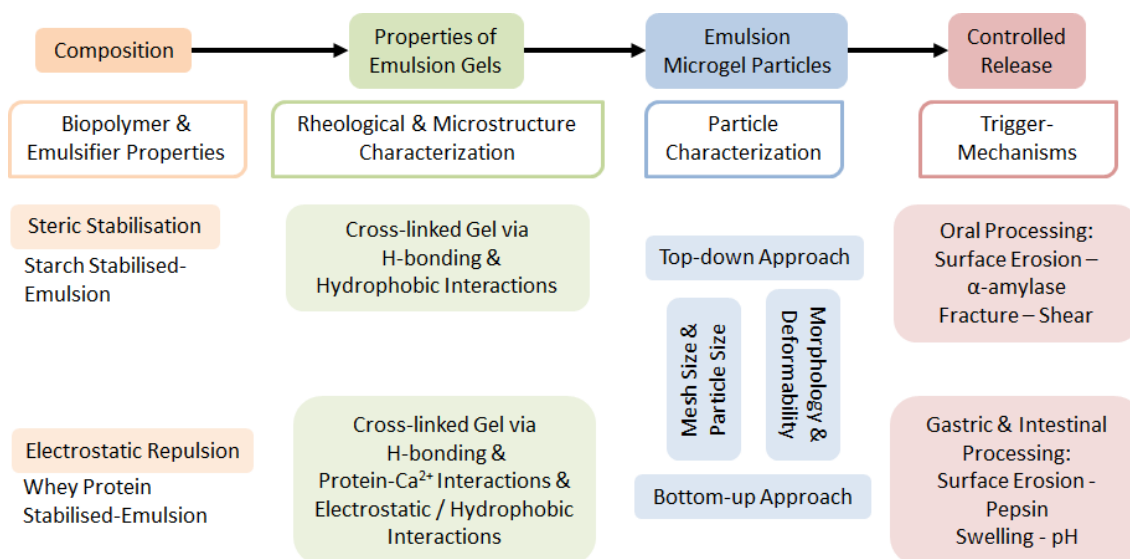


Figure 7.1 Approach of the thesis: linking polymer and emulsifier properties to control the release of nutrient during oral or gastrointestinal processing.

particles with tuneable characteristics. More specifically the rheological properties and microstructural breakdown behaviour of the model emulsion gels were first analysed. The interactions between the filler and the gel matrix were identified to understand if the emulsion droplets acted as ‘active fillers’ inside the gel (**Chapter 3 and 4**). By analysing the nature of two specific polymer networks (*i.e.*, starch gel or whey protein gel) and the interactions between the filler and the matrix, two different approaches (top-down or bottom-up) were used to design emulsion microgel particles. These emulsion microgel particles were then subjected to different environmental stresses, such as acidic pH, enzyme activity (amylase for oral relevance, pepsin or trypsin for gastrointestinal relevance) and mechanical shear (**Chapter 5 and 6**), to examine their response mechanisms.

In this general discussion, we first discuss the key findings obtained from the rheological and physicochemical properties of the two different emulsion gels (whey protein or starch). Their properties are then associated to the different design routes developed in this work. The characterization of the different emulsion microgel particles (starch versus whey protein emulsion microgel particles) are then discussed to highlight their microstructural distinctiveness and differences in responses to physiological conditions. Finally, the implications of the current findings are discussed as well as the recommendations for future work.

7.2 Summary of the main results

7.2.1 At the emulsion level: Comparison between OSA starch and whey protein

Table 7.1 summarizes the characteristics of both OSA starch stabilised-emulsions (**Chapter 3**) and heat-treated whey protein stabilised emulsions (**Chapter 4**). From a droplet size point of view, emulsification with either OSA starch or whey protein led to different sized emulsion droplets ($p < 0.05$).

Whey protein was first heat treated causing the protein to unfold and expose its hydrophobic and sulfhydryl groups to the aqueous phase. This step was necessary to allow the following cold set ionic gelation of whey protein as discussed in **Chapter 1**. Upon homogenization of the oil with heat-treated WPI, the protein will further unfold and change conformation to increase the number of contact points with the interface and decrease the interfacial tension of the oil droplets.

Similarly, OSA starch can adsorb to the O/W interface due to the presence of hydrophobic OSA groups. However from previous studies, WPI was demonstrated to be more surface active than OSA starch. In fact, heat-treated WPI was shown to reduce the interfacial tension of oil droplets to around 12 mN m^{-1} , whereas OSA starch could only lower the interfacial tension to around 22 mN m^{-1} (Schröder et al., 2017; Tesch et al., 2002; Ali et al., 2018). This difference in surface activity might be attributed to the large molecular size of OSA starch ($10^6 - 10^8 \text{ Da}$, as compared to β -lactoglobulin which is $1.84 \cdot 10^4 \text{ Da}$), which might limit the number of contact points between OSA starch and the O/W interface (Schröder et al., 2017; Dickinson, 2017).

Table 7.1 Sauter mean diameter (d_{32}) and ζ -potential at pH 7, columns with symbol (*) are significantly different ($p < 0.05$).

Emulsifier	Emulsion characteristics			
	Oil content (wt%)	d_{32} (μm)	d_{43} (μm)	ζ -potential (mV)
4 wt% OSA starch	40	0.15 ± 0.005 *	0.61 ± 0.11 *	0.1 ± 0.1 *
9.6 wt% Whey protein (heat-treated)	20	0.08 ± 0.001 *	0.36 ± 0.01 *	- 41.9 ± 2.4 *

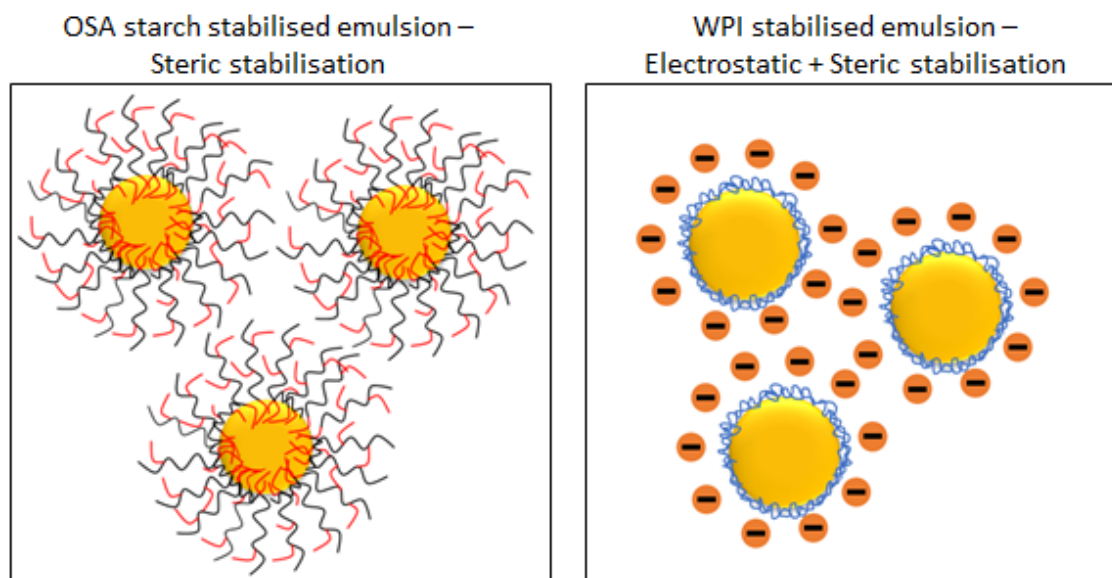


Figure 7.2 Schematic representation of emulsion droplets (denoted by yellow circles) stabilization mechanisms as a function of the emulsifiers, OSA starch with hydrophobic OSA groups in red (left) and WPI (blue) (right) at pH 7.

In the case of the ζ -potential of both types of emulsion droplets, drastic differences ($p < 0.05$) were observed (Table 7.1). The OSA starch emulsion had no net surface charge since OSA starch itself is only marginally charged as compared to WPI, the latter imparted a large negative surface charge to the emulsion droplets at pH 7. This major difference between the two emulsifiers shed light on their stabilization mechanisms. Previous studies have shown that OSA starch forms a thick layer at the O/W interface, providing the emulsion droplets with steric stabilisation, as compared to WPI, which mainly stabilizes the emulsion droplets through electrostatic repulsion (Figure 7.2) (Ettelaie et al., 2016). The steric repulsion conveyed by the OSA starch might provide several advantages to protect the emulsion droplets from destabilisation during changes in environmental conditions such as pH, temperature and ionic strength (Dickinson, 2017).

7.2.2 At the emulsion gel level: Comparison between OSA starch and whey protein emulsion gels

The design of emulsion microgel particles relies on a strong understanding of the interplay between the biopolymer matrix and emulsified droplets, such as the

concentration of biopolymer and emulsifier, the oil content, the gelation kinetics and the emulsion gel mechanical behaviour. An essential aspect of the formation of these particles is the understanding of the behaviour of the parent emulsion gel and therefore, the interactions between the emulsion droplets (or fillers) and the gel matrix. Fillers have been classed as either ‘active’ or ‘inactive’ depending on their interactions with the gel matrix (**Chapter 2**). Upon small deformation, if the elastic modulus (G') of a filled gel or emulsion gel is greater than the G' of the corresponding gel without the filler, then the filler can be considered as bound to the gel matrix, as it reinforces the gel matrix network (Dickinson, 2012; Dickinson and Chen, 1999). Active fillers are crucial in the production of emulsion microgel particles to avoid emulsion droplets from leaching out of the particles during processing whilst also allowing their targeted release at specific physiological sites depending on a change in pH, ionic strength, temperature and enzymatic activity. Therefore, before designing emulsion microgel particles, a thorough understanding of the structure of the polymer matrix and its interactions with the filler in an emulsion gel is a necessary undertaking.

The first biopolymer considered for the formation of emulsion microgel particles, in this thesis was starch (**Chapter 3**). An emulsion gel was formed by mixing sheared native starch and OSA starch stabilised-emulsion and leaving the system to gelatinize for 2 h at 4 °C. Its rheological behaviour over different variables, such as the oil and the starch polymer matrix concentration, was analysed experimentally and theoretically.

Table 7.2 summarizes the influence of oil and starch concentration on the small deformation properties of starch emulsion gels. The mesh size of starch gels were derived from the rubber elasticity theory modified by Flory (Flory, 1953) (Equation 7.1):

$$\xi^3 = \frac{\kappa_B T}{G'_m} \quad (7.1)$$

where κ_B is the Boltzmann constant, T is the temperature and G'_m the storage modulus of the starch gel. However, in the case of the emulsion gel, the contribution of the emulsion droplets to the starch gel modulus (G'_m) and phase angle ($\tan \delta_m$) need to be taken into account for a better estimation of the mesh size (ξ) of the emulsion gel. This was achieved by using the Palierne model, which takes into account the interfacial

tension, oil droplet size and oil content of the emulsion (Palierne, 1990; Palierne, 1991) (Equation 7.2):

$$G_b^*(\omega) = G_m^*(\omega) \frac{1+3\phi H(\omega)}{1-2\phi H(\omega)} \quad (7.2)$$

$$\text{where } H(\omega) = \frac{4(\gamma/R)[2G_m^*(\omega)+5G_f^*(\omega)]+[G_f^*(\omega)-G_m^*(\omega)][16G_m^*(\omega)+19G_f^*(\omega)]}{40(\gamma/R)[G_m^*(\omega)+G_f^*(\omega)]+[2G_f^*(\omega)+3G_m^*(\omega)][16G_m^*(\omega)+19G_f^*(\omega)]}$$

with, ϕ the concentration of oil, R the average radius of the emulsion droplets, γ the interfacial tension of the OSA starch, ω the frequency, G_m^* , G_f^* and G_b^* the complex shear moduli of the matrix, the emulsion droplets and the emulsion gel, respectively (Bousmina, 1999).

From an experimental analysis, the incorporation of an increased amount of emulsion droplets into the starch gel increased the elastic modulus of the emulsion gels (G'_b). For instance, the addition of 15 wt% oil in the 15 wt% starch gel led to a 75% increase in G'_b . Hence, the emulsion droplets acted as active fillers in the starch gel, probably due to the physical entanglement between both starches (*i.e.*, OSA starch and native starch), reinforcing the gel matrix (Dickinson and Chen, 1999). Several interactions were attributed to this filler-matrix association (Figure 7.3): OSA groups on the modified starch might have interacted with one another via hydrophobic interactions and adjacent native and/or OSA starch molecules might have formed hydrogen bonds (Bhosale and Singhal, 2006; Sweedman et al., 2013; Ortega-Ojeda et al., 2005).

Based on the estimated values, incorporating a low concentration of oil (5 to 10 wt%) reinforced the starch gel elastic modulus (the oil droplets were estimated to reinforce G'_m by 35%) and decreased the mesh size (from 18.6 nm to 16.3 or 14.4 nm with 5 or 10 wt% oil, respectively), confirming the 'active' influence of the emulsion droplets (Table 7.2). However, at higher concentrations of oil (15 to 20 wt%), the reinforcement of the oil droplets to G'_m was less which was highlighted by the constant $\tan \delta_m$ at increasing oil content ($\tan \delta_m = 12$ for both 15 and 20 wt% oil – 15 wt% starch emulsion gels). At high oil content, the emulsion droplet might have taken up too much space in the starch gel matrix, limiting the entanglement of the polymer chains, which reduced the reinforcement effect of the oil droplets (Sala et al., 2009b). The reduced physical entanglement of the starch molecules might allow the

Table 7.2 Final experimental elastic modulus (G'_b), phase angle ($\tan \delta$), limiting deformation value ($\dot{\gamma}_L$) of the emulsion gel containing different starch and oil concentrations, and estimated elastic modulus (G'_m) and phase angle ($\tan \delta_m$) of the starch gel matrix and derivative mesh size (ξ), columns containing symbol (*) are significantly different ($p < 0.05$) to their corresponding starch gel (15 or 20 wt%) without oil droplets, in the same column.

Gel Composition		Experimental values				Estimated theoretical values		Derivative values
Starch (wt%)	Oil (wt%)	G'_b (kPa)	$\tan \delta$	$\dot{\gamma}_L$ %	G'_m (kPa)	$\tan \delta_m$	ξ (nm)	
15	0	0.64 ±0.06	0.17	10.0 ±3.2			18.6	
	5	1.05 ±0.15	0.17	10.0 ±2.7	0.99	0.17	16.3	
	10	1.60 ±0.10*	0.14	10.0 ±4.6	1.44	0.14	14.4	
	15	2.33 ±0.03*	0.12	31.7 ±7.4*	1.99	0.12	12.9	
	20	2.83 ±0.13*	0.11	31.8 ±3.7*	2.29	0.12	11.7	
20	0	1.59 ±0.25	0.23	3.2 ±0.9			13.7	
	5	2.84 ±0.26*	0.10	25.2 ±6.3*	2.69	0.10	11.7	
	10	3.39 ±0.27*	0.10	25.3 ±2.9*	3.05	0.09	11.2	
	15	3.40 ±0.27*	0.10	32.1 ±0.1*	2.90	0.10	11.4	
	20	4.84 ±0.27*	0.10	31.5 ±3.7*	3.94	0.10	10.3	

emulsion droplets to leach out of the emulsion gel more easily during further processing. Therefore, 20 wt% oil starch-based emulsion microgel particles were not considered for the formation of emulsion microgel particles.

The second biopolymer considered to form emulsion microgel particles was whey protein (**Chapter 4**). In this case, an emulsion gel was first formed by mixing heat-treated whey protein stabilised emulsion in presence of variable concentrations of Ca^{2+} , which led to the spontaneous gelation of whey protein. Table 7.3 summarizes the influence of the oil content and Ca^{2+} concentration on the small deformation properties of the whey protein emulsion gels obtained experimentally and theoretically from Equations 7.1 and 7.2. Experimentally, the incorporation of emulsion droplets led to a significant increase of G'_b as well as a reduction of $\tan \delta$, in almost all emulsion gels. Therefore, the emulsion droplets acted as active fillers in the whey protein gel (Sala et al., 2009a). The heat-treat whey protein in the continuous phase cross-linked with adjacent protein dispersed in the aqueous phase and/or adsorbed at the O/W interface through several chemical interactions: electrostatic attraction between the

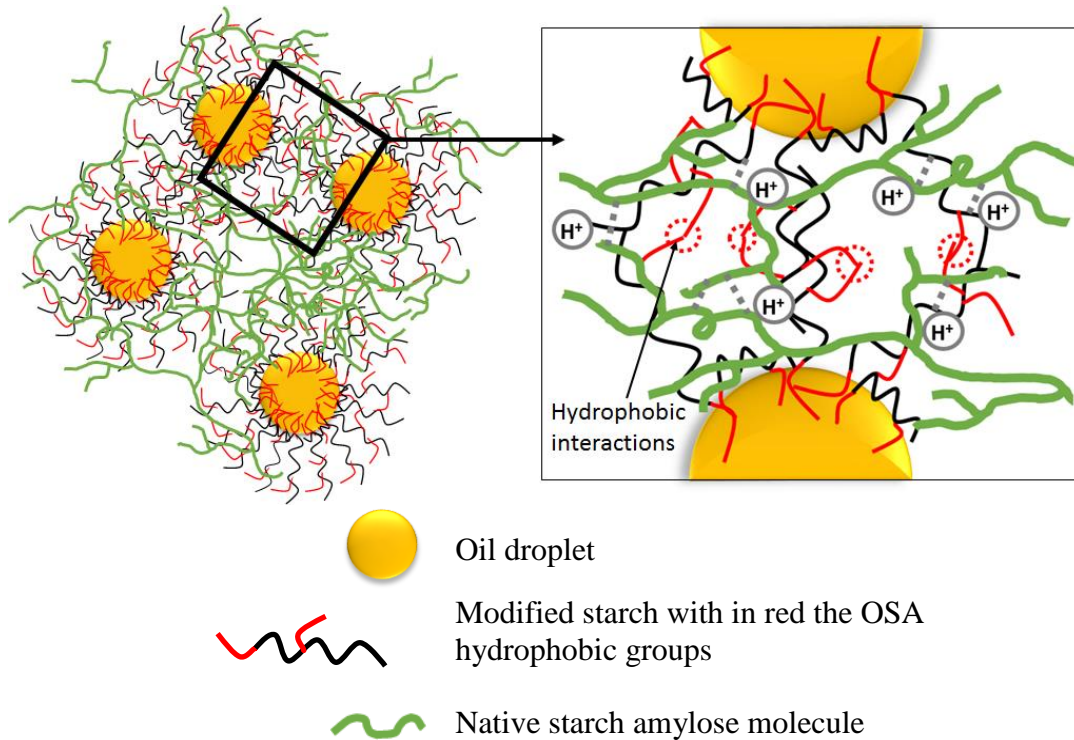


Figure 7.3 Schematic representation of starch-based emulsion gel with zooming in the region of interactions between OSA starch molecules and native starch molecules.

protein molecules due to Ca^{2+} ions screening the surface charge of the protein; ionic interactions via Ca^{2+} bridges between two carboxyl groups on the protein; hydrogen and sulfhydryl bonding between the protein molecules. Physical hydrophobic interactions would have also occurred (Figure 7.4).

Therefore, the concentration of Ca^{2+} will have an important effect on the structure and mechanical behaviour of the gels. To further understand how the concentration of Ca^{2+} affected the cross-linking of the whey protein gels and emulsion gels, the Palierne model (Equation 7.2) was used to estimate G'_m and the mesh size of the emulsion gels. At low concentration of Ca^{2+} (0.02 M), although G'_m increased as compared to G'_b without oil droplets, $\tan \delta$ stayed constant. In this case, the low addition of Ca^{2+} might have only allowed screening of the charge of the protein, causing cross-linking of the protein via electrostatic interactions without the formation of Ca^{2+} bridges (Hongprabhas et al., 1999). Hence, upon incorporation of the emulsion droplets, G'_b increases mainly due to the influence of the large elastic modulus of the emulsion droplets ($G'_f \sim 6 \text{ MPa}$) (Sok et al., 2005).

Table 7.3 Final experimental elastic modulus (G'_b), phase angle ($\tan \delta$), limiting deformation value ($\dot{\gamma}_L$) of the whey protein emulsion gel prepared at different Ca^{2+} concentrations without or with 20 wt% oil, and estimated elastic modulus (G'_m) and phase angle ($\tan \delta_m$) of the whey protein gel matrix and derivative mesh size (ξ), columns containing symbol (*) are significantly different ($p < 0.05$) to their corresponding whey protein gel without oil droplets.

Gel Composition		Experimental values				Estimated theoretical values		Derivative values
[Ca^{2+}] (M)	Oil (wt%)	G'_b (kPa)	$\tan \delta$	$\dot{\gamma}_L$ %	G'_m (kPa)	$\tan \delta_m$	ξ (nm)	
0.02	0	3.64 ±0.98	0.15	12.6 ±1.9			10.4	
	20	8.76 ±1.62	0.15	6.3 ±4.4*	7.17	0.15	8.4	
0.1	0	0.28 ±0.12	0.21	1.0 ±0.3			24.5	
	20	18.24 ±3.65*	0.14	3.2 ±1.5	15.17	0.15	6.6	
1	0	3.12 ±1.05	0.19	10.1 ±1.5			11.0	
	20	10.63 ±0.31*	0.18	6.3 ±0.0*	8.73	0.17	7.9	
1.4	0	8.12 ±2.86	0.20	5.0 ±1.4			8.0	
	20	5.74 ±2.48	0.20	3.2 ±1.6	4.67	0.20	9.7	

As the concentration of Ca^{2+} is increased (0.1 M) the formation of Ca^{2+} bridges between the protein molecules are more likely to occur increasing the cross-linking and the network density, causing an increase in G'_m and a decrease in the mesh size. The further increase in the concentration of Ca^{2+} (1 M), did not increase the elastic modulus of the gels further, possibly due to the formation of large protein aggregates caused by the excess of Ca^{2+} . The protein aggregates might disrupt the gel network weakening the network. The weakening effect with an excess of Ca^{2+} was further confirmed at 1.4 M. In this case, although the protein gel had the highest G'_b (8.1 kPa), the incorporation of the emulsion droplets led to the collapse of the gel network with $G'_m < G'_b$. The large excess of Ca^{2+} would increase the flocculation and aggregation of whey protein probably leading to a heterogeneous gel with clusters of highly cross-linked protein weakly bound together and expelling the aqueous phase (Hongprabhas et al., 1999). Therefore, upon addition of emulsion droplets, some emulsion droplets might be included in the protein clusters whilst some might be found in the expelled aqueous phase and hence weaken the emulsion gel network (Sok et al., 2005).

The different interactions between the filler and the matrix of the different emulsion gels (*i.e.*, starch or whey protein) might explain their differences in elastic modulus, limiting deformation values and theoretical mesh size. The WPI-based

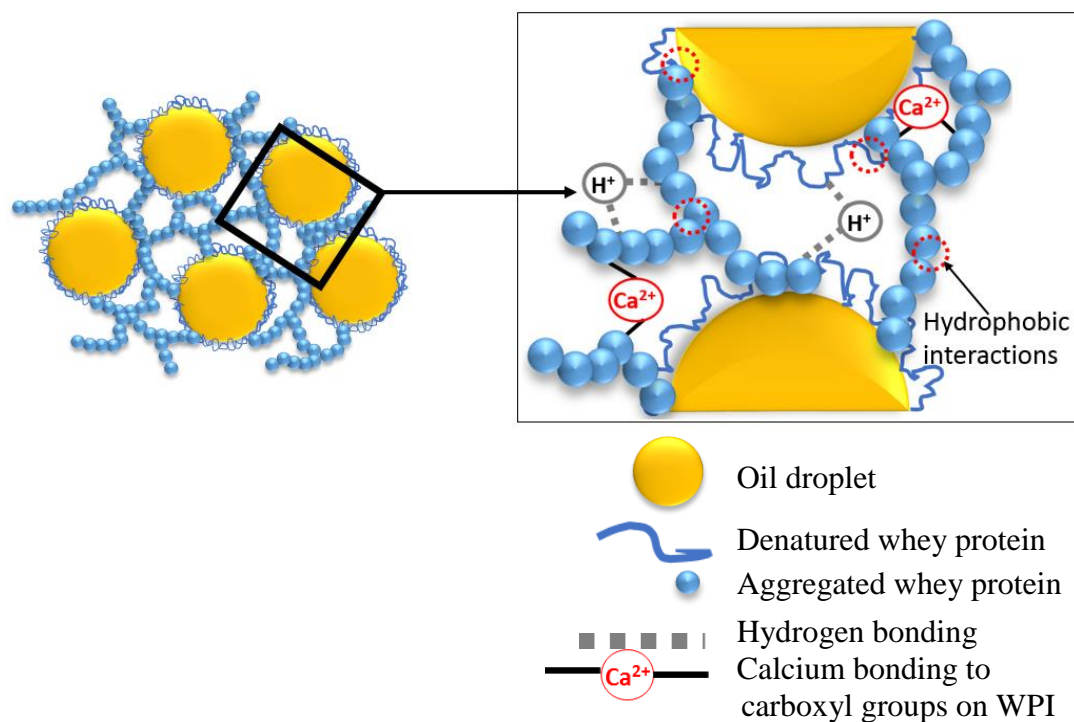


Figure 7.4 Schematic representation of whey protein-based emulsion gel with zoom in the region of interactions between WPI molecules and Ca^{2+} .

emulsion gels had an elastic modulus at least twice as large as the elastic modulus of the starch-based emulsion gel at the same oil content (20 wt%), although the concentration of biopolymer was larger in the starch-based emulsion (see Table 7.2 and Table 7.3). The presence of electrostatic interactions in the WPI emulsion gel might explain the stronger filler-matrix interactions and consequently, the larger elastic modulus. Interestingly though, the experimental and theoretical phase angle of the WPI emulsion gels was higher than the phase angle for the starch emulsion gels at the same oil content. The higher biopolymer concentration in the starch emulsion gel (15 wt% starch as compared to 9.6 wt% WPI) would have allowed a higher degree of cross-linking of the starch molecules *via* hydrogen bonding, resulting in a denser gel network as compared to the WPI emulsion gels.

Under mechanical strain, the different interactions might also explain the differences in limiting deformation values between both types of emulsion gels. The larger elastic modulus of WPI gels and corresponding emulsion gels, due to electrostatic interactions, led to a higher brittleness of the gels (Table 7.3). In comparison, starch gels and corresponding emulsion gels were more flexible (Table 7.2), probably due to the dynamic physical cross-linked network produced by the

entanglement of starch molecules that are able to adsorb the energy applied during shearing and rearrange under deformation rather than break (Xu et al., 2018).

Nevertheless, in both emulsion gels, the incorporated emulsion droplets ($d_{32} \sim 0.1 \mu\text{m}$) behaved as ‘active fillers’ reinforcing the matrices. The different gelation kinetics, cross-linking properties and behaviour of the emulsion gel under small deformation allowed one to examine two different approaches to design the emulsion microgel particles.

7.2.3 At the emulsion microgel particles level: Top-down (starch emulsion microgel particle) versus bottom-up (whey protein emulsion microgel particle) formation

The formation of starch-based emulsion microgel particles relied on the top-down approach (**Chapter 3**) due to the slow gelation kinetics but large limiting deformation values of starch gels (Figure 7.5). After gelatinization of the emulsion gel, the system was passed twice through a high pressure homogenizer causing the gel to break down into particles. The concentration of starch (15 – 20 wt%) and emulsion droplets (5 – 15 wt%) barely influenced the emulsion microgel particles size, which in average was around $24 \pm 0.5 \mu\text{m}$. An interesting observation can be made in the size difference obtained for the emulsion microgel particles in **Chapter 3** as compared to the ones in **Chapter 5**. In **Chapter 3**, the emulsion microgel particle size was below $10 \mu\text{m}$ (except for emulsion particles produced with 20 wt% starch and 15 wt% oil), whereas in **Chapter 5** the emulsion microgel particle size was above $10 \mu\text{m}$. This increase might be due to storage, as in **Chapter 3** the particles size was measured 24 h after the production of the emulsion microgel particles, whereas in **Chapter 5**, particles were made in bulk and stored in the fridge for 3 weeks during which different experiments were conducted. Hence, during storage the emulsion microgel particles might have aggregated leading to an increase in size.

In comparison, as heat-treated whey protein emulsion (9.6 wt% WPI – 20 wt% oil) gelled spontaneously with the addition of Ca^{2+} , a bottom up approach was explored (Figure 7.5). In order to optimize the design of whey protein-based emulsion microgel

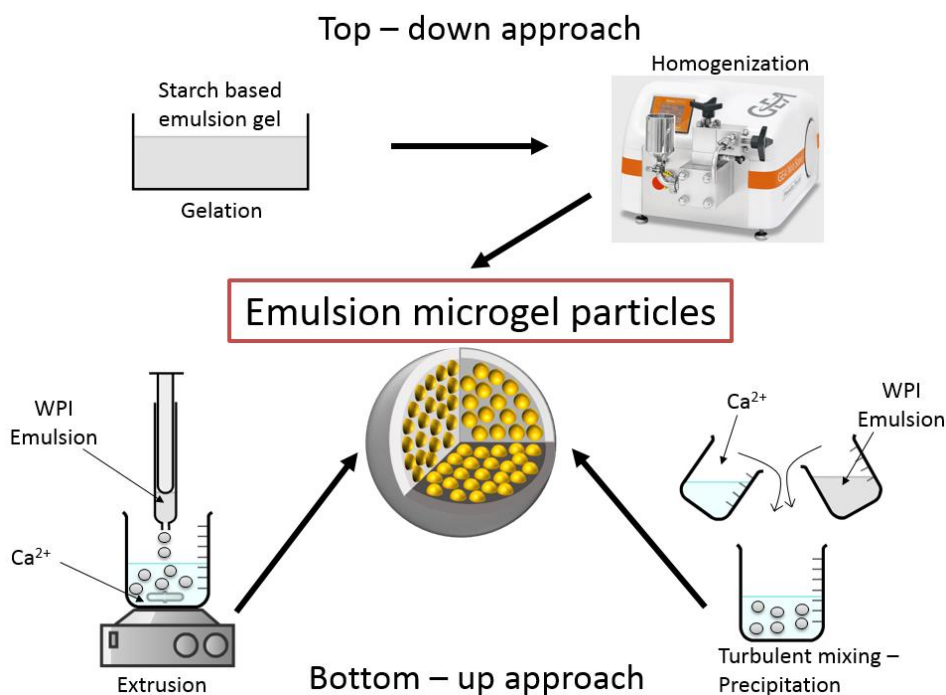


Figure 7.5 Schematic representation of the top-down and bottom-up techniques used to produce starch- or whey protein-based emulsion microgel particles, respectively.

particles, two bottom-up approaches (extrusion versus precipitation) were investigated using different concentrations of Ca^{2+} (**Chapter 4**). The different processing routes led to the creation of emulsion microgel particles of different sizes. Large particles ($\sim 900 \mu\text{m}$) were produced via the extrusion process due to a slow mixing time and Ca^{2+} flux (Table 7.4). Small particles ($\sim 15 \mu\text{m}$) were formed *via* the turbulent mixing (precipitation) technique due to a faster mixing time and Ca^{2+} flux (Table 7.4). Particles above $50 \mu\text{m}$ are reported to be detected during oral consumption (Egan et al., 2013; McClements, 2017), therefore, only small particles produced by turbulent mixing were further investigated (**Chapter 6**).

Additionally, the concentration of Ca^{2+} affected the flux, size and mesh size of the emulsion microgel particles. At 0.02 M Ca^{2+} , the emulsion microgel particles were polydisperse (with a majority of the particles being in the range of 100 to $4000 \mu\text{m}$), probably due to the low diffusive flux of Ca^{2+} as well as the low Ca^{2+} concentration which might cause bridging flocculation (Table 7.4).

Table 7.4 Summary of mixing time (t_{mix}), diffusive molecular flux of Ca^{2+} (J) and whey protein-based emulsion microgel particle size (d_{32}) as function of the different processing routes and Ca^{2+} concentrations.

Parameters	Turbulent mixing (Precipitation) technique		Extrusion technique	
	t_{mix} (s)	1.2 10^{-5}		4.3 10^{-2}
[Ca^{2+}] (M)	0.02	0.1	1.0	1.4
J (mol $m^{-2} s^{-1}$)	1.6 10^{-4}	7.8 10^{-4}	1.6 10^{-5}	2.3 10^{-5}
d_{32} (μm)	14.5	12.4	900	1200

At 0.1 M Ca^{2+} , the diffusive molar flux of Ca^{2+} was an order of magnitude faster. Although the size distribution of the emulsion microgel particles was bimodal due to aggregated particles, the size of the majority of the emulsion microgel particles were found in between 2 to 50 μm , suggesting that less particles were aggregated. Only particles formed at 0.1 M Ca^{2+} were further investigated to understand the protection and release mechanism of whey protein-based emulsion microgel particles under *in vitro* gastric and subsequent intestinal digestion (**Chapter 6**).

Therefore, emulsion droplets actively bound to gel matrix have the ability to form emulsion microgel particles. Both processing techniques (i.e., top-down and bottom-up) produced micron sized emulsion microgel particles although the physicochemical properties of the particles differed. For instance, the top-down approach produces soft particles ($G' < 10$ kPa), as strong blocks of gel might have blocked the high-pressure homogenizer. Additionally, although the different approaches formed similar sized particles, their morphology also differed. The precipitation technique produced “nearly spherical” emulsion microgel particles due to the fast mixing time and a high flow rate. In comparison, the top-down approach produced aggregated emulsion microgel particles. Under shear the emulsion gel would randomly break adjacent to emulsion droplets, which could result in aggregated emulsion droplets entrapped into a starch gel particle (Dickinson, 2012; Langley and Green, 1989).

7.2.4 Breakdown properties of starch- versus whey protein-based emulsion microgel particles during *in vitro* processing

In this thesis, the protective behaviour of the previously designed emulsion microgel particles was studied in order to examine the potential targeted release of the

encapsulated oil under either *in vitro* oral or gastrointestinal processing. By selecting appropriate biopolymers and understanding the interactions between the biopolymer matrix and the emulsion droplets as well as the small deformation properties of the emulsion microgel particles, different trigger mechanisms were observed as summarized in Table 7.5.

In vitro oral processing was studied using a ball-on-disc tribometer, to mimic oral shear using artificial saliva containing α -amylase. Starch-based emulsion microgel particles were investigated due to their known responsiveness to α -amylase (Witt et al., 2010; Reilly, 2007). The rationale behind designing emulsion microgel particles from starch was to protect emulsion droplets from destabilisation whilst still providing lubrication during oral processing. With this in mind, these particles should release a few emulsion droplets to lubricate the oral cavity although the majority of the emulsion droplets should remain encapsulated within the particles.

In contrast, *in vitro* gastrointestinal processing was examined using a static digestion model (Minekus et al., 2014), which included the gastric and intestinal phase, with pepsin at pH 3 and pancreatin (containing lipase, trypsin and chymotrypsin) and bile salts at pH 6.8, respectively. In this case the whey protein-based emulsion microgel particles were investigated due to the known resistance of WPI to pepsin and swelling at intestinal pH. The mechanical shearing effect of the stomach was not studied as relatively low peristaltic velocity (2.5 mm s^{-1}) and low force per concentration (0.2 N) were not sufficient enough to fracture the whey protein-based emulsion microgel particles (Kong and Singh, 2008). At these low shear conditions whey protein-based emulsion microgel particles were not anticipated to fracture. The

Table 7.5 Summary of the physiological-specific trigger mechanisms in relation to the biopolymer used to engineer the emulsion microgel particles

Trigger mechanisms	Starch-based emulsion microgel particles	WPI-based emulsion microgel particles
Enzyme-trigger (Chapter 5 & 6)	Surface erosion of the particles by α -amylase	Surface erosion of the particles by pepsin and proteolysis by trypsin
Mechanical shear-trigger (Chapter 5)	Fracture during oral shear	No fracture during gastric motility
pH-trigger (Chapter 6)	None	Swelling

oral phase was also excluded in the case of the protein-based emulsion microgels since enzymatic hydrolysis is only relevant in the oral phase for starch-based systems due to the presence of α -amylase, which hydrolyses α -(1 \rightarrow 4) glycosidic bonds (Reilly, 2007). The whey protein-based emulsion microgel particles were produced to protect the emulsion droplets from destabilisation during gastric processing to optimize their release during intestinal digestion. In this case, the particles should be resistant to gastric enzymes, pH and ionic strength but receptive to intestinal enzymes, pH and ionic strength.

7.2.4.1 Matrix surface erosion (enzyme-triggered mechanism)

The first trigger mechanism examined in both emulsion microgel particles was the action of specific oral or gastrointestinal enzymes. During oral processing, α -amylase is the main digestive enzyme found in saliva, involved in the hydrolysis of starch. From **Chapter 5**, α -amylase eroded the surface of the starch-based emulsion microgel as well as broke down the particles allowing the release of a few stable emulsion droplets in the continuous phase. The large estimated mesh size of the starch emulsion microgel particles (> 15 nm) might have also allowed some α -amylase (hydrodynamic radius around 3 to 4 nm and $M_w \sim 54$ kDa (Dhital et al., 2017; Cozzzone et al., 1970)) to diffuse into the physically entangled particles hydrolysing the particles from the inside-out. Interestingly, no oil coalescence was visible microscopically or macroscopically confirming that the emulsion droplets were still protected from destabilization during oral processing. The high starch content forming the matrix might have saturated the enzyme activity preventing α -amylase from digesting the OSA starch adsorbed at the O/W interface.

In comparison, during gastric processing, the surface of WPI-based emulsion microgel particles seemed to be slightly eroded by pepsin (although 85% of whey protein remained intact after *in vitro* gastric digestion, from SDS-PAGE results) and the particle size distribution barely changed (**Chapter 6**). In this case the chemical interactions (electrostatic interactions and Ca^{2+} bridges) binding the WPI molecules together might have protected the WPI from pepsinolysis either by limiting its cleavage to the active site or by restricting the diffusion of pepsin due to the estimated smaller mesh size of the particles. The pore size of the WPI emulsion microgel particles (6.5 nm at 0.1 M Ca^{2+}) might have not permitted pepsin (hydrodynamic radius around 2.3 nm (Amsden, 1998)) to diffuse into the particles. However, on entering the

intestinal phase, the dual action of trypsin and chymotrypsin (with the help of bile salts) readily hydrolysed the whey protein (specifically beta-lactoglobulin) disintegrating the emulsion microgel particles.

7.2.4.2 Fracture of the particles – mechanical shear-trigger mechanism (only relevant for starch particles)

Mechanical shear was another important trigger mechanism that starch-based emulsion microgel particles had to respond to during oral processing. In order to study the emulsion microgel particles' responsiveness to shear, the mechanical behaviour of the particles was analysed *via* tribology in the absence and presence of α -amylase.

As the main interest of this study was to understand the behaviour of the emulsion microgel particles during oral processing, an emphasis was placed on the friction force of the different samples at two low entrainment speed relevant to oral processing 3 and 50 mm s⁻¹ (Stokes et al., 2013). From Figure 7.6, it is noticeable that starch particles without oil droplets have significantly larger friction force than the emulsion microgel particles. Whilst, the incorporation of emulsion droplets led to the decrease of the friction force similar to values of O/W emulsion and sunflower oil (at both 3 and 50 mm s⁻¹). The small size of the emulsion droplets (0.08 μ m of radius) combined with the interfacial tension of OSA starch produces highly stiff emulsion droplets ($G' \sim 5.5$ MPa). Hence, under a load of 2 N, the emulsion droplets would be able to support the load whilst being compressed and entering the asperities of the PDMS, which reduces the friction force to values similar to that of sunflower oil.

In comparison, the soft starch microgel particles ($G' \sim 0.7$ kPa) were not strong enough to support the 2 N load and fractured under mechanical shear leading to a higher friction force. The slightly stiffer emulsion microgel particles ($G' > 1$ kPa) were able to support some of the load reducing the friction force. The smaller limiting deformation value of the starch particles as compared to the emulsion microgel particles, which was particularly noticeable at high starch concentration ($\dot{\gamma}_L < 5\%$ for starch particles, $\dot{\gamma}_L > 25\%$ for emulsion microgel particles, Table 7.2) confirmed that the starch particles would fracture more easily under shear as compared to the emulsion microgel particles. The latter will be able to deform and absorb the energy applied to them. The emulsion droplets, physically bound to the starch polymer matrix, would be the primary cause to the resistance of the emulsion microgel particles against

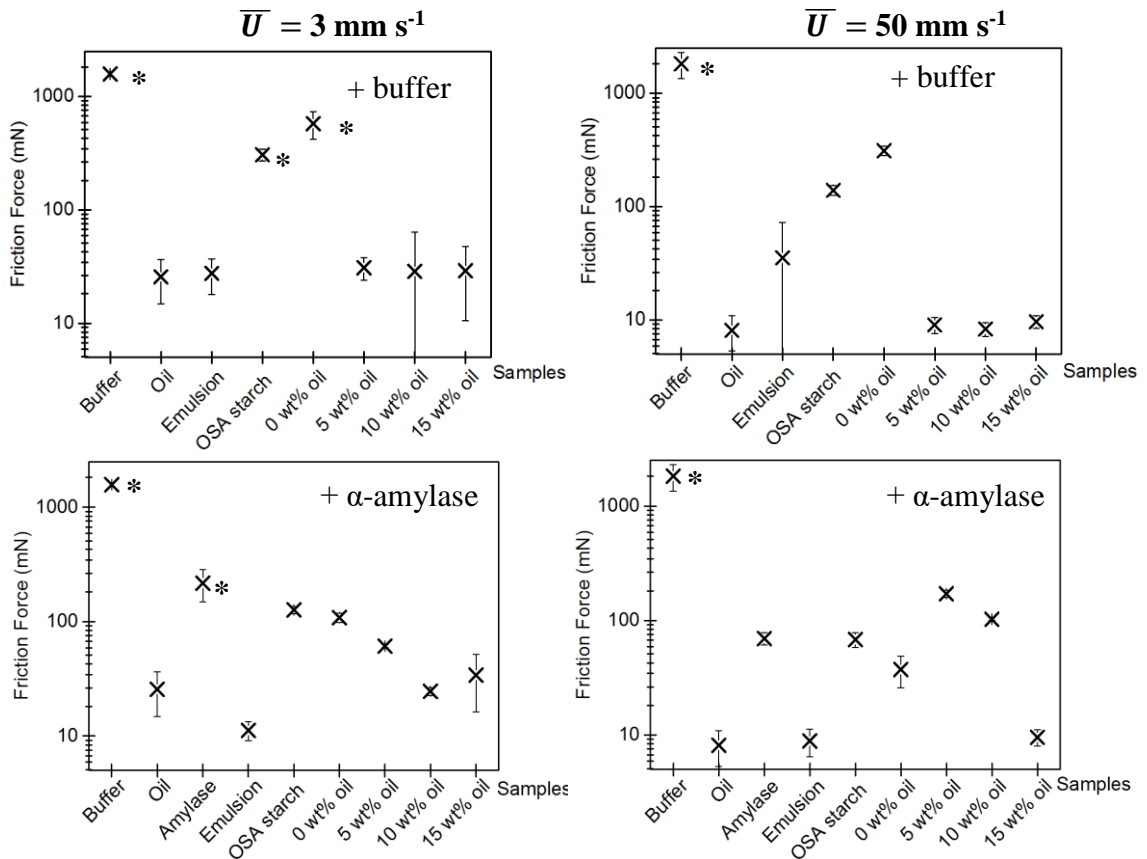


Figure 7.6 Effect of oil content and enzyme on the friction force of 15 wt% starch emulsion microgel particles depending on the lubrication regime, sample with symbol (*) are statistically different ($p < 0.05$).

shear. On entering the contact area between the tribo-pairs, the emulsion microgel particles would compress, probably releasing a few emulsion droplets, which might further explain the similarity between the friction force of the emulsion droplets and emulsion microgel particles. However, the large elastic modulus of the emulsion droplets would support the load on compression of the emulsion microgel particles, avoiding the particles from fracturing completely under shear.

The incorporation of α -amylase to the emulsion microgel particles did not significantly influence the friction force of the samples. At 3 mm s^{-1} in the absence or presence of enzyme, the emulsion microgel particles had a friction force around 35 mN (Figure 7.6). The restricted effect of α -amylase is further reinforced by the limited influence that the oil content had on the friction force of the emulsion microgel particles. At low entrainment speed (3 mm s^{-1}), all three emulsion microgel particles had similar friction forces. As the speed increased to 50 mm s^{-1} , a difference was

noticed between the samples at high oil content. At 15 wt% oil, the friction force of the emulsion microgel particles reduced to values similar to that of the emulsion droplets, suggesting fracture of the particles and possible greater release of emulsion droplets. Although the emulsion droplets were actively bound to the microgel particles and reinforced the particles, the high oil content might have acted as crack initiators in the microgel particles. Hence under mechanical shear, the starch gel matrix would disrupt more easily at high oil content resulting in a greater release of emulsion droplets (Dickinson, 2012).

Therefore, under a combination of mechanical shear and enzymatic activity, the encapsulation of emulsion droplets into starch particles provided the emulsion droplets protection against destabilisation and coalescence whilst still providing lubrication by allowing a few stable emulsion droplets to be released in the continuous phase.

The scope of the investigation only included the study of starch-based emulsion microgel particles due to their known response to oral enzyme. It would have been interesting to examine the behaviour of whey protein emulsion microgel particles, since these had a higher elastic modulus (approximately one order of magnitude higher) than the starch-based emulsion microgel particles. However, as their limiting deformation values were lower (approximately one order of magnitude lower), the whey protein-based emulsion microgel particle might have been more brittle and fracture more easily under mechanical shear.

7.2.4.3 Swelling of the particles – pH-trigger mechanism (only relevant for whey protein particles)

Environmental and physiological conditions, such as pH, ionic strength and temperature are important factors that may affect the behaviour of chemically cross-linked polymers such as whey protein. In comparison, starch polymeric network due to their uncharged entanglement are unlikely to swell over a change of pH and are hence unlikely to release emulsion droplets under a change of pH (Sweedman et al., 2013). However, to fully grasp the release behaviour of the starch-based emulsion microgel particles, their *in vitro* gastrointestinal digestion would have to be investigated.

During pH change, the biopolymer network has the ability to shrink or swell due to its capacity to bind a large amount of water *via* its hydrophilic groups, such as

hydroxyl (-OH), amide (-CONH₂), carboxyl (-COOH), sulfonate (-SO₃H) groups (Gunasekaran et al., 2007; Gupta et al., 2002). The properties of both the polymer and the media will influence the swelling capacity of the cross-linked polymer, such as the charge, concentration, cross-link density, ionization capacity, pK_a of the ionisable groups of the polymer and the pH, ionic strength, temperature, valency of ions in the surrounding media (Gupta et al., 2002). Upon swelling, the mesh size of the cross-linked polymer may increase, allowing the diffusion and release of the encapsulating material into the continuous phase (Betz et al., 2012).

According to previous studies, the swelling ratio (*i.e.*, weight difference before and after swelling due to the uptake of water) of protein hydrogels is lowest at the isoelectric point of the protein due to the minimal surface charge of the protein. Whilst at a pH away from the pI of the protein, the deprotonation of its ionisable groups would increase electrostatic interactions allowing the uptake of water molecules (via H-bonding), which causes the hydrogel to swell (Beaulieu et al., 2002; Gunasekaran et al., 2007).

Therefore, emulsion microgel particles designed from whey protein have the potential to modulate their mesh size as a function of pH, which can trigger the release of the encapsulated oil droplets. β -Lactoglobulin has an isoelectric point of 5.2, therefore at gastric pH (pH 3) the protein should be positively charged whereas at intestinal pH (pH 6.8), whey protein will be negatively charged.

To further understand the possible interactions between the water molecules and the protein, the total net charge (α) of β -lactoglobulin at pH 3 and 6.8 was calculated using the Henderson-Hasselbach equation, Equation 7.3:

$$\alpha = [10^{(pK_a - pH)} + 1]^{-1} \quad (7.3)$$

where α is the degree of dissociation of the ionisable groups.

From the amino acid composition of β -lactoglobulin (Table 7.6), the protein is expected to be highly positively charged (net charge of +20) at pH 3, whilst at pH 6.8 it is expected to be negatively charged (net charge of -6). Therefore, under gastric conditions, the positively charged emulsion microgel particles, due to protonation of the ionisable amine groups, would not be able to attract hydrogen ions, resulting in the low absorption of water and a low network swelling (Beaulieu et al., 2002). This low

swelling ratio should allow the encapsulated material to be protected against diffusion into the continuous phase or gastric degradation.

However, under intestinal condition (pH 6.8), the negatively-charged emulsion microgel particles, due to deprotonation of the carboxyl groups should be able to interact with hydrogen ions from the water molecules, resulting in a high swelling ratio and an increase in the mesh size of the particles (Beaulieu et al., 2002). The larger mesh size might allow enzymes (trypsin, chymotrypsin, lipase) to diffuse into the particle and hydrolyse the protein or the lipid molecules whilst, the emulsion droplets might also be able to diffuse out of the particles improving their accessibility to enzymes such as lipase. In **Chapter 6**, the comparison between a conventional whey protein-stabilised emulsion and whey protein-based emulsion microgel particles demonstrated that the protection of the emulsion droplets towards acidic gastric

Table 7.6 Amino acid composition of β -lactoglobulin and the pK_a values of the amino acid residue side chains (from Alexander et al., 1989 and Damodaran et al., 2008)

Type of amino acids	Amino acid residue	Number of amino acid residue	Side chains pK _a
Acid side chains	Aspartic acid	10	4.6
	Glutamic acid	16	4.6
Basic side chains	Histidine	2	7
	Lysine	16	10.2
	Arginine	3	12
Polar neutral side chains	Asparagine	5	-
	Glutamine	10	-
	Serine	7	-
	Threonine	9	-
	Valine	9	-
	Cysteine	7	8.8
Hydrophobic aromatic side chain	Phenylalanine	4	-
	Tryptophan	2	-
	Methionine	5	-
	Tyrosine	4	9.6
Hydrophobic aliphatic side chains	Alanine	19	-
	Isoleucine	10	-
	Leucine	27	-
Unique amino acids	Glycine	5	-
	Proline	8	-

destabilisation optimized the delivery and FFA release during the intestinal digestion, which indirectly confirmed the pH-responsiveness of the whey protein-emulsion microgel particles.

7.3 Concluding remarks and future directions

7.3.1 Concluding remarks

A schematic overview of the approach of this thesis was presented at the beginning of this chapter, highlighting the main outcome of this thesis: emulsion microgel particles with controlled release properties can be engineered by tuning the properties of both the biopolymer matrix and emulsion droplets (Figure 7.1).

The emulsion microgel particles contributed to the improvement of food based delivery systems for lipophilic materials. Both particles were designed using a facile and food grade processing route, employing a single biopolymer to emulsify the lipophilic molecules and form the biopolymer particle network. This thesis indicates the importance of the mechanical and physicochemical properties of the biopolymer to design emulsion microgel particles, which allow responsiveness to the targeted physiological stimuli. Emphasis was placed on the different responses of the cross-linked emulsion microgel particles during oral or gastrointestinal processing. Starch-based emulsion microgel particles were found to be suitable for the protection of lipophilic molecules against oral shear and coalescence whilst providing appropriate lubrication *via* both enzyme and shear-response mechanism. Whey protein-based emulsion microgel particles were established to protect the lipophilic molecules from harsh gastric environment whilst enabling complete release of free fatty acid during the intestinal phase due to both enzyme and pH-response mechanisms. These findings provide guidelines to develop new bio-responsive materials where these biocompatible particles offer excellent controlled release properties of lipophilic materials.

The knowledge obtained in this thesis is especially important for the design and application of emulsion microgel particles encapsulating lipophilic compounds, where improved delivery of the encapsulated material is necessary whilst providing palatable properties.

7.3.2 Future directions

This thesis has demonstrated the potential of emulsion microgel particles to control the delivery of its encapsulated material *via* different trigger mechanisms. Based on these findings, further research could be undertaken in order to fully unleash the application potential of these emulsion microgel particles:

- Testing in real food applications. In this thesis, the breakdown properties of emulsion microgel particles were elucidated in isolation. It would be of great interest to incorporate these emulsion microgel particles into real composite food systems, such as yogurt and cheese. Particularly, further research is needed to understand whether these particles retain their mechanical integrity during processing of these food applications, such as exposure to processing shear, temperature or interactions with other food components. Future research should focus on whether these emulsion microgel particles provide positive effects on the sensory properties of these food products through lubrication mechanisms by sensory panel or control release of encapsulated materials during digestion of the food products containing these particles.
- Encapsulation of bioactives and their bio-availability. Fundamental insights generated in this thesis were based on emulsion microgel particles that were encapsulating sunflower oil. As a next step, the encapsulation efficiency of bioactive lipophilic compounds such as β -carotene, vitamin D, flavonoids, or essential oil should be investigated. Research should also be undertaken to understand how these particles can help protect the encapsulated bioactive molecules against oxidation as well as investigate their behaviour under *in vitro* oral and gastrointestinal digestion using biological assays and biophysical membranes.
- *In vivo* studies. There is a greater need for *in vivo* studies to correlate the results obtain through *in vitro* studies. It might be useful to undertake sensory testing to fully appreciate the lubrication potential of the starch-based emulsion microgel particles. Clinical trials of the whey protein-based emulsion microgel particle might also be of interest to

understand the bio-accessibility of the encapsulated material during intestinal digestion.

- Reduction of solid fat content. Future research should look at investigating the lubrication behaviour of solid fat and emulsion microgel particles as a useful tool to formulate products with liquid oil whilst still providing a creamy and melting mouthfeel. Such studies should be done with quantitative sensory analysis together with in vitro lubrication tests developed as a part of this thesis.
- Biopolymer testing. There could be potential in testing different types of biopolymers, such as gelatine, chitosan, carrageenan, to formulate a wide range of microgel particles using this top down or bottom up techniques for a range of food, cosmetics and other soft matter applications with different functional needs.
- Characterisation techniques. In this thesis, we have used a range of structural and rheological techniques to characterize emulsion microgel particles. As a next step, one might consider investigating the material properties, such as modulus of single emulsion microgel particles using atomic force microscopy (AFM). Such characterization will also help to further tune individual particles with desired features, to precisely control swelling and release for use in functional food, biomedical and drug delivery applications.

7.4 References

- Alexander, L.J. et al. 1989. Complete sequence of the bovine beta-lactoglobulin cDNA. *Nucleic Acids Research*. **17**(16), p6739.
- Ali, A. et al. 2018. Effect of high pressure homogenization on the structure and the interfacial and emulsifying properties of β -lactoglobulin. *International Journal of Pharmaceutics*. **537**(1), pp.111-121.
- Amsden, B. 1998. Solute Diffusion within Hydrogels. *Mechanisms and Models. Macromolecules*. **31**(23), pp.8382-8395.

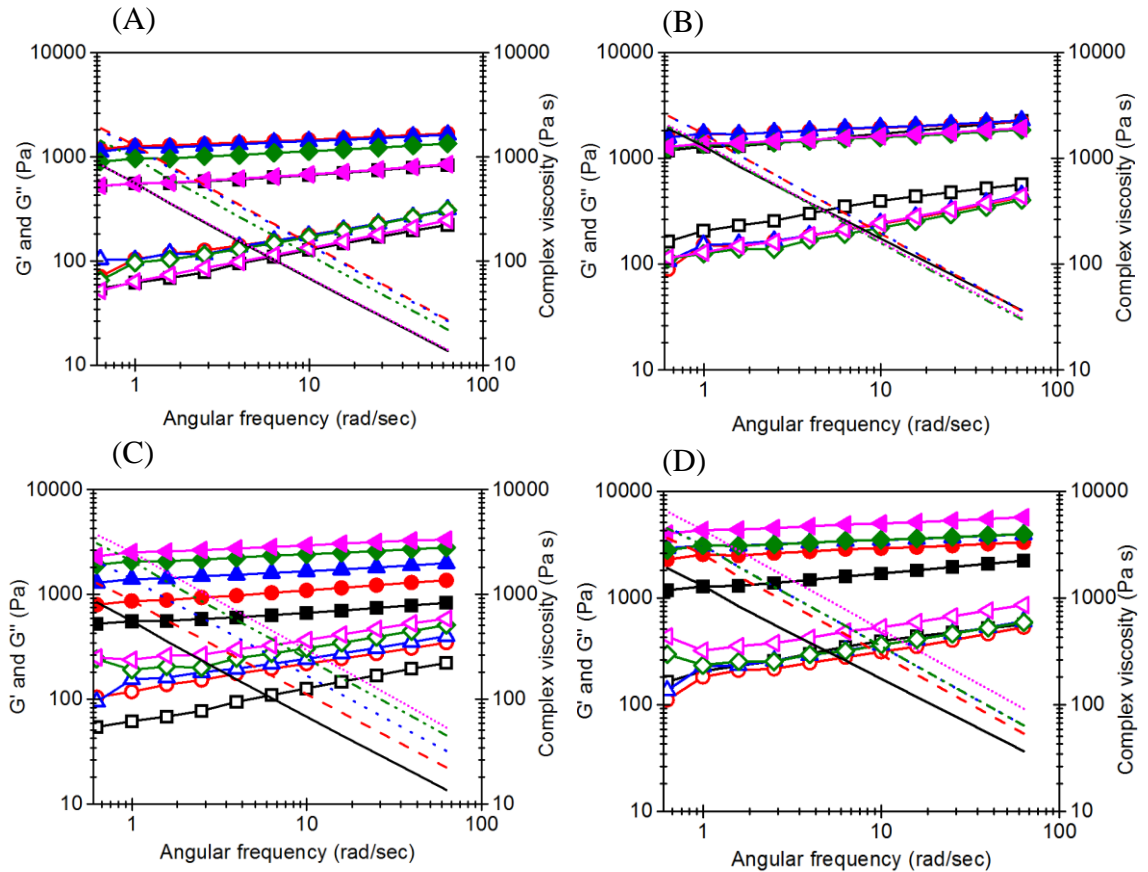
- Beaulieu, L. et al. 2002. Elaboration and characterization of whey protein beads by an emulsification/cold gelation process: application for the protection of retinol. *Biomacromolecules*. **3**(2), pp.239-248.
- Betz, M. et al. 2012. Swelling behaviour, charge and mesh size of thermal protein hydrogels as influenced by pH during gelation. *Soft Matter*. **8**(8), pp.2477-2485.
- Bhosale, R. and Singhal, R. 2006. Process optimization for the synthesis of octenyl succinyl derivative of waxy corn and amaranth starches. *Carbohydrate Polymers*. **66**(4), pp.521-527.
- Bousmina, M. 1999. Rheology of polymer blends: linear model for viscoelastic emulsions. *Rheologica Acta*. **38**(1), pp.73-83.
- Cozzone, P. et al. 1970. Characterization of Porcine Pancreatic Isoamylases Chemical and Physical Studies. *Biochimica et Biophysica Acta (BBA) - Protein Structure*. **207**(3), pp.490-504.
- Damodaran, S. et al. 2008. *Fennema's food chemistry*. 4th / by Srinivasan Damodaran, Kirk Parkin, and Owen R. Fennema. ed. London;Boca Raton;: CRC Press.
- de Wijk, R.A. et al. 2006. Perceived creaminess of semi-solid foods. *Trends in Food Science & Technology*. **17**(8), pp.412-422.
- Dhital, S. et al. 2017. Mechanisms of starch digestion by α -amylase—Structural basis for kinetic properties. *Critical Reviews in Food Science and Nutrition*. **57**(5), pp.875-892.
- Dickinson, E. 2012. Emulsion gels: The structuring of soft solids with protein-stabilized oil droplets. *Food Hydrocolloids*. **28**(1), pp.224-241.
- Dickinson, E. 2017. Hydrocolloids acting as emulsifying agents – How do they do it? *Food Hydrocolloids*.
- Dickinson, E. and Chen, J.S. 1999. Heat-Set Whey Protein Emulsion Gels: Role of Active and Inactive Filler Particles. *Journal of Dispersion Science and Technology*. **20**(1-2), pp.197-213.
- Egan, T. et al. 2013. Cold-set whey protein microgels for the stable immobilization of lipids. *Food Hydrocolloids*. **31**(2), pp.317-324.
- Ettelaie, R. et al. 2016. Steric stabilising properties of hydrophobically modified starch: Amylose vs. amylopectin. *Food Hydrocolloids*. **58**, pp.364-377.
- Flory, P.J. 1953. *Principles of Polymer chemistry*. Ithaca, NY: Cornell University Press.

- Gunasekaran, S. et al. 2007. Use of whey proteins for encapsulation and controlled delivery applications. *Journal of Food Engineering*. **83**(1), pp.31-40.
- Gupta, P. et al. 2002. Hydrogels: from controlled release to pH-responsive drug delivery. *Drug Discovery Today*. **7**(10), pp.569-579.
- Hongsprabhas, P. et al. 1999. The Structure of Cold-Set Whey Protein Isolate Gels Prepared With Ca⁺⁺. *LWT - Food Science and Technology*. **32**(4), pp.196-202.
- Kong, F. and Singh, R.P. 2008. Disintegration of solid foods in human stomach. *J Food Sci*. **73**(5), pp.R67-80.
- Langley, K.R. and Green, M.L. 1989. Compression Strength and Fracture Properties of Model Particulate Food Composites in Relation to Their Microstructure and Particle-Matrix Interaction. *Journal of Texture Studies*. **20**(2), pp.191-207.
- McClements, D.J. 2017. Designing biopolymer microgels to encapsulate, protect and deliver bioactive components: Physicochemical aspects. *Advances in Colloid and Interface Science*. **240**, pp.31-59.
- Minekus, M. et al. 2014. A standardised static in vitro digestion method suitable for food – an international consensus. *Food & Function*. **5**(6), pp.1113-1124.
- Ortega-Ojeda, F.E. et al. 2005. Gel formation in mixtures of hydrophobically modified potato and high amylopectin potato starch. *Carbohydrate Polymers*. **59**(3), pp.313-327.
- Palierne, J.F. 1990. Linear rheology of viscoelastic emulsions with interfacial tension. *Rheologica Acta*. **29**(3), pp.204-214.
- Palierne, J.F. 1991. Erratum. *Rheologica Acta*. **30**(5), pp.497-497.
- Reilly, P.J. 2007. Chapter 5 - Amylase and Cellulase Structure and Function. In: Yang, S.-T. ed. *Bioprocessing for Value-Added Products from Renewable Resources*. Amsterdam: Elsevier, pp.119-130.
- Sala, G. et al. 2009a. Deformation and fracture of emulsion-filled gels: Effect of oil content and deformation speed. *Food Hydrocolloids*. **23**(5), pp.1381-1393.
- Sala, G. et al. 2009b. Deformation and fracture of emulsion-filled gels: Effect of gelling agent concentration and oil droplet size. *Food Hydrocolloids*. **23**(7), pp.1853-1863.

- Schröder, A. et al. 2017. Interfacial properties of whey protein and whey protein hydrolysates and their influence on O/W emulsion stability. *Food Hydrocolloids*. **73**, pp.129-140.
- Sok, L.V.L. et al. 2005. Cold gelation of β -lactoglobulin oil-in-water emulsions. *Food Hydrocolloids*. **19**(2), pp.269-278.
- Stokes, J.R. et al. 2013. Oral processing, texture and mouthfeel: From rheology to tribology and beyond. *Current Opinion in Colloid & Interface Science*. **18**(4), pp.349-359.
- Sweedman, M.C. et al. 2013. Structure and physicochemical properties of octenyl succinic anhydride modified starches: A review. *Carbohydrate Polymers*. **92**(1), pp.905-920.
- Tesch, S. et al. 2002. Stabilization of emulsions by OSA starches. *Journal of Food Engineering*. **54**(2), pp.167-174.
- Witt, T. et al. 2010. Starch Digestion Mechanistic Information from the Time Evolution of Molecular Size Distributions. *Journal of Agricultural and Food Chemistry*. **58**(14), pp.8444-8452.
- Xu, J. et al. 2018. The role of chemical and physical crosslinking in different deformation stages of hybrid hydrogels. *European Polymer Journal*. **100**, pp.86-95.

Appendix A

Supplementary information for Chapter 3



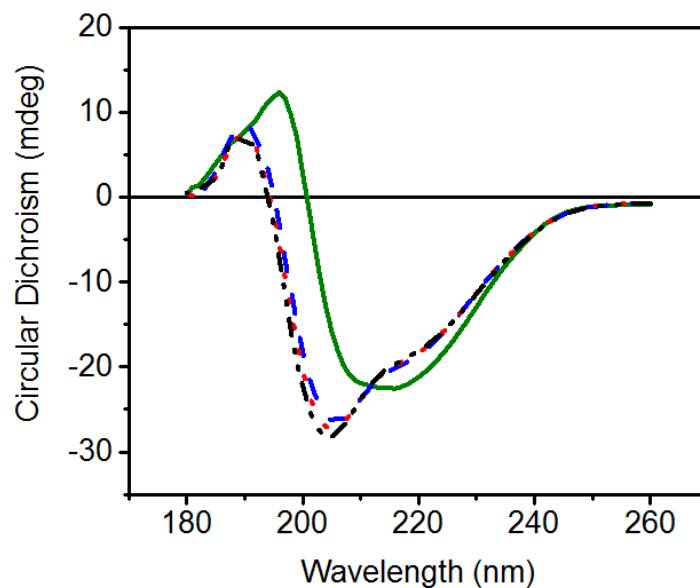
Appendix A.1 Elastic modulus (G' , filled symbols), viscous modulus (G'' , empty symbols) and complex viscosity (η^* , lines) as a function of angular frequency of 15 wt% (A) and 20 wt% native starch gel (B) prepared with different OSA starch concentrations (0 wt%, ■, solid black line; 0.5 wt%, ●, dashed red line; 1 wt%, ▲, dotted blue line; 1.5 wt%, ◆, dashed and dotted green line; 2 wt%, ◀, short dotted pink line), 15 wt% (C) and 20 wt% starch emulsion gel (D) prepared with different oil concentrations (0 wt%, ■, solid black line; 5 wt%, ●, dashed red line; 10 wt%, ▲, dotted blue line; 15 wt%, ◆, dashed and dotted green line ; 20 wt%, ◀, short dotted pink line).

Appendix A.2 Initial and final elastic modulus (G') of 15 wt% starch gel mixed with different concentration of OSA starch dispersion (0 – 2 wt%) and standard deviation; means in the same column with same superscript letter are not significantly different ($p > 0.05$) to the 15 wt% native starch gel without OSA starch.

	[OSA starch] (wt%)	Initial G' (kPa)	Final G' (kPa)
Starch gel	0	0.04 ^a ±0.006	0.64 ^a ±0.06
	0.5	0.23 ^b ±0.02	1.41 ^b ±0.12
OSA starch + Starch gel	1	0.26 ^c ±0.07	1.37 ^c ±0.20
	1.5	0.26 ^d ±0.04	1.09 ^a ±0.21
	2	0.16 ^f ±0.02	0.64 ^a ±0.05

Appendix B

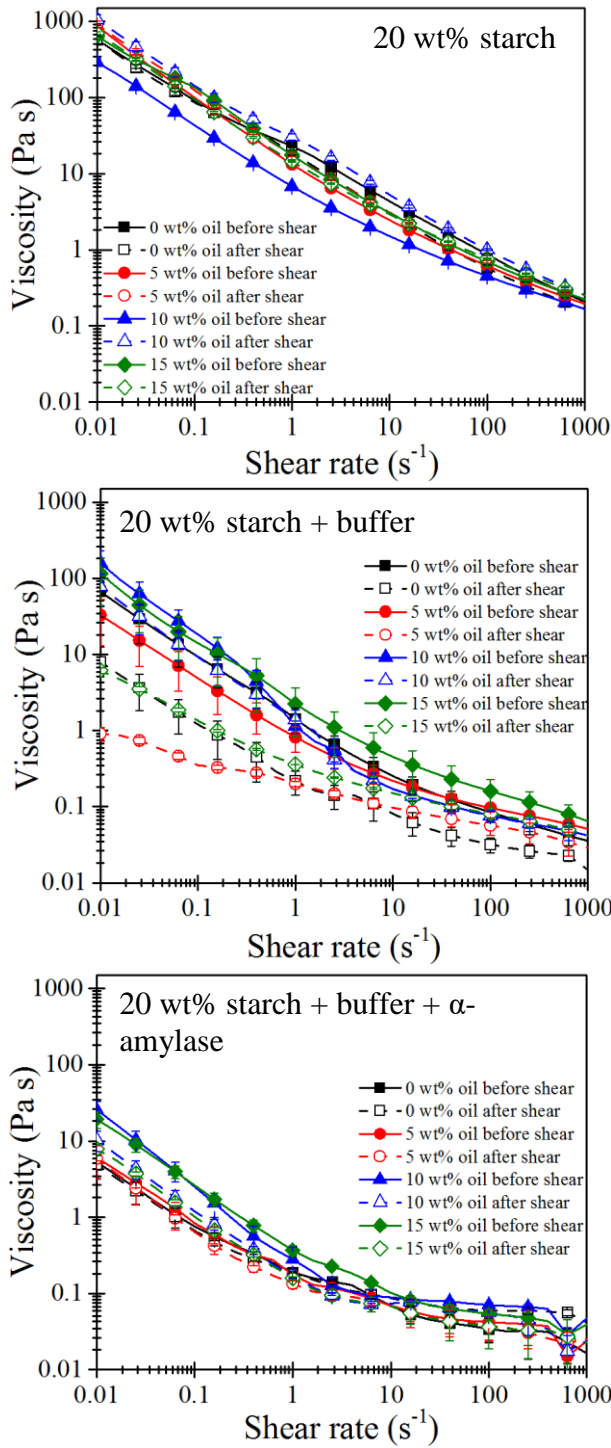
Supplementary information for Chapter 4



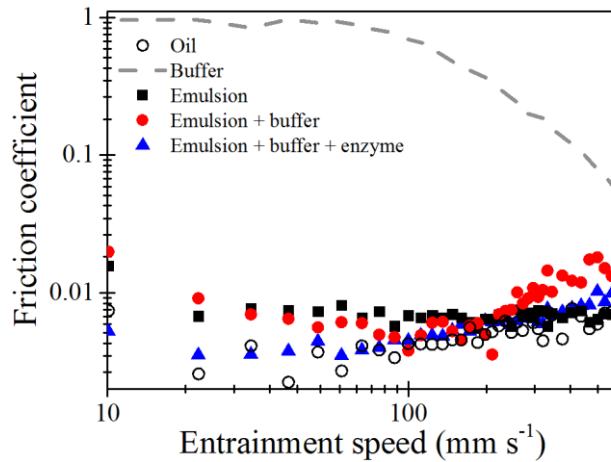
Appendix B.1 Circular dichroism of WPI at 20 °C (green full line), 75 °C (blue dashed line), 80 °C (red dotted line) and 85 °C (black dash and dotted line).

Appendix C

Supplementary information for Chapter 5



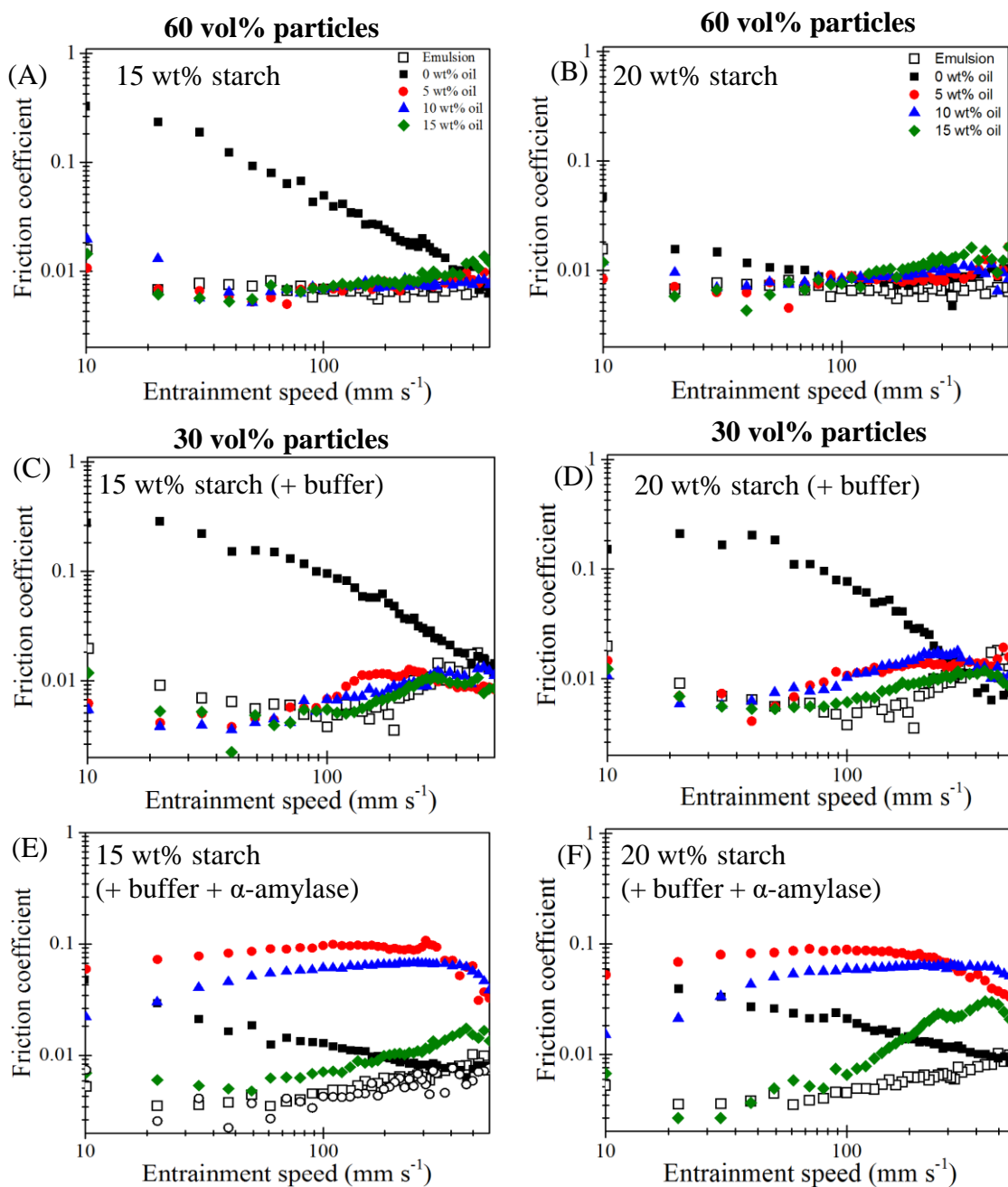
Appendix C.1 Flow curves of the emulsion microgel particles produced from 20 wt% starch.



Appendix C.2 Coefficient of friction as function of entrainment speed ($10 < \bar{U} < 100 \text{ mm s}^{-1}$) for sunflower oil, buffer with α -amylase and OSA starch stabilized emulsion in absence or presence of buffer and/or α -amylase subjected to an entrainment speed of 10 to 500 mm s^{-1} , a normal load of 2 N and at 37 °C.

Appendix C.3 Friction coefficient measured at 3 and 50 mm s^{-1} , 37 °C and 2 N of buffer, sunflower oil and emulsions under different conditions, column shown with means values \pm standard deviations with same superscript letter are significantly different ($p < 0.05$).

Entrainment speed (mm s^{-1})	Coefficient of friction	
	3	50
Buffer	0.788 ^{a,b,c,d,e} ± 0.033	0.912 ^{a,b,c,d,e} ± 0.238
Sunflower oil	0.013 ^{b,a} ± 0.005	0.004 ^{b,a} ± 0.001
Emulsion (40 wt% oil)	0.043 ^{c,a} ± 0.016	0.007 ^{c,a} ± 0.004
Emulsion + buffer (20 wt% oil)	0.042 ^{d,a} ± 0.008	0.005 ^{d,a} ± 0.001
Emulsion + buffer + α -amylase (20 wt% oil)	0.006 ^{e,a} ± 0.001	0.004 ^{e,a} ± 0.001



Appendix C.4. Coefficient of friction as function of entrainment speed of starch microgel particles encapsulating different oil content measured at 2 N and 37 °C in absence of buffer and α -amylase (A and B); in presence of buffer (50:50 w/w) without α -amylase (C and D); in presence of buffer (50:50 w/w) with α -amylase (E and F). Controls are the OSA stabilised-emulsion at the different conditions.

Appendix C.5 Friction coefficient measured at 3 mm s⁻¹, 37 °C and 2 N of the starch based particles under different conditions, column shown with means values ± standard deviations with same superscript letter are significantly different (*p* < 0.05).

Physiological Condition	Coefficient of friction		
	No buffer	+ buffer	+ buffer + α-amylase
Buffer	0.788 ±0.033 ^{a,b,c,d,e,f,g,h,i,j,k}	0.788 ±0.033 ^{a,b,c,d,e,f,g,h,i,j,k}	0.788 ±0.033 ^{a,b,c,d,e,f,g,h,i,j,k}
Sunflower oil	0.013 ±0.005 ^{b,a,d,h}	0.013 ±0.005 ^{b,a,d,h}	0.013 ±0.005 ^{b,a,d,h}
Emulsion (40 wt% oil)	0.043 ±0.016 ^{c,a,d,h}	0.042 ±0.008 ^{c,a,d,h}	0.006 ±0.001 ^{c,a,d,h}
15 wt% starch + 0 wt% oil	0.428 ±0.107 ^{d,a,b,c,e,f,g,h,i,j,k}	0.287 ±0.077 ^{d,a,b,c,e,h,i,j,k}	0.054 ±0.005 ^{d,a,b,c,f,j,k}
15 wt% starch + 5 wt% oil	0.026 ±0.007 ^{e,a,d,h}	0.015 ±0.003 ^{e,a,d,h}	0.031 ±0.001 ^{e,a}
15 wt% starch + 10 wt% oil	0.101 ±0.009 ^{f,a,d}	0.014 ±0.017 ^{f,a,d,h}	0.012 ±0.001 ^{f,a,d,h}
15 wt% starch + 15 wt% oil	0.022 ±0.010 ^{g,a,d,h}	0.015 ±0.009 ^{g,a,d,h}	0.017 ±0.009 ^{g,a,h}
20 wt% starch + 0 wt% oil	0.166 ±0.028 ^{h,a,b,c,d,e,g,I,j}	0.188 ±0.110 ^{h,a,b,c,d,e,i,j,k}	0.026 ±0.007 ^{h,a,b,c,i,j,k}
20 wt% starch + 5 wt% oil	0.021 ±0.003 ^{i,a,d,h}	0.054 ±0.015 ^{i,a,d,h}	0.024 ±0.001 ^{i,a,h}
20 wt% starch + 10 wt% oil	0.022 ±0.016 ^{j,a,d,h}	0.032 ±0.021 ^{j,a,d,h}	0.012 ±0.000 ^{j,a,d,h}
20 wt% starch + 15 wt% oil	0.061 ±0.033 ^{k,a,d}	0.055 ±0.018 ^{k,a,d,h}	0.014 ±0.001 ^{k,a,d,h}

Appendix C.6 Friction coefficient measured at 50 mm s⁻¹, 37 °C and 2 N of the starch based particles under different conditions, column shown with means values ± standard deviations with same superscript letter are significantly different (*p* < 0.05).

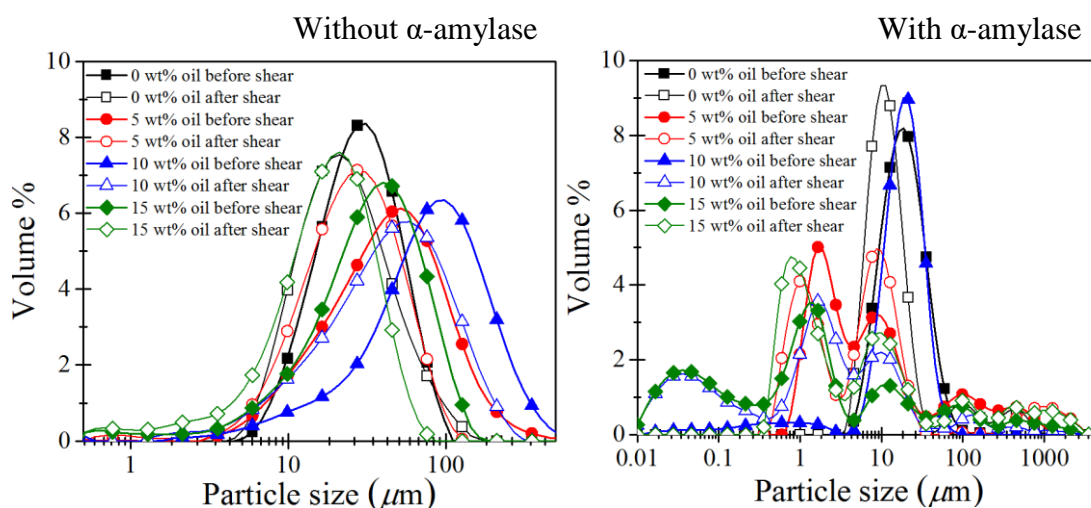
Physiological Condition	Coefficient of friction		
	No buffer	+ buffer	+ buffer + α-amylase
Buffer	0.912 ^{a,b,c,d,e,f,g} ±0.238 ^{h,i,j,k}	0.912 ^{a,b,c,d,e,f,g} ±0.238 ^{h,i,j,k}	0.912 ^{a,b,c,d,e,f,g,h,i} ±0.238 ^{j,k}
Sunflower oil	0.004 ^{b,a} ±0.001	0.004 ±0.001	0.004 ^{b,a} ±0.001
Emulsion (40 wt% oil)	0.007 ^{c,a} ±0.004	0.056 ±0.001	0.004 ^{c,a} ±0.001
15 wt% starch + 0 wt% oil	0.093± 0.014 ^{d,a}	0.156 ±0.015	0.019 ^{d,a,b,e,f,g,i,j} ±0.006 ^{,k}
15 wt% starch + 5 wt% oil	0.005 ^{e,a} ±0.001	0.005 ±0.001	0.086 ^{e,a} ±0.006
15 wt% starch + 10 wt% oil	0.005 ^{f,a} ±0.002	0.004 ±0.001	0.051 ^{f,a} ±0.001
15 wt% starch + 15 wt% oil	0.006 ^{g,a} ±0.001	0.005 ±0.001	0.005 ^{g,a} ±0.001
20 wt% starch + 0 wt% oil	0.011 ^{h,a} ±0.002	0.186 ±0.070	0.026 ^{h,a} ±0.007
20 wt% starch + 5 wt% oil	0.086 ^{i,a} ±0.006	0.006 ±0.001	0.083 ^{i,a} ±0.003
20 wt% starch + 10 wt% oil	0.051 ^{j,a} ±0.001	0.008 ±0.003	0.050 ^{j,a} ±0.001
20 wt% starch + 15 wt% oil	0.005 ^{k,a} ±0.001	0.005 ±0.001	0.005 ^{k,a} ±0.001

Appendix C.7 Friction coefficient measured at 3 mm s⁻¹, 37 °C and 2 N of the starch based particles with different oil contents, column shown with means values ± standard deviations with same superscript letter are significantly different (*p* < 0.05).

Oil content (wt%)	Coefficient of friction			
	0	5	10	15
15% Starch no buffer	0.428 ^{a, c, d, e, f} ±0.107	0.026 ^{a, e} ±0.007	0.101 ^{a, b, c, d} ±0.009 ^{e, f}	0.022 ^a ±0.010
15% Starch + buffer	0.287 ^{b, a, c, f} ±0.077	0.015 ^{b, c, e} ±0.003	0.014 ^{b, a} ±0.017	0.015 ^{b, d} ±0.009
15% Starch + buffer + α-amylase	0.054 ^{c, a, b} ±0.005	0.031 ^{c, b, e} ±0.001	0.012 ^{c, a} ±0.001	0.017 ^c ±0.009
20% Starch no buffer	0.166 ^{d, a} ±0.028	0.021 ^{d, e} ±0.003	0.022 ^{d, a} ±0.016	0.061 ^{d, b, f} ±0.033
20% Starch + buffer	0.188 ^{e, a} ±0.110	0.054 ^{e, a, b, c} ±0.015 ^{d, f}	0.032 ^{e, a} ±0.021	0.055 ^e ±0.018
20% Starch + buffer + α-amylase	0.070 ^{f, a, b} ±0.023	0.024 ^{f, e} ±0.001	0.012 ^{f, a} ±0.000	0.014 ^{f, d} ±0.001

Appendix C.8 Friction coefficient measured at 50 mm s⁻¹, 37 °C and 2 N of the starch based particles with different oil contents, column shown with means values ± standard deviations with same superscript letter are significantly different (*p* < 0.05).

Oil content (wt%)	Coefficient of friction			
	0	5	10	15
15% Starch no buffer	0.093 ±0.014 ^{a, e}	0.005 ±0.001 ^{a, c, f}	0.005 ±0.002 ^{a, c, f}	0.006 ±0.001 ^a
15% Starch + buffer	0.156 ±0.015 ^{b, c, d, e}	0.005 ±0.001 ^{b, c, f}	0.004 ±0.001 ^{b, c, f}	0.005 ±0.001 ^b
15% Starch + buffer + α-amylase	0.019 ±0.006 ^{c, b, e}	0.086 ±0.006 ^{c, a, b, d, e}	0.051 ±0.001 ^e	0.005 ±0.001 ^c
20% Starch no buffer	0.011 ±0.002 ^{d, b, e}	0.008 ±0.001 ^{d, c, f}	0.008 ±0.000 ^{d, c, f}	0.006 ±0.000 ^d
20% Starch + buffer	0.186 ±0.070 ^{e, a, c, d, f}	0.006 ±0.001 ^{e, c, f}	0.008 ±0.003 ^{e, c, f}	0.005 ±0.001 ^e
20% Starch + buffer + α-amylase	0.026 ±0.007 ^{f, b, e}	0.083 ±0.003 ^{f, a, b, d, e}	0.050 ±0.001 ^{f, a, b, d, e}	0.005 ±0.001 ^f



Appendix C.9 Particles size distribution of the emulsion microgel particles produced from 20 wt% starch before and after tribological shear.

Appendix C.10 Theoretical analysis of the relative indentation and drag force of the different samples

In the mixed lubrication regime, the total load W_T is supported by both the asperity contact and the lubricant (*i.e.*, emulsion or emulsion microgel particles) separating some regions of the surfaces. According to Otero et al. (2017) the friction coefficient μ , in the mixed regime, can be expressed in terms of the friction coefficient given by the lubricant μ_L and the one given by the asperities μ_B (Equation C.1):

$$\mu = f_\lambda^{1.2} \mu_L + (1 - f_\lambda) \mu_B \quad (\text{C.1})$$

where, f_λ is defined as the load carried by each component, $W_L = f_\lambda W_T$ for the lubricant and $W_B = (1 - f_\lambda) W_T$ for the asperities. From Figure 3.a and Figure 5., it is noticeable that the friction coefficients of all lubricants (*i.e.*, sunflower oil, emulsions, starch particles and emulsion microgel particles) (μ_L) are at least two order of magnitude lower compared to the ones obtained with the buffer (μ_B). Therefore, the term at the right side of Equation 1 can be neglected. Under this assumption, the load supported by the lubricant in terms of friction coefficients can be expressed by Equation C.2:

$$W_L = \frac{\mu_B - \mu}{\mu_B} W_T \quad (\text{C.2})$$

In order to understand the physical properties of the lubricant partially separating the contact surfaces a mechanical analysis of the emulsion droplets, starch and emulsion microgel particles in the contact area was introduced. From the Hertz theory at the contact point, the radius of contact a_H and the indentation of the contact δ can be obtained from Equation C.3 and C.4 for a point of contact supporting a load W , respectively:

$$a_H^3 = \frac{3}{4} \frac{WR^*}{E^*} \quad (\text{C.3})$$

and

$$\delta = \frac{a_H^2}{R^*} - f\left(\frac{a_H}{R}\right) \frac{W}{\pi R^* E^* (1-\nu^2)}, \quad (\text{C.4})$$

$$\text{with } \left(\frac{a_H}{R}\right) = \frac{2(1+\nu)}{\left(4+\left(\frac{a_H}{R}\right)^2\right)^{3/2}} + \frac{(1-\nu^2)}{\left(4+\left(\frac{a_H}{R}\right)^2\right)^{1/2}}, R^*, \nu \text{ and } E^* \text{ represent the reduced radius,}$$

Poisson ratio and reduced elastic modulus of the contacts formed by the particles and the PDMS contact surfaces, E^* was obtained from $E^* = \left(\frac{1-\nu^2}{E'} + \frac{1-\nu^2}{E''}\right)^{-1}$ where E' and E'' are the reduced elastic modulus of PDMS and particles, respectively. E'' was estimated from the elastic compression (Mezger, 2014) $E'' = 2G'_f(1+\nu)$, where G'_f is the shear elastic modulus of the emulsion droplets or particles. In the case of the emulsion droplets (Torres et al., 2016; van Vliet, 1988), G'_f was obtained from: $G'_f = \frac{2\gamma_T}{R}$, where γ_T is the interfacial tension of the emulsion droplets stabilised by the OSA starch, measured previously at $\gamma_T = 27 \text{ mN m}^{-1}$ (Tesch et al., 2002) and R is the radius of the particle. In the case of the particles, G'_f was obtained from measurements of the elastic modulus of the gels from which they were prepared (Torres et al., 2017).

The load (W_L) was assumed to be supported by the emulsion droplets or particles consequently, the load supported by each emulsion droplets (W_P) could also be estimated. This was achieved by relating the number of particles, forming a monolayer, inside the contact (n_p) with an effective fraction of particles ϕ_p covering the contact area: $n_p = \frac{\phi_p a_{TP}^2}{R^2}$

where a_{TP} is the Hertz contact radius between the PDMS ball and disc, calculated at 2.07 mm, using Equation C.3.

So the load per particles can be written as (Equation C.5):

$$W_P = \frac{W_L}{N_P} = \frac{1}{\phi_p} \frac{W_T R^2}{a_{TP}^2} \quad (\text{C.5})$$

Using this last expression and combining Equations C.3 and C.4, the relative indentation for a monolayer of particles in the contact can be expressed as (Equation C.6):

$$\frac{\delta}{R} = \left(\frac{a_H}{R}\right)^2 - \frac{4}{3\pi(1-\nu^2)} \left(\frac{a_H}{R}\right)^3 f\left(\frac{a_H}{R}\right) \quad (\text{C.6})$$

where the ratio a_H/R is independent of R and relates the relative indentation to the fraction of surface covered by particles ϕ_p independently of the particle radius (Equation C.7):

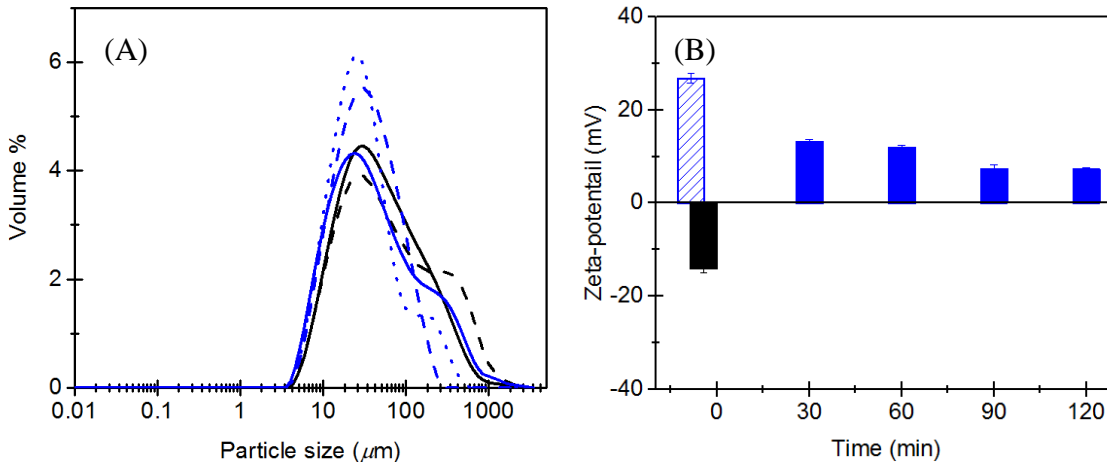
$$\frac{a_H}{R} = \left(\frac{3W_L}{4\phi_p E^* a_T p^2}\right)^{1/3} \quad (\text{C.7})$$

Appendix C.11 References

- Mezger, T.G. 2014. *The Rheology Handbook 4th Edition*. Hanover, Germany: Vincentz Network.
- Otero, J.E. et al. 2017. Friction coefficient in mixed lubrication: A simplified analytical approach for highly loaded non-conformal contacts. *Advances in Mechanical Engineering*. **9**(7), p1687814017706266.
- Tesch, S. et al. 2002. Stabilization of emulsions by OSA starches. *Journal of Food Engineering*. **54**(2), pp.167-174.
- Torres, O. et al. 2016. Emulsion microgel particles: Novel encapsulation strategy for lipophilic molecules. *Trends in Food Science & Technology*. **55**, pp.98-108.
- Torres, O. et al. 2017. Novel starch based emulsion gels and emulsion microgel particles: Design, structure and rheology. *Carbohydrate Polymers*. **178**, pp.86-94.
- van Vliet, T. 1988. Rheological properties of filled gels. Influence of filler matrix interaction. *Colloid and Polymer Science*. **266**(6), pp.518-524.

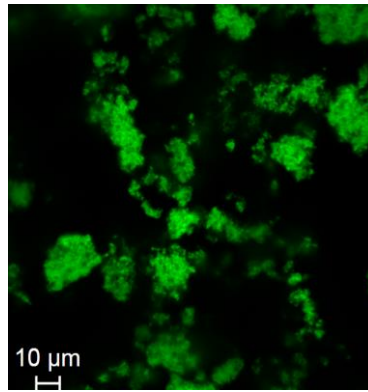
Appendix D

Supplementary information for Chapter 6



Appendix D.1 Particle size distribution (A) (black full line: before digestion, black dashed line: in buffer pH3, blue full line: SGF + pepsin 5 min, blue dashed line: SGF + pepsin 60 min, blue dotted line: SGF + pepsin 120 min) and zeta-potential (B) (black: before digestion, blue slashed: in gastric buffer pH3, blue: in gastric buffer + pepsin) of 9.6 wt% WPI based microgel particles during gastric *in vitro* digestion over time.

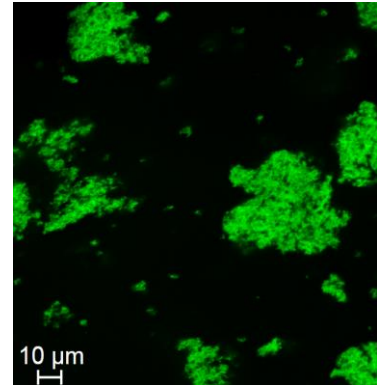
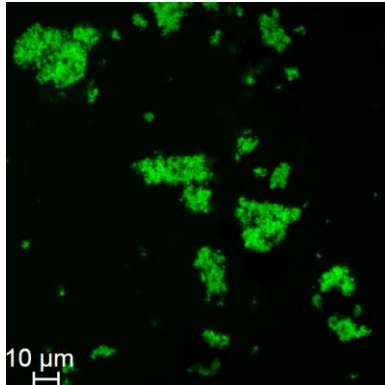
Before digestion



30 min

120 min

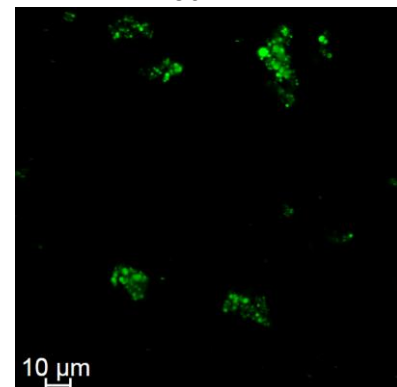
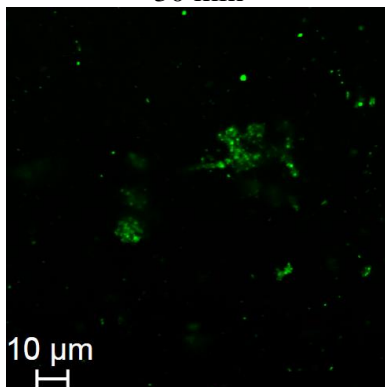
Gastric digestion



30 min

180 min

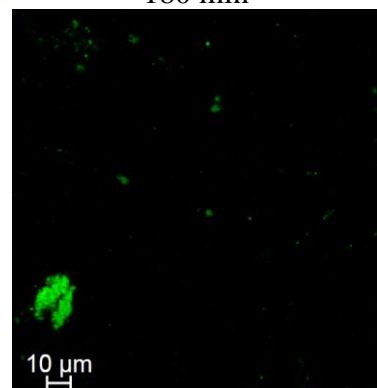
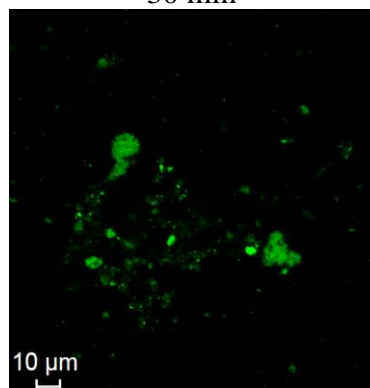
Intestinal digestion



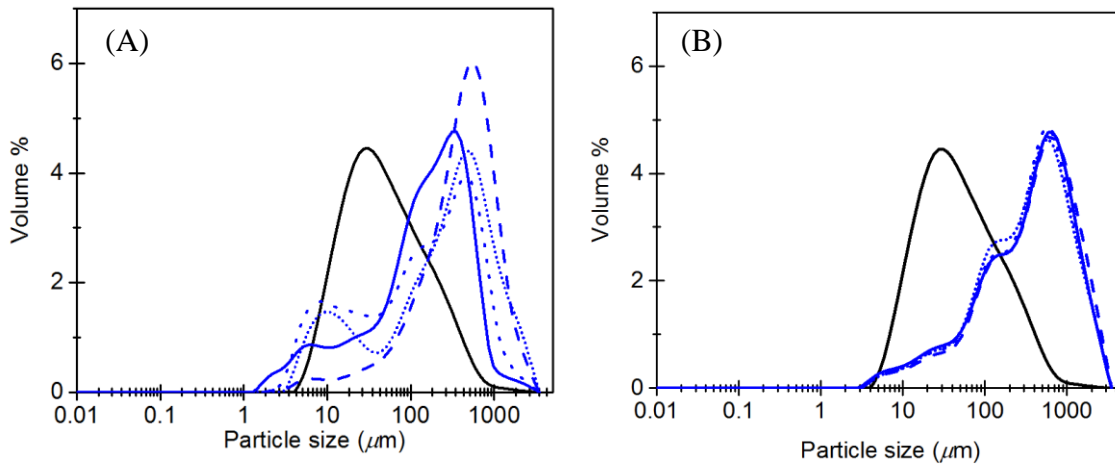
30 min

180 min

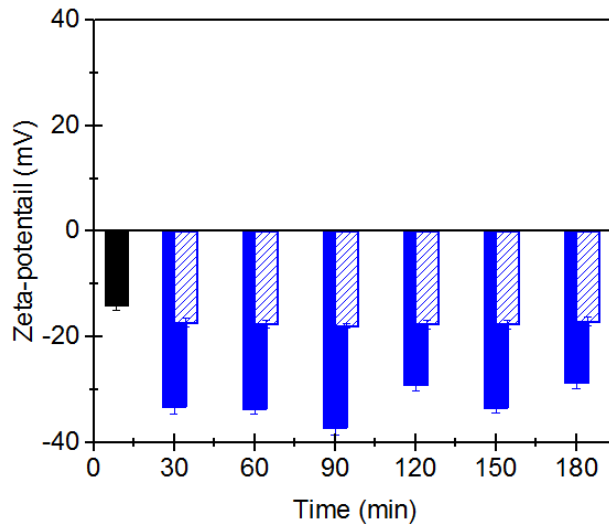
Gastric + intestinal digestion



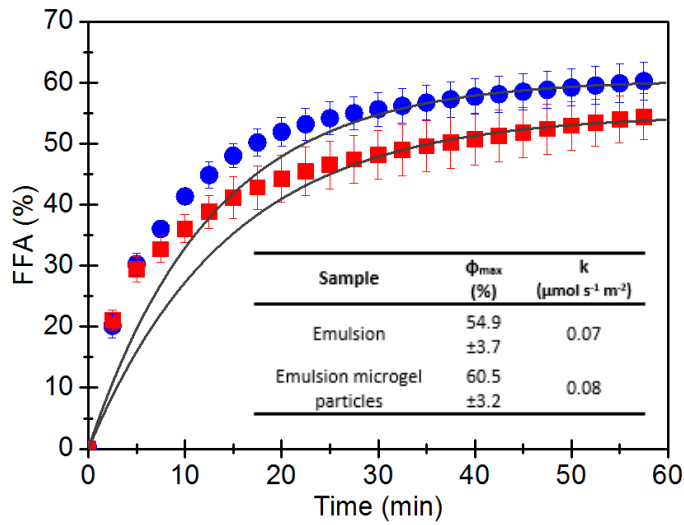
Appendix D.2 Confocal microscopy of the WPI microgel particles undergoing *in vitro* digestion (WPI stained in green).



Appendix D.3 Particle size distribution of 9.6 wt% WPI based microgel particles under intestinal *in vitro* digestion (A) and gastric + intestinal *in vitro* digestion (B) over time (black full line: before digestion, blue full line: 5 min, blue dashed line: 60 min, blue dotted line: 120 min, blue short dotted line: 180 min).



Appendix D.4 Zeta-potential of 9.6 wt% WPI microgel particles before *in vitro* intestinal digestion (black), during intestinal digestion pre-gastric digestion (blue) or post-gastric digestion (blue slashed).



Appendix D.5 Free fatty acid release during *in vitro* intestinal digestion (pre-gastric digestion) over time and release schematics of 9.6 wt% WPI stabilised emulsion (red square) and 9.6 wt% WPI emulsion microgel particles (blue circle) and mathematical modelling fit (grey line). Maximum free fatty acid release (Φ_{\max} , %), rate constant after 60 min (k , $\mu\text{mol s}^{-1} \text{m}^{-2}$) of *in vitro* intestinal digestion of different samples in the inset table (* mean statistical different at a level of $p < 0.05$)